

# Statics and Dynamics of Skyrmions Interacting with Pinning: A Review

C. Reichhardt and C. J. O. Reichhardt

*Theoretical Division and Center for Nonlinear Studies,  
Los Alamos National Laboratory,  
Los Alamos, NM 87545,  
USA*

M. V. Milošević

*NANOLab Center of Excellence,  
Department of Physics,  
University of Antwerp,  
Belgium*

(Dated: February 23, 2021)

Magnetic skyrmions are topologically stable nanoscale particle-like objects that were discovered in 2009. Since that time, intense research interest in the field has led to the identification of numerous compounds that support skyrmions over a range of conditions spanning cryogenic to room temperatures. Skyrmions can be set into motion under various types of driving, and the combination of their size, stability, and dynamics makes them ideal candidates for numerous applications. At the same time, skyrmions represent a new class of system in which the energy scales of the skyrmion-skyrmion interactions, sample disorder, temperature, and drive can compete. A growing body of work indicates that the static and dynamic states of skyrmions can be influenced strongly by pinning or disorder in the sample; thus, an understanding of such effects is essential for the eventual use of skyrmions in applications. In this article we review the current state of knowledge regarding individual skyrmions and skyrmion assemblies interacting with quenched disorder or pinning. We outline the microscopic mechanisms for skyrmion pinning, including the repulsive and attractive interactions that can arise from impurities, grain boundaries, or nanostructures. This is followed by descriptions of depinning phenomena, sliding states over disorder, the effect of pinning on the skyrmion Hall angle, the competition between thermal and pinning effects, the control of skyrmion motion using ordered potential landscapes such as one- or two-dimensional periodic asymmetric substrates, the creation of skyrmion diodes, and skyrmion ratchet effects. We highlight the distinctions arising from internal modes and the strong gyroscopic or Magnus forces that cause the dynamical states of skyrmions to differ from those of other systems with pinning, such as vortices in type-II superconductors, charge density waves, or colloidal particles. Throughout this work we also discuss future directions and open questions related to the pinning and dynamics in skyrmion systems.

## CONTENTS

I. Introduction	2	D. Continuum Based Simulations of the Dynamic Phase Diagram	30
II. Pinning in particle Like systems	5	E. 3D Skyrmion Dynamics	31
III. Models of Skyrmions and Mechanisms of Skyrmion Pinning	6	F. Further Directions for Dynamic Skyrmion Phases with Random Disorder	33
A. Particle Based Approaches to Skyrmion Dynamics and Pinning	8	VII. Pinning and the Skyrmion Hall Angle	34
IV. Micromagnetic Models	10	A. Thermal Effects	38
A. Pinning Mechanisms	11	B. Future Directions	39
B. Skyrmion Pinning by Individual versus Extended Defects and the Role of the Magnus Force	13	VIII. Nanostructured and Periodic Landscapes	40
C. Further Directions	16	A. One Dimensional Periodic Substrates and Speed-Up Effects	41
V. Collective States and Skyrmion Lattices With Pinning	17	B. Further Directions for 1D Periodic Substrates	45
A. Future Directions	21	C. Skyrmions with Two Dimensional Periodic Pinning	46
VI. Depinning Dynamics of Skyrmions with Pinning	22	1. Further Studies with Periodic Substrates	48
A. Elastic and Plastic Depinning	24	D. Asymmetric Arrays, Diodes, and Ratchets	49
B. Noise	28	E. Coupling Skyrmions to Other Quasiperiodic Lattice Structures	51
C. Avalanches	30	F. Single Skyrmion Manipulation	52
		IX. Summary	52
		Acknowledgments	52

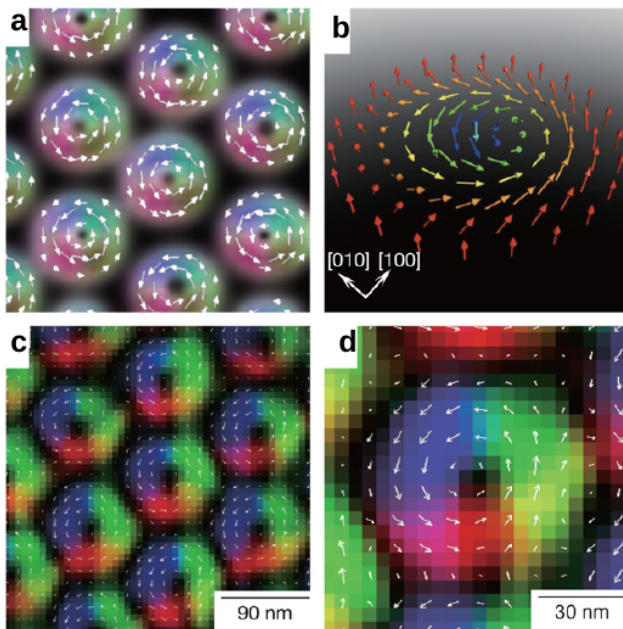


FIG. 1 Skyrmion crystal image obtained using Lorentz microscopy on thin film  $\text{Fe}_{0.5}\text{Co}_{0.5}\text{Si}$  near  $T = 25\text{K}$  from Ref. (Yu *et al.*, 2010). (a) The spin structures predicted by simulation. (b) Schematic of the spin configuration in a single skyrmion. (c) Lorentz image of the skyrmion lattice. (d) Magnified view of panel (c). Here the skyrmions are on the order of 90 nm in diameter. Reprinted by permission from: Springer Nature, X. Z. Yu *et al.*, “Real-space observation of a two-dimensional skyrmion crystal”, *Nature (London)* **465**, 901 (2010), ©2010.

References

53

## I. INTRODUCTION

The idea of a particle like magnetic texture called a skyrmion was initially proposed theoretically (Bogdanov and Yablonskii, 1989; Rößler *et al.*, 2006), and was confirmed experimentally in 2009 when neutron scattering experiments revealed a six-fold scattering pattern in the chiral magnet MnSi, indicating the presence of a collection of lines forming a two-dimensional (2D) hexagonal skyrmion lattice (Mühlbauer *et al.*, 2009). Shortly afterward, direct images of the skyrmion lattice in thin film samples were obtained using Lorentz microscopy (Yu *et al.*, 2010). Since this initial discovery, skyrmions with sizes ranging from micron scale down to 10 nm have been identified in a growing number of 2D, three-dimensional (3D), and layered materials (Heinze *et al.*, 2011; Jiang *et al.*, 2015; Milde *et al.*, 2013; Nagaosa and Tokura, 2013; Romming *et al.*, 2013; Seki *et al.*, 2012; Wang *et al.*, 2018a; Wiesendanger, 2016; Yu *et al.*, 2011).

As an applied magnetic field is increased, skyrmions emerge from the helical state in the form of a lattice, re-

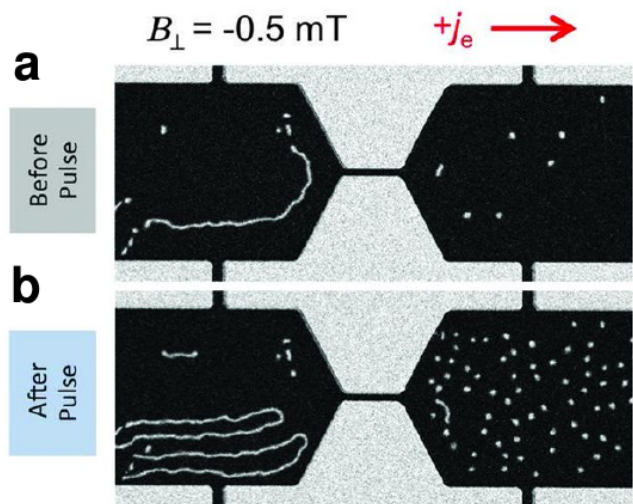


FIG. 2 Image of skyrmion creation at room temperature by passing current through a constriction (Jiang *et al.*, 2015). Here the skyrmions are approximately a micron in diameter. From W. Jiang *et al.*, *Science* **349**, 283 (2015). Reprinted with permission from AAAS.

main stable over a range of temperatures and fields, and then disappear at sufficiently high fields when the system transitions into a ferromagnetic state (Mühlbauer *et al.*, 2009; Nagaosa and Tokura, 2013). The predicted spin structure of a skyrmion lattice and of an individual skyrmion, shown schematically in Fig. 1(a, b), agrees well with the initial Lorentz microscopy images in Fig. 1(c, d) of skyrmions that are approximately 90 nm in diameter (Yu *et al.*, 2010). These first observations of skyrmions were performed at temperatures near  $T = 30\text{K}$ , but since that time numerous systems have been identified which support skyrmions at and above room temperature (Boulle *et al.*, 2016; Jiang *et al.*, 2015; Moreau-Lucaire *et al.*, 2016; Soumyanarayanan *et al.*, 2017; Tokunaga *et al.*, 2015; Wiesendanger, 2016; Woo *et al.*, 2016). Figure 2 shows images of skyrmion bubbles of diameter close to a micron created in a room temperature system (Jiang *et al.*, 2015). It is also possible to observe transitions from hexagonal to square skyrmion lattices (Karube *et al.*, 2016; Nakajima *et al.*, 2017b; Yi *et al.*, 2009), as well as new types of particle like textures such as a square meron lattice that transitions into a triangular skyrmion lattice (Yu *et al.*, 2018b).

Skyrmions can be two dimensional in thin films, (Mühlbauer *et al.*, 2009; Yu *et al.*, 2010), have a layered or pancake-like structure in layered materials, form 3D lines in bulk materials (Birch *et al.*, 2020; Milde *et al.*, 2013; Park *et al.*, 2014; Zhang *et al.*, 2018a), and even assemble into 3D lattices of particle-like hedgehogs in certain bulk systems (Fujishiro *et al.*, 2019; Lin and Batista, 2018). Different species of skyrmions can exist (Leonov and Mostovoy, 2015), including bi-skyrmions (Takagi *et al.*, 2018; Wang *et al.*, 2016; Yu *et al.*, 2014), multiply charged

skyrmions (Rybakov and Kiselev, 2019), chiral bobbars (Rybakov *et al.*, 2015; Zheng *et al.*, 2018), antiskyrmions (Hoffmann *et al.*, 2017; Nayak *et al.*, 2017), antiferromagnetic skyrmions (Akosa *et al.*, 2018; Barker and Tretiakov, 2016), magnetic bi-layer skyrmions (Zhang *et al.*, 2016c), elliptical skyrmions (Jena *et al.*, 2020), meron lattices (Gao *et al.*, 2020; Wang *et al.*, 2020b; Yu *et al.*, 2018b), bi-merons (Jani *et al.*, 2021), hopfions (Liu *et al.*, 2020; Wang *et al.*, 2019b), hedgehog textures (Fujishiro *et al.*, 2019; Zou *et al.*, 2020) and polar skyrmions (Das *et al.*, 2019). Skyrmions and similar quasiparticle textures can arise in many other non-magnetic systems including graphene (Bömerich *et al.*, 2020; Zhou *et al.*, 2020) liquid crystals (Duzgun *et al.*, 2018; Foster *et al.*, 2019; Nych *et al.*, 2017), and optical (Tsesses *et al.*, 2018) and plasmonic systems (Davis *et al.*, 2020). We highlight a variety of the possible textures in Fig. 3, including a real space image of a square meron lattice (Yu *et al.*, 2018b) in Fig. 3(a), an image of polar skyrmions (Das *et al.*, 2019) in Fig. 3(b), a half skyrmion lattice in a chiral liquid crystal system (Nych *et al.*, 2017) in Fig. 3(c), and the electric fields for an optical skyrmion (Tsesses *et al.*, 2018) in Fig. 3(d).

Skyrmions can be set into motion with an applied drive, such as a current which creates a spin torque Hall effect. The skyrmion motion can be deduced from changes in the topological Hall effect (Liang *et al.*, 2015; Schulz *et al.*, 2012) or observed through direct imaging (Jiang *et al.*, 2015, 2017b; Legrand *et al.*, 2017; Litzius *et al.*, 2017; Tolley *et al.*, 2018; Woo *et al.*, 2016, 2018; Yu *et al.*, 2012, 2014). It is also possible to move skyrmions with temperature gradients (Kong and Zang, 2013; Mochizuki *et al.*, 2014; Pöllath *et al.*, 2017; Wang *et al.*, 2020c), magnetic fields (Casiraghi *et al.*, 2019; Shen *et al.*, 2018a; Zhang *et al.*, 2018c), electric fields (Kruchkov *et al.*, 2018; White *et al.*, 2014), microwaves (Ikka *et al.*, 2018; Wang *et al.*, 2015), spin waves (Shen *et al.*, 2018b), magnons (Psaroudaki and Loss, 2018), or acoustic waves (Nepal *et al.*, 2018). Due to their size scale, mobility, and stability at room temperature, skyrmions have great potential for use in a wide range of applications such as race track memory (Everschor-Sitte *et al.*, 2018; Fert *et al.*, 2013, 2017; Müller, 2017; Suess *et al.*, 2018, 2019; Tomasello *et al.*, 2014), logic devices (Liu *et al.*, 2019; Luo *et al.*, 2018; Mankalale *et al.*, 2019; Zhang *et al.*, 2015) or novel computing architectures (Grollier *et al.*, 2020; Pinna *et al.*, 2018; Prychynenko *et al.*, 2018; Song *et al.*, 2020). Many of the proposed skyrmion-based devices would require the skyrmions to move through a nanostructured landscape in a highly controlled fashion.

A growing body of work indicates that in many skyrmion systems, pinning and the effects of quenched disorder are very important in determining both the static and dynamic skyrmion response (Fert *et al.*, 2017; Jiang *et al.*, 2017b; Litzius *et al.*, 2017; Nagaosa and

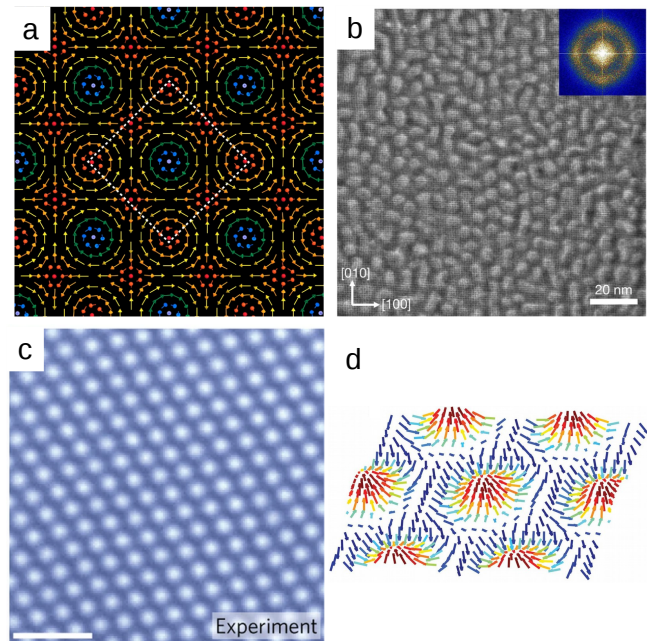


FIG. 3 Different types of skyrmionic textures in real space. (a) Schematic magnetization texture of a square meron lattice (Yu *et al.*, 2018b). Reprinted by permission from: Springer Nature, X. Z. Yu *et al.*, “Transformation between meron and skyrmion topological spin textures in a chiral magnet”, Nature (London) **564**, 95 (2018), ©2018. (b) Image of a polar skyrmion structure (Das *et al.*, 2019). Reprinted by permission from: Springer Nature, S. Das *et al.*, “Observation of room-temperature polar skyrmions”, Nature (London) **568**, 368 (2019), ©2019. (c) Image of a half skyrmion lattice in a liquid crystal system (Nych *et al.*, 2017). Reprinted by permission from: Springer Nature, A. Nych *et al.*, “Spontaneous formation and dynamics of half-skyrmions in a chiral liquid-crystal film”, Nature Phys. **13**, 1215 (2017), ©2017. (d) Vector representation of the electric field for a Neel-type optical skyrmion (Tsesses *et al.*, 2018). From S. Tsesses *et al.*, Science **361**, 993 (2018). Reprinted with permission from AAAS.

Tokura, 2013; Wiesendanger, 2016; Woo *et al.*, 2016). Initial transport studies revealed only weak skyrmion pinning effects, with a critical depinning force  $j_c$  in MnSi at  $T = 28K$  of only  $j_c \propto 10^6$  A/m<sup>2</sup> (Jonietz *et al.*, 2010; Schulz *et al.*, 2012), nearly five orders of magnitude smaller than the depinning force for magnetic domain walls. In contrast, recent work by Woo *et al.* on room temperature skyrmions in thin films showed that the pinning can be very strong, with  $j_c \propto 2.2 \times 10^{11}$  A/m<sup>2</sup> (Woo *et al.*, 2018). Similar high depinning thresholds observed in other systems (Hrabec *et al.*, 2017) indicate that a variety of pinning effects and skyrmion-pin interaction mechanisms can be important in different materials that support skyrmions, depending on the skyrmion size, dimensionality, and the characteristics of the disorder in the sample.

Skyrmion motion can be strongly modified when pin-

ning is present. For example, there is evidence that the skyrmion Hall effect is heavily impacted by pinning. The skyrmion Hall effect arises when the gyroscopic nature of the skyrmion dynamics causes the skyrmions to move at an angle called the skyrmion Hall angle  $\theta_{\text{SKH}}$  with respect to the applied drive (Everschor-Sitte and Sitte, 2014; Iwasaki *et al.*, 2013b; Nagaosa and Tokura, 2013; Zang *et al.*, 2011). Due to the skyrmion Hall effect, a skyrmion driven along a narrow strip by a current parallel to the strip does not move in the direction of the current. Instead, it translates toward the edge of the strip, where it is annihilated. This behavior imposes a limitation on the use of skyrmions in strip-based devices (Iwasaki *et al.*, 2013a). It may, however, be possible to use pinning to change the motion of skyrmions through a strip. Simulations (Kim and Yoo, 2017; Legrand *et al.*, 2017; Litzius *et al.*, 2020; Müller and Rosch, 2015; Reichhardt *et al.*, 2015b,c; Reichhardt and Reichhardt, 2016) and experiments (Jiang *et al.*, 2017b; Litzius *et al.*, 2020, 2017; Woo *et al.*, 2018) have shown that the introduction of pinning to a system not only produces a finite depinning threshold for skyrmion motion, but also generates a strong drive dependence of the skyrmion Hall angle, which increases from a very small value at low drives to the pin-free intrinsic value  $\theta_{\text{SKH}}^{\text{int}}$  as the drive increases.

There are a variety of other cases in which pinning effects can be beneficial. Thermal and diffusive motion of skyrmions has been observed in experiment (Nozaki *et al.*, 2019; Zázvorka *et al.*, 2019; Zhao *et al.*, 2020), and it will soon be important to take thermal effects into account for device creation, particularly for smaller skyrmions. For example, a skyrmion serving as an information carrier in a memory device may need to be locked in a specific location for long times, but the thermal motion present at room temperature could cause the skyrmion to wander away gradually and lose the memory of its initial position. Long term stable memory could be achieved through pinning, which could overcome the thermal effects over arbitrarily long times. It would be ideal to have tunable pinning that would be absent when rapid motion of skyrmions is needed but strong when long time stability of the skyrmion configuration is required to create a desired memory state. Already, different types of pinning have been identified that have attractive, repulsive, radially symmetric, or radially asymmetric behavior. Devices could be created by using nanoscale techniques to fabricate controlled pinning patterns in the form of lines or channels that guide skyrmions, periodic arrays that stabilize certain skyrmion configurations, or asymmetric pinning that produces skyrmion diodes, rectifiers and logic devices. For future applications it is important to develop a thorough understanding of skyrmion pinning and dynamics.

Beyond applications, interacting skyrmions driven over pinning represent a fascinating class of systems in which collective and competing effects can produce a rich vari-

ety of nonequilibrium dynamical phases (Fisher, 1998; Reichhardt and Reichhardt, 2017). The skyrmion-skyrmion interactions usually favor the formation of a triangular skyrmion lattice, while the interactions of skyrmions with random pinning favor a disordered skyrmion structure, producing a competition between crystalline and glassy states even for static skyrmion configurations. Under an applied drive, the pinning opposes the skyrmion motion, and the competition between the pinning and driving forces generates complex dynamics near the depinning threshold. Additional competing effects appear when thermal fluctuations are important. Temperature can reduce the effectiveness of the pinning, favoring an ordered state, but can also disorder the skyrmion lattice.

In this review, we focus on aspects of pinning and dynamics in skyrmion systems. We highlight what is known currently about skyrmion pinning and the variety of mechanisms that can produce it, including changes in the Dzyaloshinskii-Moriya interaction (DMI), atomic impurities, local anisotropy, sample thickness, damage tracks, missing spins, holes, or blind holes. We outline the microscopic models for pinning and skyrmion dynamics currently in use, and show that skyrmions can have attractive, repulsive, or combined attractive and repulsive interactions with pointlike or linelike disorder. Throughout this review we discuss similarities and differences between skyrmions and other systems with pinning such as superconducting vortices, sliding charge density waves, Wigner crystals, and colloidal particles. In the absence of driving, we consider disorder-induced transitions from a skyrmion crystal to different types of glassy states. When a drive is added, we describe the different types of depinning that occur, ranging from elastic to plastic, as well as the effect of disorder on bulk transport measures such as velocity-force curves, the role of temperature, and creep effects. The effects of pinning on fluctuations, the skyrmion Hall angle, and the skyrmion-skyrmion interactions are also covered. In addition to sources of random disorder, we describe the pinning and dynamics of skyrmions on ordered structures such as 2D periodic, quasiperiodic, quasi-one-dimensional (1D) periodic, and 1D asymmetric substrates, which can produce commensurate and incommensurate states, soliton motion, and diode and ratchet effects.

In each section we discuss future directions including studies of skyrmions in bulk materials, skyrmion behavior in thin films with extended or point defects, the effects of nanostructured arrays with periodic or 1D modulation, the behavior of layered materials, the coupling of skyrmions to other topological defects such as vortices in type-II superconductors, or even the effect of having different species of skyrmions coexist. In the case of 3D skyrmions, introduction of a columnar pinning landscape could create a state analogous to the Bose glass found in type-II superconductors, and could also lead to cutting

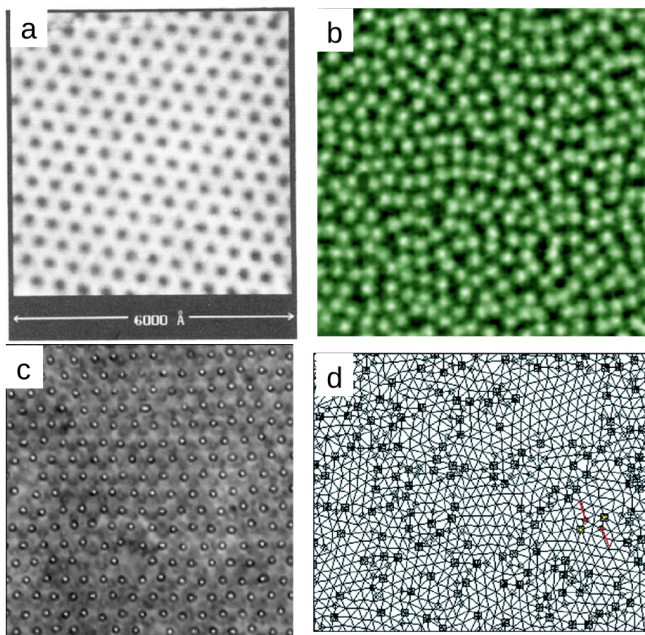


FIG. 4 (a) Image of an ordered superconducting vortex lattice obtained using a scanning tunneling microscope (Hess *et al.*, 1989). Reprinted with permission from H. F. Hess *et al.*, Phys. Rev. Lett. **62**, 214 (1989). Copyright 1989 by the American Physical Society. (b) Image of a disordered superconducting vortex lattice obtained using magneto-optical imaging (Goa *et al.*, 2001). Used with permission of IOP Publishing, Ltd, from “Real-time magneto-optical imaging of vortices in superconducting NbSe<sub>2</sub>,” P. E. Goa *et al.*, Supercond. Sci. Technol. **14**, 729, 2001; permission conveyed through Copyright Clearance Center, Inc. (c) Image of a colloidal lattice obtained with an optical microscope (Weiss *et al.*, 1998). Reprinted from J. A. Weiss *et al.*, J. Chem. Phys. **109**, 8659 (1998), with the permission of AIP publishing. (d) Delaunay triangulation of colloidal particle positions in a colloidal glass state based on an optical microscope image obtained experimentally (Pertsinidis and Ling, 2008). Reprinted with permission from A. Pertsinidis *et al.*, Phys. Rev. Lett. **100**, 028303 (2008). Copyright 2008 by the American Physical Society.

and entanglement effects as well as the possibility of creating transformer geometries. We outline potential new measures for characterizing the skyrmion structures and dynamics that are borrowed from work in vortex dynamics, soft matter, and statistical physics, such as structural measures, force chains, jamming concepts, glassy effects, and defect proliferation.

For more general reviews of other aspects of skyrmions, we refer the reader to Refs. (Bogdanov and Panagopoulos, 2020; Jiang *et al.*, 2017a; Tokura and Kanazawa, 2020) for materials that support skyrmions, Ref. (Li *et al.*, 2021) for skyrmion devices and skyrmionlike textures such as swirling quasiparticles, and to Refs. (Back *et al.*, 2020; Göbel *et al.*, 2021) for further future direc-

## II. PINNING IN PARTICLE LIKE SYSTEMS

Systems with many interacting particles coupled to some form of disorder or pinning are known to exhibit very rich static and dynamic phase behavior as a function of changing particle-particle interactions, disorder strength, and temperature. One of the best studied examples of such systems is magnetic vortices in type-II superconductors (Blatter *et al.*, 1994). In the absence of driving, the vortices can form a triangular lattice, a weakly pinned Bragg glass in which the vortices remain elastic with topological order but still have glassy properties (Giamarchi and Le Doussal, 1995; Klein *et al.*, 2001), topologically disordered vortex glass states (Fisher *et al.*, 1991; Ganguli *et al.*, 2015; Henderson *et al.*, 1996; Nattermann and Scheidl, 2000; Toft-Petersen *et al.*, 2018), entangled vortex lines (Giller *et al.*, 1997; Nelson, 1988), liquid states (Cubitt *et al.*, 1993; Safar *et al.*, 1992; Zeldov *et al.*, 1995), or reentrant liquid states (Avraham *et al.*, 2001; Banerjee *et al.*, 2000). Vortices in the presence of an external drive can exhibit elastic depinning, where the system transitions from a pinned crystal into a moving crystal state (Bhattacharya and Higgins, 1993; Di Scala *et al.*, 2012; Reichhardt and Reichhardt, 2017), or plastic depinning, where the moving state has a liquid structure (Bhattacharya and Higgins, 1993; Fily *et al.*, 2010; Jensen *et al.*, 1988; Matsuda *et al.*, 1996; Olson *et al.*, 1998a; Reichhardt and Reichhardt, 2017; Shaw *et al.*, 2012). Plastically moving vortices at higher drives can transition into a moving crystalline (Bhattacharya and Higgins, 1993; Giamarchi and Le Doussal, 1996; Koshelev and Vinokur, 1994; Olson *et al.*, 1998b; Reichhardt and Reichhardt, 2017) or moving smectic phase (Balents *et al.*, 1998; Olson *et al.*, 1998b; Pardo *et al.*, 1998). These different depinning and dynamical phase transitions produce distinct signatures in the bulk transport measures and velocity-force curves as well as changes in the vortex structure and fluctuations (Bhattacharya and Higgins, 1993; Di Scala *et al.*, 2012; Fily *et al.*, 2010; Fisher, 1998; Jensen *et al.*, 1988; Koshelev and Vinokur, 1994; Olson *et al.*, 1998b; Reichhardt and Reichhardt, 2017; Shaw *et al.*, 2012). Similar depinning and sliding dynamics occur in other systems of particle-like objects moving through quenched disorder, such as colloidal particles (Hu and Westervelt, 1995; Pertsinidis and Ling, 2008; Reichhardt and Olson, 2002a; Tierno, 2012), Wigner crystals (Cha and Fertig, 1994, 1998; Kumar *et al.*, 2018; Reichhardt *et al.*, 2001; Williams *et al.*, 1991), and certain pattern forming systems (Morin *et al.*, 2017; Sándor *et al.*, 2017; Sengupta *et al.*, 2010).

To highlight the similarities between skyrmions and other systems with pinning, in Fig. 4(a) we show an image of a triangular superconducting vortex lattice obtained using scanning tunneling microscopy (Hess *et al.*, 1989). In Fig. 4(b), a disordered vortex structure appears in an image obtained using a magneto-optical technique

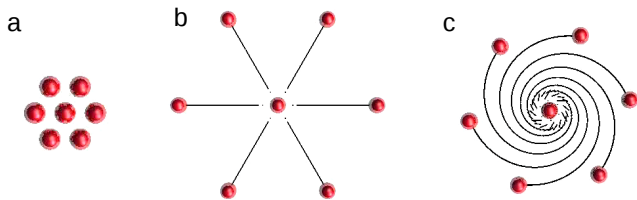


FIG. 5 Illustration of the difference between purely overdamped motion and motion with a Magnus force of strength  $\alpha_m$  for particles with finite damping,  $\alpha_d > 0$ . (a) Initial dense cluster of particles. (b) Trajectories of overdamped particles with  $\alpha_m = 0$  moving away from the center. (c) Trajectories of particles with a Magnus force  $\alpha_m > 0$  moving away from the center, showing the emergence of nonconservative rotation.

(Goa *et al.*, 2001). Figure 4(c) shows a colloidal triangular lattice observed with optical microscopy (Weiss *et al.*, 1998), while in Fig. 4(d), the colloidal lattice is distorted by strong pinning, there are numerous topological defects, and the system forms a pinned glass (Pertsinidis and Ling, 2008). If the disorder is weak, as in Fig. 4(a) and (c), the particles depin without the generation of topological defects and flow elastically, while for strong disorder, as in Fig. 4(b) and (d), the particles depin plastically with large lattice distortions or with a coexistence of pinned and moving particles.

A crucial difference between skyrmions and the vortices or colloidal particles illustrated in Fig. 4 is the fact that skyrmions experience a strong non-dissipative gyroscopic or Magnus force which generates a velocity component *perpendicular* to the net external forces acting on the skyrmion. In many of the previously studied systems, the dynamics are overdamped and the particle velocity  $\mathbf{v}_d$  is strictly aligned with the net external force  $\mathbf{F}_{\text{ext}}$ ,  $\mathbf{v}_d = \alpha_d \mathbf{F}_{\text{ext}}$ , where  $\alpha_d$  is a damping constant. In a skyrmion system, the damping term is accompanied by a Magnus force contribution to the velocity,  $\mathbf{v}_m = \alpha_m \hat{\mathbf{z}} \times \mathbf{F}_{\text{ext}}$ , which generates a velocity component perpendicular to the applied force. Here  $\alpha_m$  is the strength of the Magnus term. The ratio  $\alpha_m/\alpha_d$  for skyrmions can be as large as ten or even higher (Nagaosa and Tokura, 2013). One consequence of the Magnus force is the appearance of a skyrmion Hall effect in which the skyrmion moves at an angle  $\theta_{\text{SKH}}$  with respect to the applied driving force. The intrinsic value of this angle is given by  $\theta_{\text{SKH}}^{\text{int}} = \tan^{-1}(\alpha_m/\alpha_d)$ . The Magnus force affects the skyrmion-skyrmion interactions as well as the motion of skyrmions through pinning sites. In Fig. 5(a) we show repulsively interacting particles that have been initialized in a dense cluster and are then allowed to move away from each other. In the overdamped limit with  $\alpha_m = 0$ , Fig. 5(b) shows that the particles move radially, in the direction of the forces generated by the particle-particle interactions. In contrast, the particles in Fig. 5(c) have a finite Magnus force,  $\alpha_m > 0$ , so that in addition to the radial displacement, there is

a strong rotational component of the motion. Here the dissipative term  $\alpha_d$  is still finite, but if it were zero, only rotational motion of the particles would occur with no radial motion.

Many of the previously studied systems with pinning, including superconducting vortices, classical charges, and colloidal particles, are composed of relatively stiff particle-like objects in which the internal degrees of freedom are unimportant, making a particle-based treatment of their dynamics appropriate. In contrast, skyrmions can exhibit excitations of internal modes (Beg *et al.*, 2017; Garst *et al.*, 2017; Ikka *et al.*, 2018; Onose *et al.*, 2012) or large distortions (Gross *et al.*, 2018; Litzius *et al.*, 2017; Zeissler *et al.*, 2017) that activate additional degrees of freedom, significantly impacting the statics and dynamics. Furthermore, moving skyrmions can emit spin waves that could modify the effective skyrmion-skyrmion interactions (Koshibae and Nagaosa, 2018; Schütte and Garst, 2014). The uniformity often associated with particle-based models may also not capture the behavior of a skyrmion system well. It is possible for skyrmions to coexist with a stripe phase or ferromagnetic domains (Loudon *et al.*, 2018; Müller *et al.*, 2017; Shibata *et al.*, 2018; Yu *et al.*, 2018a), and in some systems, there is considerable dispersion in the size of the skyrmions, making the skyrmion assembly effectively polydisperse (Karube *et al.*, 2018) This contrasts strongly with superconducting vortices, which are all the same size in a given sample.

### III. MODELS OF SKYRMIONS AND MECHANISMS OF SKYRMION PINNING

One of the simplest pictures of pinning and sliding dynamics is a model of a single particle in a tilted sinusoidal potential with period  $L$ . To further simplify the problem, consider an overdamped particle that obeys the following equation of motion:

$$\alpha_d \frac{dx}{dt} = -\frac{dU(x)}{dx} + F_D. \quad (1)$$

Here  $\alpha_d$  is the damping constant,  $F_D$  is the external dc drive, and  $U(x) = A \cos(kx)$ , where  $k = 2\pi/L$ . When  $A = 0$ , the substrate disappears and the particle moves in the direction of the drive with a velocity  $v = F_D/\alpha_d$ . When  $A > 0$ , there is a finite depinning threshold  $F_c$ , indicating that there is no steady state motion unless  $F_D > F_c$ . If we set  $A = A_0/k$ , we obtain a critical force of  $F_c = A_0$ . For drives close to but above the critical force,  $F_D \gtrsim F_c$ , the particle begins to slide with a velocity  $v \propto (F_D - F_c)^\beta$  where  $\beta = 1/2$  (Fisher, 1985). At higher drives, the velocity crosses over to the clean value limit of  $v \propto F_D$ , similar to what is shown in Fig. 6.

Additional effects can be included in the single particle picture, such as a coupling to a thermal bath modeled using a fluctuating force term  $\eta(t)$  representing

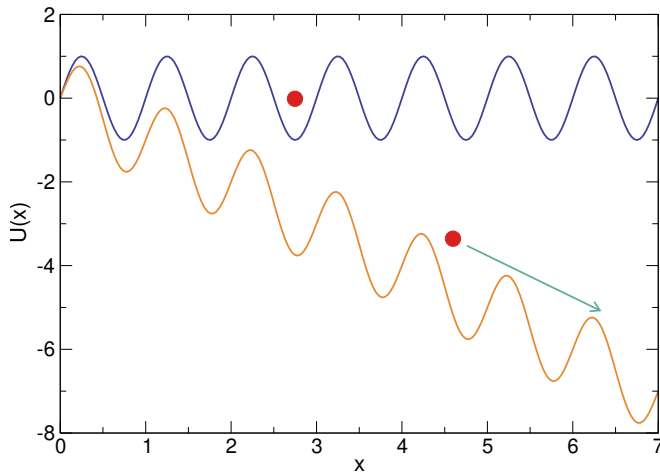


FIG. 6 The simplest system exhibiting depinning is an overdamped particle (red circle) in a sinusoidal potential  $U(x) = A \cos(kx)$  that has been tilted by a driving force  $F_D$ . The particle is pinned when  $F_D < F_c$  (blue curve), where  $F_c$  is the critical driving force that must be applied to enable the particle to slide. Steady state particle motion occurs when  $F_D > F_c$  (orange curve).

Langevin kicks. These obey the correlations  $\langle \eta(t) \rangle = 0$  and  $\langle \eta(t)\eta(t') \rangle = 2k_B T \delta(t - t')$ , where  $k_B$  is the Boltzmann constant. When  $F_D = 0$ , the particle can thermally hop with equal probability to the left or right according to an Arrhenius law, with an instantaneous velocity  $|v| \propto \exp(-U/k_B T)$  and an average velocity of zero; however, under a finite applied drive, the time-averaged velocity becomes finite since the Arrhenius jumps are now biased. In this case, the potential  $U(x)$  is replaced by  $U(x) \pm U_D(x)$ , where for a linear drive  $U_D(x) = U(x) - F_D x$ . This increases the average size of jumps in the driving direction and produces a finite velocity even for drives that are below the  $T = 0$  value of  $F_c$ , leading to the emergence of a creep regime. The creep velocity for  $F < F_c$  is of the form

$$v \propto C_A \exp\left(\frac{A - F_D}{kT}\right) \quad (2)$$

where  $C_A$  is the attempt frequency. Figure 7 shows schematic velocity-force curves at  $T = 0$  and  $T > 0$ . Even at finite temperatures, there can be a noticeable change in the velocity-force curves upon crossing the  $T = 0$  value of  $F_c$  due to a crossover from the creep motion of intermittently hopping particles for  $F_D < F_c$  to continuous flow for  $F_D > F_c$ . When multiple interacting particles are present, collective creep, plastic creep, and glassy effects can occur, which typically introduce a power law prefactor to the exponential velocity term (Feigel'man *et al.*, 1989; Luo and Hu, 2007).

It is possible to add other terms to Eq. (1), such as an inertial term  $M d^2 x / dt^2$ , where  $M$  is the mass of the particle, as well as asymmetry or disorder in the substrate. If the dc drive is supplemented with an additional

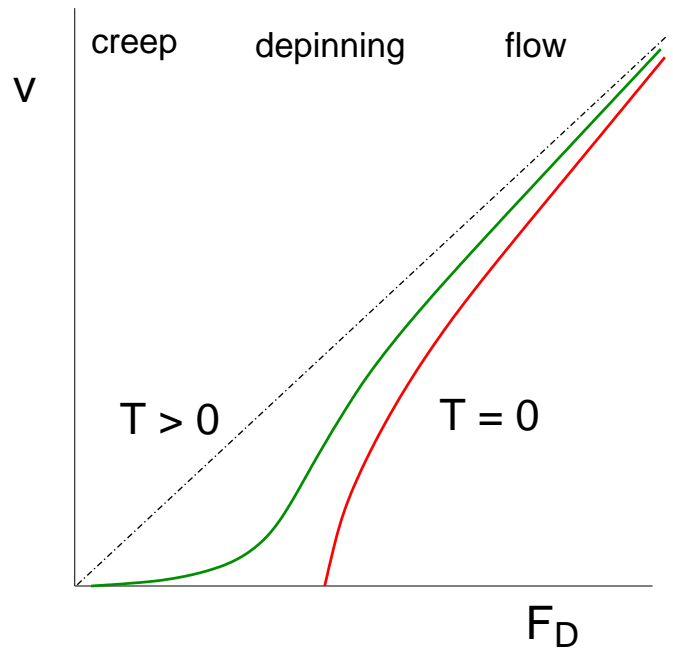


FIG. 7 Schematic velocity  $v$  vs drive  $F_D$  curves for a system with a finite depinning threshold  $F_c$  at zero temperature  $T = 0$  (red curve) and finite temperature  $T > 0$  (green curve). Creep behavior occurs for finite temperature when the velocity remains nonzero for  $F_D < F_c$ . There is a change in the shape of the  $T > 0$  velocity-force curve near  $F_c$  due to a crossover from creep to flow. The dashed line indicates the free-flow limit  $v \propto F_D$  for a system with no pinning.

ac drive of the form  $F^{ac} = A_{ac} \sin(\omega t)$ , the well known Shapiro step phenomenon appears in the form of steps in the velocity-force curves (Shapiro, 1963). The complexity of the substrate can be increased by introducing spatial variations in two dimensions, such as square or triangular pinning lattices, or by adding random disorder. For an overdamped system, the 1D picture of depinning generally captures the effects that are found even for a substrate with 2D features. Interestingly, this is not case for skyrmions, since the presence of the Magnus force causes 2D skyrmions to exhibit different dynamics than their completely 1D counterparts.

The next level of complexity is to include multiple interacting or coupled particles. For example, a dimer or trimer arrangement of particles connected by springs could be placed on a periodic 1D substrate. The best known model of such a system is the Frenkel-Kontorova model consisting of a 1D chain of elastically coupled particles moving over a 1D periodic substrate (Braun and Kivshar, 1998). This model can be extended to describe a 1D string of particles or a 2D array of particles moving in 2D or 3D and coupled to a random substrate. For example, a 2D triangular array of skyrmions could be modeled as a 2D elastic lattice. In 3D, a single 1D line-like string could be modeled as an elastically coupled array of elements extending along the length of the string.

Additional terms can be incorporated into the equation of motion to capture effects appropriate for the specific system. When the particles are coupled by unbreakable elastic springs that do not allow for exchange of neighbors, phase slips, or breaking of the lattice, the system is said to be in an elastic limit. One advantage of working in the elastic limit is that it may be possible to ignore the exact details of the specific particle-particle interactions, since the system can be modeled effectively as a collection of harmonic springs. This approximation can be used when both the pinning and the temperature are sufficiently weak that only small distortions of the lattice can occur. It has been applied for understanding depinning phenomena in systems such as directed lines (Ertas and Kardar, 1996; Kardar, 1998), superconducting vortices (Dobramysl *et al.*, 2014), sliding charge density waves (Fisher, 1985), models of friction (Vanossi *et al.*, 2013), and even plate tectonics (Carlson *et al.*, 1994). For skyrmions, elastically coupled particle models are appropriate for 2D skyrmion lattices moving over weak disorder well below the temperature at which dislocations can be created thermally, as well as for 3D coupled skyrmion lines or even a single 3D skyrmion line in 3D systems. Additional terms such as the Magnus force can be inserted into the Frenkel-Kontorova model to capture long wavelength features of the depinning and sliding states.

The next step beyond an elastically coupled system is to consider particle based models with pairwise particle-particle interactions. Here, the particles respond not only to the positions of their nearest neighbors, but also to those of more distant neighbors or even to all other particles. Models of this type allow neighbor exchange, dislocation generation, and other plastic or nonaffine events (Fisher, 1998; Reichhardt and Reichhardt, 2017). Driven particle based models that undergo depinning have been used extensively in a wide range of studies of both hard matter systems, such as superconducting vortices, and soft matter systems, such as colloidal particles and granular matter (Reichhardt and Reichhardt, 2017). Particle based models have the advantages of permitting transitions between elastic and plastic motion as well as the ability to incorporate realistic pairwise particle-particle interactions. They are also generally more computationally efficient than fully continuum models, such as micromagnetic models of skyrmions in which the full spin degrees of freedom are included. The particle-particle interaction potentials are typically more complex than simple nearest neighbor harmonic interactions, and have a range that can depend strongly on the microscopic details of the system. For example, in thin film superconductors, the vortex-vortex pairwise interactions are logarithmic, so all the particles interact with all other particles in the system as well as with image charges, while in colloidal systems with strong screening, the particles interact only out to their first or second nearest neighbors.

## A. Particle Based Approaches to Skyrmion Dynamics and Pinning

One approach for modeling skyrmions is to treat them as point particles with dynamics that evolve according to an equation of motion proposed by Thiele (Thiele, 1973) to describe a driven magnetic particle:

$$\mathcal{G} \times \dot{\mathbf{R}} + \alpha \mathcal{D} \dot{\mathbf{R}} + m \ddot{\mathbf{R}} = \mathbf{F}_D. \quad (3)$$

Here  $\mathbf{F}_D$  is the driving force,  $\alpha$  is the Gilbert damping of an individual spin,  $\alpha \mathcal{D}$  is the friction experienced by the skyrmion, and  $\mathcal{G}$  is the gyrocoupling term which acts like a magnetic field applied perpendicular to the plane. This term is analogous to the Coriolis force. The inertial term is proportional to the skyrmion mass  $m$ ; however, when  $m$  is small, this term can be neglected. Additional second derivative terms can arise due to the excitation of internal modes of the skyrmion. The Thiele equation can be extended using terms that represent a substrate potential, field gradients, thermal forces, or gyrodamping (Schütte *et al.*, 2014). Due to its flexibility, the Thiele approach has been used extensively to model the dynamics of single rigid skyrmions (Büttner *et al.*, 2015).

Particle-particle interactions of either the elastically coupled or pairwise type can be included by making further modifications to the Thiele equation. Lin *et al.* (Lin *et al.*, 2013b) proposed a particle-based model including skyrmion-skyrmion, skyrmion-pinning, and skyrmion-driving force interactions of the form:

$$\alpha_d \mathbf{v}_i + \alpha_m \hat{\mathbf{z}} \times \mathbf{v}_i = \mathbf{F}_i^{ss} + \mathbf{F}_i^p + \mathbf{F}_i^D. \quad (4)$$

Here  $\mathbf{v}_i = d\mathbf{r}_i/dt$  is the skyrmion velocity,  $\alpha_d$  is the damping constant which aligns the skyrmion velocity in the direction of the external forces, and  $\alpha_m$  is the strength of the Magnus term which aligns the skyrmion velocity in the direction perpendicular to the external forces. When both  $\alpha_d$  and  $\alpha_m$  are finite, the skyrmions move at an angle called the intrinsic skyrmion Hall angle,  $\theta_{\text{SkH}}^{\text{int}} = \tan^{-1}(\alpha_m/\alpha_d)$  with respect to an externally applied driving force. In the work of Lin *et al.* (Lin *et al.*, 2013b), the skyrmion-skyrmion interaction was modeled as a short range repulsive force of the form  $\mathbf{F}_i^{ss} = \sum_{j \neq i}^N K_1(r_{ij}) \hat{\mathbf{r}}_{ij}$ , where  $K_1$  is the modified Bessel function,  $r_{ij} = |\mathbf{r}_i - \mathbf{r}_j|$  is the distance between skyrmion  $i$  and skyrmion  $j$ , and  $\hat{\mathbf{r}}_{ij} = (\mathbf{r}_i - \mathbf{r}_j)/r_{ij}$ . In Fig. 8 we show a snapshot from a 2D particle based skyrmion simulation model illustrating the skyrmion locations, pinning site locations, and the trajectory of one of the skyrmions, which undergoes rotational motion due to the Magnus force as it moves across the pinning sites (Reichhardt *et al.*, 2015b). The model proposed by Lin *et al.* (Lin *et al.*, 2013b) has both advantages and disadvantages. It neglects inertial effects, changes in the skyrmion shape, Magnon generation, and possible many body interaction terms. On the other hand, it allows for greater computational effi-



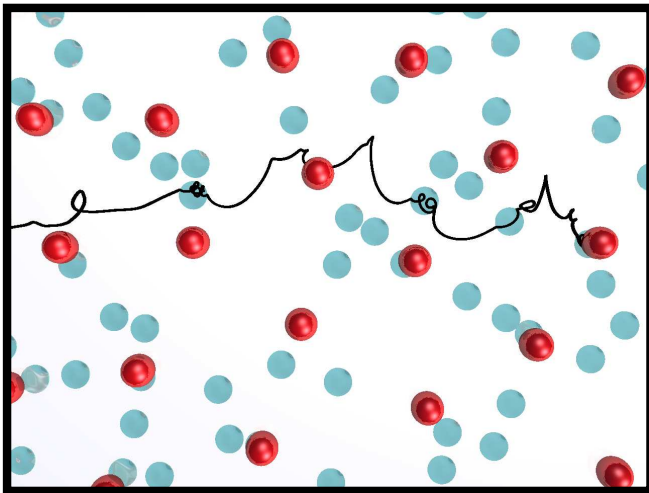


FIG. 8 Real-space image of skyrmions (dark red dots) in a particle based model driven through randomly arranged pinning sites (light blue dots) in a plastic flow phase (Reichhardt *et al.*, 2015b). The trajectory of a single skyrmion is highlighted, showing spiraling motions inside the pinning sites. Reprinted with permission from C. Reichhardt *et al.*, Phys. Rev. Lett. **114**, 217202 (2015). Copyright 2015 by the American Physical Society.

ciency compared to micromagnetic simulations, permitting many thousands of skyrmions to be simulated over long periods of time. In many cases the particle-based model successfully captures the robust general features of the system.

The particle based models can be substantially modified based on insight gained either from micromagnetic simulations or experiments. For instance, the skyrmion interactions are typically modeled as a short range repulsion; however, some micromagnetic simulations show evidence of skyrmion clustering (Leonov and Pappas, 2019; Loudon *et al.*, 2018; Rózsa *et al.*, 2016), suggesting that the skyrmion interactions extend out to longer range. Such effects could be captured by adding some form of longer range attraction to the particle based model. In other samples, the skyrmions exhibit a transition from a square to a triangular lattice, and this could be modeled by including an additional higher order symmetry term in the pairwise potential of the form (Olszewski *et al.*, 2018)

$$V(R, \theta) = K(r)(1 + A \cos^2(n_a(\theta - \phi)/2)). \quad (5)$$

Here  $\theta$  is the angle between the two skyrmions,  $\phi$  is the rotation angle of the axis, and  $n_a$  is the number of symmetry directions in the potential, where  $n_a = 4$  would favor square ordering. In some skyrmion systems, the skyrmion size can vary. This could be modeled by introducing a varying screening length  $\lambda_i$  in the skyrmion interaction potential,  $K_1(r/\lambda_i)$ , where  $\lambda_i$  would have some nonuniform distribution. It is also possible to add three-body and multi-body effects to the interaction by

including higher order potentials such as a three-body  $V_{i,j,k}$ . These potentials could be extracted from micromagnetic simulations, similar to the techniques used to model such effects in colloidal systems (Sengupta *et al.*, 2010). The skyrmion dynamics can also be modified. For example, an antiskyrmion could have a four-fold modulation of its dissipative term or different dissipation terms for different directions of driving (Kovalev and Sandhoefner, 2018). Other studies have shown that trochoidal skyrmion motion is possible, some types of which can be modeled with particle based approaches (Ritzmann *et al.*, 2018).

A variety of potentials can be used to represent the pinning term  $\mathbf{F}_i^p$ , such as the short range attraction employed in previous works (Lin *et al.*, 2013b). Other possibilities include short range repulsion, longer range pinning which could arise from strain fields or magnetic interactions, sites with competing attraction and repulsion of the type observed in micromagnetic simulations (Müller and Rosch, 2015), or long range smoothly varying landscapes. It is also possible to add a thermal term to the skyrmion equation of motion by introducing Langevin kicks (Brown *et al.*, 2018; Reichhardt and Reichhardt, 2019b).

Although the particle model does not capture all of the features found in micromagnetic simulations, in some cases it is possible to incorporate additional terms into the model in order to mimic some of these effects, such as by including a time dependence of the skyrmion interactions or the magnitude of the dissipative or Magnus forces in order to represent breathing modes. Similarly, the shape changes that skyrmions can undergo when they become compressed or elongated while in pinning sites can be modeled by modifying the particle-particle interactions when at least one of the skyrmions is inside a pinning site. Similar modifications could be applied for systems in which the shape-changing skyrmions are moving across a landscape. Other rules could be added to accommodate skyrmion creation or annihilation, such as by defining certain conditions for the combination of the external force and the pinning force which, when met, would cause the removal or addition of a skyrmion. Magnon generation could be captured by introducing retarded potentials, a dynamical pairwise skyrmion-skyrmion interaction term, or multi-body interaction effects.

The particle description can be integrated directly to examine the skyrmion dynamics; however, in order to identify ground state configurations such as crystal, liquid or pinning-stabilized disordered structures, Monte Carlo or other simulated annealing methods can be applied. In simulated annealing, the system is initialized in a high temperature state with rapidly diffusing particles, and the temperature is gradually lowered to  $T = 0$  or to the desired final temperature. The cooling must be performed sufficiently slowly that the particles can explore

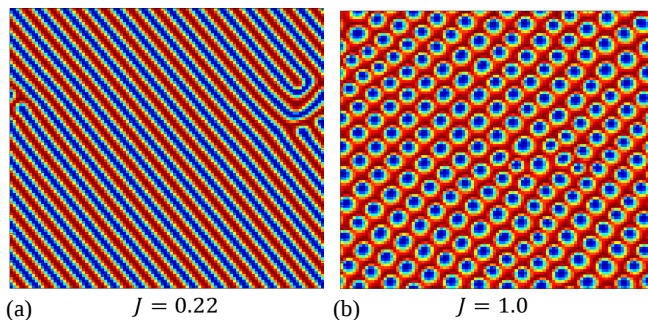


FIG. 9 Images from 2D micromagnetic simulations (Lin *et al.*, 2013a). (a) The spiral state in the absence of a magnetic field,  $H = 0$ . (b) A skyrmion lattice state for finite  $H$ . Reprinted with permission from S.-Z. Lin *et al.*, Phys. Rev. Lett. **110**, 207202 (2013). Copyright 2013 by the American Physical Society.

phase space and find a configuration that is either in or close to a ground state. The cooling rate can be tested by first considering a system containing no pinning in order to determine whether the skyrmions are able to settle into a triangular lattice.

#### IV. MICROMAGNETIC MODELS

Since skyrmions are emergent objects composed of spins, the other main modeling method that has been employed is micromagnetic simulations in which the dynamics of the spin degrees of freedom are calculated directly in the presence of different interaction terms including exchange energy, DMI, anisotropy, and magnetic fields. The starting point for these models is (Bogdanov and Yablonskii, 1989)

$$\mathcal{H} = \int d\mathbf{r}^2 \left[ \frac{J_{ex}}{2} (\nabla \mathbf{n})^2 + D \mathbf{n} \cdot \nabla \times \mathbf{n} - \mathbf{H}_a \cdot \mathbf{n} \right], \quad (6)$$

where  $J_{ex}$  is the exchange term,  $D$  is the DMI produced by spin-orbit coupling, and  $\mathbf{H}_a$  is the anisotropy term. Additional terms can be added to represent pinning, thermal forces, gradient forces, and other effects. This Hamiltonian can be integrated using the Landau-Lifshitz-Gilbert equation (Tatara *et al.*, 2008),

$$\partial_t \mathbf{n} = (\mathbf{J} \cdot \nabla) \mathbf{n} - \gamma \mathbf{n} \times \mathbf{H}_{\text{eff}} + \alpha \partial_t \mathbf{n} \times \mathbf{n}. \quad (7)$$

In many cases, the skyrmions can be modeled effectively using 2D micromagnetic simulations, but extensions to fully 3D simulations are possible. In Fig. 9(a) we show an image from a 2D micromagnetic simulation (Lin *et al.*, 2013a) of a spin system with DMI that has formed a helical state at zero magnetic field,  $H = 0$ . The same system at finite  $H$  forms a skyrmion lattice, as shown in Fig. 9(b).

The advantage of micromagnetic models is that they allow skyrmion distortions and breathing modes to oc-

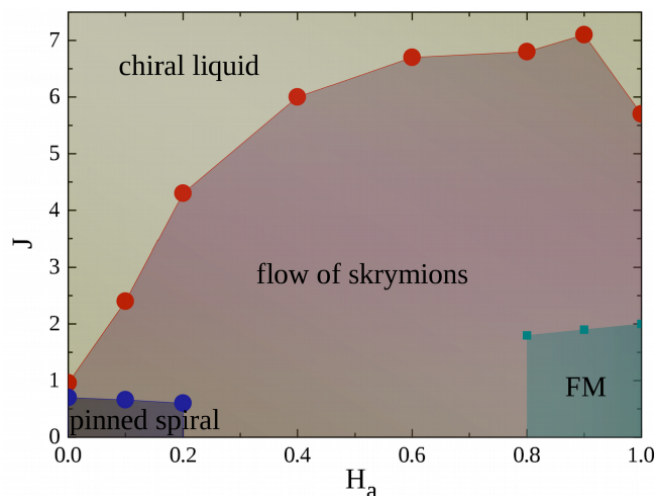


FIG. 10 The dynamic phase diagram as a function of current  $J$  vs magnetic field  $H_a$  from 2D micromagnetic simulations (Lin *et al.*, 2013a). In the absence of a current,  $J = 0$ , pinned spiral, skyrmion lattice, and ferromagnetic (FM) phases appear. At finite  $J$ , a moving skyrmion lattice and chiral liquid phase form at high drives. This indicates that it is possible to use a drive to nucleate skyrmions from a spiral or ferromagnetic state. Reprinted with permission from S.-Z. Lin *et al.*, Phys. Rev. Lett. **110**, 207202 (2013). Copyright 2013 by the American Physical Society.

cur along with skyrmion annihilation and creation. The internal dynamics of a single skyrmion can be studied in detail, and it is possible to include additional terms which can give rise to remarkably rich behaviors. Micromagnetic simulations can readily access the basic phase diagram in the absence of drive under an applied field, showing the transition from a zero field helical state to skyrmion lattices of varied density followed by the emergence of a ferromagnetic state at high fields. When a driving force is applied, even in the absence of pinning the range of magnetic fields for which skyrmions are stable changes. An example of a dynamic phase diagram as a function of current versus magnetic field for driven skyrmions in a pin-free system obtained through micromagnetic simulations appears in Fig. 10. A pinned spiral state forms at low fields, and there are regions of flowing skyrmions, a ferromagnetic state, and a high drive chiral state. These simulations indicate that application of a current can cause skyrmions to emerge from ferromagnetic or spiral states, while strong driving can destroy the skyrmions (Lin *et al.*, 2013a). Experiments have demonstrated the current-induced creation and annihilation of skyrmions in weakly pinned systems (Yu *et al.*, 2017). Current-induced nucleation of skyrmions was also observed in experiments in Co-based Heusler alloys (Akhtar *et al.*, 2019); however, these samples were strongly pinned, suggesting that pinning in combination with a drive can create skyrmions. This work also revealed that the current required to nucleate skyrmions

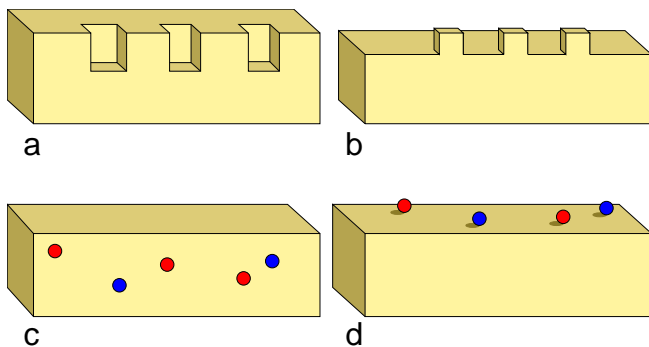


FIG. 11 Schematic illustrations of possible ways that pinning can arise in skyrmion systems. (a) Surface thickness modulations. (b) The addition of nanodots to the surface. (c) Naturally occurring atomic defects or substitutions in the bulk of the sample. (d) Adatoms on the surface of the sample.

increases with increasing magnetic field.

There are several magnetic codes available that can be used to simulate skyrmions interacting with pinning, including MuMax (Leliaert *et al.*, 2018). The disadvantage of micromagnetic simulations is that they are generally limited in the number of skyrmions that can be simulated and the time scales that can be studied. As a result, such simulations are unsuitable for examining hundreds or thousands of skyrmions interacting with pinning sites under a drive due to the relatively long transient times that can occur before the system settles into a steady state. It is also possible to use other types of numerical models for skyrmions or skyrmion-defect interactions. For example, density functional theory can be particularly powerful for extracting the energies of skyrmion-pin interactions on the atomic scale.

### A. Pinning Mechanisms

In the experiments by Schulz *et al.* (Schulz *et al.*, 2012), the motion of skyrmions was inferred from observations of changes in the topological Hall effect. This technique provided evidence of a finite depinning threshold for skyrmion motion, and in many subsequent imaging experiments, a wide range of depinning thresholds has been observed ranging from  $10^6$  to  $10^{11}$  A/m<sup>2</sup>. In superconducting vortex systems, pinning arises at locations where the order parameter of the superconducting condensate is lowered. The system can reduce its energy by placing a vortex at these locations since the condensation energy is already suppressed to zero at the vortex core (Blatter *et al.*, 1994). In the case of colloidal particles, pinning can be produced via optical trapping (Reichhardt and Olson, 2002a) or simply by providing a substrate on which the particles can be localized (Pertsinidis and Ling, 2008; Tierno, 2012), while in Wigner crystals the pinning is produced by offset charges (Reichhardt *et al.*, 2001).

For skyrmions, pinning effects can in principle arise in numerous ways. These include local changes in the DMI, missing spins, holes in thin film samples, a local change in the anisotropy, sample thickness modulations, localized changes in the magnetic field, impurity atoms embedded in the bulk, or adatoms adhering to the surface. Schematics of some of the possible pinning mechanisms appear in Fig. 11. It is possible to introduce a surface modulation by fabricating holes or antidots as in Fig. 11(a), place dots in Fig. 11(b), take advantage of naturally occurring atomic defects in the bulk such as missing atoms or substitutions as shown in Fig. 11(c), or place adatoms on the surface as in Fig. 11(d). Grain boundaries, twin boundaries, or dislocations can also serve as pinning sites in thin film systems.

There is no threshold current for skyrmion motion in micromagnetic simulations of uniform samples without defects (Lin *et al.*, 2013a). One of the first theoretical studies of skyrmion pinning was performed by Iwasaki *et al.* (Iwasaki *et al.*, 2013b), who used micromagnetic simulations with parameters appropriate for MnSi and modeled the pinning as small regions in which the local anisotropy  $A$  varied. In this system, where the ratio of the local anisotropy to the exchange term  $J$  is  $A/J = 0.2$ , the depinning threshold is  $j_c \approx 10^{10} - 10^{11}$  A/m<sup>2</sup> and the skyrmion depins elastically. Lin *et al.* used a combination of micromagnetic simulations and particle based simulations for 2D skyrmions and also found finite depinning thresholds for both cases (Lin *et al.*, 2013b).

Liu and Li (Liu and Li, 2013) considered a local exchange mechanism for producing skyrmion pinning, achieved by varying the local density of itinerant electrons. Using micromagnetics and a Thiele equation approach, they found that the skyrmion is pinned due to the lowering of the skyrmion core energy. They also showed that under perturbation by a small drive, the skyrmion performs a spiraling trajectory as it returns to the pinning site, in contrast to an overdamped particle which moves linearly back to its equilibrium position. The spiraling motion is produced by the Magnus force. When the current is large, the skyrmion is able to escape the trap and a depinning phenomenon occurs.

Muller *et al.* (Müller and Rosch, 2015) considered the interaction of a skyrmion with a hole or locally damaged region both analytically and numerically using continuum methods and the Thiele equation approach. They found that the potential generated by the hole has the interesting property of combining a longer range repulsion with a short range attraction. The competition that results when a drive is applied produces an unusual effect. The skyrmion moves around the pinning site at low drives due to the repulsion, but at high drives it jumps over the longer range repulsive barrier and is captured by the short range attraction. At even higher drives, the skyrmion escapes from the attractive part of the pinning

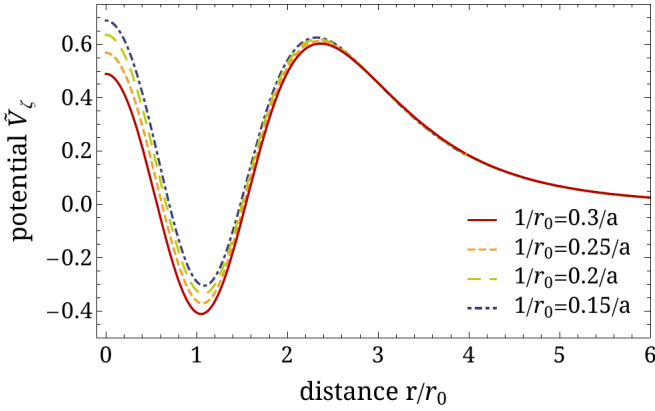


FIG. 12 The shape of the pinning potential produced by a hole in the sample, which has longer range repulsion and a short range attraction (Müller and Rosch, 2015). Reprinted with permission from J. Müller and A. Rosch, Phys. Rev. B **91**, 054410 (2015). Copyright 2015 by the American Physical Society.

site and the system enters a flow regime. The competing attractive and repulsive potential experienced by the skyrmion due to the hole is illustrated in Fig. 12.

Choi *et al.* (Choi *et al.*, 2016) used density functional theory to study the effects of atomic defects on skyrmions in MnSi. They found that if Si is substituted or if Mn is substituted by Zn or Ir, the resulting defect sites attract the skyrmions, whereas if Mn is substituted with Co, the interaction with the defect sites is repulsive.

For Co monolayers on Pt, Stosic *et al.* (Stosic *et al.*, 2017) examined the interactions of skyrmions with atomic defects and studied the pinning potentials at different locations including on or between domain walls. Figure 13 shows the total, exchange, DMI, anisotropy, and Zeeman energies as a function of the distance  $\zeta$  along the minimum energy path for the skyrmion to escape from the pinning. The insets indicate that the total energy  $G$  can be fit to an exponential power function  $G(\zeta) \propto -\exp[-(\zeta/\alpha)^\beta]$ , where  $\alpha$  and  $\beta$  are the scale and shape parameters. Stosic *et al.* found that off-center pinning sites are well described by a similar energy expression with a radial shift.

Navau *et al.* (Navau *et al.*, 2018) used micromagnetic simulations to study the properties of skyrmion-defect interactions in thin films containing DMI modulations, and also obtained analytic expressions for the skyrmion-defect forces within a rigid skyrmion model approximation. They found that the pinning is enhanced when the defect increases the DMI but weakened when the defect decreases the DMI. Anisotropic defects can be attractive, repulsive, or have a combination of the two effects.

From first principles calculations for skyrmions interacting with single-atom impurities, Fernandes *et al.* (Fernandes *et al.*, 2018) found that defects can be both attractive and repulsive or purely attractive depending on

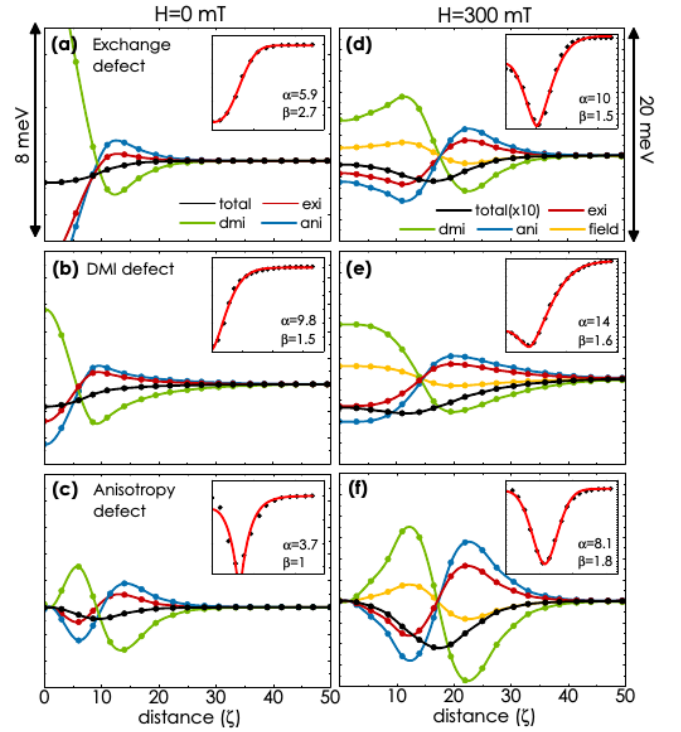


FIG. 13 The total (total), exchange (exi), Dzyaloshinskii-Moriya (dmi), anisotropy (ani), and Zeeman (field) energies plotted as a function of distance  $\zeta$  along the minimum energy path for a skyrmion to escape from the defect for three different types of defects at external fields of  $H = 0$  mT [(a)-(c)] and  $H = 300$  mT [(d)-(f)] (Stosic *et al.*, 2017). In the insets, the total energy landscape or effective pinning potential is fit to an exponential power function. Reprinted with permission from D. Stosic *et al.*, Phys. Rev. B **96**, 214403 (2017). Copyright 2017 by the American Physical Society.

the impurity type. They focused on PdFe bilayers on an Ir substrate and considered a range of defect transition metal atoms including 3d (Sc, Ti, V...) and 4d (Y, Zr, Nb...) atoms as well as Cu and Ag atoms, with the defects either located on the surface or embedded in the Pd surface layers. By analyzing the binding energy to determine whether it is positive or negative, they found that it is possible to have both attractive and repulsive interactions with various strengths that depend strongly on the element used. A key feature of this system is that strongly magnetic defects locally stiffen the skyrmion, leading to a repulsive skyrmion-defect interaction, while weakly interacting defects produce attractive pinning due to the substrate contribution. Since the pinning originates from surface atoms, it would be possible to use scanning tunneling microscopy to add atoms in prescribed patterns in order to create attractive and repulsive pinning sites that precisely control the deviations of the skyrmions. Arjana *et al.* (Arjana *et al.*, 2020) pursued this idea by examining atom by atom crafting of skyrmion defect landscapes using single, double, and

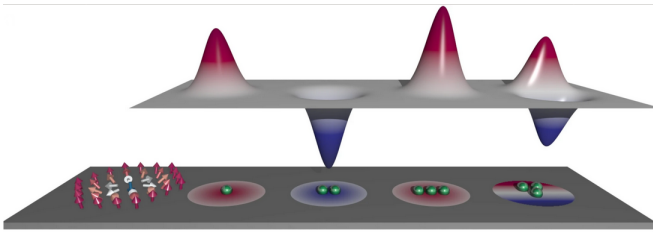


FIG. 14 Schematic of atom-by-atom construction of potential landscapes for skyrmions. The leftmost cluster of arrows illustrates the size of a typical skyrmion. Green spheres are atoms which have been placed so as to construct, from left to right, a repulsive, attractive, strongly repulsive, or combined attractive and repulsive pinning potential (Arjana *et al.*, 2020). Reprinted under CC license from I. G. Arjana *et al.*, *Sci. Rep.* **10**, 14655 (2020).

triple atom states to create repulsive, attractive, and combined repulsive and attractive pinning sites, as illustrated in Fig. 14. They also generated asymmetric landscapes and demonstrated that atomic clusters could be used to construct reservoir computing devices.

Larger scale magnetic defects can be created using a variety of nanoscale methods. These include irradiating particular regions of the sample in order to change the local magnetic properties (Fassbender *et al.*, 2009), introducing large scale thickness modulations to change the DMI (Yang *et al.*, 2015), or adding magnetic dots to the surface in a manner similar to that used for introducing pinning in superconductors (Marchiori *et al.*, 2017; Martín *et al.*, 1997). In extensive micromagnetic simulations of skyrmion trapping by larger scale magnetic defects, Toscano *et al.* (Toscano *et al.*, 2019) found that the defects can act either as attractive traps or as repulsive scatterers depending on the exchange stiffness, DMI, perpendicular anisotropy, and saturation magnetization. A defect that modifies the exchange stiffness acts as a skyrmion trap when its exchange stiffness is smaller than that of the surrounding material but as a repulsive scattering site when the exchange stiffness exceeds that of the surrounding material. Additionally, the strength of the interaction with a pinning site increases when the skyrmion becomes smaller than the size of the defect. In other micromagnetic simulations for skyrmions moving in nanostructured materials, a large region with altered local anisotropy was shown to act as a repulsive area for the skyrmions (Ding *et al.*, 2015; Wang *et al.*, 2018a).

Wang *et al.* (Wang *et al.*, 2017) introduced the concept of pinning skyrmions with magnetic field gradients and showed that the pinning strength depends on the intensity of the gradient as well as on the skyrmion size. They demonstrated that a skyrmion can be dragged and manipulated with a suitable magnetic field gradient, suggesting a new way to move skyrmions by using a magnetic tip.

Beyond the evidence for skyrmion pinning obtained

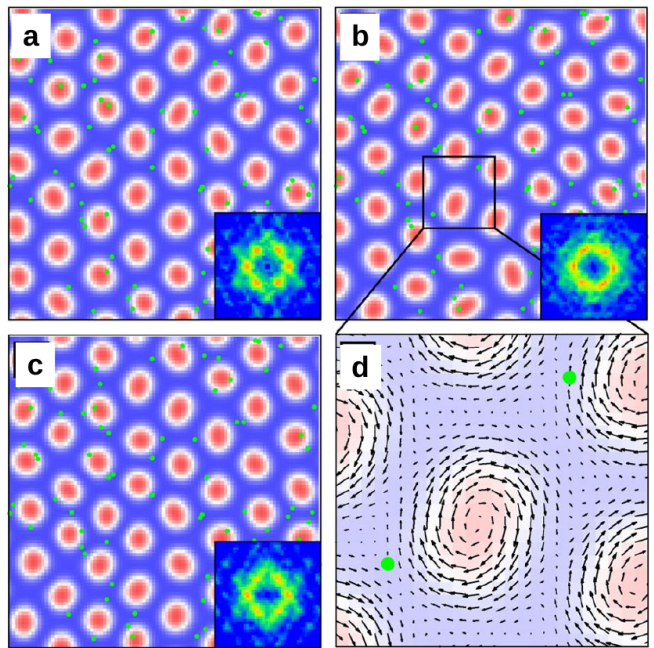


FIG. 15 Micromagnetic simulation images of the evolution of a skyrmion crystal and the distortions of the skyrmions for different times under the application of a driving current (Iwasaki *et al.*, 2013b). The times are (a)  $t = 1.30 \times 10^{-8}$  s, (b)  $t = 2.60 \times 10^{-8}$  s, and (c)  $t = 8.47 \times 10^{-8}$  s. Green dots are the defect sites and red regions are the skyrmion centers, while the insets show the corresponding structure factor measurement. Panel (d) shows a magnified view of the distortion of the circular shapes of the skyrmions in panel (c). Reprinted by permission from: Springer Nature, “Universal current-velocity relation of skyrmion motion in chiral magnets,” *Nature Commun.* **4**, 1463 (2013), J. Iwasaki *et al.*, ©2013.

from transport studies, pinning effects can also be deduced via the manipulation of individual skyrmions. Hanneken *et al.* (Hanneken *et al.*, 2016) explored the interactions between nanometer-scale skyrmions and atomic scale defects in PdFe by measuring the force needed to move a skyrmion, which revealed the presence of a range of pinning strengths. They also found that interlayer defects such as single Fe atoms interact strongly with a skyrmion while single Co adatoms on the surface are weak pinning centers; however, clusters of such adatoms can serve as strong pinning sites.

## B. Skyrmion Pinning by Individual versus Extended Defects and the Role of the Magnus Force

In many systems such as vortices in type-II superconductors, it is known that very different pinning effects can occur when the defects are extended or linelike instead of pointlike. Such extended defects can form naturally, as in the case of twin boundaries (Vlasko-Vlasov

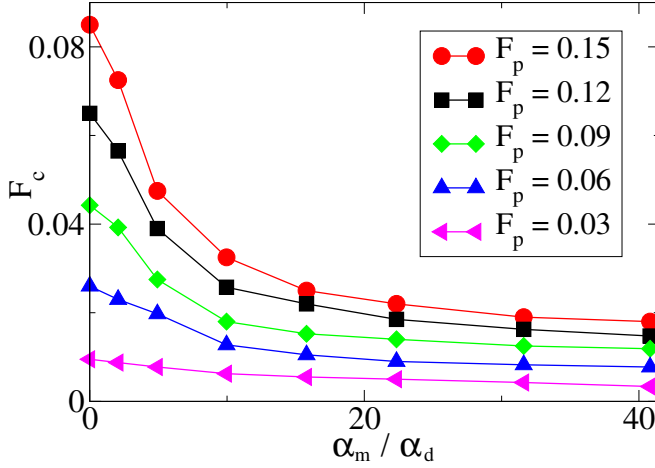


FIG. 16 The critical depinning force  $F_c$  vs the ratio  $\alpha_m/\alpha_d$  of the Magnus force to the dissipative term for 2D particle based simulations of skyrmions moving over pointlike disorder sites for varied pinning strength  $F_p$  (Reichhardt *et al.*, 2015b). The depinning threshold decreases with increasing Magnus force. Reprinted with permission from C. Reichhardt *et al.*, Phys. Rev. Lett. **114**, 217202 (2015). Copyright 2015 by the American Physical Society.

*et al.*, 1994), or they can be introduced with nanoscale techniques (Guillamón *et al.*, 2014). In superconducting vortex systems, a line defect can serve as a region of increased pinning for motion across the lines (Groth *et al.*, 1996; Vlasko-Vlasov *et al.*, 1994), but it can also produce guided or easy flow for motion of vortices along the line (Durán *et al.*, 1992; Groth *et al.*, 1996). In skyrmion systems, it was initially argued that a skyrmion can move around a point pinning site due to the Magnus effect (Nagaosa and Tokura, 2013). Micromagnetic simulations by Iwasaki *et al.* (Iwasaki *et al.*, 2013b) showed that pinning was reduced not only by this avoidance motion but also by the ability of the skyrmions to change their shape, as shown in Fig. 15.

Particle based simulations of skyrmions interacting with pointlike random pinning (Reichhardt *et al.*, 2015b) in 2D systems indicate that the depinning threshold decreases as the ratio  $\alpha_m/\alpha_d$  of the Magnus force to the dissipative term increases over a wide range of pinning strengths, as shown in Fig. 16. A schematic illustration of how the Magnus force reduces the effectiveness of the pinning for a skyrmion interacting with a point pinning site appears in Fig. 17. The black arrows indicate the direction of the attractive force from the pinning site, which always points toward the pin. The red arrows represent the Magnus force component, which is always perpendicular to the force from the pinning site. The net effect is that, although the dissipative term favors the motion of the skyrmion toward the pinning site, the Magnus force causes the skyrmion to deflect around the pinning site. In contrast, a purely overdamped particle such as a superconducting vortex moves directly toward the center

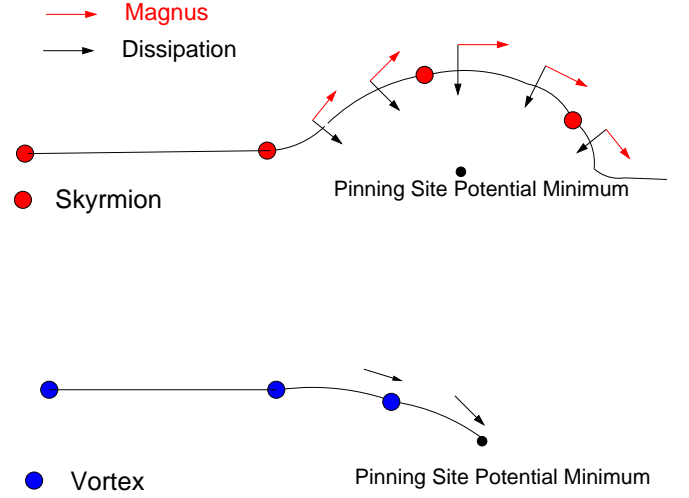


FIG. 17 Schematic of a skyrmion (red dot) with both Magnus and dissipative terms and a vortex (blue dot) with only a dissipative term interacting with an attractive point pinning site (black dot) to illustrate how the Magnus force can decrease the effectiveness of the pinning. The velocity component induced by the dissipation is indicated by black arrows, and that produced by the Magnus force is shown as red arrows. Since the Magnus force velocity component is perpendicular to the attractive force from the pinning site, the skyrmion deflects around the pinning site. In contrast, the vortex moves directly toward the potential minimum and is more likely to be trapped by the pinning site.

of the pinning site and is likely to be trapped. The deflection of the skyrmion around the pinning site depends strongly on the relative size and extent of the skyrmion compared to that of the pinning site.

Experiments by Woo *et al.* (Woo *et al.*, 2016) on room temperature ultrathin systems unexpectedly showed that the skyrmions experience strong pinning. The intrinsic pinning in these samples may not be pointlike due to the nature of the films, which contain grain boundaries or extended defects. Continuum based simulations of skyrmions (Legrand *et al.*, 2017) confirmed that grain boundaries induce skyrmion pinning and that the strength of this pinning increases for smaller grain sizes; however, there is a minimum grain size below which pinning cannot occur. One explanation for the stronger pinning by extended defects is that although the Magnus force can cause a skyrmion to skirt a point defect, the same process is not possible for an extended defect. In Fig. 18(a) we schematically illustrate the Magnus and dissipation induced velocity components of a skyrmion moving toward an extended line defect. If the defect is attractive, the dissipative term aligns the velocity toward the line defect, but the Magnus force generates a velocity component perpendicular to the line defect, causing the skyrmion trajectory to bend sideways as the skyrmion approaches the defect. If the defect line extends across the sample, the skyrmion is unable to avoid the defect,

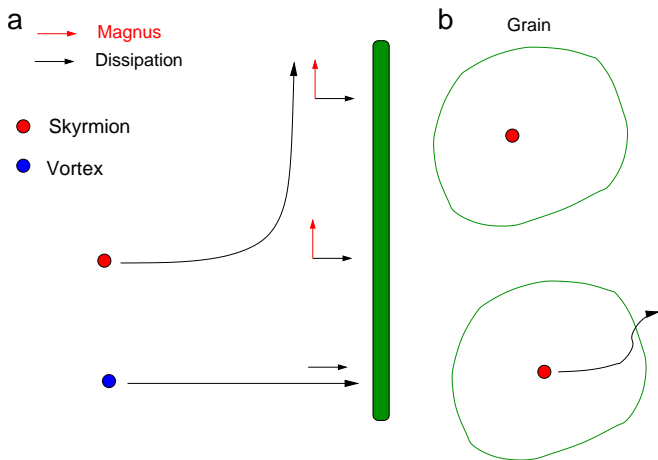


FIG. 18 (a) Schematic showing the dissipative (black arrows) and Magnus (red arrows) velocity components for a skyrmion (red dot) or vortex (blue dot) moving toward an attractive extended line defect (green). The overdamped vortex moves directly toward the line defect, while the skyrmion is deflected but gradually approaches the defect. Unlike the case for point pinning in Fig. 17, the skyrmion cannot simply move around the line defect but eventually reaches the defect and interacts with it. (b) Schematic of a skyrmion (red dot) located inside a closed grain boundary (green). The skyrmion may be deflected as it moves toward the grain boundary; however, it must cross the pinning potential minimum in order to pass through the grain boundary.

but eventually reaches and crosses it. As a result, the skyrmion experiences the full pinning potential of the line defect. This is in contrast to the point pinning situation where the skyrmion can completely avoid the pin. If a driven skyrmion is inside an extended line defect such as a grain boundary, as shown schematically in Fig. 18(b), the skyrmion trajectory may bend upon approaching the boundary due to the Magnus force, but the skyrmion eventually must pass through the potential minimum in order to exit the grain boundary, as illustrated in the lower panel of Fig. 18(b). As a result, extended defects are always more effective than point defects at exerting pinning forces on skyrmions.

A numerical test of the effect of the Magnus force on skyrmions moving perpendicular to a line defect was performed by Reichhardt *et al.* (Reichhardt and Olson Reichhardt, 2016) for a 2D skyrmion moving over a 1D pinning line. As shown in Fig. 19, when the driving direction is parallel to the pinning line, the critical current  $F_c$  is independent of the size of the Magnus term, in contrast to the decrease in critical current with increasing Magnus term found for point pinning. On the other hand, when the drive is applied perpendicular to the line defect, the depinning threshold decreases with increasing Magnus force. This effect would be most pronounced for skyrmions moving over 1D pinning features such as twin boundaries, but would likely be absent in a sample filled

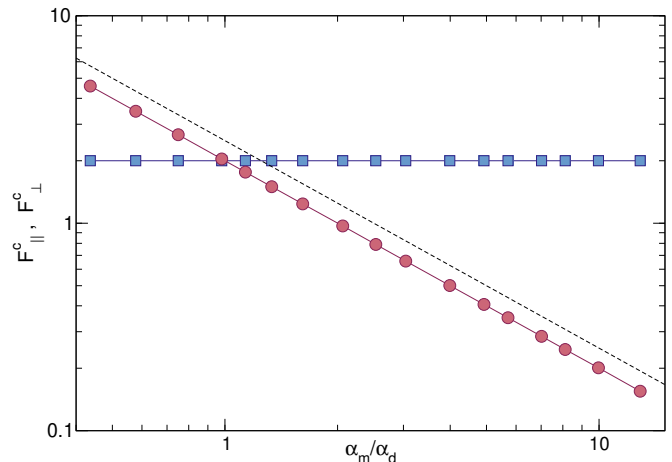


FIG. 19 2D particle based numerical simulations of a skyrmion interacting with a 1D defect line showing the critical depinning force for driving applied parallel,  $F_{\parallel}^c$  (blue squares), and perpendicular,  $F_{\perp}^c$  (red circles), to the line, vs the relative strength  $\alpha_m/\alpha_d$  of the Magnus force.  $F_{\parallel}^c$  is insensitive to the Magnus force while  $F_{\perp}^c$  decreases with increasing Magnus force. (Reichhardt and Olson Reichhardt, 2016). Reprinted with permission from C. Reichhardt *et al.*, Phys. Rev. B **94**, 094413 (2016). Copyright 2016 by the American Physical Society.

with closed grain boundaries.

The best model for the interaction between skyrmions and extended defects is dictated by the nature of the defects. For example, if the defects arise due to thickness modulations, the pinning will be short range and attractive, whereas if the defects are in the form of magnetic stripes, the pinning will be longer range with a dipolar form  $A/r^3$  and it could be either attractive or repulsive. In some cases the extended defect could have a competing potential in which the interaction with the skyrmion is repulsive at longer distances but becomes attractive close to the defect.

Navau *et al.* simulated the Thiele model for a single skyrmion interacting with an extended defect consisting of an edge (Navau *et al.*, 2016). The edge exerts a force on the skyrmion of the form  $\mathbf{f} = -f_0 e^{-d/d_0} \hat{\mathbf{n}}$ , where  $d$  is the distance between the skyrmion center of mass and the edge,  $\hat{\mathbf{n}}$  is a unit vector perpendicular to the edge, and  $d_0$  is approximately equal to the diameter of the skyrmion. The skyrmion is strongly deflected by the edge. Other work (Navau *et al.*, 2018) showed that extended defects can exert either repulsive or attractive forces on a skyrmion. The dynamics of a skyrmion interacting with an extended defect depends on both the form of the defect and the skyrmion type. Menezes *et al.* (Menezes *et al.*, 2019a) considered micromagnetic simulations of a skyrmion moving toward a heterochiral interface created with multilayers as illustrated in Fig. 20. They found that a ferromagnetic skyrmion is deflected by the interface, and that the deflection amplitude can

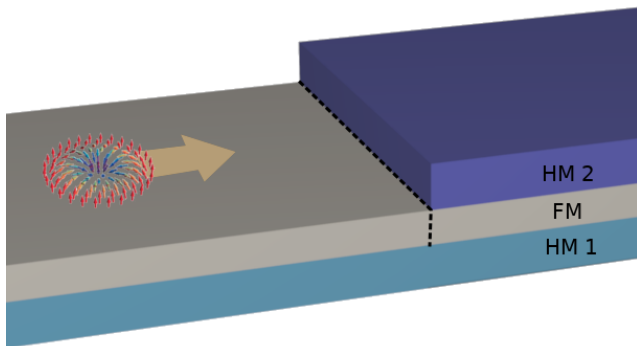


FIG. 20 Schematic of a skyrmion moving toward an interface composed of a ferromagnetic (FM) layer sandwiched between two heavy metal (HM) layers. The upper heavy metal layer is truncated in order to create a heterochiral interface (Menezes *et al.*, 2019a). The dashed line indicates the interface where the DMI changes. Reprinted with permission from R. M. Menezes *et al.*, Phys. Rev. B **99**, 104409 (2019). Copyright 2019 by the American Physical Society.

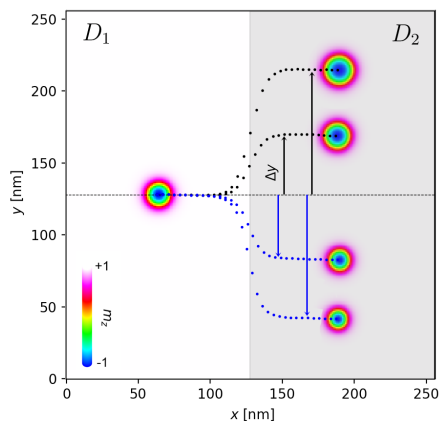


FIG. 21 Illustration of skyrmion motion through the heterochiral interface shown in Fig. 20 (Menezes *et al.*, 2019a). The initial skyrmion position is on the left side of the interface. As the relative DMI strengths  $D_1$  and  $D_2$  are varied with respect to each other, the skyrmion trajectory is deflected by a distance  $\delta y$  in the positive (black arrows) or negative (blue arrows)  $y$  direction. Reprinted with permission from R. M. Menezes *et al.*, Phys. Rev. B **99**, 104409 (2019). Copyright 2019 by the American Physical Society.

be tuned by changing the applied current or by modifying the difference in the DMI across the interface, as shown in Fig. 21. On the other hand, antiferromagnetic skyrmions experience no deflection at the interface.

### C. Further Directions

There are numerous theoretical, computational, and experimental directions for further study of the basic mechanisms of skyrmion pinning. Simulations and theory have shown that there are many ways to create attractive, repulsive, or both attractive and repulsive pinning sites, so one of the next steps is to consider how to combine these different types of pinning sites to produce novel dynamical phenomena, control the skyrmion motion, and reduce or enhance pinning. In many other systems where pinning occurs, such as for vortices in type-II superconductors, the natural or artificial defects producing the pinning reduce the superconducting condensation energy, so studies have focused on strictly attractive pinning sites. In colloidal systems, optical forces and most surface modifications also create attractive pinning sites. As a result, systems with repulsive defect sites represent a relatively unexplored regime of collective dynamics. Many skyrmions in thin films seem to show strong pinning effects from attractive pins; however, there may be a way to introduce additional repulsive defect sites that would effectively reduce the overall pinning by competing with the attractive pinning centers.

Another question is the nature of the pinning process for antiskyrmions or antiferromagnetic skyrmions. The work of Menezes *et al.* (Menezes *et al.*, 2019a) on a line defect separating two regions with different DMI suggests that antiferromagnetic skyrmions may not be very susceptible to changes in the DMI, thus reducing the number of possible methods available for pinning skyrmions of this type. This could mean that antiferromagnetic skyrmions would be more mobile than ferromagnetic skyrmions due to a reduction in the amount of pinning present; however, the lack of a Magnus effect in the antiferromagnetic skyrmions could make any pinning sites that are present more effective. It would also be interesting to explore the pinning of biskyrmions, merons, and other related objects such as skyrmionium (Kolesnikov *et al.*, 2018), as well as the role pinning plays in determining the direction of current flow. For example, Stier *et al.* (Stier *et al.*, 2021) showed in simulations that although magnetic impurities do not interfere with a uniform applied current, conducting impurities can change the current paths. If defects could be introduced that are able to move over time in response to a current, they would create a pinning landscape that can gradually be sculpted in a manner similar to electromigration. This could produce interesting memristor-like effects.

Most studies of pinning performed up until now have focused on defects in 2D; however, for 3D line like skyrmions, entirely new types of pinning effects could arise along with an array of new methods for creating 3D pinning. In 3D superconducting vortex systems, it was shown that columnar pinning enhances the critical depinning current (Civale, 1997) by trapping the vortex



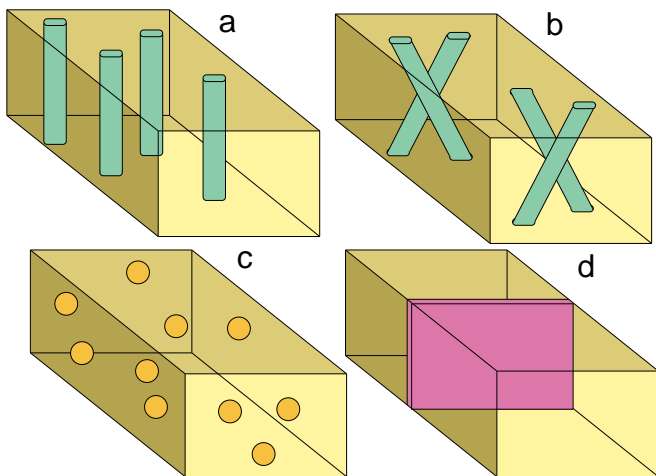


FIG. 22 Schematic of possible different types of 3D defects that could be created for bulk skyrmions. (a) Columnar defect tracks, which could induce the formation of a skyrmion Bose glass. (b) Splayed columnar defects, which could create a splayed skyrmion glass or promote skyrmion entanglement. (c) Random point defects, which could generate a skyrmion glass. (d) 3D planar defects.

line along the entire length of the pinning site, and a similar effect could occur for 3D skyrmions. Splayed columnar defects (Hwa *et al.*, 1993) could promote the entanglement of skyrmion lines, while proton irradiation could be used to create random point defects (Haberkorn *et al.*, 2012) or 3D line defects (Kafri *et al.*, 2007). In the schematic in Fig. 22 we show possible 3D pinning arrangements that could be created in skyrmion systems, including columnar, splayed, 3D point-like, and 3D planar defects. It would be interesting to learn whether 3D pinning is more effective than 2D pinning or whether it can reduce skyrmion creep at finite temperatures. Some types of defects repel skyrmions rather than attracting them, and adding 3D versions of such defects could increase the net skyrmion mobility. One possible experiment would be to irradiate bulk samples and determine whether the depinning threshold changes as measured by changes in the topological Hall effect. If a sufficiently large density of 3D defects were added to the sample, they could create percolation paths which could serve as easy flow channels for skyrmion motion, leading to a net increase rather than a net decrease in the skyrmion mobility.

In 3D samples it would be possible to place one type of pinning on the top of the sample, such as through nanopatterning or by adding adatoms, while simultaneously placing a different type of pinning on the bottom of the sample. For example, if antipinning sites are present on top of the sample and pinning sites are present on the bottom, a shear effect could arise under driving that would promote skyrmion cutting or the creation of monopoles along the skyrmion lines.

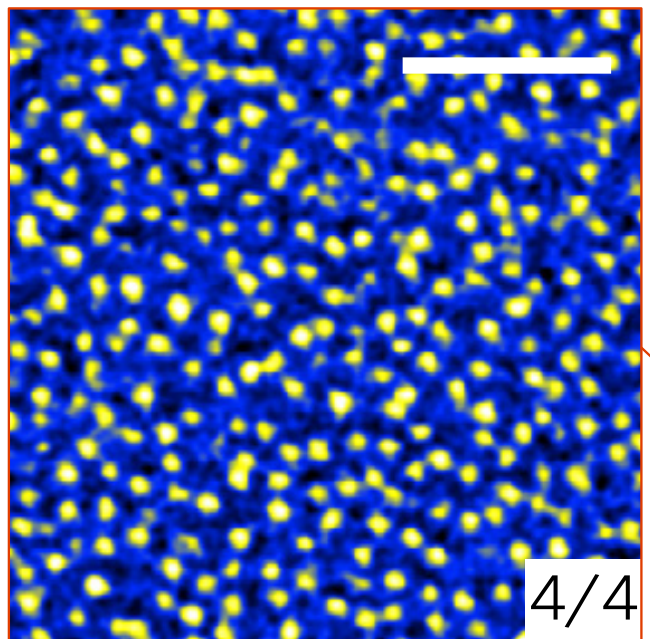


FIG. 23 Magnetic force microscope image of disordered skyrmions in Ir/Fe/Co/Pt multilayers (Soumyanarayanan *et al.*, 2017). Reprinted by permission from: Springer Nature, “Tunable room-temperature magnetic skyrmions in Ir/Fe/Co/Pt multilayers,” *Nature Mater.* **16**, 898 (2017), A. Soumyanarayanan *et al.*, ©2017.

## V. COLLECTIVE STATES AND SKYRMION LATTICES WITH PINNING

We next consider the effect of pinning on the static configurations of collectively interacting skyrmions. The very first experimental observation of skyrmions was the imaging of a skyrmion lattice with neutron scattering (Mühlbauer *et al.*, 2009), followed by direct visualization of the skyrmion lattice with Lorentz microscopy (Yu *et al.*, 2010). The fact that the skyrmions formed a lattice suggests that in these initial experiments, the pinning was relatively weak; however, it is also possible that the thermal fluctuations were large enough to wash out the effect of the pinning and create what is known as a floating solid. There are now many examples of skyrmion systems, particularly in thin films, that form disordered states (Hsu *et al.*, 2018; Karube *et al.*, 2018; Wang *et al.*, 2019a; Zhang *et al.*, 2018b). Figure 23 shows an image of disordered room temperature skyrmions in Ir/Fe/Co/Pt multilayers (Soumyanarayanan *et al.*, 2017). The manner in which the system is prepared strongly impacts whether the skyrmions form a lattice. For example, consider a sample in which the skyrmion ground state at temperature  $T_1$  is disordered. If the sample were prepared at another temperature  $T_2$  where the ground state is ordered and the temperature was suddenly changed to  $T_1$ , the skyrmions could remain in a metastable ordered lattice configuration. The metastable state could be destroyed

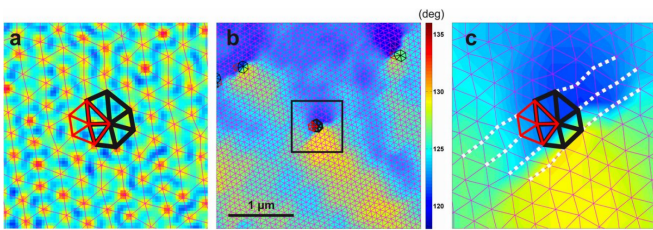


FIG. 24 Examples of Delaunay triangulations of skyrmion lattices (Rajeswari *et al.*, 2015). (a) Image of a lattice defect consisting of sevenfold-coordinated (black) and fivefold-coordinated (red) skyrmions adjacent to each other. (b) A map of the local spatial angle superimposed on top of the Delaunay triangulation with a defect at the center. (c) A close-up view of the region marked with a square in panel (b), showing the presence of a dislocation line at the domain boundary. From J. Rajeswari *et al.*, Proc. Natl. Acad. Sci. (USA) **112**, 14212 (2015).

by the application of a current or drive which allows the skyrmions to reach their disordered  $T_1$  ground state configuration.

The structure of a skyrmion lattice can be measured using the structure factor,

$$S(\mathbf{k}) = \frac{1}{N} \left| \sum_{j=1}^N e^{-i\mathbf{k}\cdot\mathbf{R}_j} \right|^2 \quad (8)$$

where  $\mathbf{R}_j$  is the position of skyrmion  $j$  and  $N$  is the total number of skyrmions being sampled. If the skyrmion forms a glass state,  $S(\mathbf{k})$  has a ring structure, while if the skyrmions are in a triangular lattice,  $S(\mathbf{k})$  has sixfold peaks. The lattice structure can also be measured by using a Voronoi or Delaunay construction to determine the fraction of sixfold coordinated particles in the system, as illustrated in Fig. 24 (Rajeswari *et al.*, 2015). These measures can also be used to identify different types of topological defects in the skyrmion lattice, such as a skyrmion with five neighbors that is connected to a skyrmion with seven neighbors to form a dislocation pair, as shown in Fig. 24(c). The dislocation pairs can glide or climb depending on the strength of the driving. It is also possible that instead of completely disordering, the skyrmion lattice can form domains defined by grain boundaries of a specific angle. The grain boundaries are decorated by 5-7 dislocation pairs and the spacing between the dislocations is determined by the angular mismatch between the skyrmion lattices in the adjacent grains (Lavergne *et al.*, 2018).

Disordered skyrmion arrangements can be produced by strong pinning, temperature, or polydispersity of the skyrmion sizes or types. In other systems containing random quenched disorder, various types of equilibrium phases can arise. For example, consider a 2D system with a triangular lattice ground state or a 3D system of lines that form a 2D ordered triangular lattice in the absence of disorder. Under increasing temperature, these

systems generally melt at a critical temperature  $T_c$ . In the 3D system, the melting transition can be first or second order, while in the 2D system it can be second order according to the Kosterlitz-Thouless-Halperin-Nelson-Young (KTHNY) mechanism, in which there is first a proliferation of dislocations followed by the proliferation of free disclinations (Kosterlitz and Thouless, 1973; Nelson and Halperin, 1979; Strandburg, 1988; Young, 1979). Evidence for 2D melting via intermediate hexatic phases in the absence of a substrate has been obtained in numerous systems, including colloidal assemblies (Zahn *et al.*, 1999) and it is even possible to observe a first order transition into a hexatic phase (Thornework *et al.*, 2017). The hexatic phase can be detected by measuring the density-density correlation function

$$g_G(|\mathbf{r} - \mathbf{r}'|) = \langle \exp(i\mathbf{G} \cdot [\mathbf{u}(\mathbf{r}) - \mathbf{u}(\mathbf{r}')]]) \rangle \quad (9)$$

and the bond-angular correlation function

$$g_6(|\mathbf{r} - \mathbf{r}'|) = \langle \exp(i6[\theta(\mathbf{r}) - \theta(\mathbf{r}')]]) \rangle. \quad (10)$$

Here  $\mathbf{G}$  is the reciprocal lattice vector,  $\mathbf{u}(\mathbf{r})$  is the particle displacement field, and  $\theta(\mathbf{r})$  is the angle with respect to the  $x$ -axis. For a 2D crystal,  $g_6(\mathbf{r})$  is constant and  $g_G(\mathbf{r})$  decays algebraically,  $g_G(\mathbf{r}) \propto r^{-n(T)}$ . In the hexatic phase,  $g_G(\mathbf{r})$  decreases exponentially while  $g_6(\mathbf{r})$  decays algebraically as  $g_6(\mathbf{r}) \propto r^{-n_6(T)}$ , where  $n_6$  approaches the value  $1/4$ . In the fluid phase, both correlation functions decay exponentially. Several recent experiments have provided evidence for a hexatic phase in skyrmion systems (Huang *et al.*, 2020; Zàzvorka *et al.*, 2020).

The more relevant situation for most skyrmion systems is when disorder is present. At  $T = 0$  in a sample with random pinning, a lattice of interacting particles takes advantage of the pinning energy  $E_p$  at the cost of the elastic energy  $E_{el}$ . If the pinning is weak, a small amount of elastic distortion can occur but the triangular symmetry of the lattice is preserved. When the disorder is stronger, the elasticity of the lattice can break down and various types of topological defects can appear. In 2D systems, a disordered KTHNY transition can occur in which the system passes from a lattice to a hexatic phase, while when the disorder is stronger, a 2D glassy state appears. Nelson (Nelson, 1983) proposed the phase diagram illustrated in Fig. 25(a) as a function of disorder versus temperature. In the absence of quenched disorder, the lattice ordering begins to disappear at a finite value of  $T$  when a transition occurs into a hexatic state or into a liquid. When quenched disorder is present, the lattice becomes disordered even for  $T = 0$ ; however, the temperature can wash out the effect of disorder, producing a thermally induced transition from a disordered non-crystalline state into a floating crystalline state which then melts into a liquid at a higher temperature. When the quenched disorder is strong enough, the

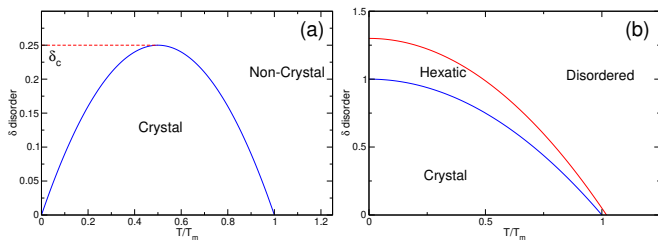


FIG. 25 (a) Schematic phase diagram as a function of quenched disorder  $\delta$  vs temperature  $T/T_m$  for a 2D system, where  $T_m$  is the melting temperature. The solid line indicates the transition from a crystal to a disordered non-crystalline state predicted by Nelson (Nelson, 1983). The disordered state can be reentrant when the temperature washes out the effect of the quenched disorder before the crystal lattice melts. The dashed red line is from the modified phase diagram proposed by Cha and Fertig (Cha and Fertig, 1995), where the system is ordered at  $T = 0$  and the low temperature disordered state does not appear until a critical amount of disorder  $\delta_c$  has been added (b) A schematic phase diagram as a function of quenched disorder  $\delta$  vs temperature  $T/T_m$  based on 2D colloidal experiments (Deuschländer *et al.*, 2013), where an intermediate hexatic phase appears between the crystal and disordered phases.

system is always in a disordered state. Cha and Fertig (Cha and Fertig, 1995) argued that at  $T = 0$  the system remains in a crystalline state until a critical amount of quenched disorder  $\delta_c$  is added, at which point the system disorders, as indicated by the horizontal dashed line in Fig. 25(a). These different scenarios depend on the size scale of the quenched disorder, since the thermal effects can only wash out the pinning before the lattice melts if the pinning sites are small. Experiments in 2D colloidal systems (Deuschländer *et al.*, 2013) suggest the phase diagram shown in Fig. 25(b), where an intermediate hexatic phase appears for zero quenched disorder and increases in extent as quenched disorder is added to the sample. In principle, a similar phase diagram could be constructed for 2D skyrmion systems in which the skyrmion size is roughly uniform.

Recent Monte Carlo simulations have shown that a 2D skyrmion lattice can melt without passing through an intermediate hexatic phase (Nishikawa *et al.*, 2019); however, there are a wide range of different 2D skyrmion systems, and as suggested in Fig. 25, quenched disorder could enhance the hexatic phase. Skyrmions in 2D are often already strongly disordered, but in a dense regime the skyrmion interactions could become strong enough to favor the formation of a hexatic phase. In addition to quenched disorder, two other mechanisms could be relevant in determining whether the skyrmion arrangement is ordered or disordered. In 2D assemblies of particles that form a triangular lattice in the absence of quenched disorder, there can be transitions to hexatic or disordered states as a function of increasing particle polydispersity. For example, polydispersity in the skyrmion

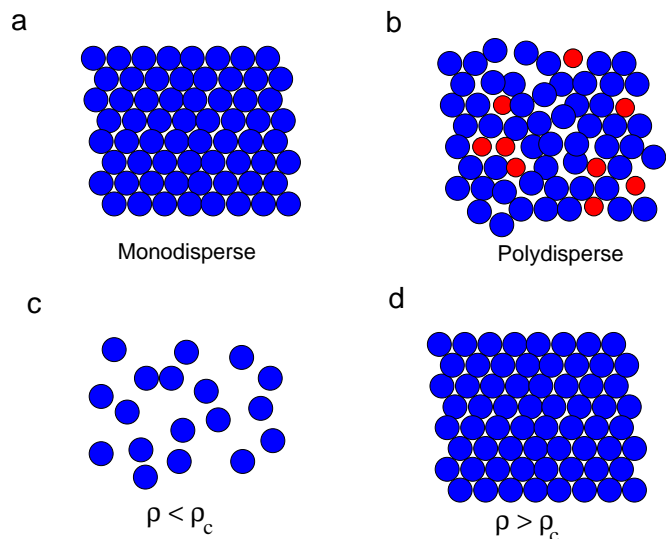


FIG. 26 Schematic illustrations of scenarios leading to disordered skyrmion structures without quenched disorder or temperature. (a,b) Disorder induced by polydispersity in the skyrmion sizes. (c,d) A jamming mechanism for skyrmions with short range contact forces. (c) Below a critical density,  $\rho < \rho_c$ , the system is liquidlike, while (d) for  $\rho > \rho_c$ , the skyrmions are in contact and form a solid.

sizes could induce the formation of a hexatic state even when the quenched disorder is weak. Simulations of 2D Lennard-Jones systems (Reza Sadr-Lahijany *et al.*, 1997) showed that, depending on the density of the sample, a dispersity in as few as 10% of the particles was sufficient to disorder the system. In other work on bidisperse Yukawa particles, doubling the charge on 10% to 20% of the particles disordered the system (Reichhardt and Olson Reichhardt, 2008). Numerical evidence by Zhang *et al.* for frustrated ferromagnetic films (Zhang *et al.*, 2017b) containing mixtures of skyrmions with different sizes indicates that polydispersity can produce disordered skyrmion states. In Fig. 26(a,b) we schematically illustrate the disordering of a monodisperse triangular solid by the introduction of some dispersity in the particle size. An open question for skyrmion systems is how much size dispersity is necessary to induce a transition from a triangular solid to a disordered state.

Another possible disordering mechanism is an effective jamming transition. In jamming, a system passes from a fluid-like state where the particles can move freely to a solid state in which the particles are in contact and the assembly has a finite response to a shear stress. The jamming concept is typically used to describe systems with short range or even hard sphere interactions, such as grains and emulsions; however, the interaction between larger skyrmions can be described as a short range repulsion, making it possible for such skyrmions to share features with emulsions. In a hard disk jamming system, there is a density or area coverage  $\phi_J$ , referred to as

“point J,” at which the disks first come into contact. For a 50:50 mixture of 2D bidisperse hard disks with a radius ratio of  $R_1/R_2 = 1.4$ ,  $\phi_J = 0.84$  (O’Hern *et al.*, 2003; Reichhardt and Reichhardt, 2014). At densities below point J, the system is a disordered fluid, while above point J, a jammed amorphous solid appears. Monodisperse disks form a triangular solid which is jammed but not disordered at a critical density  $\phi_c = 0.9$ . These results suggest that in skyrmion systems with very short range interactions, even monodisperse skyrmions will generally be disordered if they are below the jamming or solidification density. The schematic in Fig. 26(c) illustrates particles with short range interactions at a density well below the jamming or solidification density,  $\rho < \rho_c$ , while in Fig. 26(d), the same particles, which could be skyrmions, at  $\rho > \rho_c$  are in contact and form a jammed crystalline solid. It is possible that for small skyrmions or for 3D skyrmions, where a single skyrmion can interact with other skyrmions beyond nearest neighbor interactions, the skyrmions will form a lattice, while for larger skyrmions or for 2D skyrmions where the interaction range is short and reaches only nearest neighbors, the system can be described as exhibiting a jamming transition to a disordered state.

The density of skyrmions is nonmonotonic as a function of magnetic field. As a result, at intermediate fields where the skyrmion density is high, the skyrmions may form a triangular solid; however, when the skyrmion density decreases for higher or lower fields, the spacing between skyrmions could become large enough that the skyrmions no longer interact, causing the system to transition into a disordered state outside some critical window of magnetic fields. The skyrmions could exhibit two glassy states associated with the lower field low density limit, an intermediate field triangular lattice, and a higher field disordered state.

For 3D systems containing quenched disorder, such as superconducting vortex lines, a Bragg glass can form in which the system has hexagonal order but also exhibits glassy features (Giamarchi and Le Doussal, 1995; Klein *et al.*, 2001). If skyrmions in a bulk 3D sample form a Bragg glass, it could be detected through measurements of the in-plane correlation function  $g(\mathbf{r})$  or by finding a power law divergence of the Bragg peaks in a scattering measurement (Giamarchi and Le Doussal, 1995). In analogy to the transitions observed in superconducting vortex systems, 3D skyrmions could also undergo a first order transition from a Bragg glass to a liquid state or to a different type of more disordered glass.

When columnar disorder is present, 3D superconducting vortices can form a disordered Bose glass, which suggests that skyrmions in linelike disorder could form a skyrmion Bose glass. Strong disorder in a 3D skyrmion system could also produce different types of glasses such as an entangled state in which the skyrmion lines wrap around each other. These skyrmion glasses could have

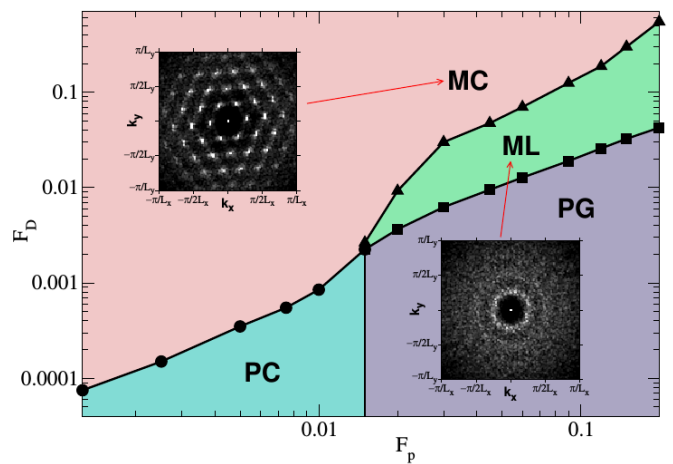


FIG. 27 Particle-based numerical simulations of a transition from a pinned crystal (PC) to a pinned glass (PG) as a function of increasing quenched disorder strength  $F_p$  (Reichhardt *et al.*, 2015b). When a driving force  $F_D$  is applied, transitions to a moving crystal (MC) or moving liquid (ML) state can occur. Upper inset: Peaks associated with crystalline ordering appear in the structure factor  $S(\mathbf{k})$ . Lower inset: Rings associated with a liquid state appear in  $S(\mathbf{k})$ . Reprinted with permission from C. Reichhardt *et al.*, Phys. Rev. Lett. **114**, 217202 (2015). Copyright 2015 by the American Physical Society.

very different properties than the vortex glasses since the skyrmions can in principle break or merge to form monopole states. In superconducting systems, glassy states can be detected through magnetization or voltage measurements, while for skyrmion systems, possible measurements that could reveal glassy features include magnetization, slow changes in the topological Hall effect, or changes in the structure factor  $S(k)$  as a function of time. The exploration of glassy states is an almost completely open field in skyrmions.

In samples with intermediate disorder, there are only a few strong pinning sites, so the system may exhibit a polydisperse state in which local ordering coexists with a series of grain boundaries (Moretti and Miguel, 2009). Conversely, there could be locally disordered regions coexisting with long range order. There are numerous experimental observations of domains and grain boundaries in skyrmion lattices (Li *et al.*, 2017; Matsumoto *et al.*, 2016a,b; Nakajima *et al.*, 2017a; Rajeswari *et al.*, 2015; Zhang *et al.*, 2016b). In such systems the depinning could involve either the motion of grain boundaries or the rotation of grains, and the depinning dynamics could be very different from those of purely ordered skyrmion lattices or completely disordered skyrmion states. Since skyrmions can change shape, the grain boundary formation process in a skyrmion lattice differs from that in a colloidal lattice or an atomic system, and certain topological defects may be less costly in a skyrmion lattice than in a system of rigid particles (Matsumoto *et al.*, 2016a).

The approach to a skyrmion glass at zero drive was observed in particle based simulations by Reichhardt *et al.* (Reichhardt *et al.*, 2015b) for skyrmions interacting with attractive point pins. At  $T = 0$  and low drives, the skyrmions form a defect-free lattice with six-fold peaks in  $S(\mathbf{k})$  and exhibit a finite elastic depinning threshold when the quenched disorder is weak. For stronger quenched disorder, the skyrmions form a disordered skyrmion glass as indicated by the ringlike structure of  $S(\mathbf{k})$ , illustrated in the lower inset of Fig. 27. Although the simulations in Fig. 27 show a transition from an ordered to a disordered state at  $T = 0$  as a function of increasing quenched disorder strength, in agreement with the predictions of Cha and Fertig (Cha and Fertig, 1995), it was not determined whether or not the transition from the pinned skyrmion crystal to the pinned skyrmion glass was of KTHNY type.

Silva *et al.* (Silva *et al.*, 2014) performed Monte Carlo simulations of skyrmion formation in the presence of pointlike nonmagnetic defects, and found that a very small number of defects could produce a disordered skyrmion structure. They also observed the emergence of bimerons for an increasing density of spin vacancies in both the spiral and the skyrmion state, as shown in Fig. 28. Silva *et al.* showed that inclusion of even 1% of spin vacancies can strongly disorder the system, but did not identify whether there is a critical amount of disorder that must be added to induce a transition from a skyrmion crystal to a disordered state (Silva *et al.*, 2014). Hoshino and Nagaosa (Hoshino and Nagaosa, 2018) theoretically studied a collective skyrmion glass phase using various methods such as replica theory from the glass literature, similar to what has been employed for other pinned systems (Giamarchi and Le Doussal, 1995). They found a number of scaling relations for the critical current and pinning frequencies, along with the key result that these quantities change sharply across the transition from the helical state to the skyrmion state. There have also been several studies demonstrating that quenched disorder can generate skyrmions (Chudnovsky and Garanin, 2018; Mirebeau *et al.*, 2018).

Transitions have been observed from square meron to hexagonal meron to hexagonal skyrmion states (Yu *et al.*, 2018b). Changes in the elastic constants can occur at these crossovers, and if the elastic constants drop below a certain level, the system can disorder near the square to hexagonal transition. It may also be possible to generate metastable glassy skyrmion states by quenching rapidly from a higher temperature liquid state to a lower temperature at which the equilibrium state is an ordered solid. In the presence of pinning, the resulting metastable supercooled liquid or glassy state could be long lived. Metastable disordered states can be distinguished from equilibrium disordered states by applying various perturbations such as a changing magnetic field. Experiments have shown that even in systems with large intrinsic disorder, an ordered skyrmion lattice can be pro-

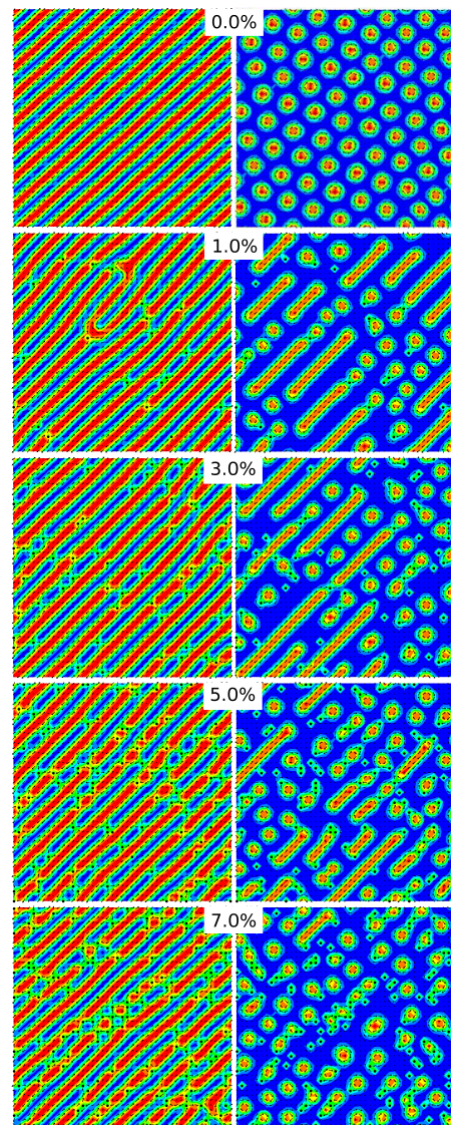


FIG. 28 Images from Monte Carlo simulations (Silva *et al.*, 2014) of spiral (left column) and skyrmion (right column) states with increasing magnetic spin vacancy densities  $\rho$ . At  $\rho = 0$ , an ordered spiral or triangular skyrmion lattice state forms. As the density of magnetic spin vacancies increases, skyrmions nucleate in the spiral state, the skyrmion lattice becomes disordered, and bimerons appear. Reprinted with permission from R. L. Silva *et al.*, Phys. Rev. B **89**, 054434 (2014). Copyright 2014 by the American Physical Society.

duced by the judicious selection of field application protocols (Gilbert *et al.*, 2019).

### A. Future Directions

There is a wide range of open issues for collective skyrmion states with disorder, such as whether there are different types of glassy states. These could include analogs to the vortex glass with point pinning in type-

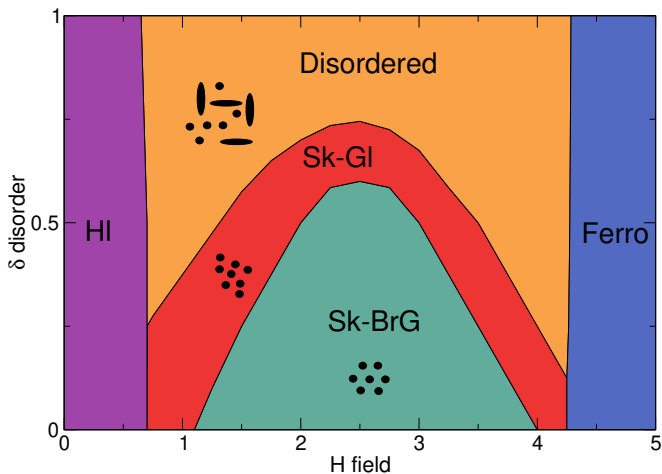


FIG. 29 Schematic of a possible phase diagram as a function of disorder strength  $\delta$  versus magnetic field  $H$  for a skyrmion system. At low fields the system is in a helical state (HI). At low disorder strength and high skyrmion density the system forms a skyrmion Bragg-Glass (Sk-BrG), and at low skyrmion densities and intermediate disorder, a skyrmion glass (Sk-GI) appears. For strong disorder, the system forms a mixed skyrmion-meron state with skyrmion breaking (Disordered). At the highest fields, the system forms a ferromagnetic state (Ferro).

II superconductors, a Bose glass, a splay glass, or even entirely new types of glassy phases that have not been observed previously. For example, for weak quenched disorder the skyrmions could form a Bragg glass, while for stronger quenched disorder they could form a skyrmion glass phase that is similar to a vortex glass. At even stronger disorder, the skyrmion lines could break up to create something like a monopole glass or a skyrmion-bimeron glass. In Fig. 29 we show a schematic of a possible phase diagram as a function of disorder strength versus magnetic field for a skyrmion system. At intermediate fields, where the skyrmion density is the highest, the system could form a skyrmion Bragg glass, while for larger disorder the skyrmions could positionally disorder to form a skyrmion glass. At the highest disorder strengths, the skyrmion lines could break up into a disordered configuration of coexisting skyrmions and bimerons. Each of these states could show unique responses to a drive, ac perturbations, retardation effects, or creep. It is an open question whether a full phase diagram for static skyrmion states can be measured as a function of quenched disorder, field, and temperature. Such a phase diagram could contain skyrmion lattice, skyrmion glass, and skyrmion liquid states similar to the vortex phase diagram observed for type-II superconductors (Crabtree and Nelson, 1997). Another question is whether a 2D or 3D skyrmion liquid phase differs from a 2D or 3D skyrmion glass phase. Since many materials now support skyrmions at room temperature, it is likely that systems will be identified in which the thermal fluc-

tuations are strong enough to create a skyrmion liquid with diffusing skyrmions. Already there is evidence for skyrmion thermal motion (Nozaki *et al.*, 2019; Zázvorka *et al.*, 2019; Zhao *et al.*, 2020) and liquid phases (Chai *et al.*, 2018). The nature of the skyrmion liquid phase could depend strongly on quenched disorder and pinning effects.

Differences between a pinned liquid and a pinned glass are detectable in correlation functions such as the density fluctuations or  $S(\mathbf{k})$ . The same measures can be used to detect the presence or absence of what is called disordered hyperuniformity, in which, unlike the behavior of a completely random system, large scale density fluctuations are suppressed (Torquato, 2016). Hyperuniformity can be used to distinguish jammed states from liquid states (Dreyfus *et al.*, 2015), and it has been observed in simulations of interacting particles with pinning (Le Thien *et al.*, 2017). The key signature of hyperuniformity is the behavior of the structure factor  $S(\mathbf{k})$  in the limit  $|\mathbf{k}| \rightarrow 0$ , given by

$$S(\mathbf{k}) \propto |\mathbf{k}|^\alpha. \quad (11)$$

An exponent  $\alpha > 0$  is indicative of hyperuniformity, while in a random configuration,  $S(\mathbf{k})$  approaches a constant value at small  $\mathbf{k}$ . There are different hyperuniform scaling regimes with  $\alpha > 1$ ,  $\alpha = 1$ , and  $0 < \alpha < 1$ . In general, larger values of  $\alpha$  indicate larger amounts of short range order. Hyperuniformity can also be characterized by measuring the number variance  $\sigma^2(R) = \langle N^2(R) \rangle - \langle N(R) \rangle^2$ , where  $N(R)$  is the number of particles in a region of radius  $R$ . For a random system,  $\sigma^2(R) \propto R^2$ , while for  $d$ -dimensional hyperuniform systems,  $\sigma^2(R) \propto R^{d-\alpha}$  when  $\alpha < 1$  and  $\sigma^2(R) \propto R^{d-1}$  when  $\alpha > 1$  (Torquato, 2016). Skyrmion assemblies are an ideal system in which to test some of the hyperuniformity concepts since skyrmions can easily be imaged over large scales.

It is an open question how all of the disordered phases described above would change for different species of skyrmions such as an antiskyrmion lattice, antiferromagnetic skyrmions, or a 3D hedgehog lattice. Each variety of skyrmion could exhibit different collective interactions in the presence of disorder.

## VI. DEPINNING DYNAMICS OF SKYRMIONS WITH PINNING

In this section we consider the dynamics of skyrmions in the presence of pinning. Skyrmions can be driven by various methods depending on whether the host system is a metal or an insulator. In the case of a metallic system, driving can be achieved through the application of a current by means of the spin torque effect (Iwasaki *et al.*, 2013a,b; Legrand *et al.*, 2017; Liang *et al.*, 2015; Nagaosa and Tokura, 2013; Schulz *et al.*, 2012; Tolley *et al.*, 2018;

Woo *et al.*, 2016; Yu *et al.*, 2012). Other driving methods include thermal gradients (Kong and Zang, 2013; Kovalev, 2014; Lin *et al.*, 2014; Mochizuki *et al.*, 2014; Pöllath *et al.*, 2017), electric fields (White *et al.*, 2014), spin currents (Shen *et al.*, 2018b), magnons (Psaroudaki and Loss, 2018), magnetic field gradients (Shen *et al.*, 2018a; Zhang *et al.*, 2018c), and acoustic waves (Nepal *et al.*, 2018). One of the first studies of skyrmion dynamics was performed by Zang *et al.* (Zang *et al.*, 2011), who showed that the skyrmion trajectories are deflected from the direction of the applied current and generate a skyrmion Hall effect, which can be very large. They also addressed the effect of pinning and identified a weak pinning or collective pinning regime along with a strong pinning regime. Direct imaging of skyrmion dynamics has been achieved with a variety of experimental techniques including Lorentz imaging, as will be discussed in more detail below.

Skyrmions produce the topological Hall effect (Nagaosa and Tokura, 2013; Neubauer *et al.*, 2009; Raju *et al.*, 2019) which combines additively with the other Hall effect terms to give a measured resistivity of

$$\rho_{xy}(H) = R_0H + R_sM(H) + \rho_{TH}(H). \quad (12)$$

Here  $R_0H$  is the ordinary Hall effect and  $R_sM(H)$  is the anomalous Hall effect, while  $\rho_{TH}$  is the topological Hall effect, which is typically obtained by accurately accounting for the contribution of the first two terms and subtracting them from  $\rho_{xy}$ . The topological Hall effect is linked to the skyrmion density according to  $\rho_{TH} = PR_0n_T\Phi_0$ , where  $P$  is the density of mobile charges,  $R_0$  is an unknown Hall resistivity from the effective charge density which is often taken to be equal to the ordinary Hall coefficient,  $n_T$  is the density of the total topological charge from the skyrmions, and  $\Phi_0 = h/e$  is the elementary flux quantum. According to this relation,  $\rho_{TH}$  is directly proportional to the number of skyrmions in the sample (Nagaosa and Tokura, 2013; Raju *et al.*, 2019).

Schulz *et al.* (Schulz *et al.*, 2012) were able to construct a skyrmion velocity-force curve based on changes observed in the topological Hall effect. They argue that for constant  $H$ ,  $\rho_{TH}$  remains constant when the skyrmions are stationary at zero current,  $j = 0$ , but that when the skyrmions begin to move under an applied current,  $\rho_{TH}$  decreases. By measuring variations of  $\rho_{xy}$  in the skyrmion phase as a function of  $j$ , they observed a drop at a specific value of  $j$  which was argued to correspond to the critical depinning threshold, and they were able to construct an effective velocity-force curve. In Fig. 30, a similar approach was used to construct a skyrmion velocity versus current curve for MnSi nanowires of different sizes (Liang *et al.*, 2015). The topological Hall effect  $\rho_{xy}^T$ , which has a value different from zero only inside the skyrmion phase, is plotted versus  $B$  for different currents in Figure 30(a). There is a decrease in the average value

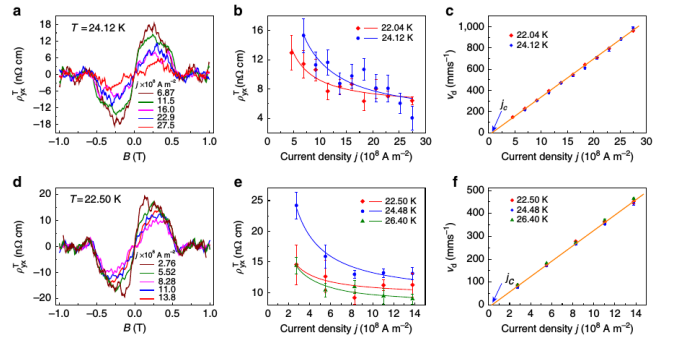


FIG. 30 Construction of skyrmion velocity-current curves based on measurements of the topological Hall effect (Liang *et al.*, 2015). Shown are transport results from two different devices, one smaller (upper row) and one larger (lower row). (a, d) The topological Hall effect  $\rho_{xy}^T$  vs magnetic field  $B$  measured at a range of applied current densities  $j$ . (b, e) The average value of  $\rho_{xy}^T$  over the range  $B = 0.2$  to  $0.4$  T vs current density  $j$  at different temperatures. (c, f) The estimated skyrmion drift velocity  $v_d$  vs current density  $j$ . Reprinted under CC license from D. Liang *et al.*, Nature Commun. **6**, 8217 (2015).

of  $\rho_{xy}^T$  with increasing  $j$ , as shown in Fig. 30(b). From this data, it is possible to extract an estimated skyrmion velocity  $v_d$ , which is plotted versus  $j$  in Fig. 30(c). The value of the critical current  $j_c$  can be obtained from a linear fit of this curve. Figure 30(d,e,f) shows that similar trends appear in a larger device. This work established that  $\rho_{xy}^T \propto 1/j$ , implying a linear increase of the skyrmion velocity with drive for drives well above  $j_c$ . There is a nonlinear dependence of  $v$  on  $j$  near the threshold current  $j_c$ . When the depinning is elastic, this nonlinear region extends only as high as currents below  $1.1j_c$ . In contrast, for plastic depinning the nonlinear regime can extend out to many multiples of  $j_c$ .

In principle, changes in the topological Hall effect as a function of current could be measured carefully as a function of drive, temperature, and magnetic field in order to map out the exact behavior of  $j_c$ . For example, a transition from elastic to plastic depinning could be accompanied by a large increase in  $j_c$ , similar to the peak effect phenomenon observed at the transition from elastic to plastic depinning in superconducting vortex systems (Reichhardt and Reichhardt, 2017). Obtaining high precision measurements of  $\rho_{xy}^T$  down to the single skyrmion level can be very difficult since all other Hall contributions must be carefully accounted for (Maccariello *et al.*, 2018; Zeissler *et al.*, 2018), so currently there are only a few studies that use changes in  $\rho_{xy}^T$  to deduce the critical depinning threshold (Liang *et al.*, 2015; Schulz *et al.*, 2012). Other studies in systems known to support skyrmions have shown the presence of a topological Hall effect that does not change with current (Leroux *et al.*, 2018). Several issues that can complicate the picture include sign changes of the topological Hall effect or the ex-

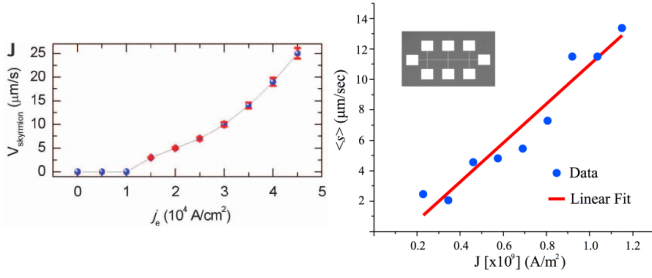


FIG. 31 Left panel: The skyrmion velocity  $V_{\text{skyrmion}}$  vs current  $j_e$  for room temperature skyrmions deduced from direct imaging (Jiang *et al.*, 2015). From W. Jiang *et al.*, Science **349**, 283 (2015). Reprinted with permission from AAAS. Right panel: The skyrmion velocity  $\langle s \rangle$  obtained from direct imaging versus current  $J$  for Pt/Co/Os/Pt thin films showing a linear fit (Tolley *et al.*, 2018). Reprinted with permission from R. Tolley *et al.*, Phys. Rev. Mater. **2**, 044404 (2018). Copyright 2018 by the American Physical Society.

istence of non-skyrmionic topological Hall effect sources (Denisov *et al.*, 2017, 2018; Maccariello *et al.*, 2018). Recent experiments in which  $\rho_{xy}^T$  was measured simultaneously with the number of skyrmions confirm that  $\rho_{xy}^T$  increases as the number of skyrmions increases; however, there is not exact quantitative agreement with the theory, and the value of  $\rho_{xy}^T$  is actually higher than would be expected from the number of counted skyrmions (Raju *et al.*, 2019).

Until now, the most common method for generating skyrmion velocity-force or velocity-current curves and obtaining the depinning threshold has been the use of direct imaging (Jiang *et al.*, 2015, 2017b; Litzius *et al.*, 2017; Tolley *et al.*, 2018; Woo *et al.*, 2016, 2018; Yu *et al.*, 2012). An example of results obtained with this technique appears in the left panel of Fig. 31 for room temperature skyrmions with a critical depinning current near  $j = 10^4$  A/cm<sup>2</sup> (Jiang *et al.*, 2015). The right panel of Fig. 31 shows the skyrmion velocity versus current in room temperature Pt/Co/Os/Pt thin films obtained from images taken with magneto-optic Kerr effect (MOKE) microscopy (Tolley *et al.*, 2018). The disadvantage of these methods is the amount of time required for imaging the skyrmion. In many cases, the images are obtained after applying a current pulse rather than under a continuous current, and the velocities must be deduced based on the skyrmion displacements rather than through a direct visualization of the skyrmion motion, making it difficult to access high frequency dynamics or effects such as hysteresis that can appear under a continuous current sweep.

### A. Elastic and Plastic Depinning

Iwasaki *et al.* (Iwasaki *et al.*, 2013b) performed micromagnetic simulations of driven skyrmions interact-

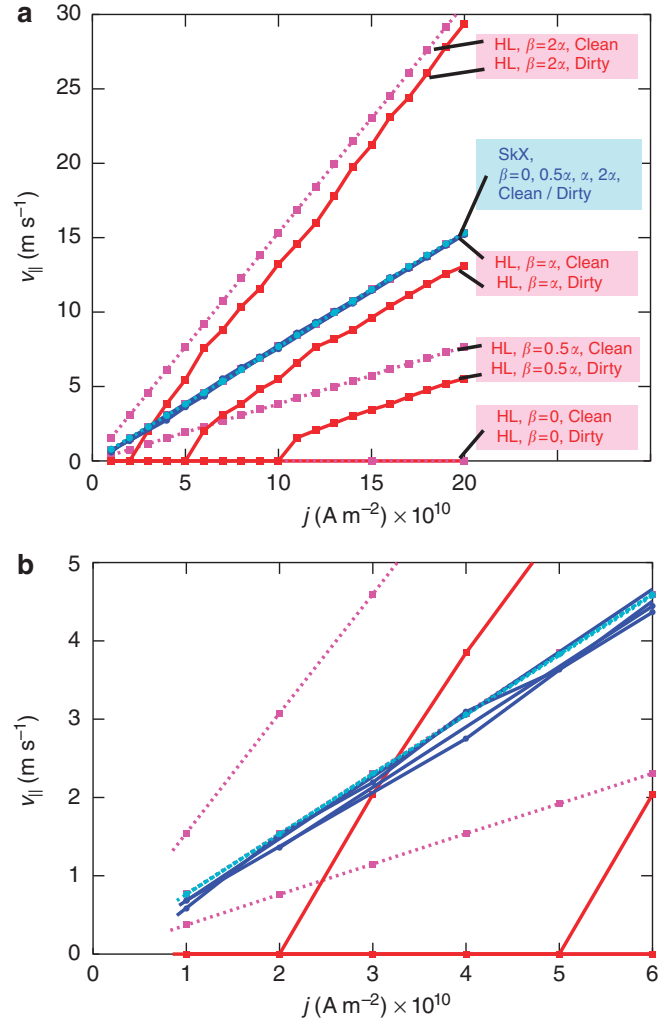


FIG. 32 Micromagnetic simulation measurements of the current-induced longitudinal velocities  $v_{\parallel}$  of the helical (HL) and skyrmion crystal (SkX) phases vs current density  $j$  in both the clean (impurity-free) and dirty limits for different values of the nonadiabatic term  $\beta$  (Iwasaki *et al.*, 2013b). Blue lines: skyrmion phases; red and magenta lines: helical phases. The skyrmions are much more weakly pinned than the helical phases and show an elastic depinning transition. (b) Magnification of panel (a) in the region of low current density. Reprinted by permission from: Springer Nature, “Universal current-velocity relation of skyrmion motion in chiral magnets,” Nature Commun. **4**, 1463 (2013), J. Iwasaki *et al.*, ©2013.

ing with weak pinning and found that the skyrmions form a triangular lattice in both the pinned and moving states. Here the pinning sites were much smaller than the skyrmion radius. The depinning threshold is zero in the absence of defects; however, when pinning is present, Iwasaki *et al.* observed elastic depinning in which each skyrmion maintains its same neighbors over time. They also found that as the ratio of the nonadiabatic portion of the interaction decreases, the criti-



cal current threshold  $j_c$  increases. The simulations revealed that the skyrmions could not only move around the defects due to the Magnus force but could also change shape. Figure 32 shows the longitudinal skyrmion velocity  $v_{\parallel}$  versus current  $j$  from simulations for skyrmion and helical phases with and without disorder. The helical phases are strongly pinned when disorder is present, but the skyrmion phases are weakly pinned. Since the skyrmions form a triangular lattice, Iwasaki *et al.* also analyzed the Bragg peaks and found that at lower drives the peaks were somewhat weaker and showed strong fluctuations, while at higher drives, the fluctuations were less pronounced and the Bragg peaks approached their pinning-free heights. This result is similar to the dynamical ordering found in superconducting vortex systems (Koshelev and Vinokur, 1994; Olson *et al.*, 1998b). Although no dislocations are generated at depinning, the system interacts more strongly with the pinning at low drives and becomes less ordered. Iwasaki *et al.* (Iwasaki *et al.*, 2013b) argue that the particle-based Thiele equation approach can be applied to understand both the depinning and the skyrmion dynamics responsible for the behavior of the velocity-force curves.

In the simulations of Iwasaki *et al.* (Iwasaki *et al.*, 2013b), the velocity-current curves were linear with  $v_{\parallel} \propto F_D$ ; however, the micromagnetic simulations could not resolve the depinning threshold  $F_c$  in the skyrmion regime. Reichhardt and Reichhardt examined a 2D particle based model for skyrmions interacting with disordered pinning substrates of varied strength (Reichhardt *et al.*, 2015b; Reichhardt and Reichhardt, 2019a), and found that the velocity force curves are consistent with  $v \propto (F_D - F_c)^\beta$  with  $\beta < 1.0$ . For elastic depinning,  $\beta < 1.0$ , while for plastic depinning,  $\beta > 1.0$  (Fisher, 1998; Reichhardt and Reichhardt, 2017); however, detailed finite size scaling has not been performed in the skyrmion simulations in order to confirm the exact values of the exponents for either the elastic or plastic depinning case. It is possible that the presence of the Magnus force could change the scaling compared to that found in overdamped systems. As for the behavior of the structure factor, Reichhardt and Reichhardt (Reichhardt and Reichhardt, 2019a) examined the magnitude  $S(k_0)$  of one of the six Bragg peaks as a function of driving force  $F_D$ . Although the skyrmions retain their sixfold ordering for all drives, there is a dip in  $S(k_0)$  just at the depinning threshold, indicating that during depinning, the lattice becomes more disordered or roughened, as also observed by Iwasaki *et al.* (Iwasaki *et al.*, 2013b).

At stronger pinning, Reichhardt and Reichhardt (Reichhardt and Reichhardt, 2019a) found a transition to a state in which, even for  $F_D = 0$ , dislocations proliferate and the skyrmions are in a glassy configuration. At higher drives, however, the skyrmions can dynamically order into a moving crystal phase. Figure 33 shows the dynamical phase diagram as a function of driving

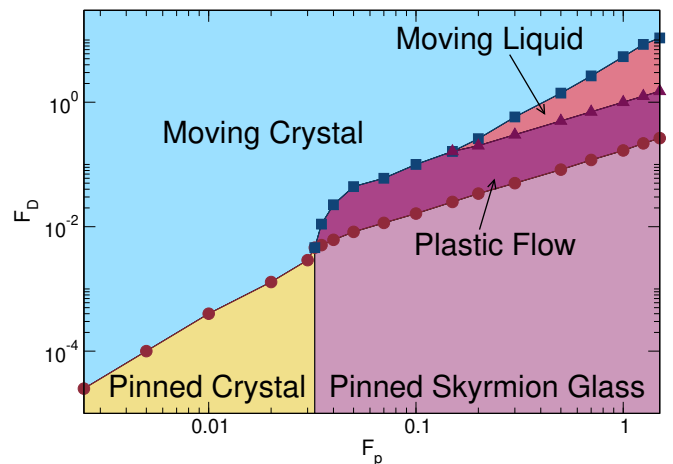


FIG. 33 Particle-based simulations of a dynamic phase diagram as a function of driving force  $F_D$  vs pinning strength  $F_p$  highlighting the transition from a pinned crystal to a pinned glass (Reichhardt and Reichhardt, 2019a). The pinned crystal depins elastically into a moving crystal phase, and the pinned skyrmion glass phase depins plastically into a plastic flow regime which transitions into the moving liquid phase. At high drives the system forms a moving crystal. The pinned to moving crystal line behaves as  $F_c \propto F_p^2$ , while the pinned glass to plastic flow line behaves as  $F_c \propto F_p$ . Reprinted with permission from C. Reichhardt *et al.*, Phys. Rev. B **99**, 104418 (2019). Copyright 2019 by the American Physical Society.

force versus pinning strength  $F_p$  obtained from a series of simulations. Here there are two pinned phases: the pinned crystal for weak disorder and the pinned glass for stronger disorder. In the pinned crystal phase, the critical driving force  $F_c \propto F_p^2$ , as expected for elastic depinning from collective pinning theory (Blatter *et al.*, 1994), while in the pinned glass phase,  $F_c \propto F_p$  as expected for plastic depinning. There is a sudden increase in  $F_c$  across the crystal to glass transition. This is similar to the peak effect phenomenon found for superconducting vortices, where the particles in the plastic or disordered phase have more local freedom to move and are better able to optimize their interactions with the randomly located pinning sites, increasing the value of  $F_c$  (Banerjee *et al.*, 2000; Bhattacharya and Higgins, 1993; Reichhardt *et al.*, 2001; Toft-Petersen *et al.*, 2018). In general, when the pinning is weaker, the relative magnitude of the jump in  $F_c$  at the transition from elastic to plastic depinning becomes more pronounced (Reichhardt and Reichhardt, 2017). Just at depinning in the elastic state, the motion can be jerky or intermittent but the particles maintain the same neighbors. On the other hand, for plastic depinning, numerous dislocations and topological objects appear in the system and there is a coexistence of pinned and flowing skyrmions in the plastic flow state, as illustrated in Fig. 34 (Reichhardt and Reichhardt, 2016). The moving liquid state in Fig. 33 is distinguished from the plastic flow state by the fact that all of the skyrmions are

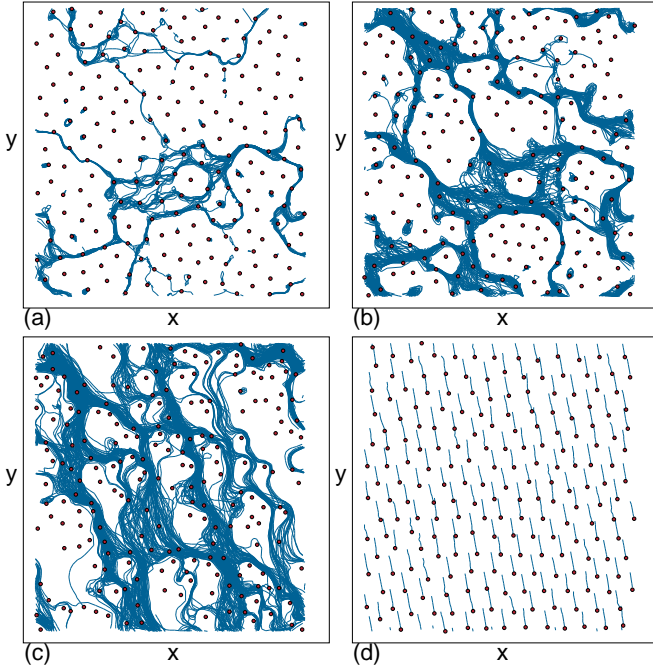


FIG. 34 The plastic flow phase just above depinning from particle-based simulations of skyrmions in strong random pinning (Reichhardt and Reichhardt, 2016). Skyrmion positions (dots) and trajectories (lines) are obtained over a fixed time period, and the drive is in the positive  $x$ -direction. (a) At a drive close to depinning, channels of flow coexist with pinned skyrmions. (b) As the drive increases, the number of pinned skyrmions decreases. (c) For higher drives, plastic flow continues to persist and the direction of motion has rotated away from the driving direction. (d) Trajectories obtained over a shorter time period at a high drive where the skyrmions are dynamically ordered and move at an angle of  $-79.8^\circ$  to the drive. Reprinted under CC license from C. Reichhardt and C. J. O. Reichhardt, *New J. Phys.* **18**, 095005 (2016).

moving simultaneously but remain disordered. At higher drives, within the particle model the skyrmions dynamically reorder into a moving crystal phase and regain their mostly sixfold ordering (Reichhardt *et al.*, 2015b; Reichhardt and Reichhardt, 2016, 2019a), (Reichhardt and Reichhardt, 2019a).

Evidence for collective plastic flow as a function of drive has been obtained with direct imaging for room temperature skyrmions in thin films. The skyrmion trajectories show a coexistence of moving and pinned regions along with specific channels or rivers in which flow is occurring, as illustrated in Fig. 35 (Montoya *et al.*, 2018). The images closely resemble the motion observed experimentally near the depinning transitions of superconducting vortices (Fisher, 1998; Matsuda *et al.*, 1996; Reichhardt and Reichhardt, 2017) and colloidal particles (Pertsinidis and Ling, 2008; Tierno, 2012) moving on random substrates. Small angle neutron scattering experiments on MnSi under current flow showed a broadening of the peaks above depinning, which could be evidence of

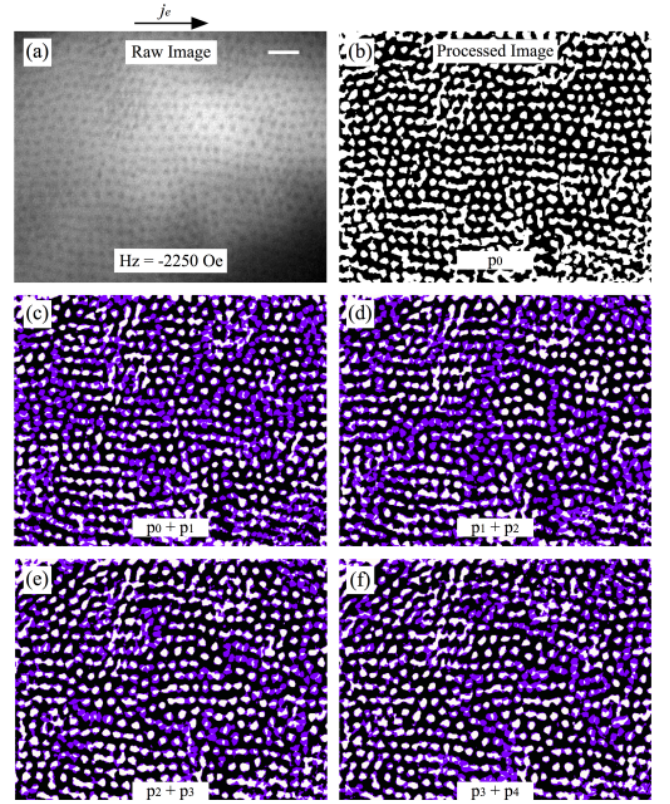


FIG. 35 Images showing current-induced plastic motion of dipole skyrmions from room temperature experiments on Ta (5 nm)/[Fe (0.34 nm)/Gd(0.4 nm)]  $\times$  100/Pt (3 nm) (Montoya *et al.*, 2018). (a) Original soft x-ray microscopy image of a close-packed skyrmion lattice. (b) Postprocessed binary image of (a) where the background has been subtracted. (c,d,e,f) Skyrmion dynamics obtained by summing images of the domain morphology before and after a current pulse is injected, where purple regions indicate places where the domain morphology has changed. Reprinted with permission from S. Montoya *et al.*, *Phys. Rev. B* **98**, 104432 (2018). Copyright 2018 by the American Physical Society.

dynamical disordering close to depinning; however, it was also argued that the broadening could arise from edge effects which produce counter-rotating domains (Okuyama *et al.*, 2019a,b).

An important difference between the experimental skyrmion system and the particle based superconducting vortex and colloidal simulations is that the skyrmions have internal degrees of freedom which can become excited. For example, one end of skyrmion (a meron) could be pinned while the meron in the other half of the skyrmion continues to move. This could be viewed as the motion of an elongated skyrmion or the emergence of a helical stripe phase.

The dynamical ordering from a plastic flow state to a more ordered state illustrated in Fig. 33 is similar to that found for superconducting vortices (Koshelev and Vinokur, 1994; Olson *et al.*, 1998b; Reichhardt and Re-

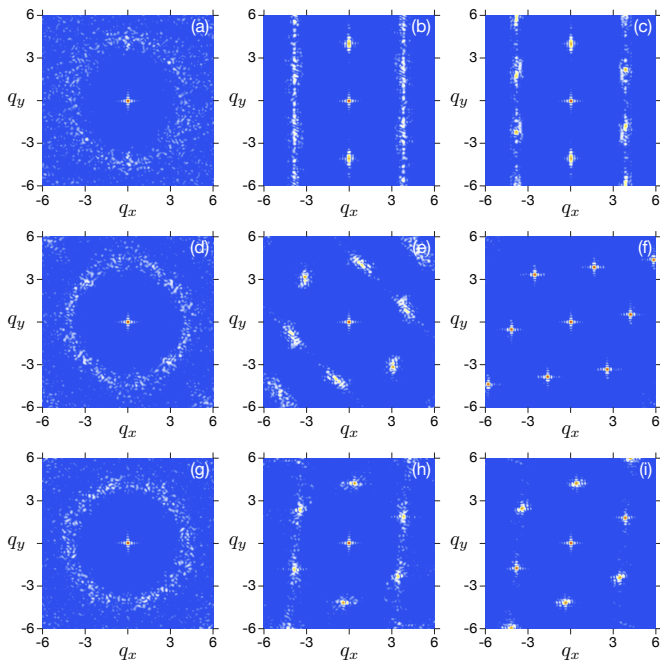


FIG. 36 Static structure factor  $S(\mathbf{q})$  from particle-based skyrmion simulations (Díaz *et al.*, 2017). The driving force increases from left to right in each row. (a-c) An overdamped system with an intrinsic Hall angle of  $\theta_{\text{SkH}}^{\text{int}} = 0$  in (a) the plastic flow state, (b) the moving smectic state, and (c) the moving anisotropic crystal state. (d-f) A system with  $\theta_{\text{SkH}}^{\text{int}} = 45^\circ$  in (d) the moving liquid state, (e) a slightly anisotropic moving crystal state, and (f) the moving crystal state. (g-i) A system with  $\theta_{\text{SkH}}^{\text{int}} = 70^\circ$  in (g) the moving liquid state, (h) a slightly anisotropic moving crystal state, and (i) the moving crystal state. Reprinted with permission from S. A. Díaz *et al.*, Phys. Rev. B **96**, 085106 (2017). Copyright 2017 by the American Physical Society.

ichhardt, 2017), colloidal particles (Reichhardt and Olson, 2002a), Wigner crystals (Reichhardt *et al.*, 2001), pattern forming systems (Reichhardt *et al.*, 2003; Xu *et al.*, 2011; Zhao *et al.*, 2013), and driven charge density waves (Danneau *et al.*, 2002; Du *et al.*, 2006; Pinsolle *et al.*, 2012). There are, however, several differences in the moving states of skyrmions with a Magnus force compared to the previously studied overdamped systems. In the 2D vortex system as well as overdamped systems in general, the moving state is typically a moving smectic in which the vortices form rows that slide past one another. Figure 36(a,b,c) shows  $S(\mathbf{k})$  at fixed drives for an overdamped particle system that could represent vortices moving over random disorder (Díaz *et al.*, 2017). At lower drives in Fig. 36(a), the structure factor has a ring shape indicative of a liquid or glass and the particles are in a disordered configuration. At higher drives in Fig. 36(b), the system starts to dynamically reorder into a moving smectic state where there are well defined chains of particles moving past each other. This creates a series of aligned dislocations and the structure factor

contains two dominant peaks. For even higher drives in Fig. 36(c), the system is still in a moving smectic state but some additional sixfold ordering is beginning to emerge, producing additional smeared peaks in  $S(\mathbf{k})$ . At still higher drives, the structure factor remains the same since the dislocations are dynamically trapped. The approach to a moving crystal state for overdamped particles such as vortices moving over random disorder has been predicted in theoretical calculations (Balents *et al.*, 1998; Giamarchi and Le Doussal, 1996) and observed in numerous simulations (Fangohr *et al.*, 2001; Giamarchi and Le Doussal, 1996; Gotcheva *et al.*, 2004; Kolton *et al.*, 1999; Moon *et al.*, 1996; Olson *et al.*, 1998b) and experiments (Pardo *et al.*, 1998).

Simulations of driven skyrmions have shown that when the Magnus force is present, the dynamically reordered state has six strong peaks, indicating the presence of a higher degree of isotropic order than what is observed in overdamped systems (Díaz *et al.*, 2017). This effect is attributed specifically to the Magnus force. Viewed from a co-moving frame, overdamped particles experience force perturbations from the substrate that are strongest in the direction of motion. It can be argued that the resulting fluctuations are equivalent to a shaking temperature  $T_{sh} \propto 1/F_D$  (Koshelev and Vinokur, 1994). For sufficiently large drives, the system freezes into a solid, but because the shaking temperature is anisotropic with  $T_{sh}^{\parallel} > T_{sh}^{\perp}$  (Balents *et al.*, 1998; Giamarchi and Le Doussal, 1996), the direction perpendicular to the drive freezes first, locking dislocations into the sample, while the direction parallel to the drive remains liquidlike. In the case of skyrmions, the Magnus force mixes the fluctuations from the driving direction into the perpendicular direction, resulting in a more isotropic shaking temperature that prevents the trapping of smectic defects and allows the system to freeze in both directions simultaneously. The isotropic nature of  $T_{sh}$  was confirmed in simulations through direct measurements of the fluctuations in both the transverse and longitudinal directions for skyrmions moving through random pinning (Díaz *et al.*, 2017). It may be possible that for very large Magnus forces, the system could form a moving smectic structure that is aligned perpendicular, rather than parallel, to the drive.

Figure 36(d,e,f) shows  $S(\mathbf{k})$  for three different drives in simulations of a 2D driven skyrmion system with random pinning where the intrinsic skyrmion Hall angle is  $\theta_{\text{SkH}}^{\text{int}} = 45^\circ$  (Díaz *et al.*, 2017). At a low drive in Fig. 36(d), the skyrmions are disordered and  $S(\mathbf{k})$  has a ringlike structure. At a higher drive in Fig. 36(e), sixfold peaks begin to emerge that are much more isotropic than the peaks observed in Fig. 36(b) at the same drive in the overdamped system, although there is still a small amount of smearing of the four side peaks. For high drives, illustrated in Fig. 36(f), there are now six sharp peaks of equal size and the skyrmions have organized into a crystal. A similar evolution of the structure fac-

tor with drive for skyrmions with  $\theta_{\text{SkH}}^{\text{int}} = 70^\circ$  appears in Fig. 36(g,h,i). Compared to the overdamped system, where a somewhat disordered crystalline state emerges that is aligned with the driving direction, the skyrmion crystalline state is very well ordered and it is *not* aligned with the driving direction. Instead, the orientation of the crystal rotates slightly with increasing drive. This is another consequence of the Magnus force, which causes the lattice to tend to align in the direction of motion rather than in the direction of the applied driving force. In an overdamped system, these two directions are the same, but in the skyrmion system, they are separated by the intrinsic skyrmion Hall angle.

The moving smectic state can also be distinguished from the moving crystal by measuring the relative motion of the particles in the co-moving frame, where the center of mass motion has been subtracted. Skyrmions exhibit a long time diffusive motion in the driving direction, but subdiffusive motion or no diffusion perpendicular to the driving direction (Díaz *et al.*, 2017). The displacements in the moving frame are given by  $\Delta_{\parallel}(t) = N^{-1} \sum_{i=1}^N [\tilde{r}_{i,\parallel}(t) - \tilde{r}_{i,\parallel}(0)]^2$ , where  $\tilde{r}_{i,\parallel} = r_{i,\parallel}(t) - R_{\parallel}^{\text{CM}}(t)$ , and  $\Delta_{\perp}(t) = N^{-1} \sum_{i=1}^N [\tilde{r}_{i,\perp}(t) - \tilde{r}_{i,\perp}(0)]^2$ , where  $\tilde{r}_{i,\perp} = r_{i,\perp}(t) - R_{\perp}^{\text{CM}}(t)$ . Here  $\mathbf{R}^{\text{CM}}$  is the center of mass in the moving frame and  $N$  is the number of skyrmions. The different phases can be identified through the power law behavior

$$\Delta(t)_{\parallel,\perp} \propto t^{\alpha_{\parallel,\perp}} \quad (13)$$

For isotropic regular diffusion,  $\alpha_{\parallel} = \alpha_{\perp} = 1$ ; for a smectic state,  $\alpha_{\parallel} \geq 1$  and  $\alpha_{\perp} = 0$ ; for a moving crystal,  $\alpha_{\parallel} = \alpha_{\perp} = 0$ ; and for a moving liquid,  $\alpha_{\parallel} \geq 1$  and  $\alpha_{\perp} \geq 1$ . Other regimes are also possible. For example, at short times there can be subdiffusive behavior with  $0 < \alpha < 1$  in either direction, but at long times a crossover to regular diffusion occurs. Within the smectic phase,  $\alpha_{\parallel} = 2$ , indicating superdiffusive or ballistic motion in the driving direction, while  $\alpha_{\perp} = 0$ . The ballistic behavior that appears even after the center of mass motion has been removed arises because the different rows in the smectic state are moving at different speeds relative to one another. In general, the moving smectic state in overdamped 2D systems always shows regular diffusion or superdiffusion in the direction parallel to the drive but no diffusion in the direction perpendicular to the drive. This is in contrast to the skyrmion system which exhibits no diffusion in either direction, indicating the emergence of a truly crystalline state as a function of drive.

## B. Noise

Noise fluctuations are a useful method for characterizing condensed matter states (Sethna *et al.*, 2001; Weissman, 1988). For skyrmion systems, transitions between

plastic flow and moving crystalline regimes can be distinguished with the power spectrum

$$S(\omega) = \left| \int \sigma(t) e^{-i2\pi\omega t} dt \right|^2 \quad (14)$$

of various time dependent quantities  $\sigma(t)$ , which could include the topological Hall resistance  $\rho_{xy}^T$ , the local magnetization, or the fluctuations in  $S(\mathbf{k})$  at a particular value of  $\mathbf{k}$ . Separate time series  $\sigma(t)$  can be obtained for different values of an applied drive in order to detect changes in the spectral response. Such measures have been used to study superconducting vortices (D'Anna *et al.*, 1995; Kolton *et al.*, 1999, 2002; Marley *et al.*, 1995; Merithew *et al.*, 1996; Olson *et al.*, 1998b), sliding charge density waves (Bloom *et al.*, 1993; Grüner *et al.*, 1981), and the motion of magnetic domain walls (Sethna *et al.*, 2001), and they could prove to be a similarly powerful technique for skyrmion systems. Particle-based simulations of vortices showed that in the plastic flow phase, the velocity noise has a broad band  $1/f^\alpha$  signature, where  $f = \omega/2\pi$  (Marley *et al.*, 1995; Olson *et al.*, 1998b). The value of the exponent  $\alpha$  determines the type of the noise. When  $\alpha = 0$ , the noise is white and has equal power in all frequencies, while  $\alpha = 1$  or a  $1/f$  signature is called pink noise and  $\alpha = 2$  or a  $1/f^2$  signature is known as brown noise or Brownian noise. Brownian noise can be produced by the trajectories of a random walk, whereas white noise has no correlations. In overdamped systems that undergo depinning, values of  $0.75 < \alpha < 1.8$  are associated with collective dynamics, and in some cases the presence of a critical point produces a distinct spectral response (Traveset *et al.*, 2002). This implies that if depinning is a critical phenomenon, it may be possible to use the noise power to determine the universality class of the depinning. In addition to broad band noise, there may be a knee at a specific frequency of the form  $S(f) \propto \tau/(1 + (2\pi\tau f)^2)$ , which approaches a constant value as  $f$  goes to zero. This type of spectrum is often associated with telegraph noise, where  $\tau$  is the characteristic time of jumps between the two states of the signal. A narrow band noise signal produces one or more peaks at characteristic frequencies that are related to a length scale in the system. For example, a random arrangement of particles moving over random disorder can have a time of flight narrow band noise peak in which the characteristic frequency is the inverse of the time required to traverse the entire sample (D'Anna *et al.*, 1995; Olson *et al.*, 1998a). Alternatively, if the particles are in a moving lattice, they can produce a washboard signal corresponding to the time required for a particle to move one lattice constant (Harris *et al.*, 1995; Klongcheongsan *et al.*, 2010; Okuma *et al.*, 2007; Olson *et al.*, 1998b; Togawa *et al.*, 2000).

In simulations, a time of flight signal can arise from the motion of a large scale structure, such as a grain boundary in a skyrmion lattice, through the periodic boundary

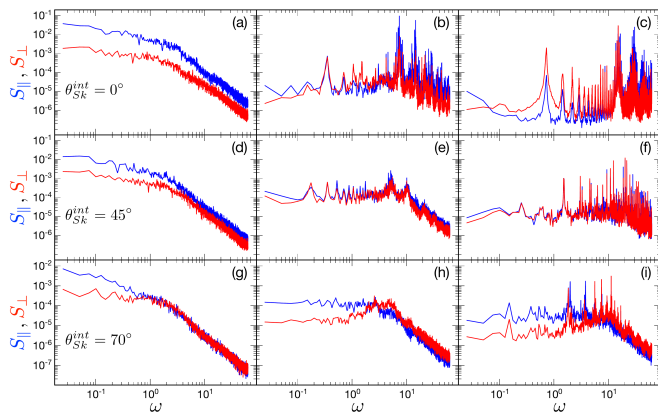


FIG. 37 Spectral density plots from particle based skyrmion simulations (Díaz *et al.*, 2017) showing  $S_{||}(\omega)$  (blue) for velocity fluctuations parallel to  $\theta_{\text{SkH}}$  and  $S_{\perp}(\omega)$  (red) for velocity fluctuations perpendicular to  $\theta_{\text{SkH}}$ . The driving force increases from left to right in each row. (a)-(c) An overdamped sample with  $\theta_{\text{SkH}}^{\text{int}} = 0^\circ$  in (a) the disordered flow state and (b,c) two drives in the moving smectic phase. (d)-(f) A sample with  $\theta_{\text{SkH}}^{\text{int}} = 45^\circ$  in (d) the disordered flow state, (e) the moving liquid phase, and (f) the moving crystal phase. (g)-(i) A sample with  $\theta_{\text{SkH}}^{\text{int}} = 70^\circ$  in (g) the disordered flow state, (h) the moving liquid phase, and (i) the moving crystal phase. Reprinted with permission from S. A. Díaz *et al.*, Phys. Rev. B **96**, 085106 (2017). Copyright 2017 by the American Physical Society.

conditions. A signal of this type typically appears at relatively low frequencies. In skyrmion experiments, narrow band noise could be produced by the periodic nucleation of skyrmions at the edge of the sample, where the time of flight would correspond to the time required for the skyrmion to cross to the other side of the sample and be annihilated. The washboard frequency of an elastic lattice moving over disorder is given by  $\omega = v/a$  (Harris *et al.*, 1995), where  $v$  is the time averaged dc velocity and  $a$  is the lattice constant. A measurement of the washboard frequency thus provides a method for determining the lattice constant. Both the time of flight and washboard narrow band signals are generated when the particles are in steady continuous motion, rather than intermittently alternating between being pinned and moving. If the system forms a continuously moving liquid, the sharp narrow band peaks in the noise spectrum would be lost, but a smoother peak could still appear that is associated with the average time between collisions of a particle with a pinning site. Figure 37 shows power spectra  $S_{||}$  and  $S_{\perp}$  of the longitudinal and transverse velocity signals from a particle based simulation of skyrmions moving over random disorder at various drives (Díaz *et al.*, 2017). In Fig. 37(a), an overdamped system in the plastic flow regime has higher noise power parallel to the drive than perpendicular to the drive, consistent with the idea that the shaking temperature from the fluctuations is largest in the direction of drive for overdamped systems

moving over quenched disorder. There is also a  $1/f^\alpha$  tail with  $\alpha \approx 1.5$ , similar to the noise observed in simulations of other overdamped systems. Figure 37(b,c) shows that at higher drives, the broad band noise signal is lost and a series of high frequency peaks appear at multiples of the washboard frequency. At much lower frequencies, the time of flight signal produces a second series of peaks which are the most pronounced in Fig. 37(c). Figures 37(d) and (g) show the lower drive plastic flow regime for skyrmion systems with a Magnus force giving  $\theta_{\text{SkH}}^{\text{int}} = 45^\circ$  and  $70^\circ$ , respectively. Here the magnitude of the noise at higher frequencies is nearly identical in both directions, in agreement with the argument that the shaking temperature for skyrmions is more isotropic than that for overdamped particles. At higher drives in Fig. 37(e, f, h, i), peaks once again appear at both the time of flight and washboard frequencies. Additional noise features can be deduced by analyzing the evolution of these peaks as a function of current. A sudden switch in the peak frequency would indicate the reorientation of the lattice or the annihilation of dislocations in the lattice.

Although skyrmions exhibit a number of dynamical features similar to those found in overdamped vortex systems, they also have some unique behaviors. For example, if a current were used to create skyrmions, this process could be detected via changes in the narrow band noise signature. In a sample where skyrmions coexist with different species of topological defects such as large ferromagnetic domains, the low frequency noise generated by the density fluctuations could be used to determine the size of the domains (Mohan *et al.*, 2009). It may also be possible to detect increases of noise as a function of increasing temperature near a 2D melting transition, where fluctuations are expected to increase strongly (Koushik *et al.*, 2013). In addition to the power spectrum, higher order measures such as the second spectrum or the noise of the noise can be analyzed to examine the persistence times of metastable processes (Merithew *et al.*, 1996). Noise has been used to measure various nonequilibrium effects such as negative velocity fluctuations (Bag *et al.*, 2017), and similar studies could be performed for driven skyrmions where the nonconservative Magnus force could produce novel effects. Skyrmion systems in which the dynamics of small numbers of skyrmions can be accessed could be ideal for studying the routes to chaos using techniques similar to previous work performed with noise in charge density wave (Levy and Sherwin, 1991) and superconducting vortex systems (Olive and Soret, 2006).

Up until this point, studies of skyrmion noise have been limited to particle based models (Díaz *et al.*, 2017; Reichhardt and Reichhardt, 2016); however, continuum based approaches could permit the exploration of additional contributions to noise from shape fluctuations or the breathing modes of the skyrmions. For example, a

moving skyrmion lattice would exhibit a washboard frequency associated with the lattice spacing, but a second much higher frequency signal could appear as a result of collective breathing modes that are excited by the motion over random disorder. In addition to noise generated purely by the internal modes of the skyrmion, other noise signatures could arise due to coupling of the internal modes with the skyrmion lattice. Experimental noise measurements in skyrmion systems are just beginning, with a recent experiment on skyrmion motion in a narrow channel showing a transition from  $1/f$  noise to narrow band noise similar to what has been seen in simulations (Sato *et al.*, 2019).

### C. Avalanches

Intermittent noise often takes the form of time windows of little or no activity interspersed with windows of large activity or avalanches. Avalanche-like behavior is a ubiquitous phenomenon in driven systems with quenched disorder (Bak *et al.*, 1988; Carlson *et al.*, 1994; Fisher, 1998; Reichhardt and Reichhardt, 2017; Sethna *et al.*, 2001), and one of the best known examples is Barkhausen noise in magnetic systems (Barkhausen, 1919; Bertotti *et al.*, 1994; Cote and Meisel, 1991; Zapperi *et al.*, 1998). Avalanches are often most clearly resolvable at low driving, where distinct jumps can be distinguished from one another.

Numerous methods exist for analyzing the avalanches. Construction of the probability distribution function of the magnitude of the velocity or other avalanche signal as a function of time can show whether the avalanches are all close to the same size, are exponentially distributed, have a specific range of sizes, or are power law distributed. A power law distribution of avalanche events is often associated with critical behavior (Bak *et al.*, 1988; Perković *et al.*, 1995). For example, if depinning in systems driven over quenched disorder is a critical phenomenon, then avalanche behavior could appear at low drives close to the depinning transition. It has been argued theoretically that the avalanches are critical only for a critical disorder strength  $R_c$ , with large avalanches that are close to the same size occurring for disorder strengths  $R < R_c$ , and exponentially distributed avalanches appearing for  $R > R_c$ ; however, it is possible to be fairly far from  $R_c$  and still observe a regime of power law distributed avalanche sizes (Perković *et al.*, 1995; Sethna *et al.*, 1993, 2001). Avalanches can occur in driven systems without thermal fluctuations; however, there are cases in which thermal effects can trigger avalanches. Both elastic and plastic systems exhibit avalanches, and in principle the avalanche distributions would change across an elastic-plastic transition. Since avalanches occur so routinely in magnetic systems, the skyrmion system is ideal for examining avalanche effects.

Skyrmion avalanches remain largely unexplored, but were studied by Díaz *et al.* (Díaz *et al.*, 2018) using a 2D particle based model in which skyrmions entered the edge of the sample under a low driving force through a series of jumps. For zero or weak Magnus forces, the avalanche sizes  $S$  and durations  $T$  are power law distributed,  $P(T) \propto T^\alpha$  and  $P(S) \propto S^\tau$ , with  $\alpha = 1.5$  and  $\tau = 1.33$ . Near a critical point there should be an additional scaling relation  $\langle S \rangle \propto T^{1/\sigma\nu z}$  between the avalanche sizes and durations (Sethna *et al.*, 2001), so that in this case,  $1/\sigma\nu z = 1.63$ . The exponents should also obey

$$\frac{\alpha - 1}{\tau - 1} = \frac{1}{\sigma\nu z} \quad (15)$$

near the critical point. In the work of Díaz *et al.*, this equality was satisfied, indicating that near depinning, the system is critical. Interestingly, for large values of  $\theta_{\text{SKH}}^{\text{int}}$ , the scaling exponents for the avalanches change but equality (15) holds, suggesting that the nature of the criticality changes with increasing Magnus force. The avalanches can also be characterized by scaling the shape of avalanches that have the same duration. In certain universality classes such as the random field Ising model, such scaling will produce a symmetric curve (Mehta *et al.*, 2002; Sethna *et al.*, 2001). Díaz *et al.* found that the avalanches in the overdamped system and in samples with weaker Magnus forces were symmetric in shape, while those for strong Magnus forces were strongly skewed. This is also correlated with the change in the avalanche exponents at strong Magnus forces. Skewed avalanche shapes can result from nondissipative effects, such as inertia which tends to speed up the avalanche at later times and produce a leftward skew, or negative mass effects which have the opposite effect and give a rightward skew (Zapperi *et al.*, 2005). Skyrmions have a tendency to be more strongly deflected at later times, which is similar to a negative mass effect. Experimental studies of avalanches or cascades in stripe and skyrmion phases that focused on jumps or changes in the pairwise correlation functions showed evidence for power law distributions of jump sizes in the skyrmion regime, as well as different avalanche exponents in the skyrmion and stripe phases (Singh *et al.*, 2019).

### D. Continuum Based Simulations of the Dynamic Phase Diagram

A variety of continuum simulation studies have explored the dynamical ordering of driven skyrmions in the presence of quenched disorder. Koshibae and Nagaosa (Koshibae and Nagaosa, 2018) used a 2D continuum model for skyrmions interacting with random point pinning to construct a driving force versus disorder strength phase diagram. They initialized the system in a skyrmion

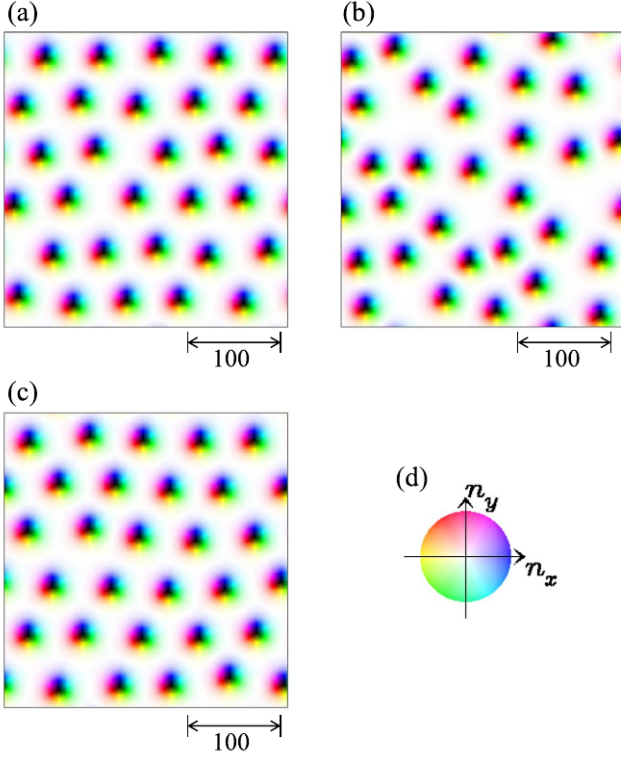


FIG. 38 Continuum simulations of current driven skyrmions interacting with weak impurities (Koshibae and Nagaosa, 2018). The magnetic field is  $h = 0.025$  and the impurity strength is  $K_{\text{imp}} = 0.01$ . (a) The initial configuration at zero drive,  $j = 0$ . (b) A glassy configuration at  $j = 0.001$ . (c) A moving skyrmion crystal at  $j = 1.0$ . (d) The color code used in panels (a-c) to represent the in-plane magnetic moment. Reprinted under CC license from W. Koshibae and N. Nagaosa, *Sci. Rep.* **8**, 6328 (2018).

lattice at a drive of  $j = 0$  as shown in Fig. 38(a). When a finite drive is applied, the skyrmions move plastically, creating a disordered structure as shown in Fig. 38(b) at  $j = 0.001$ . At higher drives, the system transitions into a moving skyrmion lattice as illustrated in Fig. 38(c) for  $j = 1.0$ . The resulting phase diagram as a function of the driving current  $j$  versus the impurity strength  $K_{\text{imp}}$  appears in Fig. 39(a,b) for two different magnetic field strengths of  $h = 0.025$  and  $h = 0.04$ , respectively. At  $h = 0.025$ , there is a pinned phase which grows in extent with increasing impurity strength, as well as large regions of moving skyrmion glass or disordered moving phases. For  $K_{\text{imp}} < 0.1$ , the moving skyrmion glass orders into a moving crystal as shown in Fig. 38. The first of two new phases that appear is a multiplication phase in which skyrmions can be created dynamically by the combination of the current and pinning effects. The second is a segregated or clustered state. For  $h = 0.04$ , there is also a decreasing phase in which skyrmions are annihilated. The segregated phase was argued to result from the modification of the skyrmion-skyrmion interactions

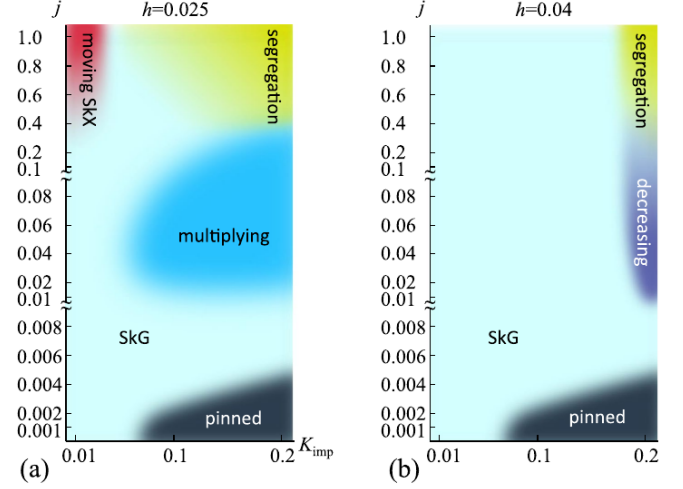


FIG. 39 Dynamic phase diagrams as a function of applied current  $j$  vs impurity strength  $K_{\text{imp}}$  from the continuum simulations illustrated in Fig. 38 (Koshibae and Nagaosa, 2018). The applied magnetic field is (a)  $h = 0.025$  and (b)  $h = 0.04$ . The different dynamic phases are labeled, including the skyrmion glass (SkG) and moving skyrmion crystal (SkX) states. Reprinted under CC license from W. Koshibae and N. Nagaosa, *Sci. Rep.* **8**, 6328 (2018).

by the emission of spin excitations, which produce an effective attractive interaction between the skyrmions. In subsequent 2D particle based simulations of skyrmions moving over strong disorder, a segregated phase was also observed that was argued to be due to a Magnus-force induced effective attraction between skyrmions that are moving at different skyrmion Hall angles (Reichhardt and Reichhardt, 2019a).

The different phases in Fig. 39 could be detected using imaging and neutron scattering techniques. They could also in principle be identified by analyzing the noise fluctuations since, as was shown previously, a change in the noise power occurs across the transition from the moving glass to the moving lattice state. The multiplying, decreasing and segregated phases shown in Fig. 39 could each have their own distinct noise signatures or changes in the topological Hall effect.

### E. 3D Skyrmion Dynamics

Although stiff 3D skyrmions can be treated with 2D models, in a fully 3D system there are numerous new effects that can appear such as skyrmion line wandering, skyrmion breaking, and skyrmion cutting or entanglement. In 3D driven superconducting vortex systems with random disorder, a variety of phases that are distinct from those found in 2D systems arise depending on the material anisotropy and the pinning strength (Chen and Hu, 2003; Olson *et al.*, 2000; Reichhardt and Reichhardt, 2017; Zhao *et al.*, 2016). In particular, the 3D vortex sys-

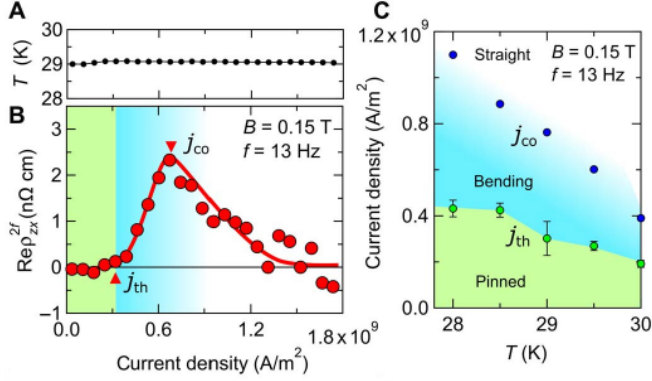


FIG. 40 Results from Hall measurements of 3D skyrmions in MnSi thin-plate samples (Yokouchi *et al.*, 2018). (a) Sample temperature  $T$  and (b) the real part of the second-harmonic Hall resistivity,  $\text{Re } \rho_{zx}^{2f}$ , vs driving current density measured at a frequency of  $f = 13$  Hz. (c) Dynamic phase diagram as a function of current density vs temperature  $T$  showing regions where the skyrmions are pinned (green), bending (blue), and straight (white). Reprinted under CC license from T. Yokouchi *et al.*, Science Adv. **4**, eaat1115 (2018).

tem often shows signatures of dynamical first order phase transitions (Chen and Hu, 2003; Olson *et al.*, 2000; Reichhardt and Reichhardt, 2017), observable as sharp jumps and hysteresis in the velocity-force curves. Similar effects could occur in skyrmion systems. Driven 3D skyrmions moving over quenched disorder could also exhibit unusual behavior such as the proliferation of monopoles in driven phases when the skyrmions break or cut (Lin and Saxena, 2016; Milde *et al.*, 2013; Schütte and Rosch, 2014; Zhang *et al.*, 2016d).

In transport experiments, Yokouchi *et al.* (Yokouchi *et al.*, 2018) examined the current-induced skyrmion motion in MnSi and found strong nonlinear signatures above the threshold current. These effects are reduced at higher drives. Figure 40(b) shows the real part of the second-harmonic Hall resistivity  $\text{Re } \rho_{zx}^{2f}$  versus current density at a fixed magnetic field. It was argued that the peak in  $\text{Re } \rho_{zx}^{2f}$  arises from the bending of the skyrmion strings just above the depinning threshold. Such bending occurs in an asymmetric manner due to the creation of a nonequilibrium or nonlinear Hall response by the DMI. At higher drives, the skyrmions become straighter and the effect is reduced. The features in  $\text{Re } \rho_{zx}^{2f}$  can be used to construct the dynamical phase diagram shown in Fig. 40(c). A pinned phase appears below the threshold current  $j_{\text{th}}$ , while the current at which the skyrmion string transitions from bent to straight is labeled  $j_{\text{co}}$ . As the temperature increases,  $j_{\text{th}}$  decreases since thermal activation makes it easier for the skyrmions to jump out of the pinning sites. There is also some experimental evidence for the unwinding of skyrmion strings in 3D systems under repeated drive pulses (Kagawa *et al.*, 2017). Pinning could be playing a role in this process since a partially unwound

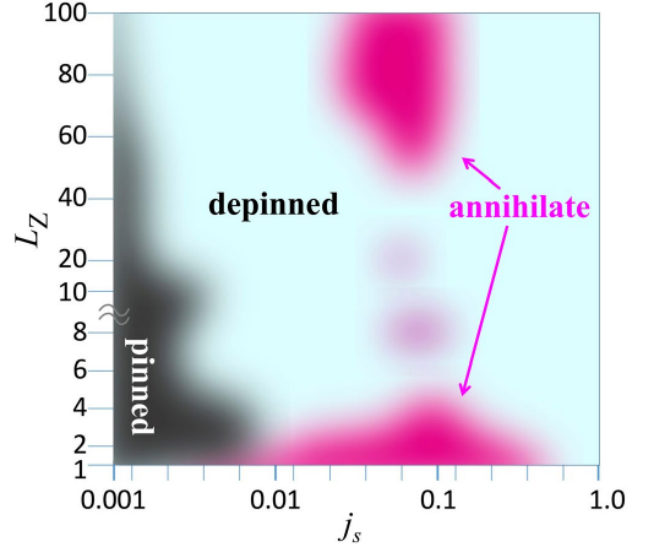


FIG. 41 Dynamic phase diagram from numerical simulations of skyrmion strings as a function of  $L_z$ , the thickness of the 3D system, vs  $j_s$ , the applied current density (Koshibae and Nagaosa, 2019). Reprinted under CC license from W. Koshibae and N. Nagaosa, Sci. Rep. **9**, 5111 (2019).

string can become trapped by the disorder during the intervals between driving pulses.

Koshibae and Nagaosa (Koshibae and Nagaosa, 2019) numerically studied a skyrmion string driven through random disorder in a 3D system for varying sample thicknesses and identified a pinned regime, a moving skyrmion regime, and regions of skyrmion string annihilation. Interestingly, they found that current-induced skyrmion annihilation occurs at a finite current for thin and thick samples, but not for samples of intermediate thicknesses, indicating that there is an optimal sample length for skyrmion stability. Figure 41 shows a dynamic phase diagram for the skyrmion string as a function of sample thickness  $L_z$  versus applied current. The extent of the pinned regime decreases with increasing  $L_z$ , meaning that it is more difficult to pin long 3D skyrmion strings than 2D skyrmions. This is in agreement with experimental observations in which the depinning threshold is low in bulk samples but high in thin films. In the regime where skyrmion annihilation does not occur, the skyrmions show pronounced roughening at low currents but become straighter at higher drives, similar to the dynamic ordering transition observed in 2D driven skyrmion assemblies with disorder (Koshibae and Nagaosa, 2018).



## F. Further Directions for Dynamic Skyrmion Phases with Random Disorder

There are many future directions for studying the collective dynamics of skyrmions with random disorder, including noise analysis, imaging, neutron scattering, or other experimental probes. Of highest priority is developing a method to obtain clear transport measures using a topological Hall effect or other signal that would allow access to the dynamics on size and time scales beyond what is possible in imaging measurements. A straightforward analysis of such transport curves could be used to determine when the skyrmions have depinned, whether they are undergoing elastic or plastic flow, and whether they pass through drive-induced transitions such as dynamical reordering, skyrmion annihilation, or skyrmion creation. This is in analogy to the fact that for driven vortices in type-II superconductors, the boundaries between different dynamic phases can generally be deduced from transport measurements alone. It would also be interesting to explore the time required for a skyrmion system to relax after a single or repeated driving pulse is applied. For example, if the skyrmions are subjected to a small ac drive, they will undergo some spiraling motion, and there could be a crossover in the response depending on whether the size of this spiral is larger or smaller than the effective dimension of the pinning or disorder sites in the sample. The addition of ac driving could also strongly influence the dc depinning threshold, and Jin *et al.* (Jin *et al.*, 2020) have found numerical evidence that an ac drive can substantially lower the dc threshold for the motion of antiferromagnetic skyrmions.

The role of boundaries is also of interest, since sample edges can be associated with the injection or annihilation of skyrmions or the presence of nonuniform edge currents. One method for eliminating edges is to consider a Corbino geometry in which the skyrmions circulate around the sample rather than entering from the edges. This geometry has been used to study vortex dynamics in type-II superconductors in the absence of edge contamination. Most work on skyrmion dynamics has been performed using dc driving; however, there should be a range of unique dynamics that can be accessed with ac driving, which could also substantially reduce the role of the sample edges. Measurements of the ac susceptibility could detect different types of dynamical response that are associated with specific frequencies, such as a pinning frequency in which each skyrmion is only oscillating within a pinning site instead of entering or exiting the pinning, or a characteristic washboard frequency that can be excited when the skyrmions are flowing elastically. There should be many different ways to observe different types of avalanche behavior in skyrmions as well. For example, if the direction of the magnetic field is changed, 3D skyrmion lines would have to reorient, and if pinning is present, this process could occur in a series of jumps

instead of the smooth behavior expected in the absence of pinning. If temperature is relevant, a finite drive could be applied below the depinning threshold in order to observe thermally activated avalanches. It would also be interesting to apply a global current simultaneously with local excitations such as local heating or a local probe to see whether large scale rearrangements of the skyrmions could be induced by a local perturbation.

Beyond 2D and 3D line-like skyrmions, unique dynamics should appear for 3D skyrmion hedgehog lattices (Fujishiro *et al.*, 2019; Lin and Batista, 2018), which could provide one of the first realizations of the depinning of a 3D particle-like lattice. This type of 3D system could be used to study inhomogeneous pinning, such as a sample in which pinning is present at the top but not at the bottom, making it possible to create a transformer geometry in a uniform field. The effects of temperature can also be explored. It is possible that near the skyrmion melting transition, there could be a divergence in the amplitude of the drive required to dynamically order the skyrmion lattice, similar to what is found in vortex systems (Koshelev and Vinokur, 1994). Both 3D skyrmion lines and point particle skyrmions could exhibit a peak effect (Banerjee *et al.*, 2000; Bhattacharya and Higgins, 1993; Cha and Fertig, 1998; Toft-Petersen *et al.*, 2018) in which the depinning threshold current strongly increases when the skyrmions transition from 3D lines to broken lines or from a 3D point particle lattice to a 3D glass. Such a peak effect could also occur as a function of drive in the form of a reentrant pinning effect, where the skyrmions form mobile straight lines at low drives, but break apart or disorder at higher drives and become pinned again.

Metastability and memory effects associated with dynamical phases are common features in other systems that exhibit depinning (Henderson *et al.*, 1996; Olson *et al.*, 2003; Paltiel *et al.*, 2000; Xiao *et al.*, 1999). Such effects can produce hysteresis in the velocity force curves or persistent memory between driving pulses that generates an increasing or decreasing response depending on the pulse duration. Memory effects could be observed by initializing skyrmions in either a metastable ordered or metastable disordered state, applying a series of drive pulses, and determining whether the metastable state gradually transitions to a stable state, similar to what has been observed for metastable states in type-II superconducting vortices (Olson *et al.*, 2003; Paltiel *et al.*, 2000; Pasquini *et al.*, 2008). Even if one skyrmion phase has a much lower equilibrium energy, when pinning is present the skyrmions may be trapped in a different phase due to the pinning barriers, so that only the application of a current gives the skyrmions access to the dynamics that will permit them to reach the low energy state. In this case, there could be a critical threshold drive that is required to destabilize the metastable state.

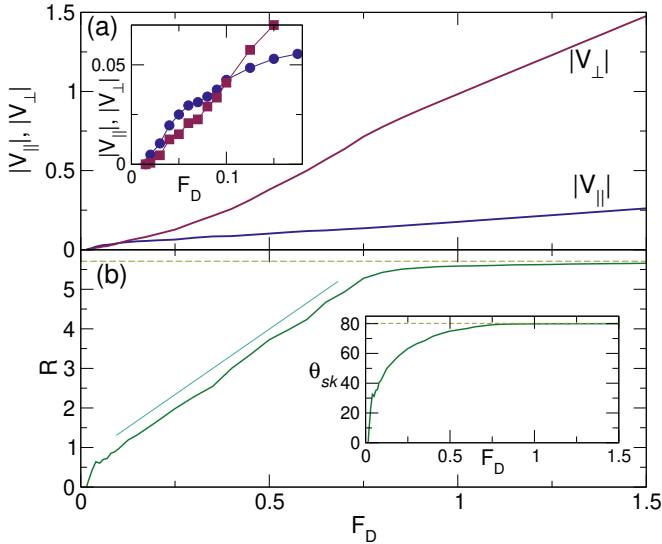


FIG. 42 Particle-based simulation measurements of the behavior of the skyrmion Hall angle  $\theta_{sk}$  for skyrmions driven over random disorder (Reichhardt and Reichhardt, 2016). (a) The skyrmion velocities in the directions parallel ( $|V_{\parallel}|$ , blue) and perpendicular ( $|V_{\perp}|$ , red) to the driving force vs  $F_D$ . Inset: a blowup of the main panel in the region just above depinning where there is a crossing of the velocity-force curves. (b) The corresponding  $R = |V_{\perp}/V_{\parallel}|$  vs  $F_D$ . The solid straight line is a linear fit and the dashed line is the clean limit value of  $R \approx 6.0$ . Inset:  $\theta_{sk} = \tan^{-1}(R)$  vs  $F_D$ . The dashed line is the clean limit value of  $\theta_{sk}$ . Reprinted under CC license from C. Reichhardt and C. J. O. Reichhardt, New J. Phys. 18, 095005 (2016).

## VII. PINNING AND THE SKYRMION HALL ANGLE

A skyrmion under an applied drive moves at an angle called the skyrmion Hall angle  $\theta_{SKH}$  with respect to the drive. This angle is proportional to the Magnus force, and in the absence of pinning, it is independent of the magnitude of the driving force (Nagaosa and Tokura, 2013; Zang *et al.*, 2011). Particle based simulations for skyrmions moving over random and periodic pinning showed that  $\theta_{SKH}$  is not constant but is nearly zero just at depinning and then increases with increasing drive before saturating at a value close to the intrinsic or pin-free value  $\theta_{SKH}^{int}$  at higher drives (Díaz *et al.*, 2017; Reichhardt *et al.*, 2015b,c; Reichhardt and Reichhardt, 2016). For a particle based simulation of a collection of skyrmions with  $\theta_{SKH}^{int} = 80.06^\circ$  driven over random pinning, Fig. 42(a) shows the average velocity in the directions parallel,  $|V_{\parallel}|$ , and perpendicular,  $|V_{\perp}|$ , to the drive versus driving force  $F_D$  (Reichhardt and Reichhardt, 2016). The corresponding ratio  $R = |V_{\perp}/V_{\parallel}|$  along with  $\theta_{SKH} = \tan^{-1}(R)$  appear in Fig. 42(b), where the dashed lines are the expected values of each quantity in the pin-free limit. The inset of Fig. 42(a) shows that there is a finite depinning threshold as well as a range of drives for which  $|V_{\parallel}| > |V_{\perp}|$ ; however, as the

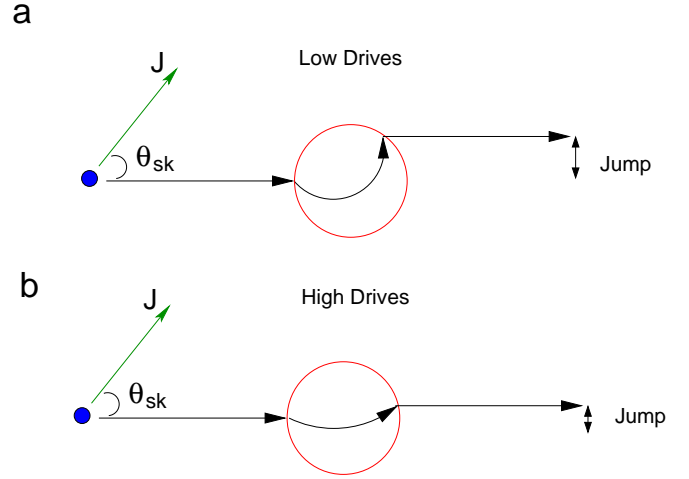


FIG. 43 A schematic illustration of how pinning can change the effective skyrmion Hall angle. The blue dot is the skyrmion and the red circle is the pinning site, while  $J$  is the direction of the applied current and  $\theta_{sk}$  is the intrinsic skyrmion Hall angle determining the direction in which the skyrmion moves with respect to the drive. (a) At low drives, the skyrmion executes a Magnus-induced orbital motion as it moves through the pinning site, leading to a side jump as the skyrmion exits the pinning site. The jump is in the direction of the current and therefore reduces the effective skyrmion Hall angle. (b) At higher drives, the skyrmion moves rapidly through the pinning site, so the magnitude of the side jump is strongly reduced.

drive increases,  $|V_{\perp}|$  grows more rapidly than  $|V_{\parallel}|$ , since the intrinsic Hall angle in the clean limit would give  $R = |V_{\perp}/V_{\parallel}| \approx 6$ . Figure 42(b) shows that over a wide range of drives,  $R$  increases roughly linearly with  $F_D$  up to  $F_D = 0.75$ , and then saturates close to its intrinsic value. As a result, at small drives the skyrmions move in the direction of the drive, but as the drive increases, they gradually develop a greater component of motion perpendicular to the drive, until at large drives they are moving along the direction of the intrinsic Hall angle. Over the drive interval in which  $R$  is linearly increasing with  $F_D$ , the skyrmions are moving plastically, while at higher drives when the skyrmions begin to move in a more coherent fashion,  $R$  starts to saturate. The same general behaviors are robust over a range of different intrinsic Hall angles, disorder strengths, and pinning densities, while when the Magnus force is zero,  $|V_{\perp}| = 0$  and  $\theta_{SKH} = 0$  for all values of  $F_D$  (Reichhardt and Reichhardt, 2016). For  $\theta_{SKH}^{int} < 50^\circ$ , the skyrmion Hall angle generally increases linearly with  $F_D$  since  $\tan^{-1}(x)$  can be expanded as  $\tan^{-1}(x) = x - x^3/3 + x^5/5 \dots$ . For small  $R$ , the first term dominates, while for  $\theta_{SKH}^{int} > 50^\circ$ , nonlinear effects appear in  $\theta_{SKH}$  with increasing  $F_D$ . In particle based simulation studies of skyrmion noise, the measured skyrmion Hall angle begins to saturate when the skyrmions begin to order, which is correlated with a reduction in the noise power (Díaz *et al.*, 2017).

The appearance of a drive dependent skyrmion Hall angle was also partially observed in continuum and Thiele equation based work by Müller *et al.* (Müller and Rosch, 2015) for a single skyrmion interacting with a single defect. A more extensive study of the evolution of  $\theta_{\text{SKH}}$  with drive was subsequently conducted using particle based simulations of skyrmion motion in a periodic pinning array (Reichhardt *et al.*, 2015c) and in random pinning (Reichhardt *et al.*, 2015b). In the work of Müller *et al.* (Müller and Rosch, 2015) and Reichhardt *et al.* (Reichhardt *et al.*, 2015b), the microscopic origin of the drive dependence of  $\theta_{\text{SKH}}$  was argued to be a side jump effect, as illustrated in Fig. 43. A skyrmion executes a Magnus-induced orbit as it moves through a pinning site, so that when the skyrmion leaves the pinning site, it has effectively jumped in the direction of the applied drive. Repeated jumps lower the effective skyrmion Hall angle compared to the pin-free situation. The motion of a skyrmion is similar to that of a charged particle in a magnetic field (Nagaosa and Tokura, 2013), and the skewed scattering of the skyrmion by a pinning site is similar to what is known as a side jump effect for electron scattering off magnetic defects, where an electron undergoes a sideways displacement when interacting with a potential as a result of spin-orbit interactions (Berger, 1970). As illustrated in Fig. 43(a), a more slowly moving skyrmion spends more time in the pinning site, resulting in a larger jump. At higher drives, when the skyrmion is moving faster, the jump is smaller and the measured skyrmion Hall angle is closer to the defect-free value, while at the highest drives, the skyrmions move so rapidly through the pinning sites that there is hardly any jump. This is illustrated in Fig. 43(b), which corresponds to the saturation of  $\theta_{\text{SKH}}$  at higher drives as observed in simulation (Díaz *et al.*, 2017; Reichhardt *et al.*, 2015b,c; Reichhardt and Reichhardt, 2016). The size of the jump is also determined by which side of the pinning site the skyrmion approaches, so that for an ensemble of different impact parameters, strongly asymmetric jumps appear as demonstrated for a single skyrmion moving through a pinning site (Reichhardt *et al.*, 2015c). This same work showed that when the Magnus force is zero, the particle can still experience a jump as it moves through the pinning site, but the jump is symmetric as a function of impact parameter, so that in the ensemble average, there is no net jump.

Fernandes *et al.* (Fernandes *et al.*, 2020) used multiscale simulations to examine the deflections of skyrmions interacting with single atom defects consisting of a Pd layer deposited on an Fe/Ir(111) surface. At low driving currents in Fig. 44(a), the trajectories indicate that the skyrmions become trapped at the defect site, while in Fig. 44(b), the driving currents are high enough that the skyrmions can escape from the defect site but experience a trajectory deflection. The magnitude of the deflection decreases as the skyrmion velocity increases. If the dis-

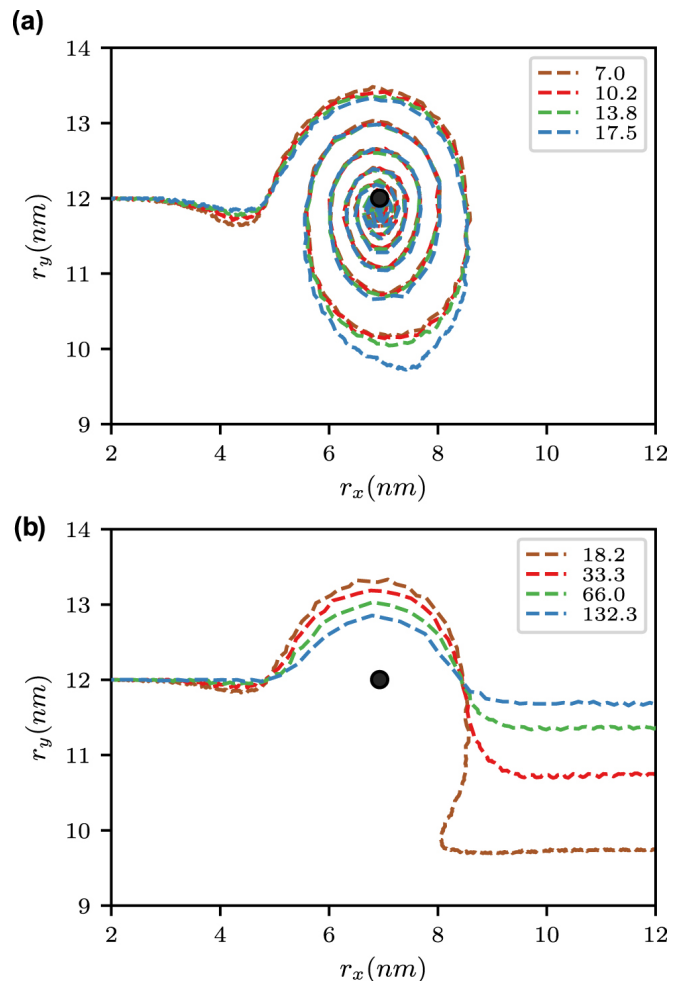


FIG. 44 Multiscale simulations of the trajectories of skyrmions scattering from a defect site consisting of a single atom (Fernandes *et al.*, 2020). The black circle indicates the position of the defect. (a) For low driving currents, the skyrmions are pinned. (b) For higher driving currents, the skyrmions can escape from the defect but their trajectories are deflected. The magnitude of the deflection decreases as the driving current increases. Reprinted under CC license from I. L. Fernandes *et al.*, *J. Phys.: Condens. Matter* **32**, 425802 (2020).

order site is repulsive rather than attractive, skyrmions are deflected in the opposite direction as they pass the defect. This work also showed that the Thiele equation approach is a reasonable approximation for capturing the skyrmion dynamics.

Jiang *et al.* (Jiang *et al.*, 2017b) performed imaging experiments of current driven skyrmions in which they could observe the drive dependence of the skyrmion Hall angle. The skyrmion motion could not be detected by any changes in the topological Hall effect but was instead deduced from the images. As illustrated in Fig. 45, four dynamical regimes appear: a pinned state at low drives, a state with finite skyrmion velocity but zero skyrmion Hall angle, a region in which the skyrmion Hall angle

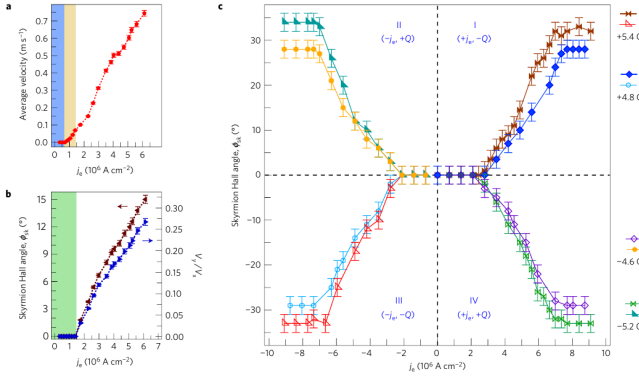


FIG. 45 Skymion velocity and skyrmion Hall angle obtained from direct imaging of the skyrmion motion (Jiang *et al.*, 2017b). (a) Average skyrmion velocity vs current density  $j_e$  showing a pinned regime of no motion (blue) and a region in which the skyrmions are moving at zero skyrmion Hall angle (orange). (b) The corresponding skyrmion Hall angle vs  $j_e$ . (c) The skyrmion Hall angle for both positive and negative driving currents  $j_e$  under both positive and negative applied magnetic fields. In each case, the skyrmion Hall angle saturates for sufficiently large magnitudes of the driving current. Reprinted by permission from: Springer Nature, “Direct observation of the skyrmion Hall effect”, Nature Phys. **13**, 162 (2017), W. Jiang *et al.*, ©2017.

increases linearly with drive, and a high drive regime in which the skyrmion Hall angle saturates to the clean limit of  $\theta_{\text{SKH}} = 30^\circ$ . The general trend is very similar to what is observed in the particle based simulations (Reichhardt *et al.*, 2015b,c; Reichhardt and Reichhardt, 2016). It would be interesting to consider a system in which the skyrmion Hall angle could be measured directly and compared to a changing topological Hall effect, since both the velocity of the skyrmion as well as the direction of skyrmion motion need to be taken into account when the magnitude of the topological Hall effect versus drive is measured.

Litzius *et al.* (Litzius *et al.*, 2017) studied skyrmions under a pulsed drive in the forward and backward directions. By obtaining images as a function of increasing drive amplitude, they constructed the skyrmion Hall angle versus current curve shown in Fig. 46. Here,  $\theta_{\text{SKH}}$  is initially low and increases with increasing drive, ultimately reaching a value close to  $\theta_{\text{SKH}} = 40^\circ$ . Imaging experiments in ferromagnetic systems (Woo *et al.*, 2018) also show a similar increase in the skyrmion Hall angle with drive. Litzius *et al.* (Litzius *et al.*, 2017) argued that the change of the skyrmion Hall angle was due to the ability of the skyrmion to change its shape or size with the applied current, rather than the side jump effect observed in the particle-based models. Using micromagnetic simulations, Tomasello *et al.* found that breathing modes of moving skyrmions excited by a current could lead to a change in the skyrmion Hall angle as a function of drive in the absence of pinning

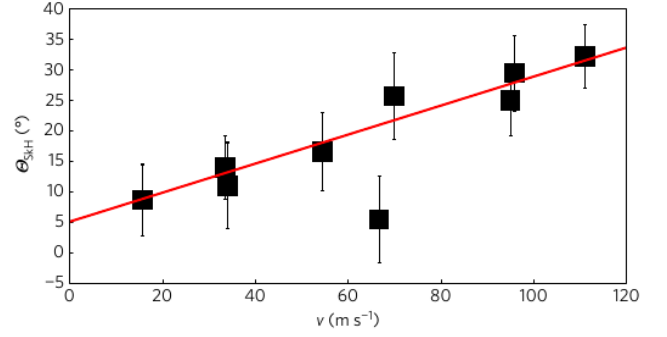


FIG. 46 Image-based experimental measurements of skyrmion Hall angle  $\theta_{\text{SKH}}$  versus skyrmion velocity  $v$  (Litzius *et al.*, 2017), showing a linear dependence. Reprinted by permission from: Springer Nature, “Skyrmion Hall effect revealed by direct time-resolved X-ray microscopy”, Nature Phys. **13**, 170 (2017), K. Litzius *et al.*, ©2017.

(Tomasello *et al.*, 2018). More recent studies by Litzius *et al.* provide evidence that there can be a high current pinning dominated regime as well as another regime in which excitations change the skyrmion Hall angle, giving rise to different scaling regimes as a function of drive (Litzius *et al.*, 2020). Current-driven studies of thin-film skyrmions in the 100 nm size range at speeds of up to 100 m/s reveal a strong dependence of the skyrmion Hall angle on drive, with an increase in the skyrmion Hall angle to a high velocity saturation value of  $\theta_{\text{SKH}} = 55^\circ$  (Juge *et al.*, 2019). The experimental observations match the continuum modeling well, showing a constant  $\theta_{\text{SKH}}$  in the absence of quenched disorder and both a finite depinning threshold and an increase of  $\theta_{\text{SKH}}$  up to a saturation value in the presence of pinning. Although this work showed that there were strong shape changes of the skyrmions due to the current in the absence of disorder, the authors argued that the changes in the skyrmion Hall angle were due to the pinning rather than to the shape fluctuations. Yu *et al.* (Yu *et al.*, 2020) investigated the motion and skyrmion Hall effect of individual and small clusters of 80 nm skyrmions in FeGe systems with low currents of  $0.96 \times 10^9$  to  $1.92 \times 10^9$  A m<sup>-2</sup>. They found an interesting effect in which a skyrmion cluster can undergo rotation as it translates. This suggests that the Magnus force can induce unusual dynamics in clusters of moving skyrmions. Zhang *et al.* imaged the motion of half skyrmions, which have a skyrmion Hall angle that is half as large as that of a full skyrmion (Zhang *et al.*, 2020). Other experiments found that shape distortions of half skyrmions could further reduce the skyrmion Hall angle (Yang *et al.*, 2020).

Most of the the experiments performed so far have been in the single or few skyrmion limit, so it would be interesting to understand what happens in the collective or lattice limit. Beyond side jump effects, it may be possible that the pinning is effectively increasing the damping

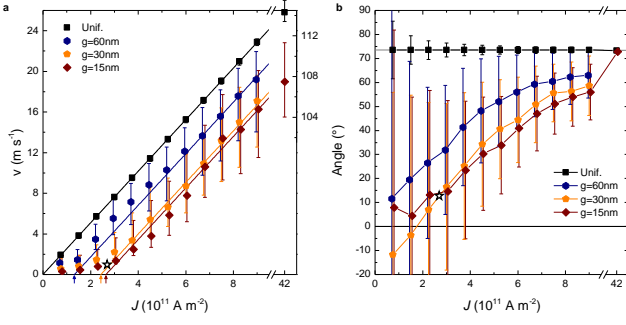


FIG. 47 Continuum simulations of skyrmion motion through a disordered landscape composed of grains of different sizes  $g$  (Legrand *et al.*, 2017). (a) Mean skyrmion velocity  $v$  vs driving current  $J$  showing a finite depinning threshold. (b) Skyrmion Hall angle vs  $J$  showing that the angle increases with increasing  $J$  from a value near zero at zero current. Reprinted with permission from W. Legrand *et al.*, Nano Lett. **17**, 2703 (2017). Copyright 2017 American Chemical Society.

on the skyrmions through some other mechanism. Since  $\theta_{\text{SKH}} \propto \tan^{-1}(\alpha_m/\alpha_d)$ , if  $\alpha_d$  is itself drive dependent, this could produce a drive dependence of  $\theta_{\text{SKH}}$ .

Several continuum-based simulations have shown a drive dependence of the skyrmion Hall angle as a function of pinning (Juge *et al.*, 2019; Kim and Yoo, 2017; Legrand *et al.*, 2017). Legrand *et al.* (Legrand *et al.*, 2017) considered pinning produced by grain boundaries, where small dense grains correspond to strong pinning. In this study, a clean system has no depinning threshold and the skyrmion Hall angle is constant, while when pinning is present, there is a finite depinning threshold and the skyrmion Hall angle is initially small and increases until reaching a saturation value, as shown in Fig. 47. This work also indicated that there is an optimal grain size for pinning, meaning that the relative size of the skyrmions and the pinning sites is important, which would be another interesting effect to study more fully. The optimal grain size could be the result of a resonance or commensuration effect, where optimal pinning occurs when the size of the pinning matches the size of the skyrmion. Due to the limited number of skyrmions simulated, the  $\theta_{\text{SKH}}$  versus drive curves contain considerable scattering. It may be possible that there are multiple regimes for  $\theta_{\text{SKH}}$  rather than only a linearly increasing regime and a saturation regime, which offers another avenue for future study. Numerical work by Juge *et al.* (Juge *et al.*, 2019) produced results similar to those of Legrand *et al.* (Legrand *et al.*, 2017), but the scattering in the data was much smaller. In these works, the skyrmion trajectories in regimes with increasing  $\theta_{\text{SKH}}$  are similar to those observed in particle based simulations (Reichhardt and Reichhardt, 2016), with a coexistence of pinned and moving skyrmions. Similar dynamics were observed in the imaging experiments of Montoya *et al.* (Montoya *et al.*, 2018). In the continuum simulations, at

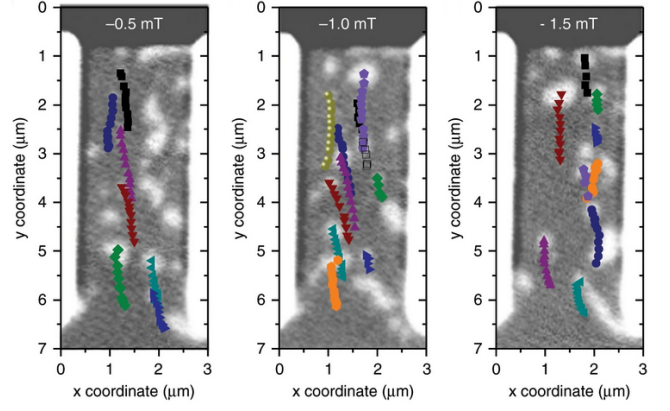


FIG. 48 Images of skyrmion motion in a multilayer system at varied magnetic fields (Zeissler *et al.*, 2020). In each case, the skyrmion Hall angle is close to  $\theta_{\text{SKH}} = 10^\circ$ . As the field is varied, the size of the skyrmion changes, so this result indicates that the skyrmion Hall angle is independent of the skyrmion diameter. Reprinted under CC license from K. Zeissler *et al.*, Nature Commun. **11**, 428 (2020).

higher drives the skyrmions moved in fairly straight trajectories along a direction close to that of the intrinsic Hall angle (Legrand *et al.*, 2017). Kim *et al.* (Kim and Yoo, 2017) performed continuum simulations that also showed a similar drive dependence of the skyrmion Hall angle.

Another question is the role of the skyrmion diameter in determining the skyrmion Hall angle. Zeissler *et al.* (Zeissler *et al.*, 2020) examined skyrmions in a magnetic multilayer under a pulsed drive and found that the skyrmion Hall angle was close to  $10^\circ$  and was independent of the diameter of the skyrmions. Figure 48 shows some of the skyrmion trajectories at varied fields, where the skyrmion diameter increases as the magnitude of the magnetic field increases but the direction of motion does not change. This work also revealed that the skyrmion trajectories are deflected by contact with disorder sites. In this case it may be possible that the disorder length scale is much larger than the skyrmion diameters, placing the system in a pinning dominated regime (Reichhardt and Reichhardt, 2020). It would be interesting to perform a separate study of the skyrmion Hall angle for varied disorder sizes to see if a change occurs when the effective pinning diameter becomes smaller rather than larger than the size of the skyrmions.

There have been numerous studies of skyrmions moving in samples with magnetic grain boundaries which show that in some cases, the disorder can enhance the skyrmion Hall angle (Salimath *et al.*, 2019). This occurs when the grains are magnetically aligned in the direction in which the skyrmions would move in the absence of disorder, creating a guidance effect in the direction of the intrinsic skyrmion Hall angle. This effect depends on the magnitude of the drive and the orientation of the grains,

but it suggests that it would be possible to control the skyrmion Hall angle through the proper orientation of extended defects.

The drive dependence of the skyrmion Hall angle indicates that a wealth of new dynamical effects can arise that are distinct from those found in previously studied overdamped systems. For example, when a skyrmion is driven over a periodic pinning array, the skyrmion Hall angle increases with drive but becomes quantized due to locking with certain symmetry angles of the periodic substrate (Reichhardt *et al.*, 2015c). Until now, the modification of the skyrmion Hall angle by pinning has only been studied for ferromagnetic skyrmions, so it would be interesting to study antiferromagnetic skyrmions, polar skyrmions, skyrmionium, antiskyrmions, and merons to see whether the effect of pinning differs depending on the nature of the skyrmion.

The antiferromagnetic skyrmion would be particularly interesting since it should have  $\theta_{\text{SkH}} = 0$  and, in principle, its dynamics would be very similar to those of vortices in superconductors. If the antiferromagnetic skyrmion is interacting with magnetic defects or magnetic pinning, then a finite skyrmion Hall effect could arise due to a side jump effect. It would also be interesting to see whether the lack of a Magnus force would lead to stronger pinning effects compared to ferromagnetic skyrmions. The skyrmion Hall angle can also be controlled using various other methods, such as internal modes (Chen *et al.*, 2019; Tomasello *et al.*, 2018), that can change and even vanish at the angular momentum compensation temperature (Hirata *et al.*, 2019), or by applying particular configurations of gate voltages (Plettenberg *et al.*, 2020). In such cases, pinning would still play a role in the dynamics, and this area is open for further investigation.

### A. Thermal Effects

Experimental observations of the skyrmion Hall effect have generally been performed at room temperature, and there are numerous indications that skyrmions can exhibit thermal effects such as Brownian motion (Nozaki *et al.*, 2019; Zázvorka *et al.*, 2019; Zhao *et al.*, 2020), which would make creep effects and thermally activated hopping from one pinning well to the next an important process. It is interesting to ask how the depinning threshold and skyrmion Hall angle behave under the combination of both pinning and temperature. Troncoso and Núñez (Troncoso and Núñez, 2014) theoretically studied thermally assisted current driven skyrmion motion in the presence of pinning, and found that the Brownian motion could be described by a stochastic Thiele equation. They observed a finite depinning threshold at zero temperature as well as a creep regime for increasing drive, as shown in Fig. 49. Reichhardt *et al.* (Reichhardt and Reichhardt, 2019b) studied the depinning of skyrmions in

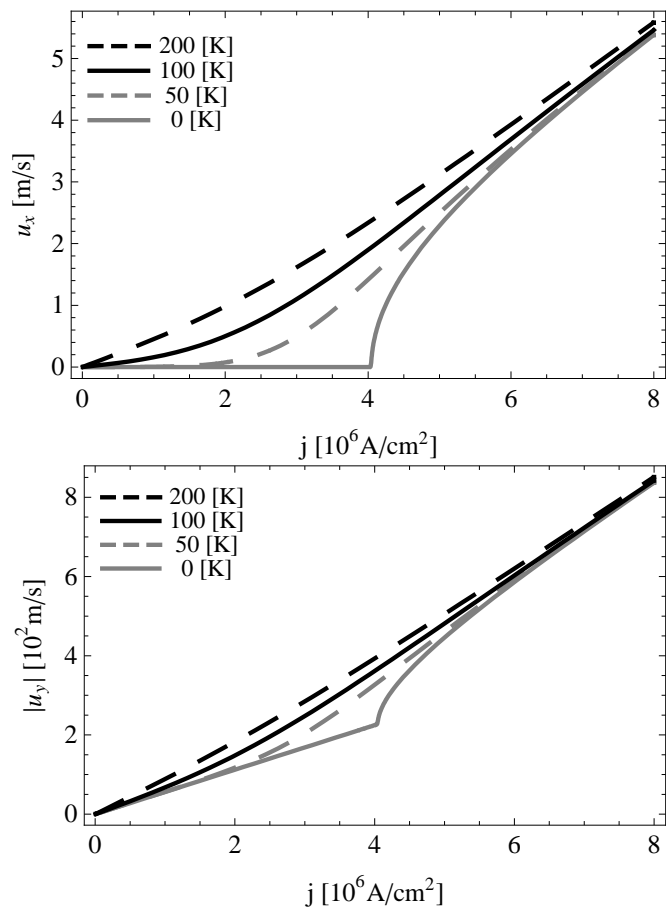


FIG. 49 Theoretical predictions for skyrmion velocity response at different temperatures, showing the existence of a creep regime below the zero-temperature depinning threshold (Troncoso and Núñez, 2014). Top panel: longitudinal velocity  $u_x$  vs driving current  $j$ ; bottom panel: transverse velocity  $u_y$  vs driving current  $j$ . Reprinted with permission from R. E. Troncoso and A. S. Núñez, Phys. Rev. B **89**, 224403 (2014). Copyright 2014 by the American Physical Society.

random disorder for increasing thermal effects in the elastic depinning regime, where the skyrmions maintain the same neighbors. At  $T = 0$  there is a well defined depinning threshold, while for increasing temperature, the depinning threshold decreases and becomes more rounded. The motion in this case can be divided into a pinned phase, an intermittent or thermally activated avalanche phase, and a high drive continuously moving phase. Figure 50(a) illustrates the measured skyrmion Hall angle  $\theta_{\text{SkH}}$  versus drive for a system at finite temperature where there is appreciable creep, and Fig. 50(b) shows  $\langle V_{\parallel} \rangle$  and  $\langle V_{\perp} \rangle$  versus  $F_D$ . There is a pinned regime with  $\langle V_{\parallel} \rangle = \langle V_{\perp} \rangle = 0$ , a creep regime with finite  $\langle V_{\parallel} \rangle$  and  $\langle V_{\perp} \rangle = 0$ , giving a skyrmion Hall angle of zero, and a flow regime in which the velocity is finite in both directions. In the latter region, the skyrmion Hall angle increases with drive and eventually saturates at the high drive limit. The appearance of a regime in which there is

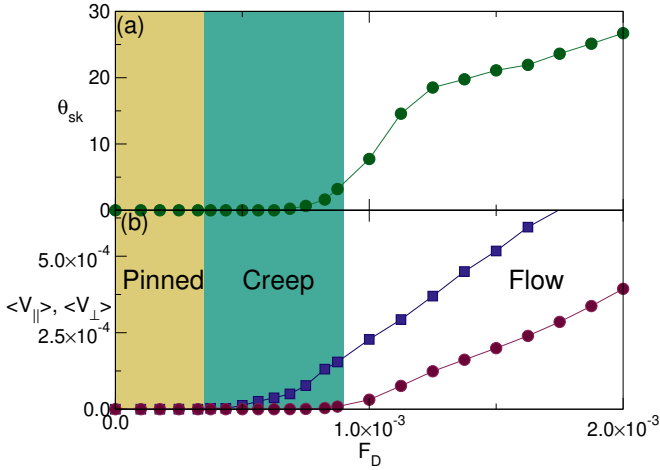


FIG. 50 Particle-based simulations of skyrmion motion with finite thermal fluctuations (Reichhardt and Reichhardt, 2019b). (a) The skyrmion Hall angle  $\theta_{sk}$  vs driving force  $F_D$ . (b) The corresponding skyrmion velocity parallel ( $\langle V_{\parallel} \rangle$ ) (blue squares) and perpendicular ( $\langle V_{\perp} \rangle$ ) (red circles) to the drive vs  $F_D$ . There is a pinned phase (yellow), a creep phase in which  $\theta_{sk}$  is close to zero (green), and a flowing phase. Republished with permission of IOP Publishing, Ltd, from “Thermal creep and the skyrmion Hall angle in driven skyrmion crystals”, C. Reichhardt and C. J. O. Reichhardt, *J. Phys.: Condens. Matter* **31**, 07LT01 (2019); permission conveyed through Copyright Clearance Center, Inc.

a finite longitudinal velocity but zero perpendicular velocity is also consistent with the observations of Jiang *et al.* just above depinning (Jiang *et al.*, 2017b).

The behavior of the skyrmion Hall angle with creep suggests that there could be multiple regimes for the evolution of  $\theta_{SKH}$  with current and velocity. Litzius *et al.* (Litzius *et al.*, 2020) studied the impact of thermal fluctuations on  $\theta_{SKH}$  in both experiment and simulations, and found distinct behaviors in the low and high current regimes. At lower currents and velocities,  $\theta_{SKH}$  increases rapidly with current, and at higher drives there is a crossover to a slower increase with current. It was argued that at low drives, the skyrmion behaves more like a particle so that  $\theta_{SKH}$  is controlled by the thermal disorder, whereas at higher drives, the internal degrees of freedom of the skyrmion become important and  $\theta_{SKH}$  is controlled by the distortions or changes of shape of the skyrmions. As shown in Fig. 51, where the skyrmion Hall angle  $\theta_{SKH}$  is plotted as a function of the skyrmion velocity  $v$  (Litzius *et al.*, 2020), the results of continuum-based simulations are consistent with experiment. In the absence of thermal disorder, there is very little change in  $\theta_{SKH}$  with velocity except at the highest values of  $v$ , where  $\theta_{SKH}$  increases slightly. When thermal disorder is present, there is a sharp increase in  $\theta_{SKH}$  at low velocities rolling over to a more gradual increase at higher velocities. The images in the insets of Fig. 51 indicate that the skyrmion becomes more distorted in shape as the veloc-

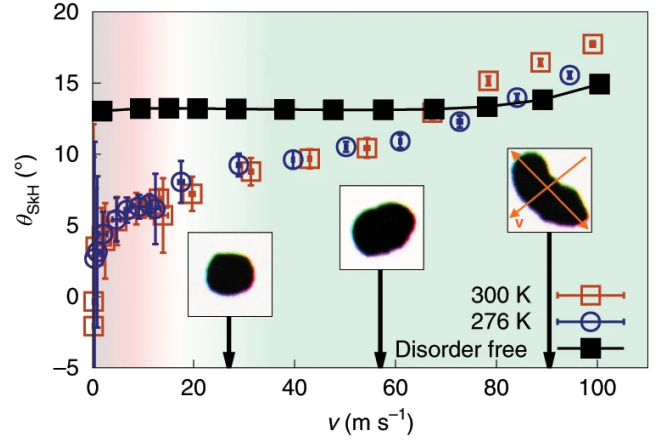


FIG. 51 Continuum simulations of the skyrmion Hall angle  $\theta_{SKH}$  versus skyrmion velocity  $v$  in a sample with no thermal disorder (black squares) and at two different finite temperatures (open symbols).  $\theta_{SKH}$  is nearly independent of velocity in the absence of temperature, but when thermal fluctuations are present,  $\theta_{SKH}$  increases with increasing velocity. The insets show the change in skyrmion shape from nearly circular at low velocities to strongly distorted at high velocities. Reprinted by permission from: Springer Nature, “The role of temperature and drive current in skyrmion dynamics,” *Nature Electron.* **3**, 30 (2020), K. Litzius *et al.*, ©2020.

ity increases. MacKinnon *et al.* (MacKinnon *et al.*, 2020) examined the role of additional interfacial spin transfer torques on driven skyrmion motion and found that it can strongly reduce the skyrmion Hall angle for skyrmion diameters that are less than 100 nm. They also observed that when disorder is present,  $\theta_{SKH}$  increases rapidly at low velocities and then increases more slowly or saturates at high velocities.

There have also been numerical studies examining the shape distortions of skyrmions at higher drives (Masell *et al.*, 2020), where the skyrmions can start developing a non-circular shape with a tail. Here there is a critical current above which the skyrmion becomes unstable. It is possible that for dense skyrmion lattices at higher currents, lattice transitions could occur due to the shape changes of the skyrmions, which could cause the skyrmion-skyrmion interactions to become more anisotropic.

## B. Future Directions

It would be interesting to examine the evolution of the skyrmion Hall angle for different types of pinning, such as short range versus long range, repulsive versus attractive, or grain boundary and extended pinning versus point pinning. Since the skyrmion Hall angle is often considered detrimental to applications, it may be possible to identify pinning or defect arrangements that reduce  $\theta_{SKH}$ , or there might even be ways to exploit the behavior of  $\theta_{SKH}$

to create new devices. The skyrmion Hall angle can also depend strongly on the skyrmion type. For example, in certain regimes  $\theta_{\text{SkH}}$  is affected by the direction of the applied current with respect to an anisotropy direction contained within the skyrmion itself, meaning that due to their anisotropy, antiskyrmions could have a rich behavior under a drive in the presence of pinning (Kovalev and Sandhoefner, 2018). Most studies have been performed using dc drives, but it would also be possible to add a high frequency ac drive component which could create breathing modes that might reduce the pinning, increase the creep, or change the skyrmion Hall angle.

Existing studies of pinning effects and the dynamical motion of skyrmions have focused on 2D systems; however, there should be a variety of interesting new effects in 3D systems. Line-like skyrmions could undergo elastic depinning of the type found for stringlike objects, but could have distinct modes of motion along the length of the line. There have already been several studies of the scaling of certain modes in 3D skyrmions (Lin *et al.*, 2019; Seki *et al.*, 2020). It would also be possible to study the roughening transition of the skyrmion lines near depinning and to analyze whether the skyrmions become more stringlike at higher drives based on changes in the fractal dimension. The skyrmions might maintain their linelike nature but become entangled, similar to entangled vortex states, and the entangled skyrmions could cut themselves free or be unable to cut and remain tangled.

Skyrmion dynamic phases and the evolution of the skyrmion Hall angle have been studied for drives arising from an applied current. It would be useful to understand whether similar or different effects occur for skyrmions subjected to different types of driving, such as thermal gradients or magnetic gradients. Existing studies have focused on uniform drives; however, introduction of nonuniform drives could produce interesting effects due to the velocity dependence of the skyrmion Hall angle. A system with a non-uniform current could exhibit clustering or other types of new effects not found in overdamped systems.

## VIII. NANOSTRUCTURED AND PERIODIC LANDSCAPES

There are already a number of proposals for using skyrmions in race track devices, which are highly confined geometries for the skyrmion. Another route for generating controlled skyrmion motion is to fabricate nanostructured pinning arrays, similar to those employed for vortices in type-II superconductors (Baert *et al.*, 1995; Berdiyrov *et al.*, 2006; Harada *et al.*, 1996; Martín *et al.*, 1997; Reichhardt *et al.*, 1998; Reichhardt and Reichhardt, 2017), vortices in Bose-Einstein condensates with optical traps (Reijnders and Duine, 2004; Tung *et al.*, 2006), cold atoms (Benassi *et al.*, 2011; Büchler *et al.*,

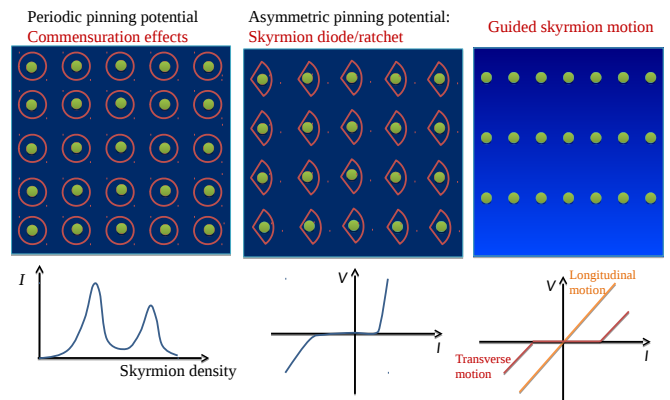


FIG. 52 Examples of skyrmions interacting with different types of nanostructured pinning. Left: 2D periodic pinning, where commensuration effects between the number of skyrmions and the number of pinning sites can occur. Center: asymmetric 2D periodic pinning which can generate ratchet and diode effects. Right: 1D periodic pinning. The lower panels show schematic transport curves that could be observed with each pinning geometry.

2003) and colloidal particles (Brunner and Bechinger, 2002; Wei *et al.*, 1998). In these systems, the particles can interact with 1D periodic substrates (Dobrovolskiy and Huth, 2015; Le Thien *et al.*, 2016; Martinoli *et al.*, 1975; Reichhardt *et al.*, 2001; Reijnders and Duine, 2004; Wei *et al.*, 1998), 2D square (Baert *et al.*, 1995; Berdiyrov *et al.*, 2006; Bohlein *et al.*, 2012; Harada *et al.*, 1996; Reichhardt and Olson, 2002b; Reichhardt *et al.*, 1998; Tung *et al.*, 2006), triangular (Brunner and Bechinger, 2002; Reichhardt and Olson, 2002b; Reichhardt *et al.*, 1998), or quasicrystalline (Kemmler *et al.*, 2006; Mikhael *et al.*, 2008; Villegas *et al.*, 2006) substrates, or arrangements with geometric frustration (Latimer *et al.*, 2013; Libál *et al.*, 2009, 2006; Ortiz-Ambriz and Tierno, 2016; Wang *et al.*, 2018b). Figure 52 illustrates three such possible pinning geometries, including a 2D periodic array of trapping sites, a periodic 1D array, and an asymmetric 2D array that can generate diode or ratchet effects.

For assemblies of particles interacting with either 1D or 2D periodic substrates, commensuration effects (Bak, 1982) can occur in which the periodicity of the lattice matches with the periodicity of the substrate. The system exhibits strong pinning under these commensurate conditions since the particle-particle interaction forces cancel via symmetry and the entire ensemble of particles behaves similarly to an isolated particle, with no additional stress or strain in the lattice caused by defects. If, however, there is some lattice mismatch or an incommensuration is present, then collective interactions between the particles become important. For example, at a particle density that is slightly above commensuration, most of the particles are located at the potential energy minima of the substrate just as in the commensurate situation, but due to the incommensuration, a small number



of particles are located on higher energy portions of the substrate. Under an applied drive, these extra particles or kinks depin first at  $F_{c1}$ , while the rest of the particles depin at a higher drive  $F_{c2}$ , producing a two step or even multiple step depinning phenomenon (Avci *et al.*, 2010; Bak, 1982; Benassi *et al.*, 2011; Bohlein *et al.*, 2012; Gutierrez *et al.*, 2009; Reichhardt *et al.*, 1997). A similar effect occurs just below commensuration, where there are vacancies or anti-kinks that depin first (Bohlein *et al.*, 2012). The commensurate condition is met whenever the number of particles  $p$  is an integer multiple of the number of substrate potential minima  $q$ ,  $p/q = 1, 2 \dots N$ . At these integer matching fillings, there is a local maximum in the depinning threshold  $F_c$  (Baert *et al.*, 1995; Berdiy- orov *et al.*, 2006; Reichhardt *et al.*, 1997, 1998). There can also be fractional commensuration effects at fillings such as  $p/q = 1/2$  or  $1/3$ , and signatures of these fractional fillings depend on the symmetry of the underlying lattice (Bak, 1982; Grigorenko *et al.*, 2003). In quasiperiodic or frustrated substrates, other types of commensuration effects can arise at integer and non-integer matchings (Kemmler *et al.*, 2006; Latimer *et al.*, 2013; Villegas *et al.*, 2006; Wang *et al.*, 2018b). Under an applied drive, these systems can exhibit a rich variety of dynamical behaviors with well defined transitions between different kinds of plastic flow, turbulent flow, and ordered flow, and the extent and number of phases depends on the commensurability, pinning strength, and direction of drive with respect to the periodicity of the substrate (Avci *et al.*, 2010; Benassi *et al.*, 2011; Bohlein and Bechinger, 2012; Bohlein *et al.*, 2012; Dobrovolskiy and Huth, 2015; Gutierrez *et al.*, 2009; Harada *et al.*, 1996; Juniper *et al.*, 2015; Le Thien *et al.*, 2016; Martinoli *et al.*, 1975; Reichhardt *et al.*, 1997; Reichhardt and Olson Reichhardt, 2011; Wang *et al.*, 2018b).

Due to their particle-like nature, skyrmions are ideal candidates for studying commensurate and incommensurate effects on various types of substrate geometries. The interaction of skyrmions with periodic pinning could be potentially useful for creating new types of devices. Additionally, the Magnus force and the internal degrees of freedom could cause skyrmions to exhibit a variety of new types of static and dynamic commensurate phases which are distinct from those found for overdamped systems.

### A. One Dimensional Periodic Substrates and Speed-Up Effects

We first consider the simplest example consisting of a skyrmion interacting with the 1D pinning array illustrated in Fig. 53. The external driving can be applied either parallel or perpendicular to the substrate periodicity, and the system has very different dynamical responses depending on the driving direction. An overdamped system would only have a finite depinning

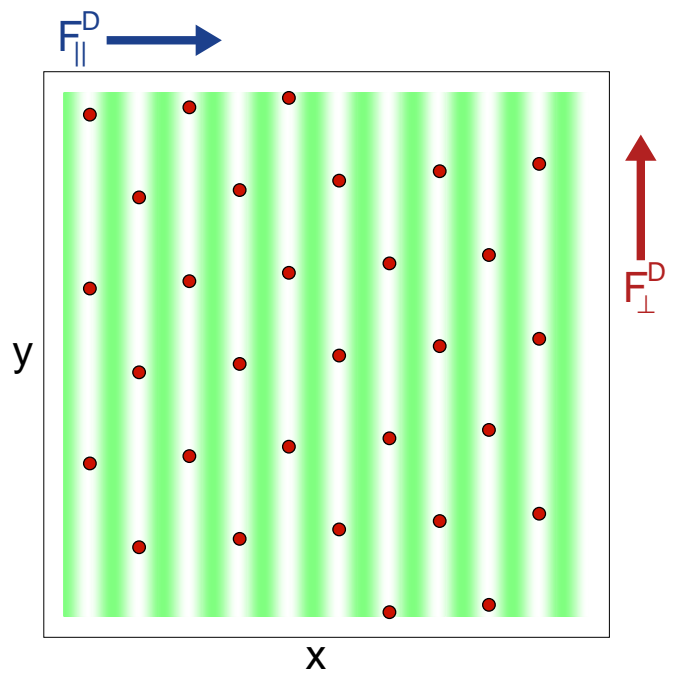


FIG. 53 An example of a periodic quasi-one-dimensional substrate for skyrmions (Reichhardt and Olson Reichhardt, 2016). The substrate is sinusoidal along the  $x$  direction. White areas indicate substrate minima while substrate maxima are colored green. The skyrmions, represented by red dots, can be driven either parallel to the substrate periodicity by  $F_{||}^D$  (blue arrow), or perpendicular to the substrate periodicity by  $F_{\perp}^D$  (red arrow). Reprinted with permission from C. Reichhardt *et al.*, Phys. Rev. B **94**, 094413 (2016). Copyright 2016 by the American Physical Society.

threshold  $F_c$  when the driving is parallel to the substrate periodicity, while driving in the perpendicular direction would simply cause the particles to slide along the potential minima. This situation changes for skyrmions with a finite Magnus force, which move at an angle with respect to the drive. The skyrmions exhibit a finite parallel depinning threshold even when the driving is perpendicular to the substrate periodicity. Reichhardt and Olson Reichhardt (Reichhardt and Olson Reichhardt, 2016) used a 2D particle based simulation to study skyrmions interacting with a periodic 1D substrate, and found that for driving parallel to the substrate periodicity direction, the critical depinning force  $F_c$  is independent of the ratio of the Magnus force to the damping strength. This is in contrast to the case of random point pinning, where  $F_c$  decreases with increasing Magnus force. The skyrmions are able to skirt around pointlike pinning sites, but they cannot avoid passing through a 1D extended pinning site. When the drive is perpendicular to the substrate periodicity direction, there is no finite depinning threshold and the skyrmions initially move only in the perpendicular direction with  $\theta_{\text{SKH}} = 0$ . As the drive increases, the Magnus force on the skyrmions in the direction parallel to the substrate periodicity increases until, above a critical

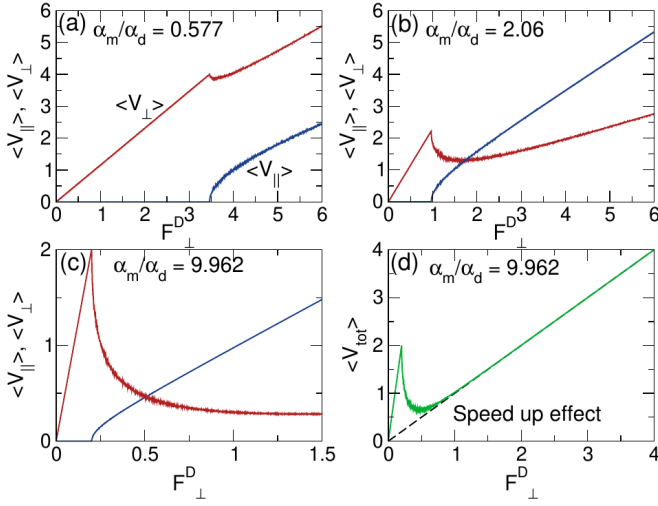


FIG. 54 Illustration of the speed up effect from particle-based simulations of skyrmion velocities parallel  $\langle V_{\parallel} \rangle$  (blue) and perpendicular  $\langle V_{\perp} \rangle$  (red) to the substrate periodicity direction for perpendicular driving  $F_{\perp}^D$  in the quasi-1D potential illustrated in Fig. 53 (Reichhardt and Olson Reichhardt, 2016). (a) At  $\theta_{\text{SkH}}^{\text{int}} = 30^\circ$ , the initial skyrmion motion is locked in the perpendicular direction. There is a drop in  $\langle V_{\perp} \rangle$  at the critical drive  $F_c^{\parallel}$  for the onset of motion in the parallel direction. At (b)  $\theta_{\text{SkH}}^{\text{int}} = 64^\circ$  and (c)  $\theta_{\text{SkH}}^{\text{int}} = 84.3^\circ$ ,  $F_c^{\parallel}$  shifts to lower drives and the drop in  $\langle V_{\perp} \rangle$  becomes more pronounced. (d) The total velocity  $\langle V_{\text{tot}} \rangle$  vs  $F_{\perp}^D$  at  $\theta_{\text{SkH}}^{\text{int}} = 84.3^\circ$ . The dashed line indicates the response  $\langle V_0 \rangle$  expected in a system with no substrate. In the speed up effect,  $\langle V_{\text{tot}} \rangle > \langle V_0 \rangle$ . Reprinted with permission from C. Reichhardt *et al.*, Phys. Rev. B **94**, 094413 (2016). Copyright 2016 by the American Physical Society.

drive, the skyrmions begin to jump over the barriers and move in both the parallel and perpendicular directions. A drive that is perpendicular to the substrate symmetry direction produces a situation similar to that of a skyrmion in a thin race track, which moves toward the edge of the track due to the Magnus force and leaves the track completely above a critical velocity. In the case of the 1D periodic substrate in a 2D sample, the skyrmion hops into the next potential minimum when the critical velocity is exceeded.

Figure 54 shows the skyrmion velocity-force curves for driving in the direction perpendicular to the substrate periodicity in the system from Fig. 53 (Reichhardt and Olson Reichhardt, 2016). In Fig. 54(a), a system with an intrinsic Hall angle of  $\theta_{\text{SkH}}^{\text{int}} = 30^\circ$  has a finite depinning threshold  $F_c^{\parallel}$  for motion in the parallel direction, and for  $0 < F_D < F_c^{\parallel}$  the skyrmion motion is locked along the perpendicular direction, giving  $\theta_{\text{SkH}} = 0$ . For  $F_D > F_c^{\parallel}$ , the skyrmion begins to move in both directions, and the onset of finite  $\langle V_{\parallel} \rangle$  is accompanied by a decrease in  $\langle V_{\perp} \rangle$ . In Fig. 54(b) and (c), systems with  $\theta_{\text{SkH}}^{\text{int}} = 64^\circ$  and  $84.3^\circ$ , respectively, show that  $F_c^{\parallel}$  drops to lower drives with increasing  $\theta_{\text{SkH}}^{\text{int}}$ , while the drop in  $\langle V_{\perp} \rangle$

at  $F_c^{\parallel}$  becomes more pronounced. Figure 54(d) illustrates the net skyrmion velocity  $\langle V \rangle = (\langle V_{\perp} \rangle^2 + \langle V_{\parallel} \rangle^2)^{1/2}$  versus  $F_{\perp}^D$  for a sample with  $\theta_{\text{SkH}}^{\text{int}} = 84.3^\circ$ , along with a dashed line indicating the velocity  $\langle V_0 \rangle$  expected in the absence of a substrate. A pinning-induced speed up effect appears near  $F_c^{\parallel}$  in which  $\langle V \rangle > \langle V_0 \rangle$ , meaning that the skyrmion is moving *faster* than it would if the substrate were not present. This speed up effect, which does not occur in overdamped systems, is produced by a combination of the Magnus force and the pinning potential. When the skyrmion is constrained by the pinning potential to move in the direction of the drive, the Magnus force-induced velocity component from the pinning  $\alpha_m F_p$  is aligned with the drive. This is added to the velocity component  $\alpha_d F_D$  produced by the drive, giving a total velocity of  $\langle V \rangle = \alpha_d F_D + \alpha_m F_p$ . Here the nonconservative Magnus force has turned the pinning force into an effective additional driving force. Speed up effects are the most prominent on 1D substrates, and have been studied numerically for a single skyrmion moving along domain walls (Xing *et al.*, 2020). They can also occur for random and 2D periodic pinning arrays. Gong *et al.* (Gong *et al.*, 2020) numerically studied skyrmion motion in random disorder and found that the skyrmion velocity can be boosted in regimes where motion in the transverse or skyrmion Hall angle direction is suppressed. This indicates that whenever the skyrmion motion along  $\theta_{\text{SkH}}^{\text{int}}$  is impeded, the Magnus force can transfer part or all of the component of motion in that direction to the direction along which the skyrmion is constrained to move.

Skyrmion speed up effects have been observed in micromagnetic simulations of race tracks (Sampaio *et al.*, 2013) and for scattering off a single pinning site in both continuum and Thiele based approaches (Müller and Rosch, 2015). Iwasaki *et al.* used both a Thiele approach and micromagnetic simulations to examine the large velocity enhancement near a boundary and showed that it is related to a colossal spin transfer torque effect (Iwasaki *et al.*, 2014). Here the velocity is enhanced by a factor of  $1/\alpha$ , where  $\alpha$  is the Gilbert damping, and the maximum velocity is determined by the magnitude of the confining force produced by the sample edge. Several other works also describe the acceleration of skyrmions along sample edges (Castell-Queralt *et al.*, 2019; Martinez *et al.*, 2018). Castell-Queralt *et al.* (Castell-Queralt *et al.*, 2019) examined the dynamics of a skyrmion moving across a rail where, in addition to skyrmion acceleration along the edge, they observed guiding and compressing effects. They found that speed ups of as much as an order of magnitude are possible compared to motion in a system without defects. Figure 55 shows the results from micromagnetic simulations (Castell-Queralt *et al.*, 2019) of a skyrmion approaching a single defect line along which the DMI interaction strength  $\delta$  has a modified value. Here  $\delta = -1$  indicates a complete suppression of the DMI and  $\delta = 1$  is the unaltered DMI interaction strength, so that

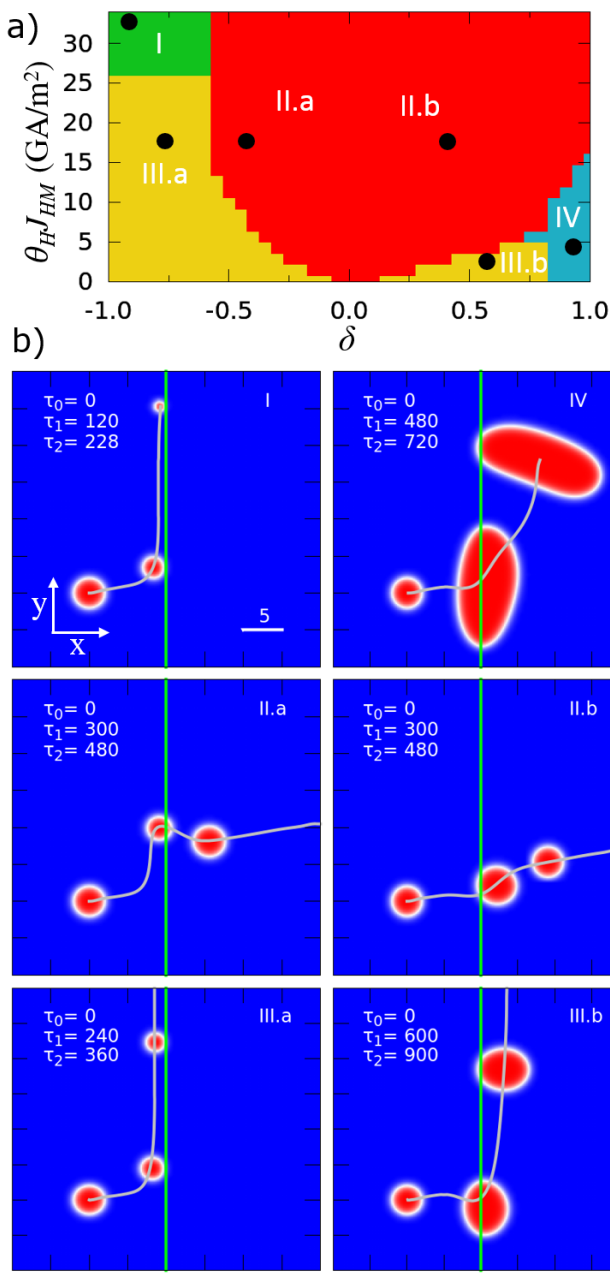


FIG. 55 Results from continuum simulations of a skyrmion interacting with a line along which the DMI has been changed by an amount  $\delta$  compared to the rest of the sample (Castell-Queralt *et al.*, 2019). (a) A phase diagram as a function of the product of the skyrmion Hall angle  $\theta_H$  and current  $J_{HM}$  vs  $\delta$ . (b) Illustration of motion in the six different regimes. The defect is indicated by a green vertical line and the skyrmion trajectory is given by the gray line. Republished with permission of the Royal Society of Chemistry, from “Accelerating, guiding, and compressing skyrmions by defect rails”, J. Castell-Queralt *et al.*, *Nanoscale* **11**, 12589 (2019); permission conveyed through Copyright Clearance Center, Inc.

$\delta < 0$  produces a skyrmion repulsion and  $\delta > 0$  causes the line to attract the skyrmion. The dynamic phase diagram in Fig. 55(a) shows the behavior as a function of the product of the skyrmion Hall angle and current versus  $\delta$ , while Fig. 55(b) illustrates the six different phases of motion. In phases I and III.a, the skyrmion is guided along the line and shrinks. In phase IV the skyrmion moves across the line but experiences strong distortion. In phases II.a and II.b the skyrmion crosses the line and is weakly deflected, while in phase III.b the skyrmion crosses the line and is strongly deflected. The same work also demonstrated skyrmion guidance using a combination of two line defects, one of which is repulsive and the other attractive, and showed that a strong acceleration effect occurs in this case.

The work of Reichhardt and Olson Reichhardt (Reichhardt and Olson Reichhardt, 2016) also focused on collective effects for skyrmions moving over 1D periodic arrays. For driving perpendicular to the substrate periodicity direction, a number of dynamical phases arise, including a pinned smectic state similar to that observed for colloidal particles and superconducting vortices in periodic 1D substrates, a disordered plastic flow state just above depinning, a moving hexatic state, and a moving crystal state. All these phases produce signatures in the different velocity components as well as changes in  $\theta_{SKH}$ , and they could be detected experimentally via neutron scattering, changes in the topological Hall effect, or noise measurements.

For a skyrmion moving over either a 1D or 2D substrate, various interference effects can arise. In general, a particle moving over a periodic substrate has a time dependent velocity modulation at a washboard frequency  $\omega_d$  which increases with increasing dc drive  $F_D$  or current  $J$ . When an ac drive  $F_{ac} = A \sin(\omega_{ac} t)$  is added to the dc drive, at certain values of  $F_{ac}$  a matching between the ac drive frequency and  $\omega_d$  occurs, creating a resonance. Such effects have been observed experimentally for superconducting vortex lattices moving over random disorder (Fiory, 1971; Harris *et al.*, 1995; Okuma *et al.*, 2011, 2007). Since the dc velocity must remain locked at a fixed value for the resonance condition to persist, a region of constant or locked velocity appears over an interval of  $F_D$  values. When the difference between the two frequencies becomes too large, the system jumps out of the velocity locked step; however, additional velocity locking steps appear whenever  $\omega_d/\omega_{ac}$  is an integer. The steps in the velocity at the resonant condition and its higher harmonics are known as Shapiro steps (Benz *et al.*, 1990; Shapiro, 1963). If the ac amplitude  $A$  is large, additional nonlinear effects can occur, producing fractional steps and strongly fluctuating regions. Shapiro steps have been observed in a wide variety of systems that exhibit depinning on periodic substrates, such as sliding charge density waves (Coppersmith and Littlewood, 1986) and vortices in type-II superconductors with 1D

and 2D periodic substrates (Martinoli *et al.*, 1975; Reichhardt *et al.*, 2000; Van Look *et al.*, 1999), All of these systems are either overdamped or have inertial effects, but none of them include Magnus forces.

In skyrmion systems, the Magnus force should produce a variety of new types of phase locking phenomena. For example, the mixing of the velocity components by the Magnus force makes it possible for locking steps to occur for any driving direction, as demonstrated in a particle based model for skyrmions moving over a periodic 1D potential with a dc drive applied parallel to the substrate periodicity and an ac drive applied either parallel or perpendicular to the dc drive (Reichhardt and Olson Reichhardt, 2015). Here Magnus induced Shapiro steps appear in the velocity-force curves, and the step widths  $\Delta F_{ac}$  oscillate according to the Bessel function  $\Delta F_{ac} = |J_n(F_x^{ac})|$ , as expected for Shapiro steps. The skyrmion orbits on a locking step are considerably more complex than those found in overdamped systems. Sato *et al.* (Sato *et al.*, 2020) measured voltage fluctuations for current induced skyrmion lattice motion in MnSi. They found a narrow band noise signal that shifted to higher frequency with increasing current, indicating that the speed of the skyrmion motion was increasing. When they added an ac driving current, a clear mode locking signal emerged with strongly enhanced narrow band noise. The plots of the dependence of the narrow band noise magnitude on the dc current density in Fig. 56(a) include a step-like regime where the narrow band signal is locked to the washboard frequency. For zero applied ac current, no step is present, but as the amplitude of the ac current increases, the width of the narrow band step  $\Delta j_{dc}$  in Fig. 56(b) increases and decreases according to the Bessel function form of Shapiro steps.

Other combinations of drives for skyrmions on 1D periodic arrays produce unusual collective effects. For example, the dc drive can be applied perpendicular to the substrate periodicity while the ac drive is either parallel or perpendicular to the dc drive. In an overdamped system, this orientation of the dc drive does not produce any interference effects; however, for the skyrmion system, phase locking effects appear, including a new phenomenon in which spikes rather than steps appear in the velocity force curves. This Shapiro spike structure occurs when the ac and dc drives are both perpendicular to the substrate periodicity (Reichhardt and Olson Reichhardt, 2017). In some cases the phase locking can cause the skyrmion to move at  $90^\circ$  with respect to the dc drive, an effect known as absolute transverse mobility (Reichhardt and Olson Reichhardt, 2003). There can also be regions in which  $V_\perp$  is negative, indicative of absolute negative mobility (Eichhorn *et al.*, 2002; Ros *et al.*, 2005) where the skyrmion is actually moving against the direction of the external drive.

Since skyrmions have internal modes with their own intrinsic frequencies, there should be a wealth of pos-

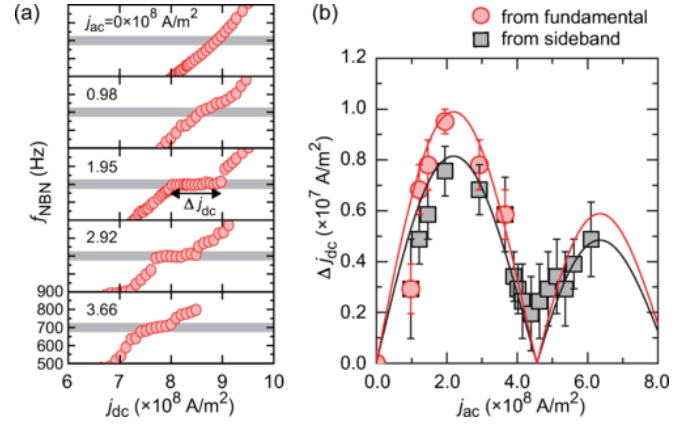


FIG. 56 Phase locking and Shapiro steps for current driven skyrmions in MnSi under combined dc and ac driving (Sato *et al.*, 2020). (a) Magnitude of the narrow band noise  $f_{\text{NBN}}$  as a function of dc driving current  $j_{\text{dc}}$  for different values of the ac current  $j_{\text{ac}}$ , showing the emergence of a locking step when  $j_{\text{ac}} = 1.95 \times 10^8 \text{ A/m}^2$ . (b) Dependence of the locking step width  $\Delta j_{\text{dc}}$  on ac current amplitude  $j_{\text{ac}}$  showing oscillations in the form of a Bessel function, as expected for a Shapiro step. Reprinted with permission from T. Sato *et al.*, Phys. Rev. B **102**, 180411(R) (2020). Copyright 2020 by the American Physical Society.

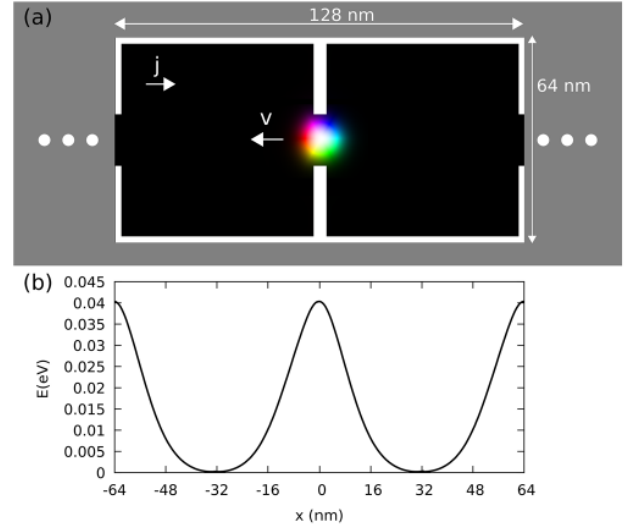


FIG. 57 (a) Micromagnetic simulation of a skyrmion moving in an infinitely long nanotrack containing periodic notches (white regions) (Leliaert *et al.*, 2019). The DMI is reduced in the notch regions compared to the rest of the nanotrack. (b) The energy landscape experienced by the skyrmion as a function of position. Republished with permission of IOP Publishing, Ltd, from “Coupling of the skyrmion velocity to its breathing mode in periodically notched nanotracks”, J. Leliaert *et al.*, J. Phys. D: Appl. Phys. **52**, 024003 (2019); permission conveyed through Copyright Clearance Center, Inc.

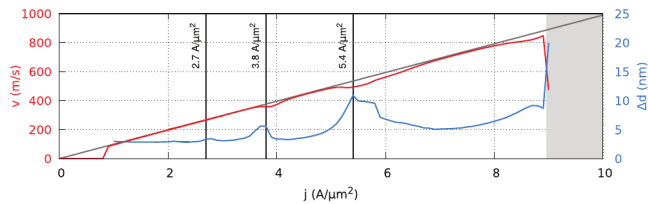


FIG. 58 From micromagnetic simulations (Leliaert *et al.*, 2019) of the periodically notched system in Fig. 57, the skyrmion velocity  $v$  (red) and skyrmion size fluctuations  $\Delta d$  (blue) vs driving current  $j$ . Resonances appear when the washboard frequency of the skyrmion motion couples with the skyrmion breathing mode. Republished with permission of IOP Publishing, Ltd, from “Coupling of the skyrmion velocity to its breathing mode in periodically notched nanotracks”, J. Leliaert *et al.*, *J. Phys. D: Appl. Phys.* **52**, 024003 (2019); permission conveyed through Copyright Clearance Center, Inc.

sible resonances involving the coupling of these modes to an external ac frequency, a substrate frequency produced by dc motion over periodic pinning, or the intrinsic washboard frequency of the skyrmion lattice. These dynamics would be quite different from those typically found for overdamped or rigid particles. There is already some work along these lines by Leliaert *et al.* (Leliaert *et al.*, 2019), who performed micromagnetic simulations of skyrmions moving through a wire with a periodic modulation of notches, as shown in Fig. 57. The notches, produced by varying the DM interaction, induce a periodic modulation of the skyrmion motion which couples to the skyrmion breathing mode, producing a series of resonances in the velocity-force curves, as illustrated in Fig. 58.

## B. Further Directions for 1D Periodic Substrates

There are a variety of potential race track memory applications of 1D periodic substrates for both bulk and thin films, including situations in which multiple interacting skyrmions could be coupled inside a nanowire with a periodic modulation. In this case, mobile kinks in the 1D skyrmion chain could reduce the effects of the skyrmion Hall angle. An example is shown schematically in Fig. 59(a), where a constriction with a periodic modulation is filled with skyrmions at a ratio just above the 1:1 matching condition. The extra skyrmion forms a kink that travels in the direction of drive. Conversely, if the system is just below the 1:1 matching, a vacancy appears which moves in the opposite direction, as shown in Fig. 59(b). The periodic modulation could be created using a periodic array of notches (Marchiori *et al.*, 2017), variations of the DMI, spatially varying damping (Zhang *et al.*, 2017a; Zhou *et al.*, 2019a), or periodic thickness modulations (Loreto *et al.*, 2019). For coupled colloidal

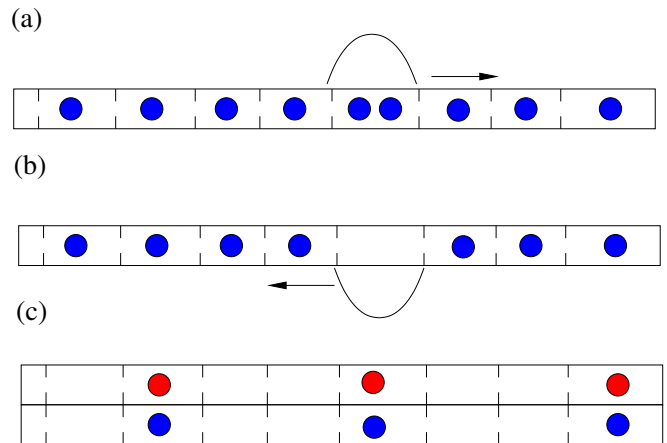


FIG. 59 (a) Schematic of skyrmions in a nanowire interacting with a 1D periodic substrate at a filling just above the 1:1 matching. The additional skyrmion creates a mobile kink that moves in the direction of drive. Every time the kink moves through the system, the skyrmion translates by one lattice constant. (b) The same, but for an anti-kink just below the 1:1 matching, which moves in the opposite direction. (c) Two coupled wires with different species of skyrmions could form skyrmions and antiskyrmions that could bind together and create skyrmion excitons.

particles on 1D periodic substrates, it was shown that the kinks can act like emergent particles with their own internal frequency, making it possible to observe phase locking of kinks under a combined dc and ac drive (Juniper *et al.*, 2015). The kinks themselves could serve as information carriers instead of the actual skyrmions. The 1D substrate need not be static; a dynamic substrate can be created using arrays of different gate voltages (Liu *et al.*, 2019) that can be turned on and off to create a flashing potential for the skyrmions. In this case, an additional frequency arises from the periodic flashing that could couple with the internal frequencies of the skyrmions. In most overdamped systems, Shapiro steps appear when a dc drive is combined with a single ac driving frequency; however, for skyrmions it was shown that biharmonic ac forces (Chen *et al.*, 2019) can lead to directed skyrmion motion even in the absence of a dc drive. Thus, having a skyrmion move over a 1D substrate under both dc and biharmonic ac drives could produce a variety of new phenomena. It would also be possible to couple together nanowires of different materials such that the skyrmions interact between the nanowires, leading to skyrmion drag effects as shown schematically in Fig. 59(c). For example, a nanowire containing antiskyrmions that couples to another nanowire containing regular skyrmions could produce an effective skyrmion exciton.

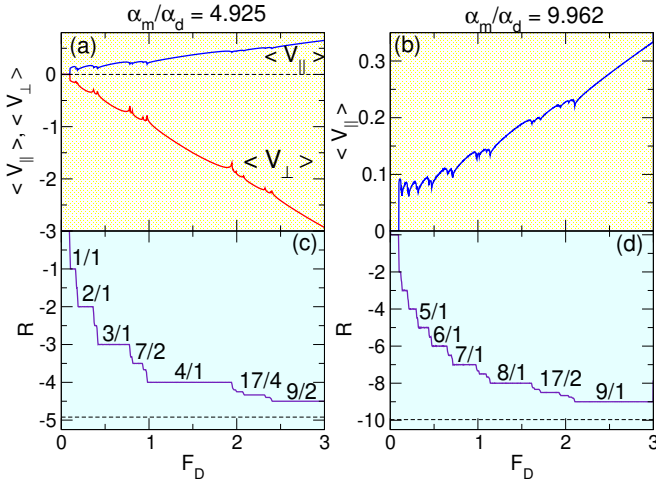


FIG. 60 Particle-based simulations of skyrmions moving over a square array of pinning sites showing quantization of the skyrmion Hall angle (Reichhardt *et al.*, 2015c). (a) The velocity parallel,  $\langle V_{\parallel} \rangle$  (blue), and perpendicular,  $\langle V_{\perp} \rangle$  (red), to the driving direction vs the dc drive amplitude  $F_D$  at a Magnus ratio to damping ratio of  $\alpha_m/\alpha_d = 4.925$ . (b)  $\langle V_{\parallel} \rangle$  vs  $F_D$  for a larger ratio  $\alpha_m/\alpha_d = 9.962$ . (c) The ratio  $R = \langle V_{\perp} \rangle / \langle V_{\parallel} \rangle = \tan(\theta_{\text{SKH}})$  vs  $F_D$  for the sample in panel (a), where steps appear at rational fractions. (d)  $R$  vs  $F_D$  for the sample in panel (b) also exhibits a series of steps. Reprinted with permission from C. Reichhardt *et al.*, Phys. Rev. B **91**, 104426 (2015). Copyright 2015 by the American Physical Society.

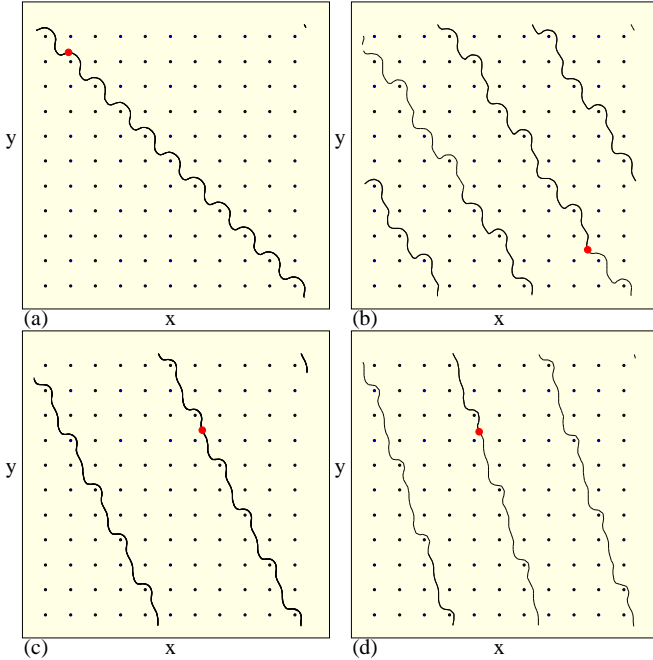


FIG. 61 Skyrmion trajectories (lines) for particle based simulations of the system in Fig. 57 with a skyrmion (red circle) moving through a periodic array of pinning sites (black dots) at (a)  $|R| = 1$ , (b)  $|R| = 5/3$ , (c)  $|R| = 2$ , and (d)  $|R| = 3$  (Reichhardt *et al.*, 2015c). Reprinted with permission from C. Reichhardt *et al.*, Phys. Rev. B **91**, 104426 (2015). Copyright 2015 by the American Physical Society.

### C. Skyrmions with Two Dimensional Periodic Pinning

Reichhardt *et al.* used a particle-based model to study a single skyrmion moving over a 2D square periodic potential (Reichhardt *et al.*, 2015c). This system has a finite depinning threshold and a drive-dependent skyrmion Hall angle  $\theta_{\text{SKH}}$ , similar to what is observed for random pinning as discussed above (Jiang *et al.*, 2017b; Kim and Yoo, 2017; Legrand *et al.*, 2017; Litzius *et al.*, 2017; Reichhardt *et al.*, 2015b; Reichhardt and Reichhardt, 2016); however, due to the square substrate symmetry, the skyrmion motion preferentially locks to certain directions  $\theta_{\text{SKH}} = \tan^{-1}(n/m)$  with integer  $m$  and  $n$ . For example, locking at  $\theta_{\text{SKH}} = 45^\circ$  occurs when  $n = 1$  and  $m = 1$  while locking at  $\theta_{\text{SKH}} = 23^\circ$  corresponds to  $n = 1$  and  $m = 2$ . For increasing drive, the skyrmion can only remain locked in its direction of motion if its net velocity  $\langle V \rangle$  decreases, so each locking step is associated with a window of negative differential mobility in which  $d\langle V \rangle/dF_D < 0$ . Cusps in both the parallel and perpendicular velocities,  $\langle V_{\parallel} \rangle$  and  $\langle V_{\perp} \rangle$ , appear at the transition from one directional locking step to the next, as shown in Fig. 60(a,b). Figure 60(c,d) illustrates the ratio  $R = \langle V_{\perp} \rangle / \langle V_{\parallel} \rangle = \tan(\theta_{\text{SKH}})$ , indicating that the skyrmion Hall angle is quantized as a function of increasing drive. On the  $|R| = 1$  step, the particle is constrained to move along  $\theta_{\text{SKH}} = 45^\circ$ , as illustrated in Fig. 61(a). The skyrmion trajectories for motion on the  $|R| = 5/3$ , 2, and 3 steps appear in Figs. 61(b), (c), and (d), respectively. In general, the integer steps are more pronounced than the fractional steps. Such directional locking should be a generic feature of ferromagnetic skyrmions moving over periodic pinning arrays. A similar directional locking effect with steps in the velocity force curves was studied for superconducting vortices (Reichhardt and Nori, 1999) and colloidal particles (Korda *et al.*, 2002; MacDonald *et al.*, 2003; Risbud and Drazer, 2014) moving over 2D periodic substrates, but in these overdamped systems, the external drive must change direction in order to generate the locking steps, whereas in the skyrmion system, the direction of the dc drive remains fixed.

Feilhauer *et al.* (Feilhauer *et al.*, 2020) employed a combined micromagnetic and Thiele equation approach to study skyrmion motion in a magnetic antidot array. They found that the skyrmion motion locks to the symmetry angles of the array and that the skyrmion Hall angle can be controlled by varying the damping, as shown in Fig. 62. By careful choice of the direction of the current pulse, a skyrmion can be steered to move into almost any other plaquette position, suggesting that this drive protocol could be a useful method for applications. There have already been some experimental efforts to create a similar type of substrate using antidot lattices (Saha *et al.*, 2019).

Locking of the skyrmion motion to particular symmetry directions of 2D periodic arrays could be harnessed

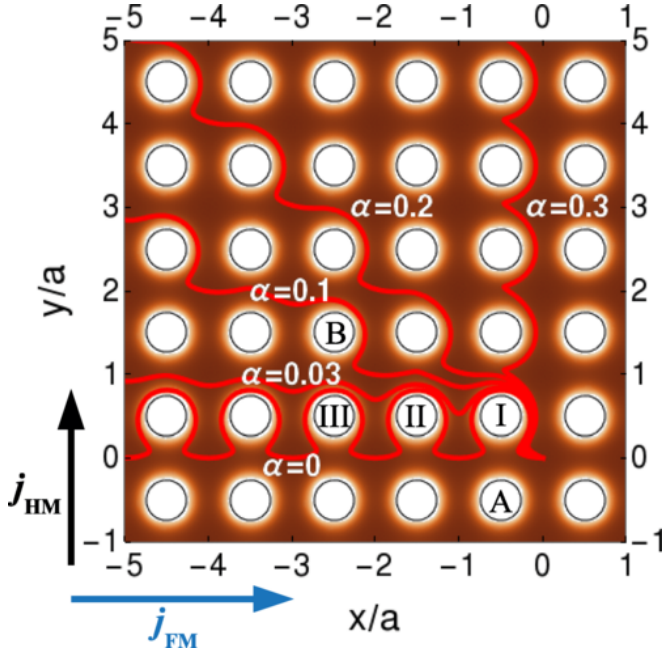


FIG. 62 Combined micromagnetic and analytic calculations of skyrmion trajectories (red lines) in a square array of magnetic dots for different values of the damping coefficient  $\alpha$  (Feilhauer *et al.*, 2020). By varying the direction of the applied current pulse, the skyrmion can be steered to any selected position in the array. Reprinted with permission from J. Feilhauer *et al.*, Phys. Rev. B **102**, 184425 (2020). Copyright 2020 by the American Physical Society.

to create a topological sorting device for different species of skyrmions with slightly different values of  $\theta_{\text{SkH}}^{\text{int}}$ . Here, one species would lock to a symmetry direction of the substrate while the other species would not, producing a lateral separation of the species over time. A demonstration of this separation effect was achieved in simulations by Vizarim *et al.* for a bidisperse assembly of skyrmions driven through a square obstacle array (Vizarim *et al.*, 2020a). This procedure is similar to that used in microfluidic systems, and suggests that skyrmion bubbles with a carefully selected size could be separated from skyrmion bubbles of other size. Using particle-based simulations, Vizarim *et al.* also showed that a skyrmion interacting with a 2D periodic array under a dc drive and one or more ac drives can undergo a variety of controlled motions (Vizarim *et al.*, 2020c) and can exhibit non-monotonic behavior of the skyrmion Hall angle (Vizarim *et al.*, 2020b). Another interesting effect observed in particle based models of skyrmions driven over periodic arrays is skyrmion clustering or segregation. This is similar to the segregated states found for strong random pinning in both continuum (Koshibae and Nagaosa, 2018) and particle based simulations (Reichhardt and Reichhardt, 2019a).

Reichhardt *et al.* also studied collective static arrangements of skyrmions interacting with square pinning ar-

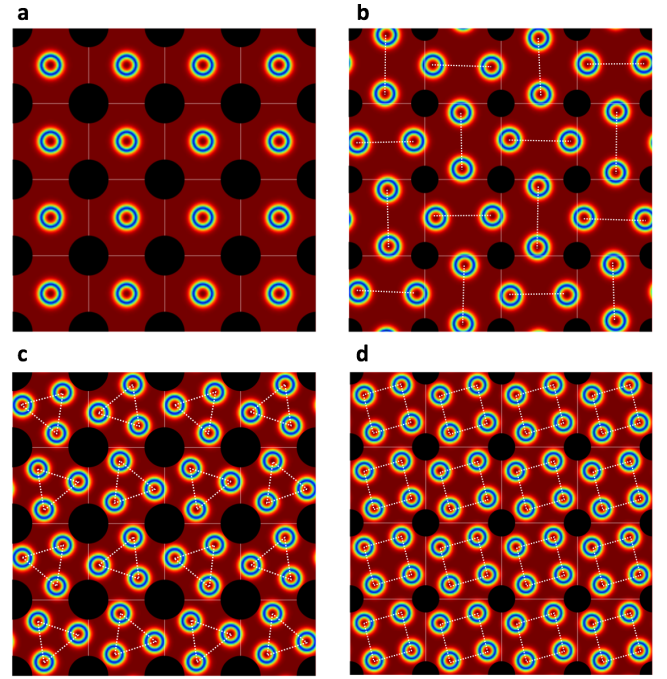


FIG. 63 Continuum simulations of chiral liquid crystal skyrmions (blue rings) interacting with a periodic array of obstacles (black circles) (Duzgun *et al.*, 2020). (a) A filling ratio of  $f = 1$  where the skyrmions form a square lattice. (b) Alternating dimer ordering for  $f = 2$ . (c) A trimer arrangement at  $f = 3$ . (d) An ordered quadrimer state at  $f = 4$ . Republished with permission of the Royal Society of Chemistry, from “Commensurate states and pattern switching via liquid crystal skyrmions trapped in a square lattice”, A. Duzgun *et al.*, Soft Matter **16**, 3338 (2020); permission conveyed through Copyright Clearance Center, Inc.

rays as a function of skyrmion density using a particle based model (Reichhardt *et al.*, 2018). When the number of skyrmions  $N_{sk}$  is an integer multiple of the number of pinning sites  $N_p$ , a series of commensurate states appear in which different types of skyrmion crystals can be stabilized, including square or triangular lattices. Ordered skyrmion lattices can also form at rational filling fractions  $f \equiv N_{sk}/N_p$  such as  $f = 1/2$ , where the skyrmions adopt a checkerboard pattern. The  $f = 1.65$  and  $f = 2.0$  configurations were also observed in continuum-based simulations for a square array of pinning sites produced by local changes in the anisotropy (Koshibae and Nagaosa, 2018).

Duzgun *et al.* explored the ordering of liquid crystal skyrmions interacting with a square array of defects using continuum based simulations (Duzgun *et al.*, 2020). At a one-to-one matching of  $f = 1$ , the skyrmions form a square lattice as illustrated in Fig. 63(a). Fillings of  $f = 2, 3$ , and 4 produce dimer, trimer, and quadrimer states as shown in Fig. 63(b-d). At some filling fractions such as  $f = 2$ , the skyrmions deform into elongated states in order to match the substrate symmetry better.

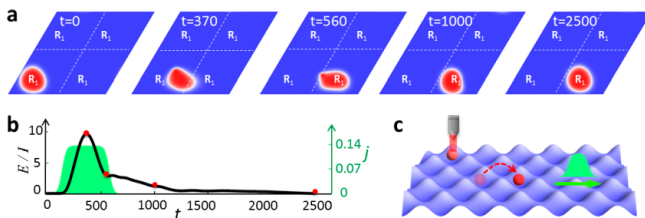


FIG. 64 Numerical model for the motion of a skyrmion over a moiré pattern formed by a van der Waals 2D magnet (Tong *et al.*, 2018). (a) The red region indicates the location of the skyrmion as a function of time. (b) The time profile of the applied current  $j$  (green) and the energy of the skyrmion  $E/I$  during the motion illustrated in panel (a). (c) A schematic of the use of a spin-polarized scanning tunneling microscopy tip (gray) to write a skyrmion, which is then moved from one substrate minimum to another with a current pulse (green). Reprinted with permission from Q. Tong *et al.*, Nano Lett. **18**, 7194 (2018). Copyright 2018 American Chemical Society.

Observation of skyrmion motion in systems with two periodic surfaces can be achieved using moiré patterns in van der Waals 2D magnets (Tong *et al.*, 2018). The moiré patterns are generated by introducing a lateral modulation of the interlayer magnetic coupling for different atomic angles. In the case of weak interlayer coupling, a skyrmion can be viewed as moving over a periodic substrate composed of trapping sites formed by the moiré pattern. Figure 64(a) shows the periodic motion that can be induced by the pattern. In Fig. 64(b), application of a current pulse can cause the skyrmion to jump from one side of a trapping barrier to the other. Tong *et al.* proposed that the 2D moiré trapping array could be used to create a stable background substrate for controlled skyrmion motion for various applications (Tong *et al.*, 2018).

Skyrmions have also been studied in 2D arrays of artificial spin ice geometries. Here, a skyrmion is placed in a double well potential, and the position of the skyrmion on either end of the well can be mapped onto an effective spin direction. Figure 65 shows schematically how such structures could be made using a thickness modulation (Ma *et al.*, 2016). The skyrmions form a spin ice ordering very similar to that observed for superconducting vortices (Libál *et al.*, 2009) and colloidal particles (Libál *et al.*, 2006) on square and hexagonal double well artificial ice arrays. Unlike the vortices and colloidal particles, the skyrmions can change size or deform. As a result, a transition can occur from a frustrated state in which each skyrmion occupies only one side of the double well to an unfrustrated state in which a single skyrmion stretches out and occupies the center of the well, as shown in Fig. 65(d-e). There have also been studies of so-called artificial skyrmion lattices in a 2D array of magnetic dots, where the individual dots contain skyrmion states (Gilbert *et al.*, 2015; Zhang *et al.*,

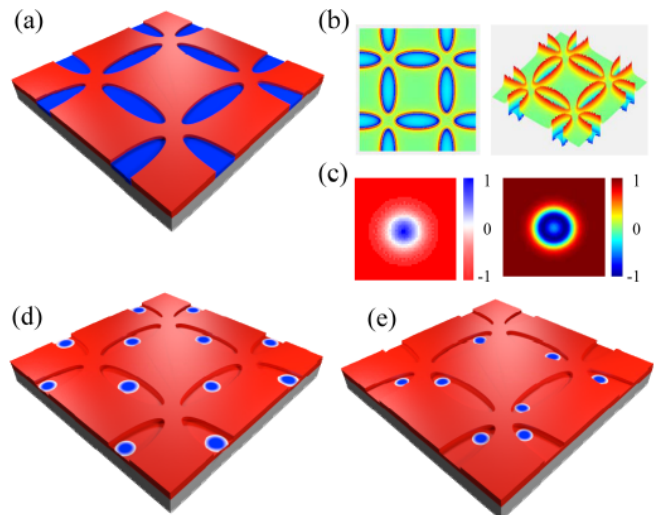


FIG. 65 An artificial ice geometry for skyrmions (Ma *et al.*, 2016). (a) The geometry is constructed using elliptical blind holes with opposite magnetization directions inside and outside the holes. (b) The perpendicular or  $z$  component of the resulting stray field. (c) Images of the spin configuration (left) and the topological density distribution (right) of an isolated individual skyrmion. (d) Large skyrmions sit at the center of each blind hole to form a non-frustrated configuration. (e) Small skyrmions sit at one end of each blind hole and form a frustrated state. Reprinted with permission from F. Ma *et al.*, Phys. Rev. B **94**, 144405 (2016). Copyright 2016 by the American Physical Society.

2016a). The next step in such work would be to see whether skyrmions in adjacent dots could be coupled, or if the entire system could be placed on a ferromagnetic substrate that would permit the skyrmions to hop directly from one dot to the next.

### 1. Further Studies with Periodic Substrates

A wide variety of avenues of study are available for skyrmions on 2D periodic substrates created by a range of methods. New types of skyrmion-based memory devices could be produced by storing information in certain skyrmion configurations that could be changed by the application of a current. At fillings slightly away from commensuration, a well defined number of kinks or antikinks are present that act like emergent particles with their own dynamics. It would be interesting to explore whether the Magnus force or the internal degrees of freedom of the skyrmions would change the dynamics of kinks and antikinks compared to what is observed in overdamped or rigid particle systems. When thermal fluctuations become relevant, the kinks or antikinks could form their own lattice and exhibit melting phenomena. Up to now, numerical work on incommensurate states has focused on particle-based models, so new studies based



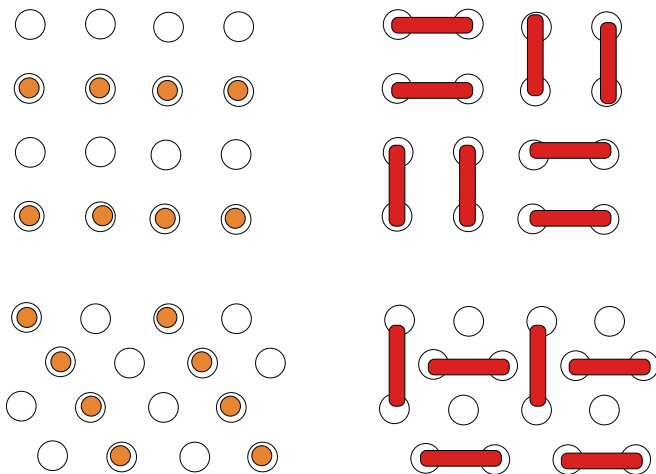


FIG. 66 Schematic of possible orderings on square and triangular pinning arrays (open circles) at half filling. Left: Skyrmion (orange circles) orderings. Right: The skyrmions elongate into meron pairs (red rectangles) to create a 1:1 filling for the square pinning array, but still leave unoccupied pins in the triangular pinning array.

on micromagnetic calculations could reveal many additional effects related to the ability of the skyrmion to change its shape. These could include a variety of new types of commensuration and dynamical effects that do not appear in overdamped or inertial systems. For example, a system containing twice as many pinning sites as particles normally forms a square or striped sublattice as illustrated in Fig. 66. If the pinning is strong enough, however, the skyrmions can elongate to form pairs of merons that cover each lattice site, representing an effective dimer covering model that has numerous possible ordered states. Triangular substrates at half filling would form strongly frustrated states if the skyrmions elongate into meron pairs.

The strong gyroscopic motion of skyrmions makes it possible to explore coupled skyrmions oscillating in dense 2D arrays of dots where each dot can have different materials properties. The coupled oscillations could pass through a series of locking transitions as a function of some form of ac driving. The sliding dynamics of skyrmions over a periodic array would also be an interesting avenue of study. For example, Koshibae and Nagaosa (Koshibae and Nagaosa, 2018) showed that skyrmion creation and annihilation occurs at certain drives and pinning strengths when skyrmions are moving through random arrays. On periodic arrays, such events may be much better controlled. For instance, a skyrmion could move a specific number of lattice sites before it is annihilated, or a new skyrmion is created, or some combination of these effects occurs. Under superimposed ac and dc driving, a resonance could arise between the ac drive and the motion of the skyrmions over the substrate or the skyrmion breathing modes. Similar effects could be stud-

ied for other systems such as merons, combined meron-skyrmion lattices, antiskyrmions, and antiferromagnetic skyrmions. Periodic pinning arrays could be created in bulk systems as well, where the pinning could either be only present on the surface or could pass through the bulk in the form of columnar defects of the type that can be generated using patterned irradiation.

#### D. Asymmetric Arrays, Diodes, and Ratchets

In a ratchet device, an applied ac drive leads to the net dc motion of a particle. Ratcheting motion in overdamped systems is typically achieved using an asymmetric pinning potential (Hänggi and Marchesoni, 2009; Reimann, 2002). The flashing of an asymmetric substrate in a thermal system can generate stochastic ratchet transport, while higher dimensional ratchet effects can occur on symmetric substrates if time symmetry is broken by a chiral ac drive. Ratchet effects have been studied extensively in particle-based systems such as colloidal particles (Rousselet *et al.*, 1994; Xiao *et al.*, 2011), vortices in type II superconductors (Lee *et al.*, 1999; Lin *et al.*, 2011; Olson *et al.*, 2001; Shklovskij *et al.*, 2014; Villegas *et al.*, 2003), and cold atoms (Salger *et al.*, 2009). There are also examples of ratchet effects in magnetic systems, where domain walls interacting with asymmetric dot arrays undergo ratcheting motion under various types of external ac driving (Franken *et al.*, 2012; Herrero-Albillos *et al.*, 2018; Marconi *et al.*, 2011). Ratchet effects have generally been studied in overdamped systems; however, additional effects appear when terms such as inertia are included in the equation of motion (Hänggi and Marchesoni, 2009; Reimann, 2002). Skyrmions, as particle-like objects, represent a natural system in which to study ratchet effects, and their strong non-dissipative Magnus force can produce new effects distinct from what has been observed previously in other ratchet systems.

The first proposal for a skyrmion ratchet involved a 1D asymmetric substrate, studied by Reichhardt *et al.* (Reichhardt *et al.*, 2015a) using a particle based approach. The skyrmions move in 2D on the substrate potential illustrated in Fig. 67, which has the form

$$U(x) = U_0[\sin(2\pi x/a) + 0.25\sin(4\pi x/a)] \quad (16)$$

where  $a$  is the substrate periodicity. In the overdamped limit, if an ac drive is applied in the direction of the substrate periodicity (the  $x$ -direction), a standard ratchet effect arises in which the particle can translate by one or more substrate periods in the easy ( $+x$ ) direction under each cycle of an ac drive. The depinning threshold is finite for both the easy ( $+x$ ) and hard ( $-x$ ) directions; however, the depinning threshold is larger in the hard direction, so that in the dc limit, the system acts as a diode. If the ac drive is applied in the perpendicular or  $y$ -direction in an overdamped system, there is no

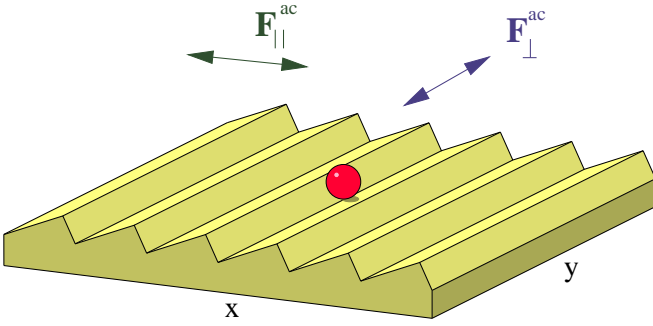


FIG. 67 Schematic of a quasi-one-dimensional asymmetric ratchet potential (Reichhardt *et al.*, 2015a). A skyrmion (red circle) can be driven by an ac current applied parallel ( $F_{\parallel}^{ac}$ , green arrow) or perpendicular ( $F_{\perp}^{ac}$ , blue arrow) to the substrate periodicity direction. An overdamped particle would exhibit no ratcheting effect under  $F_{\perp}^{ac}$ , but due to the Magnus effect, a skyrmion can undergo ratcheting motion under either ac driving direction. Reprinted under CC license from C. Reichhardt *et al.*, New J. Phys. **17**, 073034 (2015).

ratchet effect since no symmetry is broken. In the case of skyrmions with a finite Magnus force, which move at an angle  $\theta_{\text{SkH}}$  with respect to the driving direction, a ratchet effect can occur even when the ac drive is purely perpendicular to the substrate periodicity direction. This is termed a Magnus ratchet effect. Figure 68 shows the velocity component in both the parallel and perpendicular directions for the system in Fig. 67 under perpendicular ac driving  $F_{\perp}^{ac}$ . The inset of Fig. 68(a) indicates that an overdamped system produces no ratchet effect, while Fig. 68(a,b,c) illustrates ratcheting motion in samples with various intrinsic skyrmion Hall angles. The ratchet velocities have well defined quantized values, and there are regions of ac amplitude over which no ratchet effect occurs. The inset in Fig. 68(c) shows a blow up of a single step where there are also fractional ratchet steps. In this system, the skyrmions execute complex 2D orbits while ratcheting.

Ma *et al.* (Ma *et al.*, 2017) used particle based simulations to consider skyrmions interacting with 2D asymmetric arrays in which the pinning sites have a density gradient. They found that, depending on whether the ac drive is applied parallel or perpendicular to the substrate periodicity direction, an entirely new type of ratchet effect called a vector ratchet can appear, in which the direction of motion of the skyrmions can be tuned by up to  $360^\circ$  by varying the amplitude of the ac driving.

Göbel and Mertig (Göbel and Mertig, 2021) performed numerical continuum modeling of skyrmions interacting with a patterned race track to show that the skyrmion Hall angle can be used to create a skyrmion ratchet. Figure 69(a) illustrates the race track geometry with a ratcheting skyrmion orbit appearing as a function of time under an oscillating drive. The Magnus force is responsible for creating the 2D orbit that is necessary to induce

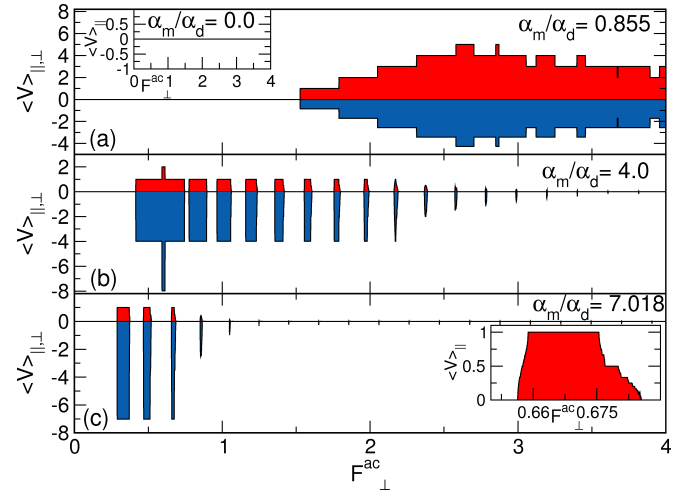


FIG. 68 Particle based simulations of skyrmion ratchet motion under perpendicular driving  $F_{\perp}^{ac}$  on the asymmetric substrate illustrated in Fig. 67 (Reichhardt *et al.*, 2015a). Panels (a,b,c) show velocities parallel,  $\langle V_{\parallel} \rangle$  (red), and perpendicular,  $\langle V_{\perp} \rangle$  (blue), to the substrate asymmetry as a function of ac driving force magnitude  $F_{\perp}^{ac}$  for different values of the Magnus force to damping force ratio  $\alpha_m/\alpha_d$ . Ratcheting with quantized velocity values occurs in both the parallel and perpendicular directions above a threshold value of  $F_{\perp}^{ac}$ , and there can be drive windows in which no ratcheting motion occurs. Inset of (a): For an overdamped system, no ratcheting occurs in either direction at any value of  $F_{\perp}^{ac}$ . Inset of (c): a blow up of panel (c) highlighting the presence of fractional velocity steps. Reprinted under CC license from C. Reichhardt *et al.*, New J. Phys. **17**, 073034 (2015).

the ratchet effect. Figure 69(b) shows that the skyrmion propagates deterministically as a function of time, while Fig. 69(c) illustrates the skyrmion velocity versus relative position. Göbel and Mertig explain that the skyrmion ratchet differs from a standard overdamped ratchet due to the fact that the Magnus force allows velocity components to be created perpendicular to the confining force produced by the sample edges.

Migita *et al.* (Migita *et al.*, 2020) considered continuum simulations of skyrmions in asymmetric constricted geometries under an oscillating magnetic field. Here the diameter of the skyrmion oscillates as a function of time, producing a unidirectional translation of the skyrmion.

Even in the absence of a substrate, a skyrmion ratchet effect can emerge. Chen *et al.* used continuum based modeling to show that it is possible to produce a skyrmion ratchet effect using biharmonic ac driving (Chen *et al.*, 2019). Under certain conditions, directed motion appears when the internal modes of the skyrmions induce an asymmetric shape oscillation. The motion can be controlled by varying the ac drive parameters. Further studies by Chen *et al.* extended this same mechanism by coupling the skyrmion to a linear defect in order to take advantage of the speed up effect and create an ultrafast ratchet effect (Chen *et al.*, 2020).

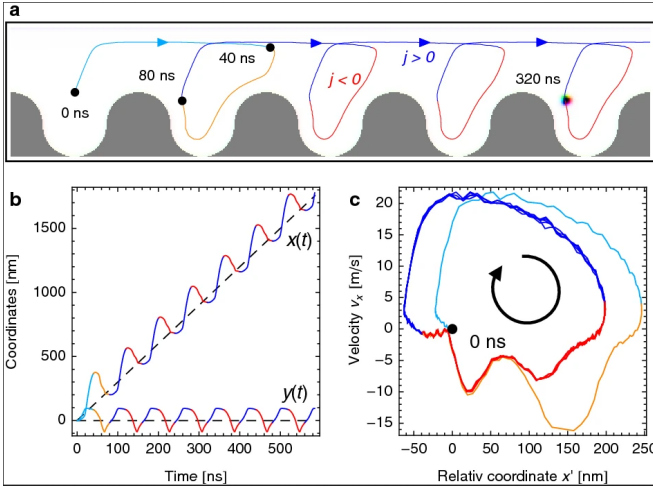


FIG. 69 Thiele-based simulations showing the operation of a ratchet mechanism in a skyrmion racetrack (Göbel and Mertig, 2021). (a) An asymmetry in the racetrack edge combines with the Magnus force to produce a 2D orbit that translates over time. (b) A plot of the position of the skyrmion as a function of time showing a deterministic ratcheting motion in the positive  $x$  direction. (c) The shape of the skyrmion orbit as a function of  $x$  direction velocity  $v_x$  vs the relative displacement in  $x$  from the average position. Reprinted under CC license from B. Göbel and I. Mertig, *Sci. Rep.* **11**, 3020 (2021).

Wang *et al.* (Wang *et al.*, 2015) found that under an oscillating field, the changing shape of the skyrmion can produce directional motion in the absence of a substrate. A similar wiggling skyrmion propagation mechanism based on parametric pumping in an oscillating electric field was studied by Yuan *et al.* (Yuan *et al.*, 2019). There have also been proposals to drive gyroscopic skyrmion motion by means of steps in the magnetic anisotropy (Zhou *et al.*, 2019b). These results indicate that in skyrmion systems, there are many possible ways in which to achieve the temporal or spatial symmetry breaking that is required to produce a ratchet effect. It would also be interesting to consider the breathing modes of skyrmions produced by biharmonic drives. These could be coupled to 1D, 2D periodic, or asymmetric periodic substrates in order to determine whether the breathing could strongly enhance the directed motion or make it easier to control.

Due to the rich dynamics of skyrmions in terms of both Magnus force and the internal modes, there are many more types of ratchet effects that could be studied. One effect that has only been considered briefly is collective ratchets. In overdamped systems, collective interactions between particles can produce incommensurate states in which the solitons themselves can undergo ratcheting motion. In these collective states, it is possible for ratchet reversals to occur (Hänggi and Marchesoni, 2009). If there are variations in the skyrmion sizes or different coexist-

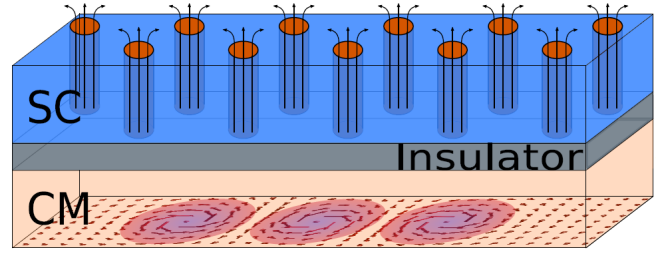


FIG. 70 Schematic of the coupling between a chiral ferromagnet (CM, tan) containing a skyrmion crystal (purple) and a superconducting film (SC, blue) (Dahir *et al.*, 2019). The materials are separated by a thin insulating barrier (gray) to ensure that only the magnetic fields from the skyrmion lattice pass into the superconductor. The attractive interaction between vortices and skyrmions generates vortices (orange) in the superconductor. Reprinted with permission from S. M. Dahir *et al.*, *Phys. Rev. Lett.* **122**, 097001 (2019). Copyright 2019 by the American Physical Society.

ing species of skyrmions, it could be possible to realize a ratchet system in which one skyrmion size or species is ratcheted more effectively or in a different direction than the other sizes or species. It would be very interesting to consider ratchet effects in collectively interacting skyrmion assemblies. Since the skyrmions have internal modes, it may even be possible to realize propagating skyrmion breathing modes. Such modes could have low dissipation and could be used as another method for transmitting information. Experimentally, asymmetric substrates could be created using periodic gradients in the sample thickness, DMI, doping, irradiation, or the magnetic field.

### E. Coupling Skyrmions to Other Quasiperiodic Lattice Structures

Another method for creating periodic structures that can act like pinning sites is to cause the skyrmions to interact with other topological objects, such as vortices in a type-II superconductor. More generally, there is interest in coupling skyrmions to superconductors in order to control certain topological aspects of the superconductor (Mascot *et al.*, 2021). Several studies have already examined interactions between superconducting vortices and skyrmions (Baumard *et al.*, 2019; Dahir *et al.*, 2019; Hals *et al.*, 2016). Figure 70 shows a schematic from Dahir *et al.* of a chiral ferromagnet coupled to a superconducting thin film through an insulating layer (Dahir *et al.*, 2019). In this case, the skyrmions produce a vortex-antivortex lattice in the superconductor. Baumard *et al.* (Baumard *et al.*, 2019) considered a thin film superconductor in which Pearl vortices are induced by the skyrmions. In these systems, the ratio of the number of skyrmions to the number of vortices can be tuned with a magnetic field, and the skyrmions experience an effective periodic

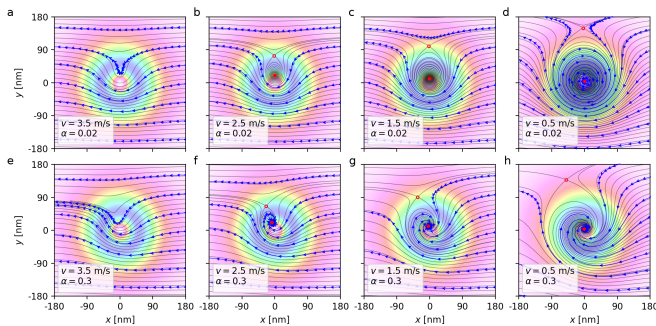


FIG. 71 Micromagnetic calculations (arrows) and Thiele equation calculations (thin lines) of skyrmion trajectories in the moving frame produced by interactions with a moving superconducting vortex (Menezes *et al.*, 2019b). The background coloring represents the  $z$  component of the magnetization from the vortex that would appear in the absence of the skyrmion. Open dots represent fixed saddle points and filled dots indicate stable spiral points. Reprinted with permission from R. M. Menezes *et al.*, Phys. Rev. B **100**, 014431 (2019). Copyright 2019 by the American Physical Society.

substrate produced by the periodicity of the vortex lattice. Further approaches include studying the effect of a driving current on such systems, where the voltage response in the superconductor could be used as a means to detect the motion of the skyrmions. The effects of either naturally occurring or artificially nanostructured pinning could also be explored. Menezes *et al.* (Menezes *et al.*, 2019b) calculated the dynamics of skyrmions interacting with a moving superconducting vortex using both micromagnetic simulations and the Thiele equation. In Fig. 71, the skyrmion trajectories in the moving frame exhibit gyroscopic spiraling motion, and in some cases skyrmions are captured by the vortex core. Recently Palermo *et al.* demonstrated experimentally that skyrmions could be used to tailor a pinning potential for vortices in a type-II superconductor (Palermo *et al.*, 2020). Future directions include analyzing different types of skyrmions interacting with vortices, or considering vortices in bulk rather than thin film systems.

## F. Single Skyrmion Manipulation

By dragging a single particle through a random disordered background or through a bath of other particles, it is possible to produce a local probe of colloidal assemblies (Olson Reichhardt and Reichhardt, 2008; Puertas and Voigtmann, 2014) or superconducting vortices (Auslaender *et al.*, 2009; Kafri *et al.*, 2007; Reichhardt, 2009; Straver *et al.*, 2008). The features in the velocity-force curves obtained for the probe particle can be used to gain insight about the behavior of the bulk system, such as changes in the viscosity and pinning force as well as the existence of cutting or entanglement. A similar local probe technique could be applied to a skyrmion system

by dragging individual skyrmions with some form of tip or by coupling an individual skyrmion to a driven object. Wang *et al.* (Wang *et al.*, 2020a) have proposed to use an optical tweezer to manipulate skyrmions by optically trapping and dragging the skyrmion. In this case, if the tip speed is too fast, the skyrmion could break away from the tip. Other possible methods for creating a local probe include dragging a skyrmion with a magnetic tip or even dragging a group of skyrmions with an array of optical traps or magnetic tips.

Along these lines, there is also the possibility that skyrmion systems could host Majorana fermion states (Rex *et al.*, 2019; Yang *et al.*, 2016). Thus, one application of skyrmion manipulation could be to drag Majorana-containing skyrmions around one another on a patterned substrate in order to create braided Majorana states for qubit operations. Such operations have been proposed for superconducting vortex systems with Majorana states in the vortex core (Ma *et al.*, 2020). The vortices are coupled to a periodic pinning array and a magnetic tip is used to perform a representative set of braiding moves that contain all of the necessary operations for quantum logic gates. A similar approach could be used for skyrmions.

## IX. SUMMARY

Skyrmions are attracting increasing interest as new materials continue to be identified which support different skyrmion species as well as related topological objects. Since skyrmions can be manipulated or driven by a variety of techniques, the role of pinning or quenched disorder will become a more important aspect of future skyrmion studies. There is already considerable evidence that skyrmions can experience both weak and strong pinning effects depending on the sample thickness or material type, and it has been demonstrated that skyrmions exhibit a rich phenomenology of dynamics, including gyroscopic motion and the skyrmion Hall angle, all of which appear to depend on the nature of the disorder as well as on the drive. Due to the presence of the Magnus force, both individual and collective skyrmion states undergo new types of pinning and depinning phenomena that are distinct from those previously studied in overdamped systems. Pinning and dynamic effects of skyrmions interacting with disordered or ordered substrates are of technological importance for skyrmion applications, and the Magnus effects in the skyrmion system open a new field in equilibrium and nonequilibrium statistical mechanics.

## ACKNOWLEDGMENTS

We gratefully acknowledge the support of the U.S. Department of Energy through the LANL/LDRD program

for this work. This work was supported by the US Department of Energy through the Los Alamos National Laboratory. Los Alamos National Laboratory is operated by Triad National Security, LLC, for the National Nuclear Security Administration of the U. S. Department of Energy (Contract No. 892333218NCA000001).

## REFERENCES

- Akhtar, W, A. Hrabec, S. Chouaieb, A. Haykal, I. Gross, M. Belmeguenai, M. S. Gabor, B. Shields, P. Maletinsky, A. Thiaville, S. Rohart, and V. Jacques (2019), “Current-induced nucleation and dynamics of skyrmions in a Co-based Heusler alloy,” *Phys. Rev. Appl.* **11**, 034066.
- Akosa, C A, O. A. Tretiakov, G. Tatara, and A. Manchon (2018), “Theory of the topological spin Hall effect in antiferromagnetic skyrmions: Impact on current-induced motion,” *Phys. Rev. Lett.* **121**, 097204.
- Arjana, I G, I. L. Fernandes, J. Chico, and S. Lounis (2020), “Sub-nanoscale atom-by-atom crafting of skyrmion-defect interaction profiles,” *Sci. Rep.* **10**, 14655.
- Auslaender, O M, L. Luan, E. W. J. Straver, J. E. Hoffman, N. C. Koshnick, E. Zeldov, D. A. Bonn, R. Liang, W. N. Hardy, and K. A. Moler (2009), “Mechanics of individual isolated vortices in a cuprate superconductor,” *Nature Phys.* **5**, 35.
- Avcı, S, Z. L. Xiao, J. Hua, A. Imre, R. Divan, J. Pearson, U. Welp, W. K. Kwok, and G. W. Crabtree (2010), “Matching effect and dynamic phases of vortex matter in  $\text{Bi}_2\text{Sr}_2\text{CaCu}_2\text{O}_8$  nanoribbon with a periodic array of holes,” *Appl. Phys. Lett.* **97**, 042511.
- Avraham, N, B. Khaykovich, Y. Myasoedov, M. Rappaport, H. Shtrikman, D. E. Feldman, T. Tamegai, P. H. Kes, M. Li, M. Konczykowski, K. van der Beek, and E. Zeldov (2001), “‘Inverse’ melting of a vortex lattice,” *Nature* **411**, 451–454.
- Back, C, V. Cros, H. Ebert, K. Everschor-Sitte, A. Fert, M. Garst, Tianping Ma, S. Mankovsky, T. L. Monchesky, M. Mostovoy, N. Nagaosa, S. S. P. Parkin, C. Pfleiderer, N. Reyren, A. Rosch, Y. Taguchi, Y. Tokura, K. von Bergmann, and Jiadong Zang (2020), “The 2020 skyrmionics roadmap,” *J. Phys. D* **53** (36), 363001.
- Baert, M, V. V. Metlushko, R. Jonckheere, V. V. Moshchalkov, and Y. Bruynseraede (1995), “Composite flux-line lattices stabilized in superconducting films by a regular array of artificial defects,” *Phys. Rev. Lett.* **74**, 3269.
- Bag, B, G. Shaw, S. S. Banerjee, S. Majumdar, A. K. Sood, and A. K. Grover (2017), “Negative velocity fluctuations and non-equilibrium fluctuation relation for a driven high critical current vortex state,” *Sci. Rep.* **7**, 5531.
- Bak, P (1982), “Commensurate phases, incommensurate phases and the devil’s staircase,” *Rep. Prog. Phys.* **45**, 587.
- Bak, P, C. Tang, and K. Wiesenfeld (1988), “Self-organized criticality,” *Phys. Rev. A* **38**, 364.
- Balents, L, M. C. Marchetti, and L. Radzihovsky (1998), “Nonequilibrium steady states of driven periodic media,” *Phys. Rev. B* **57**, 7705.
- Banerjee, S S, S. Ramakrishnan, A. K. Grover, G. Ravikumar, P. K. Mishra, V. C. Sahni, C. V. Tomy, G. Balakrishnan, D. McK. Paul, P. L. Gammel, D. J. Bishop, E. Bucher, M. J. Higgins, and S. Bhattacharya (2000), “Peak effect, plateau effect, and fishtail anomaly: The reentrant amorphization of vortex matter in  $2\text{H-NbSe}_2$ ,” *Phys. Rev. B* **62**, 11838.
- Barker, J, and O. A. Tretiakov (2016), “Static and dynamical properties of antiferromagnetic skyrmions in the presence of applied current and temperature,” *Phys. Rev. Lett.* **116**, 147203.
- Barkhausen, H (1919), “Zwei mit Hilfe der neuen Verstärker entdeckte Erscheinungen,” *Z. Phys.* **20**, 401.
- Baumard, J, J. Cayssol, F. S. Bergeret, and A. Buzdin (2019), “Generation of a superconducting vortex via Néel skyrmions,” *Phys. Rev. B* **99**, 014511.
- Beg, M, M. Albert, M.-A. Bisotti, D. Cortés-Ortuño, W. Wang, R. Carey, M. Vousden, O. Hovorka, C. Ciccarelli, C. S. Spencer, C. H. Marrows, and H. Fangohr (2017), “Dynamics of skyrmionic states in confined helimagnetic nanostructures,” *Phys. Rev. B* **95**, 014433.
- Benassi, A, A. Vanossi, and E. Tosatti (2011), “Nanofriction in cold ion traps,” *Nature Commun.* **2**, 236.
- Benz, S P, M. S. Rzchowski, M. Tinkham, and C. J. Lobb (1990), “Fractional giant Shapiro steps and spatially correlated phase motion in 2D Josephson arrays,” *Phys. Rev. Lett.* **64**, 693.
- Berdiyorov, G R, M. V. Milosevic, and F. M. Peeters (2006), “Novel commensurability effects in superconducting films with antidot arrays,” *Phys. Rev. Lett.* **96**, 207001.
- Berger, L (1970), “Side-jump mechanism for the Hall effect of ferromagnets,” *Phys. Rev. B* **2**, 4559.
- Bertotti, G, G. Durin, and A. Magni (1994), “Scaling aspects of domain wall dynamics and Barkhausen effect in ferromagnetic materials,” *J. Appl. Phys.* **75**, 5490.
- Bhattacharya, S, and M. J. Higgins (1993), “Dynamics of a disordered flux line lattice,” *Phys. Rev. Lett.* **70**, 2617.
- Birch, M T, D. Cortes-Ortuno, L. A. Turnbull, M. N. Wilson, F. Gross, N. Traeger, A. Laurenson, N. Bukin, S. H. Moody, M. Weigand, G. Schuetz, H. Popescu, R. Fan, P. Steadman, J. A. T. Verezhak, G. Balakrishnan, J. C. Loudon, A. C. Twitchett-Harrison, O. Hovorka, H. Fangohr, F. Y. Grin, J. Graefe, and P. D. Hatton (2020), “Real-space imaging of confined magnetic skyrmion tubes,” *Nature Commun.* **11** (1), 1726.
- Blatter, G, M. V. Feigel’man, V. B. Geshkenbein, A. I. Larkin, and V. M. Vinokur (1994), “Vortices in high-temperature superconductors,” *Rev. Mod. Phys.* **66**, 1125–1388.
- Bloom, I, A. C. Marley, and M. B. Weissman (1993), “Nonequilibrium dynamics of discrete fluctuators in charge-density waves in  $\text{NbSe}_3$ ,” *Phys. Rev. Lett.* **71**, 4385.
- Bogdanov, A N, and C. Panagopoulos (2020), “Physical foundations and basic properties of magnetic skyrmions,” *Nature Rev. Phys.* **2** (9), 492–498.
- Bogdanov, A N, and D. A. Yablonskii (1989), “Thermodynamically stable ‘vortices’ in magnetically ordered crystals. The mixed state of magnets,” *Sov. Phys. JETP* **68**, 101–103.
- Bohlein, T, and C. Bechinger (2012), “Experimental observation of directional locking and dynamical ordering of colloidal monolayers driven across quasiperiodic substrates,” *Phys. Rev. Lett.* **109**, 058301.
- Bohlein, T, J. Mikhael, and C. Bechinger (2012), “Observation of kinks and antikinks in colloidal monolayers driven across ordered surfaces,” *Nature Mater.* **11**, 126.
- Bömerich, T, L. Heinen, and A. Rosch (2020), “Skyrmion and tetarton lattices in twisted bilayer graphene,” *Phys. Rev. B* **102**, 100408.

- Boulle, O, J. Vogel, H. Yang, S. Pizzini, D. de Souza Chaves, A. Locatelli, T. O. Mendes, A. Sala, L. D. Buda-Prejbeanu, O. Klein, M. Belmeguenai, Y. Roussigné, A. Stashkevich, S. M. Chérif, L. Aballe, M. Foerster, M. Chshiev, S. Auffret, I. M. Miron, and G. Gaudin (2016), “Room-temperature chiral magnetic skyrmions in ultrathin magnetic nanostructures,” *Nature Nanotechnol.* **11**, 449–454.
- Braun, O M, and Y. S. Kivshar (1998), “Nonlinear dynamics of the Frenkel-Kontorova model,” *Phys. Rep.* **306**, 1–108.
- Brown, B L, U. C. Täuber, and M. Pleimling (2018), “Effect of the Magnus force on skyrmion relaxation dynamics,” *Phys. Rev. B* **97**, 020405(R).
- Brunner, M, and C. Bechinger (2002), “Phase behavior of colloidal molecular crystals on triangular light lattices,” *Phys. Rev. Lett.* **88**, 248302.
- Büchler, H P, G. Blatter, and W. Zwerger (2003), “Commensurate-incommensurate transition of cold atoms in an optical lattice,” *Phys. Rev. Lett.* **90**, 130401.
- Büttner, F, C. Moutafis, M. Schneider, B. Krüger, C. M. Günther, J. Geilhufe, C. v. Korff Schmising, J. Mohanty, B. Pfau, S. Schaffert, A. Bisig, M. Foerster, T. Schulz, C. A. F. Vaz, J. H. Franken, H. J. M. Swagten, M. Kläui, and S. Eisebitt (2015), “Dynamics and inertia of skyrmionic spin structures,” *Nature Phys.* **11**, 225–228.
- Carlson, J M, J. S. Langer, and B. E. Shaw (1994), “Dynamics of earthquake faults,” *Rev. Mod. Phys.* **66**, 657.
- Casiraghi, A, H. Corte-León, V. Vafaei, F. Garcia-Sanchez, G. Durin, M. Pasquale, G. Jakob, M. Kläui, and O. Kazakova (2019), “Individual skyrmion manipulation by local magnetic field gradients,” *Commun. Phys.* **2**, 145.
- Castell-Queralt, J, L. Gonzalez-Gomez, N. Del-Valle, A. Sanchez, and C. Navau (2019), “Accelerating, guiding, and compressing skyrmions by defect rails,” *Nanoscale* **11** (26), 12589–12594.
- Cha, M-C, and H. A. Fertig (1994), “Topological defects, orientational order, and depinning of the electron solid in a random potential,” *Phys. Rev. B* **50**, 14368.
- Cha, M-C, and H. A. Fertig (1995), “Disorder-induced phase transitions in two-dimensional crystals,” *Phys. Rev. Lett.* **74**, 4867.
- Cha, M-C, and H. A. Fertig (1998), “Peak effect and the transition from elastic to plastic depinning,” *Phys. Rev. Lett.* **80**, 3851.
- Chai, Y, P. Lu, H. Du, J. Shen, Y. Ma, K. Zhai, L. Wang, Y. Shi, H. Li, W. Wang, and Y. Sun (2018), “Observation of skyrmion liquid in a chiral magnet,” *arXiv e-prints*, arXiv:1811.01555 [cond-mat.mtrl-sci].
- Chen, Q-H, and X. Hu (2003), “Nonequilibrium phase transitions of vortex matter in three-dimensional layered superconductors,” *Phys. Rev. Lett.* **90**, 117005.
- Chen, W, L. Liu, Y. Ji, and Y. Zheng (2019), “Skyrmion ratchet effect driven by a biharmonic force,” *Phys. Rev. B* **99**, 064431.
- Chen, W, L. Liu, and Y. Zheng (2020), “Ultrafast ratchet dynamics of skyrmions by defect engineering in materials with poor conductivity under gigahertz magnetic fields,” *Phys. Rev. Applied* **14**, 064014.
- Choi, H C, S.-Z. Lin, and J.-X. Zhu (2016), “Density functional theory study of skyrmion pinning by atomic defects in MnSi,” *Phys. Rev. B* **93**, 115112.
- Chudnovsky, E M, and D. A. Garanin (2018), “Skyrmion glass in a 2D Heisenberg ferromagnet with quenched disorder,” *New J. Phys.* **20**, 03300.
- Civale, L (1997), “Vortex pinning and creep in high-temperature superconductors with columnar defects,” *Supercond. Sci. Technol.* **10**, A11.
- Coppersmith, S N, and P. B. Littlewood (1986), “Interference phenomena and mode locking in the model of deformable sliding charge-density waves,” *Phys. Rev. Lett.* **57**, 1927.
- Cote, P J, and L. V. Meisel (1991), “Self-organized criticality and the Barkhausen effect,” *Phys. Rev. Lett.* **67**, 1334.
- Crabtree, G W, and D. R. Nelson (1997), “Vortex physics in high-temperature superconductors,” *Phys. Today* **50**, 38.
- Cubitt, R, E. M. Forgan, G. Yang, S. L. Lee, D. McK. Paul, H. A. Mook, M. Yethiraj, P. H. Kes, T. W. Li, A. A. Menovsky, Z. Tarnawski, and K. Mortensen (1993), “Direct observation of magnetic flux lattice melting and decomposition in the high- $T_c$  superconductor  $\text{Bi}_{2.15}\text{Sr}_{1.95}\text{CaCu}_2\text{O}_{8+x}$ ,” *Nature* **365**, 407–411.
- Dahir, S M, A. F. Volkov, and I. M. Eremin (2019), “Interaction of skyrmions and Pearl vortices in superconductor-chiral ferromagnet heterostructures,” *Phys. Rev. Lett.* **122**, 097001.
- D’Anna, G, P. L. Gammel, H. Safar, G. B. Alers, D. J. Bishop, J. Giapintzakis, and D. M. Ginsberg (1995), “Vortex-motion-induced voltage noise in  $\text{YBa}_2\text{Cu}_3\text{O}_{7-\delta}$  single crystals,” *Phys. Rev. Lett.* **75**, 3521.
- Danneau, R, A. Ayari, D. Rideau, H. Requardt, J. E. Lorenzo, L. Ortega, P. Monceau, R. Currat, and G. Grübel (2002), “Motif ordering of a charge-density wave in the sliding state,” *Phys. Rev. Lett.* **89**, 106404.
- Das, S, Y. L. Tang, Z. Hong, M. A. P. Goncalves, M. R. McCarter, C. Klewe, K. X. Nguyen, F. Gómez-Ortiz, P. Shafer, E. Arenholz, V. A. Stoica, S.-L. Hsu, B. Wang, C. Ophus, J. F. Liu, C. T. Nelson, S. Saremi, B. Prasad, A. B. Mei, D. G. Schlom, J. Íñiguez, P. García-Fernández, D. A. Muller, L. Q. Chen, J. Junquera, L. W. Martin, and R. Ramesh (2019), “Observation of room-temperature polar skyrmions,” *Nature (London)* **568**, 368–372.
- Davis, T J, D. Janoschka, P. Dreher, B. Frank, F.-J. M. zu Heringdorf, and H. Giessen (2020), “Ultrafast vector imaging of plasmonic skyrmion dynamics with deep sub-wavelength resolution,” *Science* **368** (6489), 386.
- Denisov, K S, I. V. Rozhansky, N. S. Averkiev, and E. Lähderanta (2017), “A nontrivial crossover in topological Hall effect regimes,” *Sci. Rep.* **7**, 17204.
- Denisov, K S, I. V. Rozhansky, N. S. Averkiev, and E. Lähderanta (2018), “General theory of the topological Hall effect in systems with chiral spin textures,” *Phys. Rev. B* **98**, 195439.
- Deuschländer, S, T. Horn, H. Löwen, G. Maret, and P. Keim (2013), “Two-dimensional melting under quenched disorder,” *Phys. Rev. Lett.* **111**, 098301.
- Di Scala, N, E. Olive, Y. Lansac, Y. Fily, and J. C. Soret (2012), “The elastic depinning transition of vortex lattices in two dimensions,” *New J. Phys.* **14**, 123027.
- Díaz, S A, C. Reichhardt, D. P. Arovas, A. Saxena, and C. J. O. Reichhardt (2018), “Avalanches and criticality in driven magnetic skyrmions,” *Phys. Rev. Lett.* **120**, 117203.
- Díaz, S A, C. J. O. Reichhardt, D. P. Arovas, A. Saxena, and C. Reichhardt (2017), “Fluctuations and noise signatures of driven magnetic skyrmions,” *Phys. Rev. B* **96**, 085106.
- Ding, J, X. Yang, and T. Zhu (2015), “Manipulating current induced motion of magnetic skyrmions in the magnetic nanotrack,” *J. Phys. D: Appl. Phys.* **48**, 115004.
- Dobramysl, U, M. Pleimling, and U. C. Täuber (2014), “Pinning time statistics for vortex lines in disordered environ-

- ments,” *Phys. Rev. E* **90**, 062108.
- Dobrovolskiy, O V, and M. Huth (2015), “Dual cut-off direct current-tunable microwave low-pass filter on superconducting Nb microstrips with asymmetric nanogrooves,” *Appl. Phys. Lett.* **106**, 142601.
- Dreyfus, R, Y. Xu, T. Still, L. A. Hough, A. G. Yodh, and S. Torquato (2015), “Diagnosing hyperuniformity in two-dimensional, disordered, jammed packings of soft spheres,” *Phys. Rev. E* **91**, 012302.
- Du, C, Y.-R. Lee, C.-Y. Lo, H.-H. Lin, S.-L. Chang, M.-T. Tang, Y. P. Stetsko, and J.-J. Lee (2006), “Direct measurement of spatial distortions of charge density waves in  $K_{0.3}MoO_3$ ,” *Appl. Phys. Lett.* **88**, 241916.
- Durán, C A, P. L. Gammel, R. Wolfe, V. J. Fratello, D. J. Bishop, J. P. Rice, and D. M. Ginsberg (1992), “Real-time imaging of the magnetic flux distribution in superconducting  $YBa_2Cu_3O_{7-\delta}$ ,” *Nature (London)* **357**, 474–477.
- Duzgun, A, C. Nisoli, C. J. O. Reichhardt, and C. Reichhardt (2020), “Commensurate states and pattern switching via liquid crystal skyrmions trapped in a square lattice,” *Soft Matter* **16** (13), 3338–3343.
- Duzgun, A, J. V. Selinger, and A. Saxena (2018), “Comparing skyrmions and merons in chiral liquid crystals and magnets,” *Phys. Rev. E* **97**, 062706.
- Eichhorn, R, P. Reimann, and P. Hänggi (2002), “Brownian motion exhibiting absolute negative mobility,” *Phys. Rev. Lett.* **88**, 190601.
- Ertas, D, and M. Kardar (1996), “Anisotropic scaling in threshold critical dynamics of driven directed lines,” *Phys. Rev. B* **53**, 3520.
- Everschor-Sitte, K, J. Masell, R. M. Reeve, and M. Kläui (2018), “Perspective: Magnetic skyrmions - Overview of recent progress in an active research field,” *J. Appl. Phys.* **124**, 240901.
- Everschor-Sitte, K, and M. Sitte (2014), “Real-space Berry phases: Skyrmion soccer (invited),” *J. Appl. Phys.* **115**, 172602.
- Fangohr, H, S. J. Cox, and P. A. J. de Groot (2001), “Vortex dynamics in two-dimensional systems at high driving forces,” *Phys. Rev. B* **64**, 064505.
- Fassbender, J, J. Grenzer, O. Roshchupkina, Y. Choi, J. S. Jiang, and S. D. Bader (2009), “The effect of ion irradiation and annealing on exchange spring magnets,” *J. Appl. Phys.* **105**, 023902.
- Feigel'man, M V, V. B. Geshkenbein, A. I. Larkin, and V. M. Vinokur (1989), “Theory of collective flux creep,” *Phys. Rev. Lett.* **63**, 2303.
- Feilhauer, J, S. Saha, J. Tobik, M. Zelent, L. J. Heyderman, and M. Mruzckiewicz (2020), “Controlled motion of skyrmions in a magnetic antidot lattice,” *Phys. Rev. B* **102**, 184425.
- Fernandes, I L, J. Bouaziz, S. Blügel, and S. Lounis (2018), “Universality of defect-skyrmion interaction profiles,” *Nature Commun.* **9**, 4395.
- Fernandes, I L, J. Chico, and S. Lounis (2020), “Impurity-dependent gyrotropic motion, deflection and pinning of current-driven ultrasmall skyrmions in  $pdfe/ir(111)$  surface,” *J. Phys.: Condens. Matter* **32**, 425802.
- Fert, A, V. Cros, and J. Sampaio (2013), “Skyrmions on the track,” *Nat. Nanotechnol.* **8**, 152.
- Fert, A, N. Reyren, and V. Cros (2017), “Magnetic skyrmions: advances in physics and potential applications,” *Nature Rev. Mater.* **2**, 17031.
- Fily, Y, E. Olive, N. Di Scala, and J. C. Soret (2010), “Critical behavior of plastic depinning of vortex lattices in two dimensions: Molecular dynamics simulations,” *Phys. Rev. B* **82**, 134519.
- Fiory, A T (1971), “Quantum interference effects of a moving vortex lattice in Al films,” *Phys. Rev. Lett.* **27**, 501.
- Fisher, D S (1985), “Sliding charge-density waves as a dynamic critical phenomenon,” *Phys. Rev. B* **31**, 1396.
- Fisher, D S (1998), “Collective transport in random media: From superconductors to earthquakes,” *Phys. Rep.* **301**, 113.
- Fisher, D S, M. P. A. Fisher, and D. A. Huse (1991), “Thermal fluctuations, quenched disorder, phase transitions, and transport in type-II superconductors,” *Phys. Rev. B* **43**, 130.
- Foster, D, C. Kind, P. J. Ackerman, J.-S. B. Tai, M. R. Dennis, and I. I. Smalyukh (2019), “Two-dimensional skyrmion bags in liquid crystals and ferromagnets,” *Nature Phys.* **15** (7), 655.
- Franken, J H, H. J. M. Swagten, and B. Koopmans (2012), “Shift registers based on magnetic domain wall ratchets with perpendicular anisotropy,” *Nature Nanotechnol.* **7**, 499–503.
- Fujishiro, Y, N. Kanazawa, T. Nakajima, X. Z. Yu, K. Ohishi, Y. Kawamura, K. Kakurai, T. Arima, H. Mitamura, A. Miyake, K. Akiba, M. Tokunaga, A. Matsuo, K. Kindo, T. Koretsune, R. Arita, and Y. Tokura (2019), “Topological transitions among skyrmion- and hedgehog-lattice states in cubic chiral magnets,” *Nature Commun.* **10**, 1059.
- Ganguli, S C, H. Singh, G. Saraswat, R. Ganguly, V. Bagwe, P. Shirage, A. Thamizhavel, and P. Raychaudhuri (2015), “Disordering of the vortex lattice through successive destruction of positional and orientational order in a weakly pinned  $Co_{0.0075}NbSe_2$  single crystal,” *Sci. Rep.* **5**, 10613.
- Gao, S, H. D. Rosales, F. A. Gómez Albarracín, V. Tsurkan, G. Kaur, T. Fennell, P. Steffens, M. Boehm, P. Čermák, A. Schneidewind, E. Ressouche, D. C. Cabra, C. Rüegg, and O. Zaharko (2020), “Fractional antiferromagnetic skyrmion lattice induced by anisotropic couplings,” *Nature (London)* **586**, 37.
- Garst, M, J. Waizner, and D. Grundler (2017), “Collective spin excitations of helices and magnetic skyrmions: review and perspectives of magnonics in non-centrosymmetric magnets,” *J. Phys. D: Appl. Phys.* **50**, 293002.
- Giamarchi, T, and P. Le Doussal (1995), “Elastic theory of flux lattices in the presence of weak disorder,” *Phys. Rev. B* **52**, 1242.
- Giamarchi, T, and P. Le Doussal (1996), “Moving glass phase of driven lattices,” *Phys. Rev. Lett.* **76**, 3408.
- Gilbert, D A, A. J. Grutter, P. M. Neves, G.-J. Shu, G. Zimányi, B. B. Maranville, F.-C. Chou, K. Krycka, N. P. Butch, S. Huang, and J. A. Borchers (2019), “Precipitating ordered skyrmion lattices from helical spaghetti and granular powders,” *Phys. Rev. Mater.* **3**, 014408.
- Gilbert, D A, B. B. Maranville, A. L. Balk, B. J. Kirby, P. Fischer, D. T. Pierce, J. Unguris, J. A. Borchers, and K. Liu (2015), “Realization of ground-state artificial skyrmion lattices at room temperature,” *Nature Commun.* **6**, 8462.
- Giller, D, A. Shaulov, R. Prozorov, Y. Abulafia, Y. Wolfus, L. Burlachkov, Y. Yeshurun, E. Zeldov, V. M. Vinokur, J. L. Peng, and R. L. Greene (1997), “Disorder-induced transition to entangled vortex solid in Nd-Ce-Cu-O crystal,” *Phys. Rev. Lett.* **79**, 2542.

- Goa, P E, H. Hauglin, M. Baziljevich, E. Il'yashenko, P. L. Gammel, and T. H. Johansen (2001), "Real-time magneto-optical imaging of vortices in superconducting NbSe<sub>2</sub>," *Supercond. Sci. Technol.* **14**, 729.
- Göbel, B, and I. Mertig (2021), "Skyrmion ratchet propagation: utilizing the skyrmion Hall effect in AC racetrack storage devices," *Sci. Rep.* **11**, 3020.
- Göbel, B, I. Mertig, and O. A. Tretiakov (2021), "Beyond skyrmions: Review and perspectives of alternative magnetic quasiparticles," *Phys. Rep.* **895**, 1.
- Gong, X, H. Y. Yuan, and X. R. Wang (2020), "Current-driven skyrmion motion in granular films," *Phys. Rev. B* **101**, 064421.
- Gotcheva, V, A. T. J. Wang, and S. Teitel (2004), "Lattice gas dynamics: Application to driven vortices in two dimensional superconductors," *Phys. Rev. Lett.* **92**, 247005.
- Grigorenko, A N, S. J. Bending, M. J. Van Bael, M. Lange, V. V. Moshchalkov, H. Fangohr, and P. A. J. de Groot (2003), "Symmetry locking and commensurate vortex domain formation in periodic pinning arrays," *Phys. Rev. Lett.* **90**, 237001.
- Grollier, J, D. Querlioz, K. Y. Camsari, K. Everschor-Sitte, S. Fukami, and M. D. Stiles (2020), "Neuromorphic spintronics," *Nature Electron.* **3** (7), 360–370.
- Gross, I, W. Akhtar, A. Hrabec, J. Sampaio, L. J. Martínez, S. Chouaieb, B. J. Shields, P. Maletinsky, A. Thiaville, S. Rohart, and V. Jacques (2018), "Skyrmion morphology in ultrathin magnetic films," *Phys. Rev. Mater.* **2**, 024406.
- Groth, J, C. Reichhardt, C. J. Olson, S. B. Field, and F. Nori (1996), "Vortex plastic motion in twinned superconductors," *Phys. Rev. Lett.* **77**, 3625.
- Grüner, G, A. Zawadowski, and P. M. Chaikin (1981), "Non-linear conductivity and noise due to charge-density-wave depinning in NbSe<sub>3</sub>," *Phys. Rev. Lett.* **46**, 511.
- Guillamón, I, R. Córdoba, J. Sesé, J. M. De Teresa, M. R. Ibarra, S. Vieira, and H. Suderow (2014), "Enhancement of long-range correlations in a 2D vortex lattice by an incommensurate 1D disorder potential," *Nature Phys.* **10**, 851.
- Gutierrez, J, A. V. Silhanek, J. Van de Vondel, W. Gillijns, and V. V. Moshchalkov (2009), "Transition from turbulent to nearly laminar vortex flow in superconductors with periodic pinning," *Phys. Rev. B* **80**, 140514.
- Haberkorn, N, B. Maiorov, I. O. Usov, M. Weigand, W. Hirata, S. Miyasaka, S. Tajima, N. Chikumoto, K. Tanabe, and L. Civale (2012), "Influence of random point defects introduced by proton irradiation on critical current density and vortex dynamics of Ba(Fe<sub>0.925</sub>Co<sub>0.075</sub>)<sub>2</sub>As<sub>2</sub> single crystals," *Phys. Rev. B* **85**, 014522.
- Hals, K M D, M. Schechter, and M. S. Rudner (2016), "Composite topological excitations in ferromagnet-superconductor heterostructures," *Phys. Rev. Lett.* **117**, 017001.
- Hänggi, P, and F. Marchesoni (2009), "Artificial Brownian motors: Controlling transport on the nanoscale," *Rev. Mod. Phys.* **81**, 387.
- Hanneken, C, A. Kubetzka, K. von Bergmann, and R. Wiesendanger (2016), "Pinning and movement of individual nanoscale magnetic skyrmions via defects," *New J. Phys.* **18**, 055009.
- Harada, K, O. Kamimura, H. Kasai, T. Matsuda, A. Tonomura, and V. V. Moshchalkov (1996), "Direct observation of vortex dynamics in superconducting films with regular arrays of defects," *Science* **274**, 1167.
- Harris, J M, N. P. Ong, R. Gagnon, and L. Taillefer (1995), "Washboard frequency of the moving vortex lattice in YBa<sub>2</sub>Cu<sub>3</sub>O<sub>6.93</sub> detected by ac-dc interference," *Phys. Rev. Lett.* **74**, 3684.
- Heinze, S, K. von Bergmann, M. Menzel, J. Brede, A. Kubetzka, R. Wiesendanger, G. Bihlmayer, and S. Blügel (2011), "Spontaneous atomic-scale magnetic skyrmion lattice in two dimensions," *Nature Phys.* **7**, 713–718.
- Henderson, W, E. Y. Andrei, M. J. Higgins, and S. Bhattacharya (1996), "Metastability and glassy behavior of a driven flux-line lattice," *Phys. Rev. Lett.* **77**, 2077.
- Herrero-Albillos, J, C. Castán-Guerrero, F. Valdés-Bango, J. Bartolomé, F. Bartolomé, F. Kronast, A. Hierro-Rodríguez, L. M. Álvarez Prado, J. I. Martín, M. Vélez, J. M. Alameda, J. Sesé, and L. M. García (2018), "2d magnetic domain wall ratchet: The limit of submicrometric holes," *Mater. Design* **138**, 111.
- Hess, H F, R. B. Robinson, R. C. Dynes, J. M. Valles, and J. V. Waszczak (1989), "Scanning-tunneling-microscope observation of the Abrikosov flux lattice and the density of states near and inside a fluxoid," *Phys. Rev. Lett.* **62**, 214.
- Hirata, Y, D.-H. Kim, S. K. Kim, D.-K. Lee, S.-H. Oh, D.-Y. Kim, T. Nishimura, T. Okuno, Y. Futakawa, H. Yoshikawa, A. Tsukamoto, Y. Tserkovnyak, Y. Shiota, T. Moriyama, S.-B. Choe, K.-J. Lee, and T. Ono (2019), "Vanishing skyrmion Hall effect at the angular momentum compensation temperature of a ferrimagnet," *Nature Nanotechnol.* **14**, 232–236.
- Hoffmann, M, B. Zimmermann, G. P. Müller, D. Schürhoff, N. S. Kiselev, C. Melcher, and S. Blügel (2017), "Antiskyrmions stabilized at interfaces by anisotropic Dzyaloshinskii-Moriya interactions," *Nature Commun.* **8**, 308.
- Hoshino, S, and N. Nagaosa (2018), "Theory of the magnetic skyrmion glass," *Phys. Rev. B* **97**, 024413.
- Hrabec, A, J. Sampaio, M. Belmeguenai, I. Gross, R. Weil, S. M. Chérif, A. Stashkevich, V. Jacques, A. Thiaville, and S. Rohart (2017), "Current-induced skyrmion generation and dynamics in symmetric bilayers," *Nature Commun.* **8**, 15765.
- Hsu, P-J, L. Rózsa, A. Finco, L. Schmidt, K. Palotás, E. Vedmedenko, L. Udvardi, L. Szunyogh, A. Kubetzka, K. von Bergmann, and R. Wiesendanger (2018), "Inducing skyrmions in ultrathin Fe films by hydrogen exposure," *Nature Commun.* **9**, 1571.
- Hu, J, and R. M. Westervelt (1995), "Collective transport in two-dimensional magnetic bubble arrays," *Phys. Rev. B* **51**, 17279(R).
- Huang, P, T. Schonenberger, M. Cantoni, L. Heinen, A. Magrez, A. Rosch, F. Carbone, and H. M. Ronnow (2020), "Melting of a skyrmion lattice to a skyrmion liquid via a hexatic phase," *Nature Nanotechnol.* **15** (9), 761.
- Hwa, T, P. Le Doussal, D. R. Nelson, and V. M. Vinokur (1993), "Flux pinning and forced vortex entanglement by splayed columnar defects," *Phys. Rev. Lett.* **71**, 3545.
- Ikka, M, A. Takeuchi, and M. Mochizuki (2018), "Resonance modes and microwave-driven translational motion of a skyrmion crystal under an inclined magnetic field," *Phys. Rev. B* **98**, 184428.
- Iwasaki, J, W. Koshibae, and N. Nagaosa (2014), "Colossal spin transfer torque effect on skyrmion along the edge," *Nano Lett.* **14**, 4432–4437.



- Iwasaki, J, M. Mochizuki, and N. Nagaosa (2013a), “Current-induced skyrmion dynamics in constricted geometries,” *Nature Nanotechnol.* **8**, 742–747.
- Iwasaki, J, M. Mochizuki, and N. Nagaosa (2013b), “Universal current-velocity relation of skyrmion motion in chiral magnets,” *Nat. Commun.* **4**, 1463.
- Jani, H, J.-C. Lin, J. Chen, J. Harrison, F. Maccherozzi, J. Schad, S. Prakash, C.-B. Eom, A. Ariando, T. Venkatesan, and P. G. Radaelli (2021), “Antiferromagnetic half-skyrmions and bimerons at room temperature,” *Nature (London)* **590**, 74.
- Jena, J, B. Göbel, T. Ma, V. Kumar, R. Saha, I. Mertig, C. Felser, and S. S. P. Parkin (2020), “Elliptical Bloch skyrmion chiral twins in an antiskyrmion system,” *Nature Commun.* **11** (1), 1115.
- Jensen, H J, A. Brass, and A. J. Berlinsky (1988), “Lattice deformations and plastic flow through bottlenecks in a two-dimensional model for flux pinning in type-II superconductors,” *Phys. Rev. Lett.* **60**, 1676.
- Jiang, W, G. Chen, K. Liu, J. Zang, S. G. E. te Velthuis, and A. Hoffmann (2017a), “Skyrmions in magnetic multilayers,” *Phys. Rep.* **704**, 1–49.
- Jiang, W, P. Upadhyaya, W. Zhang, G. Yu, M. B. Jungfleisch, F. Y. Fradin, J. E. Pearson, Y. Tserkovnyak, K. L. Wang, O. Heinonen, S. G. E. te Velthuis, and A. Hoffmann (2015), “Blowing magnetic skyrmion bubbles,” *Science* **349**, 283–286.
- Jiang, W, X. Zhang, G. Yu, W. Zhang, X. Wang, M. B. Jungfleisch, J. E. Pearson, X. Cheng, O. Heinonen, K. L. Wang, Y. Zhou, A. Hoffmann, and S. G. E. te Velthuis (2017b), “Direct observation of the skyrmion Hall effect,” *Nature Phys.* **13**, 162.
- Jin, Z, T. T. Liu, W. H. Li, X. M. Zhang, Z. P. Hou, D. Y. Chen, Z. Fan, M. Zeng, X. B. Lu, X. S. Gao, M. H. Qin, and J.-M. Liu (2020), “Dynamics of antiferromagnetic skyrmions in the absence or presence of pinning defects,” *Phys. Rev. B* **102**, 054419.
- Jonietz, F, S. Mühlbauer, C. Pfleiderer, A. Neubauer, W. Münzer, A. Bauer, T. Adams, R. Georgii, P. Böni, R. A. Duine, K. Everschor, M. Garst, and A. Rosch (2010), “Spin transfer torques in MnSi at ultralow current densities,” *Science* **330**, 1648.
- Juge, R, S.-G. Je, D. de Souza Chaves, L. D. Buda-Prejbeanu, J. Peña-García, J. Nath, I. M. Miron, K. G. Rana, L. Aballe, M. Foerster, F. Genuzio, T. O. Mentès, A. Locatelli, F. Maccherozzi, S. S. Dhesi, M. Belmeguenai, Y. Roussigné, S. Auffret, S. Pizzini, G. Gaudin, J. Vogel, and O. Boulle (2019), “Current-driven dynamics of magnetic skyrmions in an ultrathin film: experiments and modelling,” *Phys. Rev. Appl.* **12**, 044007.
- Juniper, M P N, A. V. Straube, R. Besseling, D. G. A. L. Aarts, and R. P. A. Dullens (2015), “Microscopic dynamics of synchronization in driven colloids,” *Nature Commun.* **6**, 7187.
- Kafri, Y, D. R. Nelson, and A. Polkovnikov (2007), “Unzipping vortices in type-II superconductors,” *Phys. Rev. B* **76**, 144501.
- Kagawa, F, H. Oike, W. Koshibae, A. Kikkawa, Y. Okamura, Y. Taguchi, N. Nagaosa, and Y. Tokura (2017), “Current-induced viscoelastic topological unwinding of metastable skyrmion strings,” *Nature Commun.* **8**, 1332.
- Kardar, M (1998), “Nonequilibrium dynamics of interfaces and lines,” *Phys. Rep.* **301**, 85.
- Karube, K, J. S. White, D. Morikawa, C. D. Dewhurst, R. Cubitt, A. Kikkawa, X. Yu, Y. Tokunaga, T. Arima, H. M. Rønnow, Y. Tokura, and Y. Taguchi (2018), “Disordered skyrmion phase stabilized by magnetic frustration in a chiral magnet,” *Sci. Adv.* **4**, eaar7043.
- Karube, K, J. S. White, N. Reynolds, J. L. Gavilano, H. Oike, A. Kikkawa, F. Kagawa, Y. Tokunaga, H. M. Rønnow, Y. Tokura, and Y. Taguchi (2016), “Robust metastable skyrmions and their triangular-square lattice structural transition in a high-temperature chiral magnet,” *Nature Mater.* **15**, 1237–1242.
- Kemmler, M, C. Gürlich, A. Sterck, H. Pöhler, M. Neuhaus, M. Siegel, R. Kleiner, and D. Koelle (2006), “Commensurability effects in superconducting Nb films with quasiperiodic pinning arrays,” *Phys. Rev. Lett.* **97**, 147003.
- Kim, J-V, and M.-W. Yoo (2017), “Current-driven skyrmion dynamics in disordered films,” *Appl. Phys. Lett.* **110**, 132404.
- Klein, T, I. Joumard, S. Blanchard, J. Marcus, R. Cubitt, T. Giamarchi, and P. Le Doussal (2001), “A Bragg glass phase in the vortex lattice of a type II superconductor,” *Nature* **413**, 404–406.
- Klongcheongsan, T, T. J. Bullard, and U. C. Täuber (2010), “Nonequilibrium steady states of driven magnetic flux lines in disordered type-II superconductors,” *Supercond. Sci. Technol.* **23**, 025023.
- Kolesnikov, A G, M. E. Steblyi, A. S. Samardak, and A. V. Ognev (2018), “Skyrmionium – high velocity without the skyrmion Hall effect,” *Sci. Rep.* **8**, 16966.
- Kolton, A B, D. Domínguez, and N. Grønbech-Jensen (1999), “Hall noise and transverse freezing in driven vortex lattices,” *Phys. Rev. Lett.* **83**, 3061.
- Kolton, A B, R. Exartier, L. F. Cugliandolo, D. Domínguez, and N. Grønbech-Jensen (2002), “Effective temperature in driven vortex lattices with random pinning,” *Phys. Rev. Lett.* **89**, 227001.
- Kong, L, and J. Zang (2013), “Dynamics of an insulating skyrmion under a temperature gradient,” *Phys. Rev. Lett.* **111**, 067203.
- Korda, P T, M. B. Taylor, and D. G. Grier (2002), “Kinetically locked-in colloidal transport in an array of optical tweezers,” *Phys. Rev. Lett.* **89**, 128301.
- Koshelev, A E, and V. M. Vinokur (1994), “Dynamic melting of the vortex lattice,” *Phys. Rev. Lett.* **73**, 3580.
- Koshibae, W, and N. Nagaosa (2018), “Theory of current-driven skyrmions in disordered magnets,” *Sci. Rep.* **8**, 6328.
- Koshibae, W, and N. Nagaosa (2019), “Dynamics of skyrmion in disordered chiral magnet of thin film form,” *Sci. Rep.* **9**, 5111.
- Kosterlitz, J M, and D. J. Thouless (1973), “Ordering, metastability and phase transitions in two-dimensional systems,” *J. Phys. C* **6**, 1181.
- Koushik, R, S. Kumar, K. R. Amin, M. Mondal, J. Jesudasan, A. Bid, P. Raychaudhuri, and A. Ghosh (2013), “Correlated conductance fluctuations close to the Berezinskii-Kosterlitz-Thouless transition in ultrathin NbN films,” *Phys. Rev. Lett.* **111**, 197001.
- Kovalev, A A (2014), “Skyrmionic spin Seebeck effect via dissipative thermomagnonic torques,” *Phys. Rev. B* **89**, 241101.
- Kovalev, A A, and S. Sandhoefner (2018), “Skyrmions and antiskyrmions in quasi-two-dimensional magnets,” *Front. Phys.* **6**, 98.

- Kruchkov, A J, J. S. White, M. Bartkowiak, I. Živković, A. Magrez, and H. M. Rønnow (2018), “Direct electric field control of the skyrmion phase in a magnetoelectric insulator,” *Sci. Rep.* **8**, 10466.
- Kumar, M, A. Laitinen, and P. Hakonen (2018), “Unconventional fractional quantum Hall states and Wigner crystallization in suspended Corbino graphene,” *Nature Commun.* **9**, 2776.
- Latimer, M L, G. R. Berdiyrov, Z. L. Xiao, F. M. Peeters, and W. K. Kwok (2013), “Realization of artificial ice systems for magnetic vortices in a superconducting MoGe thin film with patterned nanostructures,” *Phys. Rev. Lett.* **111**, 067001.
- Lavergne, F A, A. Curran, D. G. A. L. Aarts, and R. P. A. Dullens (2018), “Dislocation-controlled formation and kinetics of grain boundary loops in two-dimensional crystals,” *Proc. Natl. Acad. Sci. (USA)* **115**, 6922–6927.
- Le Thien, Q, D. McDermott, C. J. Olson Reichhardt, and C. Reichhardt (2016), “Orientational ordering, buckling, and dynamic transitions for vortices interacting with a periodic quasi-one-dimensional substrate,” *Phys. Rev. B* **93**, 014504.
- Le Thien, Q, D. McDermott, C. J. O. Reichhardt, and C. Reichhardt (2017), “Enhanced pinning for vortices in hyperuniform pinning arrays and emergent hyperuniform vortex configurations with quenched disorder,” *Phys. Rev. B* **96**, 094516.
- Lee, C S, B. Jankó, I. Derényi, and A. L. Barabási (1999), “Reducing vortex density in superconductors using the ‘ratchet’ effect,” *Nature (London)* **400**, 337.
- Legrand, W, D. Maccariello, N. Reyren, K. Garcia, C. Moutafis, C. Moreau-Luchaire, S. Collin, K. Bouzehouane, V. Cros, and A. Fert (2017), “Room-temperature current-induced generation and motion of sub-100 nm skyrmions,” *Nano Lett.* **17**, 2703–2712.
- Leliaert, J, M. Dvornik, J. Mulkers, J. De Clercq, M. V. Milosević, and B. Van Waeyenberge (2018), “Fast micromagnetic simulations on GPU – recent advances made with mumax<sup>3</sup>,” *J. Phys. D: Appl. Phys.* **51**, 123002.
- Leliaert, J, P. Gypens, M. V. Milosević, B. Van Waeyenberge, and J. Mulkers (2019), “Coupling of the skyrmion velocity to its breathing mode in periodically notched nanotracks,” *J. Phys. D: Appl. Phys.* **52**, 024003.
- Leonov, A O, and M. Mostovoy (2015), “Multiply periodic states and isolated skyrmions in an anisotropic frustrated magnet,” *Nature Commun.* **6**, 8275.
- Leonov, A O, and C. Pappas (2019), “Skyrmion clusters and conical droplets in bulk helimagnets with cubic anisotropy,” *Phys. Rev. B* **99**, 144410.
- Leroux, M, M. J. Stolt, S. Jin, D. V. Pete, C. Reichhardt, and B. Maiorov (2018), “Skyrmion lattice topological Hall effect near room temperature,” *Sci. Rep.* **8**, 15510.
- Levy, J, and M. Sherwin (1991), “Poincaré sections of charge-density-wave dynamics: Mode locking,” *Phys. Rev. Lett.* **67**, 2846.
- Li, S, W. Kang, X. Zhang, T. Nie, Y. Zhou, K. L. Wang, and W. Zhao (2021), *Mater. Horiz.* **X**, XXXX.
- Li, Z-A, F. Zheng, A. H. Tavabi, J. Caron, C. Jin, H. Du, A. Kovács, M. Tian, M. Farle, and R. E. Dunin-Borkowski (2017), “Magnetic skyrmion formation at lattice defects and grain boundaries studied by quantitative off-axis electron holography,” *Nano Lett.* **17**, 1395–1401.
- Liang, D, J. P. DeGrave, M. J. Stolt, Y. Tokura, and S. Jin (2015), “Current-driven dynamics of skyrmions stabilized in MnSi nanowires revealed by topological Hall effect,” *Nature Commun.* **6**, 8217.
- Libál, A, C. J. Olson Reichhardt, and C. Reichhardt (2009), “Creating artificial ice states using vortices in nanostructured superconductors,” *Phys. Rev. Lett.* **102**, 237004.
- Libál, A, C. Reichhardt, and C. J. Olson Reichhardt (2006), “Realizing colloidal artificial ice on arrays of optical traps,” *Phys. Rev. Lett.* **97**, 228302.
- Lin, N S, T. W. Heitmann, K. Yu, B. L. T. Plourde, and V. R. Misko (2011), “Rectification of vortex motion in a circular ratchet channel,” *Phys. Rev. B* **84**, 144511.
- Lin, S-Z, and C. D. Batista (2018), “Face centered cubic and hexagonal close packed skyrmion crystals in centrosymmetric magnets,” *Phys. Rev. Lett.* **120**, 077202.
- Lin, S-Z, C. D. Batista, C. Reichhardt, and A. Saxena (2014), “ac current generation in chiral magnetic insulators and skyrmion motion induced by the spin Seebeck effect,” *Phys. Rev. Lett.* **112**, 187203.
- Lin, S-Z, C. Reichhardt, C. D. Batista, and A. Saxena (2013a), “Driven skyrmions and dynamical transitions in chiral magnets,” *Phys. Rev. Lett.* **110**, 207202.
- Lin, S-Z, C. Reichhardt, C. D. Batista, and A. Saxena (2013b), “Particle model for skyrmions in metallic chiral magnets: Dynamics, pinning, and creep,” *Phys. Rev. B* **87**, 214419.
- Lin, S-Z, and A. Saxena (2016), “Dynamics of Dirac strings and monopolelike excitations in chiral magnets under a current drive,” *Phys. Rev. B* **93**, 060401(R).
- Lin, S-Z, J.-X. Zhu, and A. Saxena (2019), “Kelvin modes of a skyrmion line in chiral magnets and the associated magnon transport,” *Phys. Rev. B* **99**, 140408.
- Litzius, K, J. Leliaert, P. Bassirian, D. Rodrigues, S. Kromin, I. Limesh, J. Zazvorka, K.-J. Lee, J. Mulkers, N. Kerber, D. Heinze, N. Keil, R. M. Reeve, M. Weigand, B. Van Waeyenberge, G. Schütz, K. Everschor-Sitte, G. S. D. Beach, and M. Kläui (2020), “The role of temperature and drive current in skyrmion dynamics,” *Nature Electron.* **3** (1), 30–36.
- Litzius, K, I. Limesh, B. Krüger, P. Bassirian, L. Caretta, K. Richter, F. Büttner, K. Sato, O. A. Tretiakov, J. Förster, R. M. Reeve, M. Weigand, I. Bykova, H. Stoll, G. Schütz, G. S. D. Beach, and M. Kläui (2017), “Skyrmion Hall effect revealed by direct time-resolved X-ray microscopy,” *Nature Phys.* **13**, 170.
- Liu, Y, W. Hou, X. Han, and J. Zang (2020), “Three-dimensional dynamics of a magnetic hopfion driven by spin transfer torque,” *Phys. Rev. Lett.* **124**, 127204.
- Liu, Y, N. Lei, C. Wang, X. Zhang, W. Kang, D. Zhu, Y. Zhou, X. Liu, Y. Zhang, and W. Zhao (2019), “Voltage-driven high-speed skyrmion motion in a skyrmion-shift device,” *Phys. Rev. Appl.* **11**, 014004.
- Liu, Y-H, and Y.-Q. Li (2013), “A mechanism to pin skyrmions in chiral magnets,” *J. Phys.: Condens. Matt.* **25**, 076005.
- Loreto, R P, X. Zhang, Y. Zhou, M. Ezawac, X. Liu, and C. I. L. de Araujo (2019), “Manipulation of magnetic skyrmions in a locally modified synthetic antiferromagnetic racetrack,” *J. Mag. Mag. Mater.* **482**, 155–159.
- Loudon, J C, A. O. Leonov, A. N. Bogdanov, M. Ciomaga Hatnean, and G. Balakrishnan (2018), “Direct observation of attractive skyrmions and skyrmion clusters in the cubic helimagnet Cu<sub>2</sub>OSeO<sub>3</sub>,” *Phys. Rev. B* **97**, 134403.

- Luo, M-B, and X. Hu (2007), “Depinning and creep motion in glass states of flux lines,” *Phys. Rev. Lett.* **98**, 267002.
- Luo, S, M. Song, X. Li, Y. Zhang, J. Hong, X. Yang, X. Zou, N. Xu, and L. You (2018), “Reconfigurable skyrmion logic gates,” *Nano Lett.* **18**, 1180–1184.
- Ma, F, C. Reichhardt, W. Gan, C. J. Olson Reichhardt, and W. S. Lew (2016), “Emergent geometric frustration of artificial magnetic skyrmion crystals,” *Phys. Rev. B* **94**, 144405.
- Ma, X, C. J. Olson Reichhardt, and C. Reichhardt (2017), “Reversible vector ratchets for skyrmion systems,” *Phys. Rev. B* **95**, 104401.
- Ma, X, C. J. O. Reichhardt, and C. Reichhardt (2020), “Braiding Majorana fermions and creating quantum logic gates with vortices on a periodic pinning structure,” *Phys. Rev. B* **101**, 024514.
- Maccariello, D, W. Legrand, N. Reyren, K. Garcia, K. Bouzehouane, S. Collin, V. Cros, and A. Fert (2018), “Electrical detection of single magnetic skyrmions in metallic multilayers at room temperature,” *Nature Nanotechnol.* **13**, 233–237.
- MacDonald, M P, G. C. Spalding, and K. Dholakia (2003), “Microfluidic sorting in an optical lattice,” *Nature (London)* **426**, 421–424.
- MacKinnon, C R, S. Lepadatu, T. Mercer, and P. R. Bissell (2020), “Role of an additional interfacial spin-transfer torque for current-driven skyrmion dynamics in chiral magnetic layers,” *Phys. Rev. B* **102**, 214408.
- Mankalale, M G, Z. Zhao, J.-P. Wang, and S. S. Sapatnekar (2019), “SkyLogic - A proposal for a skyrmion logic device,” *IEEE Trans. Electron Devices* **66**, 1990–1996.
- Marchiori, E, P. J. Curran, J. Kim, N. Satchell, G. Burnell, and S. J. Bending (2017), “Reconfigurable superconducting vortex pinning potential for magnetic disks in hybrid structures,” *Sci. Rep.* **7**, 45182.
- Marconi, V I, A. B. Kolton, J. A. Capitán, J. A. Cuesta, A. Pérez-Junquera, M. Vélez, J. I. Martín, and J. M. R. Parrondo (2011), “Crossed-ratchet effects and domain wall geometrical pinning,” *Phys. Rev. B* **83**, 214403.
- Marley, A C, M. J. Higgins, and S. Bhattacharya (1995), “Flux flow noise and dynamical transitions in a flux line lattice,” *Phys. Rev. Lett.* **74**, 3029–3032.
- Martín, J I, M. Vélez, J. Nogués, and I. K. Schuller (1997), “Flux pinning in a superconductor by an array of submicrometer magnetic dots,” *Phys. Rev. Lett.* **79**, 1929.
- Martinez, J C, W. S. Lewb, W. L. Ganb, and M. B. A. Jalil (2018), “Theory of current-induced skyrmion dynamics close to a boundary,” *J. Mag. Mag. Mater.* **465**, 685–691.
- Martinoli, P, O. Daldini, C. Leemann, and E. Stocker (1975), “A. C. quantum interference in superconducting films with periodically modulated thickness,” *Solid State Commun.* **17**, 205.
- Mascot, E, J. Bedow, M. Graham, S. Rachel, and D. K. Morr (2021), “Topological superconductivity in skyrmion lattices,” *npj Quantum Mater.* **6**, X.
- Masell, J, D. R. Rodrigues, B. F. McKeever, and K. Everschor-Sitte (2020), “Spin-transfer torque driven motion, deformation, and instabilities of magnetic skyrmions at high currents,” *Phys. Rev. B* **101**, 214428.
- Matsuda, T, K. Harada, H. Kasai, O. Kamimura, and A. Tonomura (1996), “Observation of dynamic interaction of vortices with pinning centers by Lorentz microscopy,” *Science* **271**, 1393–1395.
- Matsumoto, T, Y.-G. So, Y. Kohno, H. Sawada, Y. Ikuhara, and N. Shibata (2016a), “Direct observation of  $\Sigma 7$  domain boundary core structure in magnetic skyrmion lattice,” *Sci. Adv.* **2**, e1501280.
- Matsumoto, T, Y.-G. So, Y. Kohno, H. Sawada, R. Ishikawa, Y. Ikuhara, and N. Shibata (2016b), “Jointed magnetic skyrmion lattices at a small-angle grain boundary directly visualized by advanced electron microscopy,” *Sci. Rep.* **6**, 35880.
- Mehta, A P, A. C. Mills, K. A. Dahmen, and J. P. Sethna (2002), “Universal pulse shape scaling function and exponents: Critical test for avalanche models applied to Barkhausen noise,” *Phys. Rev. E* **65**, 046139.
- Menezes, R M, J. Mulkers, C. C. de Souza Silva, and M. V. Milosević (2019a), “Deflection of ferromagnetic and antiferromagnetic skyrmions at heterochiral interfaces,” *Phys. Rev. B* **99**, 104409.
- Menezes, R M, J. F. S. Neto, C. C. de Souza Silva, and M. V. Milošević (2019b), “Manipulation of magnetic skyrmions by superconducting vortices in ferromagnet-superconductor heterostructures,” *Phys. Rev. B* **100**, 014431.
- Merithew, R D, M. W. Rabin, M. B. Weissman, M. J. Higgins, and S. Bhattacharya (1996), “Persistent metastable states in vortex flow at the peak effect in NbSe<sub>2</sub>,” *Phys. Rev. Lett.* **77**, 3197.
- Migita, K, K. Yamada, and Y. Nakatani (2020), “Controlling skyrmion motion in an angelfish-type racetrack memory by an AC magnetic field,” *Appl. Phys. Express* **13** (7), 073003.
- Mikhael, J, J. Roth, L. Helden, and C. Bechinger (2008), “Archimedean-like tiling on decagonal quasicrystalline surfaces,” *Nature (London)* **454**, 501–504.
- Milde, P, D. Köhler, J. Seidler, L. M. Eng, A. Bauer, A. Chacon, J. Kindervater, S. Mühlbauer, C. Pfleiderer, S. Buhrandt, C. Schütte, and A. Rosch (2013), “Unwinding of a skyrmion lattice by magnetic monopoles,” *Science* **340**, 1076–1080.
- Mirebeau, I, N. Martin, M. Deutsch, L. J. Bannenberg, C. Pappas, G. Chaboussant, R. Cubitt, C. Decorse, and A. O. Leonov (2018), “Spin textures induced by quenched disorder in a reentrant spin glass: Vortices versus “frustrated” skyrmions,” *Phys. Rev. B* **98**, 014420.
- Mochizuki, M, X. Z. Yu, S. Seki, N. Kanazawa, W. Koshihara, M. Zang, J. and Mostovoy, Y. Tokura, and N. Nagaosa (2014), “Thermally driven ratchet motion of a skyrmion microcrystal and topological magnon Hall effect,” *Nature Mater.* **13**, 241–246.
- Mohan, S, J. Sinha, S. S. Banerjee, A. K. Sood, S. Ramakrishnan, and A. K. Grover (2009), “Large low-frequency fluctuations in the velocity of a driven vortex lattice in a single crystal of 2H-NbSe<sub>2</sub> superconductor,” *Phys. Rev. Lett.* **103**, 167001.
- Montoya, S A, R. Tolley, I. Gilbert, S.-G. Je, M.-Y. Im, and E. E. Fullerton (2018), “Spin-orbit torque induced dipole skyrmion motion at room temperature,” *Phys. Rev. B* **98**, 104432.
- Moon, K, R. T. Scalettar, and G. T. Zimányi (1996), “Dynamical phases of driven vortex systems,” *Phys. Rev. Lett.* **77**, 2778.
- Moreau-Luchaire, C, C. Moutafis, N. Reyren, J. Sampaio, C. A. F. Vaz, N. Van Horne, K. Bouzehouane, K. Garcia, C. Deranlot, P. Warnicke, P. Wohlhüter, J.-M. George, M. Weigand, J. Raabe, V. Cros, and A. Fert (2016), “Additive interfacial chiral interaction in multilayers for stabiliza-

- tion of small individual skyrmions at room temperature,” *Nature Nanotech.* **11**, 444–448.
- Moretti, P, and M.-C. Miguel (2009), “Irreversible flow of vortex matter: Polycrystal and amorphous phases,” *Phys. Rev. B* **80**, 224513.
- Morin, A, N. Desreumaux, J.-B. Caussin, and D. Bartolo (2017), “Distortion and destruction of colloidal flocks in disordered environments,” *Nature Phys.* **13**, 63.
- Mühlbauer, S, B. Binz, F. Jonietz, C. Pfleiderer, A. Rosch, A. Neubauer, R. Georgii, and P. Böni (2009), “Skyrmion lattice in a chiral magnet,” *Science* **323**, 915.
- Müller, J (2017), “Magnetic skyrmions on a two-lane race-track,” *New J. Phys.* **19**, 025002.
- Müller, J, J. Rajeswari, P. Huang, Y. Murooka, H. M. Rønnow, F. Carbone, and A. Rosch (2017), “Magnetic skyrmions and skyrmion clusters in the helical phase of  $\text{Cu}_2\text{OSeO}_3$ ,” *Phys. Rev. Lett.* **119**, 137201.
- Müller, J, and A. Rosch (2015), “Capturing of a magnetic skyrmion with a hole,” *Phys. Rev. B* **91**, 054410.
- Nagaosa, N, and Y. Tokura (2013), “Topological properties and dynamics of magnetic skyrmions,” *Nature Nanotechnol.* **8**, 899.
- Nakajima, H, A. Kotani, M. Mochizuki, K. Harada, and S. Mori (2017a), “Formation process of skyrmion lattice domain boundaries: The role of grain boundaries,” *Appl. Phys. Lett.* **111**, 192401.
- Nakajima, T, H. Oike, A. Kikkawa, E. P. Gilbert, N. Booth, K. Kakurai, Y. Taguchi, Y. Tokura, F. Kagawa, and T. Arima (2017b), “Skyrmion lattice structural transition in MnSi,” *Science Adv.* **3**, e1602562.
- Nattermann, T, and S. Scheidl (2000), “Vortex-glass phases in type-II superconductors,” *Adv. Phys.* **49**, 607–704.
- Navau, C, N. Del-Valle, and A. Sanchez (2016), “Analytical trajectories of skyrmions in confined geometries: Skyrmionic racetracks and nano-oscillators,” *Phys. Rev. B* **94**, 184104.
- Navau, C, N. Del-Valle, and A. Sanchez (2018), “Interaction of isolated skyrmions with point and linear defects,” *J. Mag. Mater.* **465**, 709–715.
- Nayak, A K, V. Kumar, T. Ma, P. Werner, E. Pippel, R. Sahoo, F. Damay, U. K. Rößler, C. Felser, and S. S. P. Parkin (2017), “Magnetic antiskyrmions above room temperature in tetragonal Heusler materials,” *Nature (London)* **548**, 561–566.
- Nelson, D R (1983), “Reentrant melting in solid films with quenched random impurities,” *Phys. Rev. B* **27**, 2902.
- Nelson, D R (1988), “Vortex entanglement in high- $T_c$  superconductors,” *Phys. Rev. Lett.* **60**, 1973.
- Nelson, D R, and B. I. Halperin (1979), “Dislocation-mediated melting in two dimensions,” *Phys. Rev. B* **19**, 2457.
- Nepal, R, U. Güngördü, and A. A. Kovalev (2018), “Magnetic skyrmion bubble motion driven by surface acoustic waves,” *Appl. Phys. Lett.* **112**, 112404.
- Neubauer, A, C. Pfleiderer, B. Binz, A. Rosch, R. Ritz, P. G. Niklowitz, and P. Böni (2009), “Topological Hall effect in the A phase of MnSi,” *Phys. Rev. Lett.* **102**, 186602.
- Nishikawa, Y, K. Hukushima, and W. Krauth (2019), “Solid-liquid transition of skyrmions in a two-dimensional chiral magnet,” *Phys. Rev. B* **99**, 064435.
- Nozaki, T, Y. Jibiki, M. Goto, E. Tamura, T. Nozaki, H. Kubota, A. Fukushima, S. Yuasa, and Y. Suzuki (2019), “Brownian motion of skyrmion bubbles and its control by voltage applications,” *Appl. Phys. Lett.* **114**, 012402.
- Nych, A, J. Fukuda, U. Ognysta, S. Žumer, and I. Mušević (2017), “Spontaneous formation and dynamics of half-skyrmions in a chiral liquid-crystal film,” *Nature Phys.* **13** (12), 1215.
- O’Hern, C S, L. E. Silbert, A. J. Liu, and S. R. Nagel (2003), “Jamming at zero temperature and zero applied stress: The epitome of disorder,” *Phys. Rev. E* **68**, 011306.
- Okuma, S, H. Imaizumi, D. Shimamoto, and N. Kokubo (2011), “Quantum melting and lattice orientation of driven vortex matter,” *Phys. Rev. B* **83**, 064520.
- Okuma, S, J. Inoue, and N. Kokubo (2007), “Suppression of broadband noise at mode locking in driven vortex matter,” *Phys. Rev. B* **76**, 172503.
- Okuyama, D, M. Bleuel, J. S. White, Q. Ye, J. Krzywon, G. Nagy, Z. Q. Im, I. Zivkovic, M. Bartkowiak, H. M. Ronnow, S. Hoshino, J. Iwasaki, N. Nagaosa, A. Kikkawa, Y. Taguchi, Y. Tokura, D. Higashi, J. D. Reim, Y. Nambu, and T. J. Sato (2019a), “Deformation of the magnetic skyrmion lattice in MnSi under electric current flow,” *Commun. Phys.* **2**, 79.
- Okuyama, D, M. Bleuel, J. S. White, Q. Ye, J. Krzywon, G. Nagy, Z. Q. Im, I. Zivkovic, M. Bartkowiak, H. M. Rønnow, S. Hoshino, J. Iwasaki, N. Nagaosa, A. Kikkawa, Y. Taguchi, Y. Tokura, D. Higashi, J. D. Reim, Y. Nambu, and T. J. Sato (2019b), “Deformation of the moving magnetic skyrmion lattice in MnSi under electric current flow,” *Commun. Phys.* **2**, 79.
- Olive, E, and J. C. Soret (2006), “Chaotic dynamics of superconductor vortices in the plastic phase,” *Phys. Rev. Lett.* **96**, 027002.
- Olson, C J, C. Reichhardt, B. Jankó, and F. Nori (2001), “Collective interaction-driven ratchet for transporting flux quanta,” *Phys. Rev. Lett.* **87**, 177002.
- Olson, C J, C. Reichhardt, and F. Nori (1998a), “Fractal networks, braiding channels, and voltage noise in intermittently flowing rivers of quantized magnetic flux,” *Phys. Rev. Lett.* **80**, 2197.
- Olson, C J, C. Reichhardt, and F. Nori (1998b), “Nonequilibrium dynamic phase diagram for vortex lattices,” *Phys. Rev. Lett.* **81**, 3757.
- Olson, C J, C. Reichhardt, R. T. Scalettar, G. T. Zimányi, and N. Grønbech-Jensen (2003), “Metastability and transient effects in vortex matter near a decoupling transition,” *Phys. Rev. B* **67**, 184523.
- Olson, C J, G. T. Zimányi, A. B. Kolton, and N. Grønbech-Jensen (2000), “Static and dynamic coupling transitions of vortex lattices in disordered anisotropic superconductors,” *Phys. Rev. Lett.* **85**, 5416.
- Olson Reichhardt, C J, and C. Reichhardt (2008), “Viscous decoupling transitions for individually dragged particles in systems with quenched disorder,” *Phys. Rev. E* **78**, 011402.
- Olszewski, M W, M. R. Eskildsen, C. Reichhardt, and C. J. O. Reichhardt (2018), “Structural transitions in vortex systems with anisotropic interactions,” *New J. Phys.* **20**, 023005.
- Onose, Y, Y. Okamura, S. Seki, S. Ishiwata, and Y. Tokura (2012), “Observation of magnetic excitations of skyrmion crystal in a helimagnetic insulator  $\text{Cu}_2\text{OSeO}_3$ ,” *Phys. Rev. Lett.* **109**, 037603.
- Ortiz-Ambriz, A, and P. Tierno (2016), “Engineering of frustration in colloidal artificial ices realized on microfeatured grooved lattices,” *Nature. Commun.* **7**, 10575.
- Palermo, X, N. Reyren, S. Mesoraca, A. V. Samokhvalov, S. Collin, F. Godel, A. Sander, K. Bouzehouane, J. Santa-

- maria, V. Cros, A. I. Buzdin, and J. E. Villegas (2020), “Tailored flux pinning in superconductor-ferromagnet multilayers with engineered magnetic domain morphology from stripes to skyrmions,” *Phys. Rev. Applied* **13**, 014043.
- Paltiel, Y, E. Zeldov, Y. N. Myasoedov, H. Shtrikman, S. Bhattacharya, M. J. Higgins, Z. L. Xiao, E. Y. Andrei, P. L. Gammel, and D. J. Bishop (2000), “Dynamic instabilities and memory effects in vortex matter,” *Nature (London)* **403**, 398–401.
- Pardo, F, F. de la Cruz, P. L. Gammel, E. Bucher, and D. J. Bishop (1998), “Observation of smectic and moving-Bragg-glass phases in flowing vortex lattices,” *Nature (London)* **396**, 348.
- Park, H S, X. Yu, S. Aizawa, T. Tanigaki, T. Akashi, Y. Takahashi, T. Matsuda, N. Kanazawa, Y. Onose, D. Shindo, A. Tonomura, and Y. Tokura (2014), “Observation of the magnetic flux and three-dimensional structure of skyrmion lattices by electron holography,” *Nature Nanotechnol* **9**, 337–342.
- Pasquini, G, D. Pérez Daroca, C. Chilotte, G. S. Lozano, and V. Bekkeris (2008), “Ordered, disordered, and coexistent stable vortex lattices in NbSe<sub>2</sub> single crystals,” *Phys. Rev. Lett.* **100**, 247003.
- Perković, O, K. Dahmen, and J. P. Sethna (1995), “Avalanches, Barkhausen noise, and plain old criticality,” *Phys. Rev. Lett.* **75**, 4528.
- Pertsinidis, A, and X. S. Ling (2008), “Statics and dynamics of 2D colloidal crystals in a random pinning potential,” *Phys. Rev. Lett.* **100**, 028303.
- Pinna, D, F. Abreu Araujo, J.-V. Kim, V. Cros, D. Querlioz, P. Bessiere, J. Droulez, and J. Grollier (2018), “Skyrmion gas manipulation for probabilistic computing,” *Phys. Rev. Appl.* **9**, 064018.
- Pinsolle, E, N. Kirova, V. L. R. Jacques, A. A. Sinchenko, and D. Le Bolloc’h (2012), “Creep, flow, and phase slippage regimes: An extensive view of the sliding charge-density wave revealed by coherent X-ray diffraction,” *Phys. Rev. Lett.* **109**, 256402.
- Plettenberg, J, M. Stier, and M. Thorwart (2020), “Steering of the skyrmion Hall angle by gate voltages,” *Phys. Rev. Lett.* **124**, 207202.
- Pöllath, S, J. Wild, L. Heinen, T. N. G. Meier, M. Kronseder, L. Tutsch, A. Bauer, H. Berger, C. Pfeleiderer, J. Zweck, A. Rosch, and C. H. Back (2017), “Dynamical defects in rotating magnetic skyrmion lattices,” *Phys. Rev. Lett.* **118**, 207205.
- Prychynenko, D, M. Sitte, K. Litzius, B. Krüger, G. Bourianoff, M. Kläui, J. Sinova, and K. Everschor-Sitte (2018), “Magnetic skyrmion as a nonlinear resistive element: A potential building block for reservoir computing,” *Phys. Rev. Appl.* **9**, 014034.
- Psaroudaki, C, and D. Loss (2018), “Skyrmions driven by intrinsic magnons,” *Phys. Rev. Lett.* **120**, 237203.
- Puertas, A M, and T. Voigtmann (2014), “Microrheology of colloidal systems,” *J. Phys.: Condens. Matter* **26**, 243101.
- Rajeswari, J, P. Huang, G. F. Mancini, Y. Murooka, T. Latychevskaia, D. McGruther, M. Cantoni, E. Baldini, J. S. White, A. Magrez, T. Giamarchi, H. M. Rønnow, and F. Carbone (2015), “Filming the formation and fluctuation of skyrmion domains by cryo-Lorentz transmission electron microscopy,” *Proc. Natl. Acad. Sci. (USA)* **112**, 14212–14217.
- Raju, M, A. Yagil, A. Soumyanarayanan, A. K. C. Tan, A. Almoalem, F. Ma, O. M. Auslaender, and C. Panagopoulos (2019), “The evolution of skyrmions in Ir/Fe/Co/Pt multilayers and their topological Hall signature,” *Nature Commun.* **10**, 696.
- Reichhardt, C (2009), “Vortices wiggled and dragged,” *Nature Phys.* **5**, 15.
- Reichhardt, C, and F. Nori (1999), “Phase locking, devil’s staircases, Farey trees, and Arnold tongues in driven vortex lattices with periodic pinning,” *Phys. Rev. Lett.* **82**, 414.
- Reichhardt, C, and C. J. Olson (2002a), “Colloidal dynamics on disordered substrates,” *Phys. Rev. Lett.* **89**, 078301.
- Reichhardt, C, and C. J. Olson (2002b), “Novel colloidal crystalline states on two-dimensional periodic substrates,” *Phys. Rev. Lett.* **88**, 248301.
- Reichhardt, C, C. J. Olson, N. Grønbech-Jensen, and F. Nori (2001), “Moving Wigner glasses and smectics: dynamics of disordered Wigner crystals,” *Phys. Rev. Lett.* **86**, 4354.
- Reichhardt, C, C. J. Olson, and F. Nori (1997), “Dynamic phases of vortices in superconductors with periodic pinning,” *Phys. Rev. Lett.* **78**, 2648.
- Reichhardt, C, C. J. Olson, and F. Nori (1998), “Commensurate and incommensurate vortex states in superconductors with periodic pinning arrays,” *Phys. Rev. B* **57**, 7937.
- Reichhardt, C, and C. J. Olson Reichhardt (2003), “Absolute transverse mobility and ratchet effect on periodic two-dimensional symmetric substrates,” *Phys. Rev. E* **68**, 046102.
- Reichhardt, C, and C. J. Olson Reichhardt (2008), “Disordering transitions and peak effect in polydisperse particle systems,” *Phys. Rev. E* **77**, 041401.
- Reichhardt, C, and C. J. Olson Reichhardt (2011), “Dynamical ordering and directional locking for particles moving over quasicrystalline substrates,” *Phys. Rev. Lett.* **106**, 060603.
- Reichhardt, C, and C. J. Olson Reichhardt (2015), “Shapiro steps for skyrmion motion on a washboard potential with longitudinal and transverse ac drives,” *Phys. Rev. B* **92**, 224432.
- Reichhardt, C, and C. J. Olson Reichhardt (2016), “Magnus-induced dynamics of driven skyrmions on a quasi-one-dimensional periodic substrate,” *Phys. Rev. B* **94**, 094413.
- Reichhardt, C, and C. J. Olson Reichhardt (2017), “Shapiro spikes and negative mobility for skyrmion motion on quasi-one-dimensional periodic substrates,” *Phys. Rev. B* **95**, 014412.
- Reichhardt, C, C. J. Olson Reichhardt, I. Martin, and A. R. Bishop (2003), “Dynamical ordering of driven stripe phases in quenched disorder,” *Phys. Rev. Lett.* **90**, 026401.
- Reichhardt, C, D. Ray, and C. J. Olson Reichhardt (2015a), “Magnus-induced ratchet effects for skyrmions interacting with asymmetric substrates,” *New J. Phys.* **17**, 073034.
- Reichhardt, C, D. Ray, and C. J. O. Reichhardt (2015b), “Collective transport properties of driven skyrmions with random disorder,” *Phys. Rev. Lett.* **114**, 217202.
- Reichhardt, C, D. Ray, and C. J. O. Reichhardt (2015c), “Quantized transport for a skyrmion moving on a two-dimensional periodic substrate,” *Phys. Rev. B* **91**, 104426.
- Reichhardt, C, D. Ray, and C. J. O. Reichhardt (2018), “Nonequilibrium phases and segregation for skyrmions on periodic pinning arrays,” *Phys. Rev. B* **98**, 134418.
- Reichhardt, C, and C. J. O. Reichhardt (2014), “Aspects of jamming in two-dimensional athermal frictionless systems,” *Soft Matter* **10**, 2932.
- Reichhardt, C, and C. J. O. Reichhardt (2016), “Noise fluctuations and drive dependence of the skyrmion Hall effect

- in disordered systems,” *New J. Phys.* **18**, 095005.
- Reichhardt, C, and C. J. O. Reichhardt (2017), “Depinning and nonequilibrium dynamic phases of particle assemblies driven over random and ordered substrates: A review,” *Rep. Prog. Phys.* **80**, 026501.
- Reichhardt, C, and C. J. O. Reichhardt (2019a), “Nonlinear transport, dynamic ordering, and clustering for driven skyrmions on random pinning,” *Phys. Rev. B* **99**, 104418.
- Reichhardt, C, and C. J. O. Reichhardt (2019b), “Thermal creep and the skyrmion Hall angle in driven skyrmion crystals,” *J. Phys.: Condens. Matter* **31**, 07LT01.
- Reichhardt, C, and C. J. O. Reichhardt (2020), “Plastic flow and the skyrmion hall effect,” *Nature Commun.* **11**, 738.
- Reichhardt, C, R. T. Scalettar, G. T. Zimányi, and N. Grønbech-Jensen (2000), “Phase-locking of vortex lattices interacting with periodic pinning,” *Phys. Rev. B* **61**, R11914(R).
- Reijnders, J W, and R. A. Duine (2004), “Pinning of vortices in a Bose-Einstein condensate by an optical lattice,” *Phys. Rev. Lett.* **93**, 060401.
- Reimann, P (2002), “Brownian motors: noisy transport far from equilibrium,” *Phys. Rep.* **361**, 57.
- Rex, S, I. V. Gornyi, and A. D. Mirlin (2019), “Majorana bound states in magnetic skyrmions imposed onto a superconductor,” *Phys. Rev. B* **100**, 064504.
- Reza Sadr-Lahijany, M, P. Ray, and H. E. Stanley (1997), “Dispersivity-driven melting transition in two-dimensional solids,” *Phys. Rev. Lett.* **79**, 3206.
- Risbud, S R, and G. Drazer (2014), “Directional locking in deterministic lateral-displacement microfluidic separation systems,” *Phys. Rev. E* **90**, 012302.
- Ritzmann, U, S. von Malottki, J.-V. Kim, S. Heinze, J. Sinova, and B. Dupé (2018), “Trochoidal motion and pair generation in skyrmion and antiskyrmion dynamics under spin-orbit torques,” *Nature Electron.* **1**, 451–457.
- Romming, N, C. Hanneken, M. Menzel, J. E. Bickel, B. Wolter, K. von Bergmann, A. Kubetzka, and R. Wiesendanger (2013), “Writing and deleting single magnetic skyrmions,” *Science* **341**, 636–639.
- Ros, A, R. Eichhorn, J. Regtmeier, T. T. Duong, P. Reimann, and D. Anselmetti (2005), “Brownian motion: Absolute negative particle mobility,” *Nature (London)* **436**, 928.
- Rößler, U K, A. N. Bogdanov, and C. Pfleiderer (2006), “Spontaneous skyrmion ground states in magnetic metals,” *Nature (London)* **442**, 797–801.
- Rousselet, J, L. Salome, A. Ajdari, and J. Prost (1994), “Directional motion of brownian particles induced by a periodic asymmetric potential,” *Nature (London)* **370**, 446.
- Rózsa, L, A. Deák, E. Simon, R. Yanes, L. Udvardi, L. Szunyogh, and U. Nowak (2016), “Skyrmions with attractive interactions in an ultrathin magnetic film,” *Phys. Rev. Lett.* **117**, 157205.
- Rybakov, F N, A. B. Borisov, S. Blügel, and N. S. Kiselev (2015), “New type of particlelike state in chiral magnets,” *Phys. Rev. Lett.* **115**, 117201.
- Rybakov, F N, and N. S. Kiselev (2019), “Chiral magnetic skyrmions with arbitrary topological charge,” *Phys. Rev. B* **99**, 064437.
- Safar, H, P. L. Gammel, D. A. Huse, D. J. Bishop, J. P. Rice, and D. M. Ginsberg (1992), “Experimental evidence for a first-order vortex-lattice-melting transition in untwinned, single crystal  $\text{YBa}_2\text{Cu}_3\text{O}_7$ ,” *Phys. Rev. Lett.* **69**, 824.
- Saha, S, M. Zelent, S. Finizio, M. Mruczkiewicz, S. Tacchi, A. K. Suszka, S. Wintz, N. S. Bingham, J. Raabe, M. Krawczyk, and L. J. Heyderman (2019), “Formation of néel-type skyrmions in an antidot lattice with perpendicular magnetic anisotropy,” *Phys. Rev. B* **100**, 144435.
- Salger, T, S. Kling, T. Hecking, C. Geckeler, L. Morales-Molina, and M. Weitz (2009), “Directed transport of atoms in a Hamiltonian quantum ratchet,” *Science* **326**, 1241–1243.
- Salimath, A, A. Abbout, A. Brataas, and A. Manchon (2019), “Current-driven skyrmion depinning in magnetic granular films,” *Phys. Rev. B* **99**, 104416.
- Sampaio, J, V. Cros, S. Rohart, A. Thiaville, and A. Fert (2013), “Nucleation, stability and current-induced motion of isolated magnetic skyrmions in nanostructures,” *Nature Nanotechnol.* **8**, 839–844.
- Sándor, Cs, A. Libál, C. Reichhardt, and C. J. O. Reichhardt (2017), “Dynamic phases of active matter systems with quenched disorder,” *Phys. Rev. E* **95**, 032606.
- Sato, T, A. Kikkawa, Y. Taguchi, Y. Tokura, and F. Kagawa (2020), “Mode locking phenomena of the current-induced skyrmion-lattice motion in microfabricated  $\text{MnSi}$ ,” *Phys. Rev. B* **102**, 180411.
- Sato, T, W. Koshibae, A. Kikkawa, T. Yokouchi, H. Oike, Y. Taguchi, N. Nagaosa, Y. Tokura, and F. Kagawa (2019), “Slow steady flow of a skyrmion lattice in a confined geometry probed by narrow-band resistance noise,” *Phys. Rev. B* **100**, 094410.
- Schulz, T, R. Ritz, A. Bauer, M. Halder, M. Wagner, C. Franz, C. Pfleiderer, K. Everschor, M. Garst, and A. Rosch (2012), “Emergent electrodynamics of skyrmions in a chiral magnet,” *Nature Phys.* **8**, 301.
- Schütte, C, and M. Garst (2014), “Magnon-skyrmion scattering in chiral magnets,” *Phys. Rev. B* **90**, 094423.
- Schütte, C, J. Iwasaki, A. Rosch, and N. Nagaosa (2014), “Inertia, diffusion, and dynamics of a driven skyrmion,” *Phys. Rev. B* **90**, 174434.
- Schütte, C, and A. Rosch (2014), “Dynamics and energetics of emergent magnetic monopoles in chiral magnets,” *Phys. Rev. B* **90**, 174432.
- Seki, S, M. Garst, J. Waizner, R. Takagi, N. D. Khanh, Y. Okamura, K. Kondou, F. Kagawa, Y. Otani, and Y. Tokura (2020), “Propagation dynamics of spin excitations along skyrmion strings,” *Nature Commun.* **11** (1), 256.
- Seki, S, X. Z. Yu, S. Ishiwata, and Y. Tokura (2012), “Observation of skyrmions in a multiferroic material,” *Science* **336**, 198–201.
- Sengupta, A, S. Sengupta, and G. I. Menon (2010), “Driven disordered polymorphic solids: Phases and phase transitions, dynamical coexistence and peak effect anomalies,” *Phys. Rev. B* **81**, 144521.
- Sethna, J P, K. Dahmen, S. Kartha, J. A. Krumhansl, B. W. Roberts, and J. D. Shore (1993), “Hysteresis and hierarchies: Dynamics of disorder-driven first-order phase transformations,” *Phys. Rev. Lett.* **70**, 3347.
- Sethna, J P, K. A. Dahmen, and C. R. Myers (2001), “Crackling noise,” *Nature (London)* **410**, 242–250.
- Shapiro, S (1963), “Josephson currents in superconducting tunneling: The effect of microwaves and other observations,” *Phys. Rev. Lett.* **11**, 80.
- Shaw, G, P. Mandal, S. S. Banerjee, A. Niazi, A. K. Rastogi, A. K. Sood, S. Ramakrishnan, and A. K. Grover (2012), “Critical behavior at depinning of driven disordered vortex matter in  $2\text{H-NbS}_2$ ,” *Phys. Rev. B* **85**, 174517.

- Shen, L C, J. Xia, G. P. Zhao, X. C. Zhang, M. Ezawa, O. A. Tretiakov, X. X. Liu, and Y. Zhou (2018a), “Dynamics of the antiferromagnetic skyrmion induced by a magnetic anisotropy gradient,” *Phys. Rev. B* **98**, 134448.
- Shen, M, Y. Zhang, J. Ou-Yang, X. Yang, and L. You (2018b), “Motion of a skyrmionium driven by spin wave,” *Appl. Phys. Lett.* **112**, 062403.
- Shibata, K, T. Tanigaki, T. Akashi, H. Shinada, K. Harada, K. Niitsu, D. Shindo, and N. Kanazawa (2018), “Current-driven motion of domain boundaries between skyrmion lattices and helical magnetic structure,” *Nano Lett.* **18**, 929–933.
- Shklovskij, V A, V. V. Sosedkin, and O. V. Dobrovolskiy (2014), “Vortex ratchet reversal in an asymmetric washboard pinning potential subject to combined dc and ac stimuli,” *J. Phys.: Condens. Matter* **26**, 025703.
- Silva, R L, L. D. Secchin, W. A. Moura-Melo, A. R. Pereira, and R. L. Stamps (2014), “Emergence of skyrmion lattices and bimerons in chiral magnetic thin films with nonmagnetic impurities,” *Phys. Rev. B* **89**, 054434.
- Singh, A, J. C. T. Lee, K. E. Avila, Y. Chen, S. A. Montoya, E. E. Fullerton, P. Fischer, K. A. Dahmen, S. D. Kevan, M. K. Sanyal, and S. Roy (2019), “Scaling of domain cascades in stripe and skyrmion phases,” *Nature Commun.* **10**, 1988.
- Song, K M, J.-S. Jeong, B. Pan, X. Zhang, J. Xia, S. Cha, T.-E. Park, K. Kim, S. Finizio, J. Raabe, J. Chang, J. Zhou, W. Zhao, W. Kang, H. Ju, and S. Woo (2020), “Skyrmion-based artificial synapses for neuromorphic computing,” *Nat. Electron.* **3**, 148–155.
- Soumyanarayanan, A, M. Raju, A. L. Gonzalez-Oyarce, A. K. C. Tan, M.-Y. Im, A. P. Petrovic, P. Ho, K. H. Khoo, M. Tran, C. K. Gan, F. Ernult, and C. Panagopoulos (2017), “Tunable room-temperature magnetic skyrmions in Ir/Fe/Co/Pt multilayers,” *Nature Mater.* **16**, 898.
- Stier, M, R. Strobel, S. Krause, W. Häusler, and M. Thorwart (2021), “Role of impurity clusters for the current-driven motion of magnetic skyrmions,” *Phys. Rev. B* **103**, 054420.
- Stosic, D, T. B. Ludermir, and M. V. Milosević (2017), “Pinning of magnetic skyrmions in a monolayer Co film on Pt(111): Theoretical characterization and exemplified utilization,” *Phys. Rev. B* **96**, 214403.
- Strandburg, K J (1988), “Two-dimensional melting,” *Rev. Mod. Phys.* **60**, 161.
- Straver, E W J, J. E. Hoffman, O. M. Auslaender, D. Rugar, and K. A. Moler (2008), “Controlled manipulation of individual vortices in a superconductor,” *Appl. Phys. Lett.* **93**, 172514.
- Suess, D, C. Vogler, F. Bruckner, P. Heistracher, and C. Abert (2018), “A repulsive skyrmion chain as a guiding track for a racetrack memory,” *AIP Advances* **8**, 115301.
- Suess, D, C. Vogler, F. Bruckner, P. Heistracher, F. Slanovc, and C. Abert (2019), “Spin torque efficiency and analytic error rate estimates of skyrmion racetrack memory,” *Sci. Rep.* **9**, 4827.
- Takagi, R, X. Z. Yu, J. S. White, K. Shibata, Y. Kaneko, G. Tatara, H. M. Rønnow, Y. Tokura, and S. Seki (2018), “Low-field bi-skyrmion formation in a noncentrosymmetric chimney ladder ferromagnet,” *Phys. Rev. Lett.* **120**, 037203.
- Tatara, G, H. Kohno, and J. Shibata (2008), “Microscopic approach to current-driven domain wall dynamics,” *Phys. Rep.* **468**, 213.
- Thiele, A A (1973), “Steady-state motion of magnetic domains,” *Phys. Rev. Lett.* **30**, 230.
- Thorneywork, A L, J. L. Abbott, D. G. A. L. Aarts, and R. P. A. Dullens (2017), “Two-dimensional melting of colloidal hard spheres,” *Phys. Rev. Lett.* **118**, 158001.
- Tierno, P (2012), “Depinning and collective dynamics of magnetically driven colloidal monolayers,” *Phys. Rev. Lett.* **109**, 198304.
- Toft-Petersen, R, A. B. Abrahamsen, S. Balog, L. Porcar, and M. Laver (2018), “Decomposing the Bragg glass and the peak effect in a type-II superconductor,” *Nature Commun.* **9**, 901.
- Togawa, Y, R. Abiru, K. Iwaya, H. Kitano, and A. Maeda (2000), “Direct observation of the washboard noise of a driven vortex lattice in a high-temperature superconductor,  $\text{Bi}_2\text{Sr}_2\text{CaCu}_2\text{O}_y$ ,” *Phys. Rev. Lett.* **85**, 3716.
- Tokunaga, Y, X. Z. Yu, J. S. White, H. M. Rønnow, D. Morikawa, Y. Taguchi, and Y. Tokura (2015), “A new class of chiral materials hosting magnetic skyrmions beyond room temperature,” *Nature Commun.* **6**, 7638.
- Tokura, Y, and N. Kanazawa (2020), “Magnetic skyrmion materials,” *Chem. Rev.* **X**, XXXX.
- Tolley, R, S. A. Montoya, and E. E. Fullerton (2018), “Room-temperature observation and current control of skyrmions in Pt/Co/Os/Pt thin films,” *Phys. Rev. Mater.* **2**, 044404.
- Tomasello, R, A. Giordano, S. Chiappini, R. Zivieri, G. Siracusano, V. Puliafito, I. Medlej, A. La Corte, B. Azzerboni, M. Carpentieri, Z. Zeng, and G. Finocchio (2018), “Micro-magnetic understanding of the skyrmion Hall angle current dependence in perpendicularly magnetized ferromagnets,” *Phys. Rev. B* **98**, 224418.
- Tomasello, R, E. Martinez, R. Zivieri, L. Torres, M. Carpentieri, and G. Finocchio (2014), “A strategy for the design of skyrmion racetrack memories,” *Sci. Rep.* **4**, 6784.
- Tong, Q, F. Liu, J. Xiao, and W. Yao (2018), “Skyrmions in the moiré of van der Waals 2D magnets,” *Nano Lett.* **18**, 7194–7199.
- Torquato, S (2016), “Hyperuniformity and its generalizations,” *Phys. Rev. E* **94**, 022122.
- Toscano, D, S. A. Leonel, P. Z. Coura, and F. Sato (2019), “Building traps for skyrmions by the incorporation of magnetic defects into nanomagnets: Pinning and scattering traps by magnetic properties engineering,” *J. Mag. Mater.* **480**, 171–185.
- Traveset, A, R. A. White, and K. A. Dahmen (2002), “Crackling noise, power spectra, and disorder-induced critical scaling,” *Phys. Rev. B* **66**, 024430.
- Troncoso, R E, and A. S. Núñez (2014), “Thermally assisted current-driven skyrmion motion,” *Phys. Rev. B* **89**, 224403.
- Tsesses, S, E. Ostrovsky, K. Cohen, B. Gjonaj, N. H. Lindner, and G. Bartal (2018), “Optical skyrmion lattice in evanescent electromagnetic fields,” *Science* **361** (6406), 993–996.
- Tung, S, V. Schweikhard, and E. A. Cornell (2006), “Observation of vortex pinning in Bose-Einstein condensates,” *Phys. Rev. Lett.* **97**, 240402.
- Van Look, L, E. Rosseel, M. J. Van Bael, K. Temst, V. V. Moshchalkov, and Y. Bruynseraede (1999), “Shapiro steps in a superconducting film with an antidot lattice,” *Phys. Rev. B* **60**, 6998(R).
- Vanossi, A, N. Manini, M. Urbakh, S. Zapperi, and E. Tosatti (2013), “Colloquium: Modeling friction: From nanoscale to mesoscale,” *Rev. Mod. Phys.* **85**, 529.
- Villegas, J E, M. I. Montero, C.-P. Li, and I. K. Schuller (2006), “Correlation length of quasiperiodic vortex lat-

- tices,” *Phys. Rev. Lett.* **97**, 027002.
- Villegas, J E, Savel'ev S., F. Nori, E. M. Gonzalez, J. V. Anguita, R. García, and J. L. Vicent (2003), “A superconducting reversible rectifier that controls the motion of magnetic flux quanta,” *Science* **302**, 1188.
- Vizarim, N P, C. Reichhardt, C. J. O. Reichhardt, and P. A. Venegas (2020a), “Skyrmion dynamics and topological sorting on periodic obstacle arrays,” *New J. Phys.* **22**, 053025.
- Vizarim, N P, C. Reichhardt, P. A. Venegas, and C. J. O. Reichhardt (2020b), “Shapiro steps and nonlinear skyrmion Hall angles for dc and ac driven skyrmions on a two-dimensional periodic substrate,” *Phys. Rev. B* **102**, 104413.
- Vizarim, N P, C. J. O. Reichhardt, P. A. Venegas, and C. Reichhardt (2020c), “Skyrmion pinball and directed motion on obstacle arrays,” *J. Phys. Commun.* **4**, 085001.
- Vlasko-Vlasov, V K, L. A. Dorosinskii, A. A. Polyanskii, V. I. Nikitenko, U. Welp, B. W. Veal, and G. W. Crabtree (1994), “Study of the influence of individual twin boundaries on the magnetic flux penetration in  $\text{YBa}_2\text{Cu}_3\text{O}_{7-\delta}$ ,” *Phys. Rev. Lett.* **72**, 3246.
- Wang, C, D. Xiao, X. Chen, Y. Zhou, and Y. Liu (2017), “Manipulating and trapping skyrmions by magnetic field gradients,” *New J. Phys.* **19**, 083008.
- Wang, L, Q. Feng, Y. Kim, R. Kim, K. H. Lee, S. D. Pollard, Y. J. Shin, H. Zhou, W. Peng, D. Lee, W. Meng, H. Yang, J. H. Han, M. Kim, Q. Lu, and T. W. Noh (2018a), “Ferroelectrically tunable magnetic skyrmions in ultrathin oxide heterostructures,” *Nature Materials* **17**, 1087–1094.
- Wang, L, C. Liu, N. Mehmood, G. Han, Y. Wang, X. Xu, C. Feng, Z. Hou, Y. Peng, X. Gao, and G. Yu (2019a), “Construction of a room-temperature Pt/Co/Ta multilayer film with ultrahigh-density skyrmions for memory application,” *ACS Appl. Mater. Interfaces* **11**, 12098–12104.
- Wang, W, M. Beg, B. Zhang, W. Kuch, and H. Fangohr (2015), “Driving magnetic skyrmions with microwave fields,” *Phys. Rev. B* **92**, 020403(R).
- Wang, W, Y. Zhang, G. Xu, L. Peng, B. Ding, Y. Wang, Z. Hou, X. Zhang, X. Li, E. Liu, S. Wang, J. Cai, F. Wang, J. Li, F. Hu, G. Wu, B. Shen, and X.-X. Zhang (2016), “A centrosymmetric hexagonal magnet with superstable biskyrmion magnetic nanodomains in a wide temperature range of 100-340 K,” *Adv. Mater.* **28**, 6887.
- Wang, X-G, L. Chotorlishvili, V. K. Dugaev, A. Ernst, I. V. Maznichenko, N. Arnold, C. Jia, J. Berakdar, I. Mertig, and J. Barnaš (2020a), “The optical tweezer of skyrmions,” *npj Comput. Mater.* **6**, 140.
- Wang, X S, A. Qaiumzadeh, and A. Brataas (2019b), “Current-driven dynamics of magnetic hopfions,” *Phys. Rev. Lett.* **123**, 147203.
- Wang, Y J, Y. P. Feng, Y. L. Zhu, Y. L. Tang, L. X. Yang, M. J. Zou, W. R. Geng, M. J. Han, X. W. Guo, B. Wu, and X. L. Ma (2020b), “Polar meron lattice in strained oxide ferroelectrics,” *Nature Mater.* **19** (8), 881.
- Wang, Y-L, X. Ma, J. Xu, Z.-L. Xiao, A. Snezhko, R. Divan, L. E. Ocola, J. E. Pearson, B. Janko, and W.-K. Kwok (2018b), “Switchable geometric frustration in an artificial-spin-ice-superconductor heterosystem,” *Nature Nanotechnol.* **13**, 560.
- Wang, Z, M. Guo, H.-A. Zhou, L. Zhao, T. Xu, R. Tomasello, H. Bai, Y. Dong, S.-G. Je, W. Chao, H.-S. Han, S. Lee, K.-S. Lee, Y. Yao, W. Han, C. Song, H. Wu, Carpentieri M., G. Finocchio, M.-Y. Im, S.-Z. Lin, and W. Jiang (2020c), “Thermal generation, manipulation and thermoelectric detection of skyrmions,” *Nature Electron.* **3**, 672.
- Wei, Q-H, C. Bechinger, D. Rudhardt, and P. Leiderer (1998), “Experimental study of laser-induced melting in two-dimensional colloids,” *Phys. Rev. Lett.* **81**, 2606.
- Weiss, J A, A. E. Larsen, and D. G. Grier (1998), “Interactions, dynamics, and elasticity in charge-stabilized colloidal crystals,” *J. Chem. Phys.* **109**, 8659.
- Weissman, M B (1988), “ $1/f$  noise and other slow, nonexponential kinetics in condensed matter,” *Rev. Mod. Phys.* **60**, 537.
- White, J S, K. Prša, P. Huang, A. A. Omrani, I. Živković, M. Bartkowiak, H. Berger, A. Magrez, J. L. Gavilano, G. Nagy, J. Zang, and H. M. Rønnow (2014), “Electric-field-induced skyrmion distortion and giant lattice rotation in the magnetoelectric insulator  $\text{Cu}_2\text{OSeO}_3$ ,” *Phys. Rev. Lett.* **113**, 107203.
- Wiesendanger, R (2016), “Nanoscale magnetic skyrmions in metallic films and multilayers: a new twist for spintronics,” *Nature Reviews Materials* **1**, 16044.
- Williams, F I B, P. A. Wright, R. G. Clark, E. Y. Andrei, G. Deville, D. C. Glattli, O. Probst, B. Etienne, C. Dorin, C. T. Foxon, and J. J. Harris (1991), “Conduction threshold and pinning frequency of magnetically induced Wigner solid,” *Phys. Rev. Lett.* **66**, 3285.
- Woo, S, K. Litzius, B. Krüger, M.-Y. Im, L. Caretta, K. Richter, M. Mann, A. Krone, R. M. Reeve, M. Weigand, P. Agrawal, I. Lemesh, M.-A. Mawass, P. Fischer, M. Kläui, and G. S. D. Beach (2016), “Observation of room-temperature magnetic skyrmions and their current-driven dynamics in ultrathin metallic ferromagnets,” *Nature Mater.* **15**, 501.
- Woo, S, K. M. Song, X. C. Zhang, Y. Zhou, M. Ezawa, X. X. Liu, S. Finizio, J. Raabe, N. J. Lee, S. I. Kim, S. Y. Park, Y. Kim, J. Y. Kim, D. Lee, O. Lee, J. W. Choi, B. C. Min, H. C. Koo, and J. Chang (2018), “Current-driven dynamics and inhibition of the skyrmion Hall effect of ferrimagnetic skyrmions in GdFeCo films,” *Nature Commun.* **9**, 959.
- Xiao, K, Y. Roichman, and D. G. Grier (2011), “Two-dimensional optical thermal ratchets based on Fibonacci spirals,” *Phys. Rev. E* **84**, 011131.
- Xiao, Z L, E. Y. Andrei, and M. J. Higgins (1999), “Flow induced organization and memory of a vortex lattice,” *Phys. Rev. Lett.* **83**, 1664.
- Xing, X, J. Åkerman, and Y. Zhou (2020), “Enhanced skyrmion motion via strip domain wall,” *Phys. Rev. B* **101**, 214432.
- Xu, X B, H. Fangohr, Z. H. Wang, M. Gu, S. L. Liu, D. Q. Shi, and S. X. Dou (2011), “Vortex dynamics for low- $\kappa$  type-II superconductors,” *Phys. Rev. B* **84**, 014515.
- Yang, G, P. Stano, J. Klinovaja, and D. Loss (2016), “Majorana bound states in magnetic skyrmions,” *Phys. Rev. B* **93**, 224505.
- Yang, H, A. Thiaville, S. Rohart, A. Fert, and M. Chshiev (2015), “Anatomy of Dzyaloshinskii-Moriya interaction at Co/Pt interfaces,” *Phys. Rev. Lett.* **115**, 267210.
- Yang, S, K.-W. Moon, C. Kim, D.-H. Kim, J. Shin, J. Hong, S. K. Kim, and C. Hwang (2020), “Control of the half-skyrmion Hall effect and its application to adder-subtractor,” *Adv. Quantum Technol.* **4**, 2000060.
- Yi, S D, S. Onoda, N. Nagaosa, and J. H. Han (2009), “Skyrmions and anomalous Hall effect in a Dzyaloshinskii-Moriya spiral magnet,” *Phys. Rev. B* **80**, 054416.
- Yokouchi, T, S. Hoshino, N. Kanazawa, A. Kikkawa, D. Morikawa, K. Shibata, T. Arima, Y. Taguchi, F. Ka-



- gawa, N. Nagaosa, and Y. Tokura (2018), “Current-induced dynamics of skyrmion strings,” *Sci. Adv.* **4**, eaat1115.
- Young, A P (1979), “Melting and the vector Coulomb gas in two dimensions,” *Phys. Rev. B* **19**, 1855.
- Yu, X, D. Morikawa, Y. Tokunaga, M. Kubota, T. Kurumaji, H. Oike, M. Nakamura, F. Kagawa, Y. Taguchi, T. Arima, M. Kawasaki, and Y. Tokura (2017), “Current-induced nucleation and annihilation of magnetic skyrmions at room temperature in a chiral magnet,” *Adv. Mater.* **29**, 1606178.
- Yu, X, D. Morikawa, T. Yokouchi, K. Shibata, N. Kanazawa, F. Kagawa, T. Arima, and Y. Tokura (2018a), “Aggregation and collapse dynamics of skyrmions in a non-equilibrium state,” *Nature Phys.* **14**, 832.
- Yu, X Z, N. Kanazawa, Y. Onose, K. Kimoto, W. Z. Zhang, S. Ishiwata, Y. Matsui, and Y. Tokura (2011), “Near room-temperature formation of a skyrmion crystal in thin-films of the helimagnet FeGe,” *Nature Mater.* **10**, 106–109.
- Yu, X Z, N. Kanazawa, W. Z. Zhang, T. Nagai, T. Hara, K. Kimoto, Y. Matsui, Y. Onose, and Y. Tokura (2012), “Skyrmion flow near room temperature in an ultralow current density,” *Nature Commun.* **3**, 988.
- Yu, X Z, W. Koshibae, Y. Tokunaga, K. Shibata, Y. Taguchi, N. Nagaosa, and Y. Tokura (2018b), “Transformation between meron and skyrmion topological spin textures in a chiral magnet,” *Nature (London)* **564**, 95–98.
- Yu, X Z, D. Morikawa, K. Nakajima, K. Shibata, N. Kanazawa, T. Arima, N. Nagaosa, and Y. Tokura (2020), “Motion tracking of 80-nm-size skyrmions upon directional current injections,” *Science Adv.* **6**, eaaz9744.
- Yu, X Z, Y. Onose, N. Kanazawa, J. H. Park, J. H. Han, Y. Matsui, N. Nagaosa, and Y. Tokura (2010), “Real-space observation of a two-dimensional skyrmion crystal,” *Nature (London)* **465**, 901.
- Yu, X Z, Y. Tokunaga, Y. Kaneko, W. Z. Zhang, K. Kimoto, Y. Matsui, Y. Taguchi, and Y. Tokura (2014), “Biskyrmion states and their current-driven motion in a layered manganite,” *Nature Commun.* **5**, 3198.
- Yuan, H Y, X. S. Wang, M.-H. Yung, and X. R. Wang (2019), “Wiggling skyrmion propagation under parametric pumping,” *Phys. Rev. B* **99**, 014428.
- Zahn, K, R. Lenke, and G. Maret (1999), “Two-stage melting of paramagnetic colloidal crystals in two dimensions,” *Phys. Rev. Lett.* **82**, 2721.
- Zang, J, M. Mostovoy, J. H. Han, and N. Nagaosa (2011), “Dynamics of skyrmion crystals in metallic thin films,” *Phys. Rev. Lett.* **107**, 136804.
- Zapperi, S, C. Castellano, F. Colaiori, and G. Durin (2005), “Signature of effective mass in crackling-noise asymmetry,” *Nature Phys.* **1**, 46–49.
- Zapperi, S, P. Cizeau, G. Durin, and H. E. Stanley (1998), “Dynamics of a ferromagnetic domain wall: Avalanches, depinning transition, and the Barkhausen effect,” *Phys. Rev. B* **58**, 6353.
- Zázvorka, J, F. Dittrich, Y. Ge, N. Kerber, K. Raab, T. Winkler, K. Litzius, M. Veis, P. Virnau, and M. Kläui (2020), “Skyrmion lattice phases in thin film multilayer,” *Advanced Functional Materials* **30** (46), 2004037.
- Zázvorka, J, F. Jakobs, D. Heinze, N. Keil, S. Kromin, S. Jaiswal, K. Litzius, G. Jakob, P. Virnau, D. Pinna, K. Everschor-Sitte, L. Rózsa, A. Donges, U. Nowak, and M. Kläui (2019), “Thermal skyrmion diffusion used in a reshuffler device,” *Nature Nanotechnol.* **14** (7), 658–661.
- Zeissler, K, S. Finizio, C. Barton, A. J. Huxtable, J. Massey, J. Raabe, A. V. Sadovnikov, S. A. Nikitov, R. Brearton, T. Hesjedal, G. van der Laan, M. C. Rosamond, E. H. Linfield, G. Burnell, and C. H. Marrows (2020), “Diameter-independent skyrmion Hall angle observed in chiral magnetic multilayers,” *Nature Commun.* **11** (1), 428.
- Zeissler, K, S. Finizio, K. Shahbazi, J. Massey, F. Al Ma’Mari, D. M. Bracher, A. Kleibert, M. C. Rosamond, E. H. Linfield, T. A. Moore, J. Raabe, G. Burnell, and C. H. Marrows (2018), “Discrete Hall resistivity contribution from Néel skyrmions in multilayer nanodiscs,” *Nature Nanotechnol.* **13**, 1161–1166.
- Zeissler, K, M. Mruczkiewicz, S. Finizio, J. Raabe, P. M. Shepley, A. V. Sadovnikov, S. A. Nikitov, K. Fallon, S. McFadzean, S. McVitie, T. A. Moore, G. Burnell, and C. H. Marrows (2017), “Pinning and hysteresis in the field dependent diameter evolution of skyrmions in Pt/Co/Ir superlattice stacks,” *Sci. Rep.* **7**, 15125.
- Zeldov, E, D. Majer, M. Konczykowski, V. B. Geshkenbein, V. M. Vinokur, and H. Shtrikman (1995), “Thermodynamic observation of first-order vortex-lattice melting transition in  $\text{Bi}_2\text{Sr}_2\text{CaCu}_2\text{O}_8$ ,” *Nature* **375**, 373–376.
- Zhang, S, G. van der Laan, J. Müller, L. Heinen, M. Garst, A. Bauer, H. Berger, C. Pfleiderer, and T. Hesjedal (2018a), “Reciprocal space tomography of 3D skyrmion lattice order in a chiral magnet,” *Proc. Natl. Acad. Sci. (USA)* **115**, 6386–6391.
- Zhang, S, A. K. Petford-Long, and C. Phatak (2016a), “Creation of artificial skyrmions and antiskyrmions by anisotropy engineering,” *Sci. Rep.* **6**, 31248.
- Zhang, S, J. Zhang, Y. Wen, E. M. Chudnovsky, and X. Zhang (2018b), “Determination of chirality and density control of Néel-type skyrmions with in-plane magnetic field,” *Commun. Phys.* **1**, 36.
- Zhang, S, X. Zhang, J. Zhang, A. Ganguly, J. Xia, Y. Wen, Q. Zhang, G. Yu, Z. Hou, W. Wang, Y. Peng, G. Xiao, A. Manchon, J. Kosel, Y. Zhou, and X.-X. Zhang (2020), “Direct imaging of an inhomogeneous electric current distribution using the trajectory of magnetic half-skyrmions,” *Science Adv.* **6**, eaay1876.
- Zhang, S L, A. Bauer, H. Berger, C. Pfleiderer, G. van der Laan, and T. Hesjedal (2016b), “Imaging and manipulation of skyrmion lattice domains in  $\text{Cu}_2\text{OSeO}_3$ ,” *Appl. Phys. Lett.* **109**, 192406.
- Zhang, S L, W. W. Wang, D. M. Burn, H. Peng, H. Berger, A. Bauer, C. Pfleiderer, G. van der Laan, and T. Hesjedal (2018c), “Manipulation of skyrmion motion by magnetic field gradients,” *Nature Commun.* **9**, 2115.
- Zhang, X, M. Ezawa, and Y. Zhou (2015), “Magnetic skyrmion logic gates: conversion, duplication and merging of skyrmions,” *Sci. Rep.* **5**, 9400.
- Zhang, X, J. Xia, G. P. Zhao, X. Liu, and Y. Zhou (2017a), “Magnetic skyrmion transport in a nanotrack with spatially varying damping and non-adiabatic torque,” *IEEE Trans. Magn.* **53**, 1500206.
- Zhang, X, J. Xia, Y. Zhou, X. Liu, H. Zhang, and M. Ezawa (2017b), “Skyrmion dynamics in a frustrated ferromagnetic film and current-induced helicity locking-unlocking transition,” *Nature Commun.* **8**, 1717.
- Zhang, X, Y. Zhou, and M. Ezawa (2016c), “Magnetic bilayer-skyrmions without skyrmion Hall effect,” *Nature Commun.* **7**, 10293.
- Zhang, X-X, A. S. Mishchenko, G. De Filippis, and N. Nagaosa (2016d), “Electric transport in three-dimensional

- skyrmion/monopole crystal,” *Phys. Rev. B* **94**, 174428.
- Zhao, H J, V. R. Misko, and F. M. Peeters (2013), “Dynamics of self-organized driven particles with competing range interaction,” *Phys. Rev. E* **88**, 022914.
- Zhao, H J, W. Wu, W. Zhou, Z. X. Shi, V. R. Misko, and F. M. Peeters (2016), “Reentrant dynamics of driven pancake vortices in layered superconductors,” *Phys. Rev. B* **94**, 024514.
- Zhao, L, Z. Wang, X. Zhang, X. Liang, J. Xia, K. Wu, H.-A. Zhou, Y. Dong, G. Yu, K. L. Wang, X. Liu, Y. Zhou, and W. Jiang (2020), “Topology-dependent Brownian gyromotion of a single skyrmion,” *Phys. Rev. Lett.* **125**, 027206.
- Zheng, F, F. N. Rybakov, A. B. Borisov, D. Song, S. Wang, Z.-A. Li, H. Du, N. S. Kiselev, J. Caron, A. Kovács, M. Tian, Y. Zhang, S. Blügel, and R. E. Dunin-Borkowski (2018), “Experimental observation of chiral magnetic bobbers in B20-type FeGe,” *Nature Nanotechnol.* **13**, 451–455.
- Zhou, H, H. Polshyn, T. Taniguchi, K. Watanabe, and A. F. Young (2020), “Solids of quantum Hall skyrmions in graphene,” *Nature Phys.* **16** (2), 154.
- Zhou, L, R. Qin, Y.-Q. Zheng, and Y. Wang (2019a), “Skyrmion Hall effect with spatially modulated Dzyaloshinskii-Moriya interaction,” *Front. Phys.* **14**, 53602.
- Zhou, Y, R. Mansell, and S. van Dijken (2019b), “Driven gyrotropic skyrmion motion through steps in magnetic anisotropy,” *Sci. Rep.* **9**, 6525.
- Zou, J, S. Zhang, and Y. Tserkovnyak (2020), “Topological transport of deconfined hedgehogs in magnets,” *Phys. Rev. Lett.* **125**, 267201.